IEEE
Robotics & Automation MAGAZINE

Vol. 15, No. 3 September 2008
ISSN 1070-9932

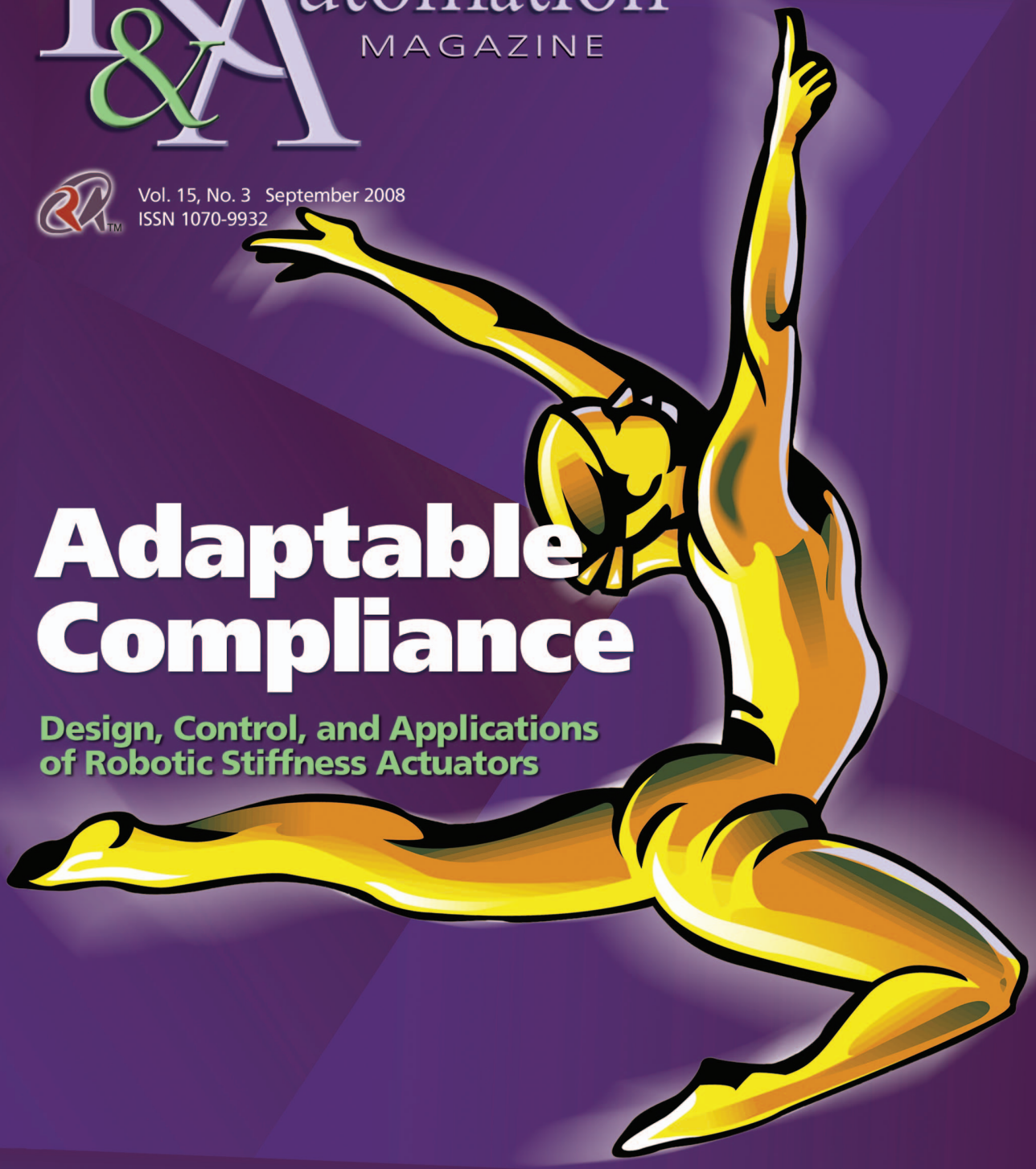

Adaptable Compliance

Design, Control, and Applications of Robotic Stiffness Actuators

IEEE

IEEE Robotics & Automation MAGAZINE

Vol. 15, No. 3 September 2008
ISSN 1070-9932

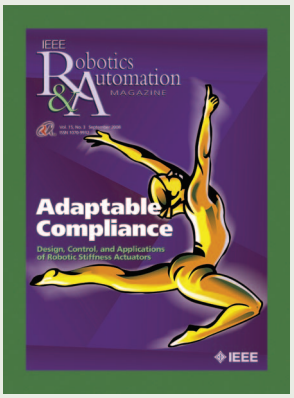

This special issue provides a balanced overview of the current research across the field of a new generation of actuators with controllable stiffness that benefits many different robotic applications and covers different designs and control strategies.

Image: ©Punchstock

FEATURES

DEPARTMENTS

Digital Object Identifier 10.1109/MRA.2008.927699

IEEE Robotics & Automation Magazine
(ISSN 1070-9932) (IRAMEB) is published quarterly by the Institute of Electrical and Electronics Engineers, Inc. Headquarters: 3 Park Avenue, 17th Floor, New York, NY 10016-5997 USA, Telephone: +1 212 419 7900. Responsibility for the content rests upon the authors and not upon the IEEE, the Society or its members. IEEE Service Center (for orders, subscriptions, address changes): 445 Hoes Lane, P.O. Box 1331, Piscataway, NJ 08855-1331 USA. Telephone: +1 732 981 0060. Individual copies: IEEE members $20.00 (first copy only), nonmembers $86.00 per copy. Subscription rates: Annual subscription rates included in IEEE Robotics and Automation Society member dues. Subscription rates available on request. Copyright and reprint permission: Abstracting is permitted with credit to the source. Libraries are permitted to photocopy beyond the limits of U.S. Copyright law for the private use of patrons (1) those post-1977 articles that carry a code at the bottom of the first page, provided the per-copy fee indicated in the code is paid through the Copyright Clearance Center, 222 Rosewood Drive, Danvers, MA 01923 USA; (2) pre-1978 articles without a fee. For other copying, reprint, or republication permission, write Copyrights and Permissions Department, IEEE Service Center, 445 Hoes Lane, Piscataway, NJ 08854. Periodicals postage paid at New York and additional mailing offices. Postmaster: Send address changes to IEEE Robotics and Automation Magazine, IEEE, 445 Hoes Lane, Piscataway, NJ 08854 USA. Canadian GST #125634188

PRINTED IN THE U.S.A.

FROM THE EDITOR'S DESK

The Gurus Behind RAS WWW

I thought it would be nice to show you the gurus behind the RAS WWW developments, on the left, between me and our new "robotic head" you see Olaf van Zandwijk. On the right is Hubert Flisijn. They are the real programmers behind the great new high-tech developments of the RAS WWW.

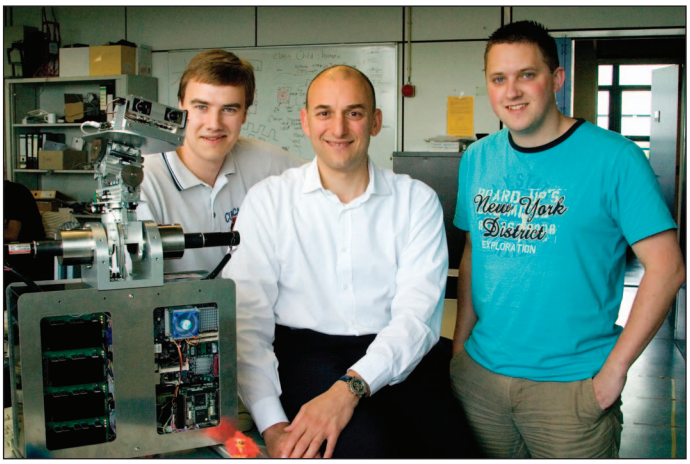

This has been a busy period. For those of you who were at the student party at ICRA08 in Pasadena, you have seen that, as Alex Zelinsky said, our Society goes beyond high-quality science and engineering and is becoming a real community, where a couple of professors risk losing face by going onstage as The RASOR and try playing songs they never played together live—I loved it!

Going back to business, this issue on adaptable compliance/variable stiffness for robotic applications guest edited by Bram Vanderborght, Thomas Sugar, and Dirk Lefeber has broken a record of 27 submissions of which only six were accepted for publication in this issue. Great job, guys!

I invite you once again to go to http://wiki.ieee-ras.org and use our Society wiki to comment on the contributions of the position papers of Herman Bruyninckx on robotics software and of Wolfram Burgard on probabilistic approaches on robotics navigation. You can express your opinion on the subject, which we may then partially publish in the magazine.

Authors have started submitting multimedia attachments, which is a great development for our magazine. We are on the edge of redesigning the magazine, and if you have suggestions or complaints about the current structure and layout, I would be very pleased to know your opinion.

In this issue, we have the second part of the tutorial on medical robotics contributed by Gabor Fichtinger, Peter Kazanzides, Allison M. Okamura, Gregory D. Hager, Louis L. Whitcomb, and Russell H. Taylor. Prof. Taylor was a corecipient of the RAS Pioneer Award for his groundbreaking work in surgical robotics. As usual, for any comments, suggestions, or criticism, do not hesitate to contact us. I hope you will enjoy the issue!

Stefano Stramigioli
S.Stramigioli@ieee.org

Digital Object Identifier 10.1109/MRA.2008.928313

IEEE Robotics & Automation MAGAZINE

A Publication of the
IEEE ROBOTICS AND AUTOMATION SOCIETY
Volume 15, No. 3 September 2008 ISSN 1070-9932

Tightening the Chord Between Academia and Industry

After a successful IEEE International Conference on Robotics and Automation (ICRA) that marked the silver anniversary of our flagship conference (from Atlanta in 1984 to Pasadena in 2008), I am writing this column while attending the IEEE/International Federation of Robotics (IFR) Joint Forum on Innovation and Entrepreneurship in Robotics and Automation (IERA) in Munich (see my message in the March issue), as part of Automatica 2008 (the largest biennial fair in robotics and automation in Europe), in parallel with two annual local events [the symposium of the German Association for Pattern Recognition, and Robotik organized by the German Society for Robotics (DGR)].

With ICRA and IERA, we are looking forward to another long summer on the road to conferences and meetings, which will take me—among others—to Xi'an, China, for the International Conference on Advanced Intelligent Mechatronics (AIM) in early July, to Washington, DC, for the Conference on Automation and Science Engineering (CASE) in late August, and to Nice in late September for the International Conference on Intelligent Robots and Systems (IROS).

This is a good and vibrant time for our field. The robotics industry is a more than US$10 billion enterprise worldwide, with a growth rate estimated to be about 8% annually. In Munich, I gave a keynote talk on "The Importance of Close Collaboration Between Academia and Industry—Successful Examples from Recent Years and Future Challenges." During the event, the European Commission announced a policy to boost European robotics (see "Robots in the News" at www.ieee-ras.org/news). The European Union will double its investments between 2007 and 2010 with almost €400 million to support European robotics research. This ambitious program aims to forge stronger links between academia and industry and plans to fund a widespread experimentation by academic researchers and industry.

Both Japan and Korea have ongoing, aggressive national plans to promote their competitiveness in robotics. The Japanese strategy for creating new industries includes robotics as one of the seven areas of emphasis, while Korean robotics is one of the ten next-generation growth engines. Interestingly enough, a policy change is taking place in the United States after years of inadequate government funding. A Congressional Robotics Caucus was established in June 2007: IEEE-USA with the IEEE Robotics

Digital Object Identifier 10.1109/MRA.2008.928306

and Automation Society (RAS) has played an active role in its formation and serves as a member of the caucus' advisory committee (see http://www.ieeeusa.org/communications/presidentscolumn/Lefevre/jun.asp).

The group acts as a resource for caucus members on the state of robotics technology and key issues facing the robotics industry. Growth in the industry means job opportunities for IEEE and RAS Members and gives us new vigor to educate and train our students and graduates in robotics and automation with the challenge of working on new and exciting projects that will have positive effects on our lives and lifestyles.

As with my previous messages, you will find the highlights from our boards, mostly based on the outcome of our Spring Administrative Committee (AdCom) meeting in Pasadena. Detailed reports are available in the "Society News" column in this issue. Indeed, as a new experiment, three of the next board meetings (Conference Activities Board, Publications Activities Board, and Technical Activities Board) will take place for the first time at CASE, in preparation for the Fall AdCom meeting in Nice during IROS: the intent of this strategic choice is to bring Society officers to get acquainted with our newest RAS annual conference on automation and science engineering.

Conference Activities Board (CAB)

- RAS is the sole financial sponsor of ten conferences, financial cosponsor of 17 others, and technical cosponsor of more than 20 conferences. While ICRA remains our flagship conference, other conferences place their proceedings on *IEEE Xplore* with RAS' imprimatur and impact the financial health of our Society. The paperwork involved with these conference operations is swamping our volunteers, especially the CAB and RAS treasurers. To offload much of the routine work, AdCom in Pasadena approved hiring a part-time assistant for the CAB, who will report to Shigeki Sugano, associate vice-president of the CAB. Other societies are increasingly hiring such assistants for similar reasons.
- Speaking of ICRA, it used to be the case that AdCom chose the location of future ICRAs after competitive presentations. In recent years, this decision has been left to the CAB, and future ICRAs have now been planned out till 2015. This amount of forward planning is probably not good for the Society, as it does not allow for the tracking of changes in the field or emergence of new robotics geographical regions or interest groups. AdCom approved a proposal to limit the advance selection of ICRAs to no more than five years, which means that ICRA 2016 will be chosen in 2011. An open call for ICRA proposals will be issued one year in advance, and AdCom will once again choose between the finalists. This could be done in an open forum to allow the community to participate.
- ICRA 2008 was the second year of operation of the Conference Editorial Board (CEB). Although there was some initial hesitation, it is fair to say that the community generally considers the CEB to be a resounding success and to have improved the quality of reviews and decision making for ICRA papers. The reputation of ICRA has been reestablished in terms of attending and presenting one's best work. The inaugural editor-in-chief of the CEB, Seth Hutchinson, deserves a strong vote of thanks for launching the CEB and ensuring its proper functioning. It is no surprise that Seth was asked to be the next editor-in-chief of *IEEE Transactions on Robotics (T-RO)* starting October 2008, succeeding Alessandro De Luca. The Steering Committee for Technical Programs, led by Vijay Kumar, took on the task of selecting a replacement. Four highly capable and respected individuals put their names into the hat for election, which is testimony to the importance our Society now places on the CEB and ICRA. After a close election, Antonio Bicchi was elected to replace Seth as the new CEB editor-in-chief, effective after ICRA 2008. We thank Antonio for stepping forward to undertake this important position.

Financial Activities Board (FAB)

- The five winners of the 2008 Initiatives Competition were approved during AdCom in Pasadena. The total requested amount from the five approved initiatives was US$75,000. Based on the availability of funds (US$63,000) and what was requested for, all five initiatives are funded, some with reduced amount.
- Promptly after AdCom, the RAS first-pass budget for 2009 has been submitted to the financial analyst at IEEE, including publication rates, conference budgets, and all new activities that have financial impact. As usual, the goal is to keep RAS on a sound financial path while investing in return to our members.

Industrial Activities Board (IAB)

- RAS is working cooperatively with IFR to support activities that promote innovation of new robotics products and services. The IERA forum also recognizes outstanding invention and entrepreneurship in robotics and automation through an award that is judged by an international panel. A report of this year's forum can be found in the "Industry/Research News" column in this issue.
- An important public relations role for the robotics community is to inform the general public about the likely future trends of robotics and automation technology. Technology road maps for robot technology and products with 5-, 10-, and 20-year timelines are being prepared by both government and industry with considerable work done in Korea, Japan, and Europe.

Early-stage road-mapping activity has commenced in the United States. The IAB is currently compiling road-mapping material and resources that will be published on the RAS Web site.

- Much of today's robotics is based on experimental demonstration platforms. To transform robotics into a full product and service-based industry will require industry standards. There is a general expectation that robots will work and operate in public places. Without robots meeting stringent safety and environment standards, deployment in public places will not be possible. IAB has a Standards Committee that is working closely with IEEE Standards; the committee is chaired by Erwin Prassler. The current focus of the Standards Committee is on robot middleware that will allow the development of common platforms for sensors and systems software. Working groups on standards commenced activities at ICRA 2008.
- IAB is working closely with the editor-in-chief of *IEEE Robotics and Automation Magazine* to develop a regular one-page column on industrial activities. The first column will report on innovations in robotics and automation with a focus on new technologies and products.

Member Activities Board (MAB)

- The first Local and Student Chapters Workshop, http://www.mech.uwa.edu.au/spns/clw/, was organized within the frame of ICRA 2008 in Pasadena as a means to share, reinforce, and brainstorm various chapters' activities. The goal of this workshop was to build a support group for the chapters to encourage members, network with other chapters, and help the RAS Committee figure out how to best assist these groups. RAS awarded travel grants so that nine out of 39 local chapters and one out of 18 student chapters could come and participate in the event. MAB Chair Alícia Casals and Chair of Student Activities Committee Carol Reiley presented the possibilities of both kind of chapters and the future of RAS committees. Each chapter chair gave a brief presentation about their chapter activities giving place to a discussion on how RAS could help and how chapters could cooperate for the benefit of all the members.
- From the presentations, a common activity was to start and promote local robotics competitions, and, consequently, two initiatives were put forth to help chapters with these competitions. A first motion approved by AdCom was the generation of a competition resource wikipage aimed to pull the chapters together and serve as a repository of rules, competitions, organizing tools, as well as providing a Robot Competition Quick Start Kit, which would give information and advice on how to organize a competition easily. Additionally, and complementarily, the second initiative was to the regular chapter grants: MAB will encourage local competitions by coordinating a grant pool.

Publications Activities Board (PAB)

- The latest impact factor (IF) from 2007 journal citation report (JCR) has just come out. For *IEEE Transactions on Automation Science and Engineering* (*T-ASE*), the IF is 1.229, indicating that for each paper published in 2005 and 2006 in *T-ASE*, it was cited by 2007 papers published in all the journals in the ISI database 1.229 times on the average. In view that the first issue of *T-ASE* was published in July 2004, this is the first time that *T-ASE* has a complete IF. The IF for 2006 was 0.929.
- The highest 2007 IF in the category of automation and control systems is 2.824 by *IEEE Transactions on Automatic Control*. The IF for *IEEE Robotics and Automation Magazine* is 0.892, and the IF for *IEEE/ASME Transactions on Mechatronics* is 0.908.
- For *T-RO*, there were mistakes in the calculation of its IF. The editor-in-chief of *T-RO*, Alessandro De Luca, gathered data and submitted it to the IEEE, which is discussing with JCR staff to correct this issue. This is very unfortunate, especially in view that 2006 IF for *T-RO* was wrongly calculated by JCR, and it was corrected only after a major effort by De Luca and the IEEE.

Technical Activities Board (TAB)

- Worldwide research in robotics and automation is thriving. Please visit http://goldberg.berkeley.edu/vpta/ for information on joining or proposing RAS Technical Committees (TCs), inviting Distinguished Lecturers to speak, and other opportunities for participating.
- Our 22 TCs are more active than ever, playing the role of research amplifiers rather than capacitors. This year, TAB initiated a triennial review for all TCs: RAS TCs are initiated to grow research in a new topic or re-energize research in an established topic related to robotics and automation. RAS TCs are expected to retire after six to nine years as their topic becomes established to make room for new TCs. TAB Associate Vice Presidents Eugenio Guglielmelli and Yasuhisa Hasegawa coordinated the first triennial review of eight TCs during ICRA, and three were retired. Two new TCs were proposed and approved, one on robot learning and one on marine robotics. Please see tab.ieee-ras.org for details and information on how to join.
- The RAS Distinguished Lecturer program has also been expanded, from 15 to 24 speakers, eight from each major region, including nine speakers from underrepresented regions. We have developed a new database with info on each speaker (see Web site mentioned earlier).
- A successful and well-attended Graduates of Last Decade (GOLD) reception was hosted at ICRA, and the program will be extended to CASE in August.

These GOLD gatherings are just perfect to bring along the experience from recent graduates to the students of our Society.

- TAB is working with *IEEE Robotics and Automation Magazine* Editor-in-Chief Stefano Stramigioli to develop a regular column for TCs and welcomes ideas and contributions from all RAS members.
- After the expansion of the Distinguished Lecturer (DL) program with an increase from 15 to 24 lecturers, the transportation budget has been increased from US$10,000 to US$15,000 a year. The DL program is a wonderful opportunity to disseminate robotics and automation among various chapters and sections.

Electronic Products and Service Board (EPSB)

Despite its name, EPSB is only a standing committee, which has been massively involved in the restructuring of our Web site over the past couple of years.

By the time this issue will be in print, Version 2 of the Web site will be online! Great efforts have been made to get a versatile, robust, easy-to-use and high-tech portal facility for RAS. The developing team chaired by Stefano Stramigioli and the gurus behind the scene, Olaf van Zandwijk and Hubert Flisijn, has found a way to implement a completely new database structure, which will support volunteers in their work and help members in searching information and archiving historical data and multimedia documents, and has given the site a completely new look. It is now possible to maintain one's own agenda for robotics and automation-related activities and couple it to the Google calendar or Outlook easily. These are just few of the new useful features, which can be checked out at http://www.ieee-ras.org.

As you can see, RAS and its volunteers keep themselves active with new ideas and initiatives, inspired by one common mission: promote robotics and automation worldwide. Please send your comments to me, any of the officers, or our Society Activities Coordinator Rosalyn Snyder. Contact information for RAS officers and committee chairs is on our home page.

Bruno Siciliano
siciliano@ieee.org
RAS President 2008–2009

Adaptable Compliance or Variable Stiffness for Robotic Applications

Bram Vanderborght, Thomas Sugar, and Dirk Lefeber

Exciting new robots are being developed that will operate in a different environment from traditional industrial factories or research laboratories. Researchers are working worldwide to create robots that are integrated into our daily lives. For the advancement of these new robots, compliant, safe, and new actuators are one of the important issues turning energy into safe motion. The biological counterpart is the muscle tendon structure that has functional performance characteristics and a neuromechanical control system that has far more superior capabilities. The superior power to weight ratio, force to weight ratio, and sensing characteristics limit the development of machines that can match motion, safety, and energy efficiency of a human or other animal. One of the key differences of biological systems is their adaptable compliance or variable stiffness compared with the traditional stiff electrical drives used for the standard industrial robotic applications, which require accurate, reference-trajectory tracking. More and more applications such as robots in close human or robot proximity, legged autonomous robots, and rehabilitation devices and prostheses demand a different set of design specifications, for which the use of compliant actuators can be beneficial as compared with the traditional stiff actuation schemes.

To tackle the problems related to design and control, both the actuator and the controller need to be completely reconsidered. Researchers are developing original mechanical designs. Different designs that are being developed include the mechanical impedance adjuster, where the effective length of the spring can be changed by a slider to control the stiffness, and the Jack Spring actuator, where the number of active coils in a helical spring is adjusted. In the mechanically adjustable compliance and controllable equilibrium position actuator (MACCEPA), the stiffness is varied by changing the pretension or the preload of the spring by altering the attachment position of the spring. New developments for the controller cannot include traditional schemes because they are designed for high-performance tracking and do not include criteria to minimize energy consumption or ensure human safety.

This special issue covers different designs and control strategies of controllable stiffness actuators and their robotic applications. An incredible number of 28 high-quality articles were received, which showed the interest among the research community. The six published articles provide a balanced overview of the current research across the field of a new generation of actuators with controllable stiffness that benefit many different robotic applications.

Digital Object Identifier 10.1109/MRA.2008.927694

Controllable compliant actuators can be divided into active compliant actuators, where a controller of a stiff actuator mimics the behavior of a spring, and passive compliant actuators, which consist of a compliant element that is able to store and release energy. The article "Soft Robotics" by Albu-Shäffer et al. clearly develops both types of actuators to achieve controllable stiffness for soft robotics. The first section of the article describes a mature technology of torque-controlled lightweight robots that are successfully demonstrated in different robotic devices. The second section describes a variable impedance actuation system, with compliance added into the hardware. They present an analysis on the advantages and disadvantages between both approaches.

The article "Toward Soft Robots You Can Depend On" by Filippini et al. describes three different arrangements of the agonist-antagonist actuation scheme to implement the variable stiffness actuation paradigm. The ability to change the effective transmission stiffness during motion is used to achieve high performance while minimizing injury risks by accidental impacts with humans, limiting an impact below a given threshold. This article describes a comparative analysis among performance, safety, and dependability.

In their article, "Series Compliance for an Efficient Running Gait," Hurst and Rizzi explain that a physical spring must be used to minimize impacts and increase energy storage in running robots. The spring-loaded inverted pendulum model is used to describe the center-of-mass motion. One variation is discussed where the actuator with mechanically adjustable series compliance (AMASC) actuator is used in the biped with mechanically adjustable series compliance (BiMASC) to control the leg length, leg angle, and leg stiffness. They also describe a second biped MABEL, a monopod named Thumper, where the stiffness is not mechanically adjustable but only controlled using software. Thumper has now performed successful hopping experiments.

In their article, "Powered Ankle-Foot Prosthesis," Au and Herr show how compliant actuation is beneficial for ankle-foot prosthetic technology. During the stance phase, a motor series spring and an additional parallel spring store energy, which is released at push off. The article focuses on the design of the ankle-foot prosthesis, selecting a parallel spring to mimic the quasi-static stiffness during controlled dorsiflexion phase of slow walking. The parallel spring effectively lowers the force borne by a series elastic actuator. Springs help to protect the mechanism from damage during foot collision, and a parallel spring helps to satisfy bandwidth requirements.

In their article, "Compliant Actuation of Rehabilitation Robots," Vallery et al. describe the gait rehabilitation robot

lower-extremity powered exoskeleton (LOPES). Position-controlled devices are not completely suitable for rehabilitation therapy because they predominantly enforce motion patterns, whereas a device with compliant actuation allows active patient participation during therapy. Such interactive-control algorithms assist the patient only when it is needed. The exoskeleton is powered by series elastic actuation and controlled with a virtual model control. The article focuses both on advantages and disadvantages of compliant actuation for rehabilitation.

For the upper extremity, the arm rehabilitation robot actuated with the novel moment arm manipulation for remote induction of net effective torque actuator is described in "Pulling Your Strings" by Sulzer et al. The goal is to build a low-cost home rehabilitation system. Both the concepts of the novel actuator and the application are described. The joint is driven by two motors: one controls the moment arm, and the other controls the cable tension to achieve variable compliance. The first tests with healthy participants show that the device is able to produce two training paradigms currently used in rehabilitation: the first one produces forces to guide the user toward a desired trajectory (guidance), and a second approach pushes the user away from a desired trajectory (error augmentation).

We believe that variable stiffness actuators will become increasingly important in robotics because of the growing fields of medical robotics, rehabilitation robotics, legged humanoids, and limit cycle walkers. Safety is crucial when robots interact closely with humans, and these new actuators can be inherently passive and compliant. Energy autonomy is a must when building humanoids and walkers.

The advancements in actuator technology will clearly facilitate the development of new applications, especially robots that will collaborate directly with humans and robots that have to move efficiently and safely. Still, much work needs to be performed both on the design of the actuator itself as well as the control technology to take full benefit of the new possibilities. Hopefully, this special issue contributes to this emerging research field and inspires new developments.

ICRA 2008 at Pasadena

The 25th IEEE International Conference on Robotics and Automation (ICRA) took place in Pasadena, California, 19–23 May 2008. More than one third of the 1,332 participants from 35 countries were students. ICRA 2008 featured the following:

- 12 tracks of regular papers
- plenary talks by Andrew Blake, Naomi Leonard, and Mitsuo Kawato
- 22 workshops and tutorials on topics ranging from wearable robots to the DARPA Urban Challenge
- the RAS Space Robotics Challenge and the Human-Robot Interaction (HRI) Challenge
- just for fun, a student party with the Robotics and Automation Society Officers Rock (RASOR) and a comics contest.

The ICRA 2008 program committee accepted 661 of the 1,463 paper submissions (about 46%) and 22 of the 29 stand-alone video submissions. The final program included papers and videos from 34 different countries, led by the United States, Japan, Germany, Canada, and France. The chart below shows the distribution by country.

All the accepted papers are available on *IEEE Xplore*. The videos were included on the ICRA DVD Proceedings and will soon be available on the RAS Web site.

Thanks to Program Chairs Gaurav Sukhatme and Stefan Schaal, and General Chairs Maja Mataric and Paul Shenker, and the rest of the ICRA team, including all the student volunteers for their efforts.

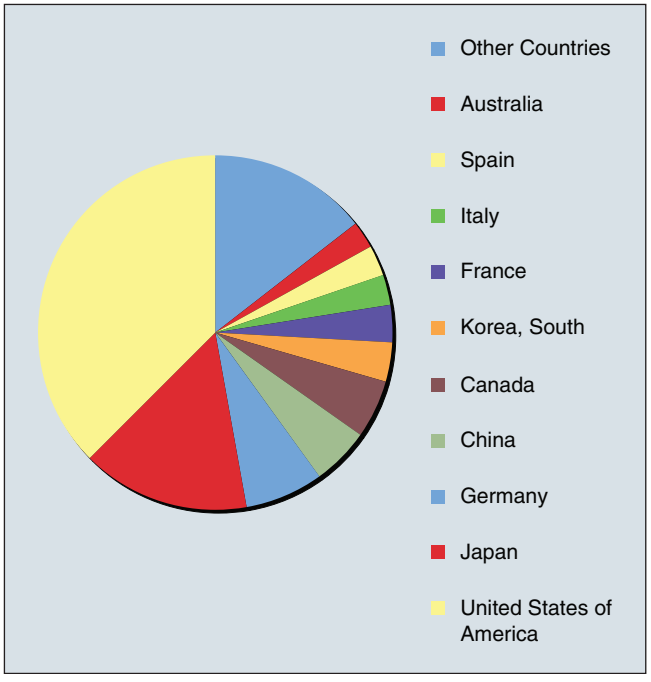

Distribution of papers in ICRA 2008 program.

Digital Object Identifier 10.1109/MRA.2008.928305

Photographs from ICRA 2008 are available on the conference Web site http://robotics.usc.edu/~nkoenig/icra2008_photos. All ICRA photographs shown here, which are not otherwise credited are courtesy of the ICRA photographers Nate Koenig, Emily Mower, and Carl Oberg.

ICRA 2008 Awards

The following outstanding video and papers were selected for awards:

- Best conference paper: "Planning in Information Space for a Quadrotor Helicopter in a GPS Denied Environment" by Ruijie He, Sam Prentice, and Nicholas Roy
- Best student paper: "Decentralized Feedback Controllers for Multi-Agent Teams in Environments with Obstacles" by Nora Ayanian (student author) and Vijay Kumar
- Best automation paper: "Fabrication of Functional Gel-Microbead for Local Environment Measurement in Microchip" by Hisataka Maruyama, Fumihito Arai, and Toshio Fukuda
- Best vision paper (Endowed by Ben Wegbreit): "Accelerated Appearance-Only SLAM" by Mark Cummins and Paul Newman
- Best manipulation paper (Endowed by Ben Wegbreit): "Adaptive Grasping by Multi Fingered Hand with Tactile Sensor Based on Robust Force and Position Control" by Taro Takahashi, Toshimitsu Tsuboi, Takeo Kishida, Yasunori Kawanami, Satoru Shimizu, Masatsugu Iribe, Tetsuharu Fukushima, and Masahiro Fujita
- KUKA service robotics best paper: "VSA-II: A Novel Prototype of Variable Stiffness Actuator for Safe and Performing Robots Interacting with Humans" by Riccardo Schiavi, Giorgio Grioli, Soumen Sen, and Antonio Bicchi
- Best video: "The OmniTread OT-4 Serpentine Robot" by Johann Borenstein and Adam Borrell.

The finalists were as follows:

Best conference paper finalists:

- "Employing Wave Variables for Coordinated Control of Robots with Distributed Control Architecture" by Christian Ott and Yoshihiko Nakamura
- "Trajectory Generation for Dynamic Bipedal Walking through Qualitative Model Based Manifold Learning" by Subramanian Ramamoorthy and Benjamin Kuipers
- "Consensus Learning for Distributed Coverage Control" by Mac Schwager, Jean-Jacques E. Slotine, and Daniela Rus.

Best student paper finalists (the names of nominated students are in bold):

- "Hybrid Simulation of a Dual-Arm Space Robot Colliding with a Floating Object" by **Ryohei Takahashi**, Hiroto Ise, Daisuke Sato, Atsushi Konno, and Masaru Uchiyama
- "Partial Barrier Coverage: Using Game Theory to Optimize Probability of Undetected Intrusion in Polygonal Environments" by **Stephen Kloder** and Seth Hutchinson
- "Gecko-Inspired Climbing Behaviors on Vertical and Overhanging Surfaces" by **Daniel Santos**, **Barrett**

Heyneman, Sangbae Kim, Noe Esparza, and Mark Cutkosky

- "High Quality 3D LIDAR from Low Cost 2D Ranging Under General Vehicle Motion" by **Alastair Harrison** and Paul Newman.

Best automation paper finalists:

- "Dynamic Analysis of a High-Bandwidth, Large-Strain, PZT Cellular Muscle Actuator with Layered Strain Amplification" by Thomas Secord, Jun Ueda, and Harry Asada
- "Actuator with Layered Strain Amplification" by Thomas Secord, Jun Ueda, and Harry Asada
- "Event-Based Two Degree-of-Freedom Control for Micro-/Nanoscale Systems Based on Differential Flatness" by Ruoting Yang, T. J. Tarn, and Mingjun Zhang
- "On the Design of Traps for Feeding 3D Parts on Vibratory Tracks" by Onno Goemans and Frank van der Stappen.

Best manipulation paper finalists:

- "Skilled-Motion Planning of Multi-Body Systems Based upon Riemannian Distance" by Masahiro Sekimoto, Suguru Arimoto, Ji-Hun Bae, and Sadao Kawamura
- "Transportation of Hard Disk Media Using Electrostatic Levitation and Tilt Control" by Ewoud Frank van West, Akio Yamamoto, and Toshiro Higuchi
- "Manipulating Articulated Objects with Interactive Perception" by Dov Katz and Oliver Brock
- "Synergistic Design of a Humanoid Hand with Hybrid DC Motor—SMA Array Actuators Embedded in the Palm" by Josiah Rosmarin and Harry Asada.

Best vision paper finalists:

- "Image Moments-Based Ultrasound Visual Servoing" by Rafik Mebarki, Alexandre Krupa, and Francois Chaumette
- "Accurate Calibration of Intrinsic Camera Parameters" by Observing Parallel Light Pairs by Ryusuke Sagawa and Yasushi Yagi
- "Information-Optimal Selective Data Return for Autonomous Rover Traverse Science and Survey" by David R. Thompson, Trey Smith, and David Wettergreen
- "Robust and Efficient Stereo Feature Tracking for Visual Odometry" by Andrew E. Johnson, Steven B. Goldberg, Yang Cheng, and Larry H. Matthies.

Best video finalists:

- "Magmites—Wireless Resonant Magnetic Microrobots" by Dominic R. Frutiger, Bradley Kratochvil, Karl Vollmers, and Bradley J. Nelson
- "Preliminary Report: Rescue Robot at Crandall Canyon, Utah, Mine Disaster" by Robin R. Murphy, Jeffery Kravitz, Ken Peligren, James Milward, and Jeff Stanway.

KUKA service robotics best paper finalists:

- "Efficient Airport Snow Shoveling by Applying Autonomous Multi-Vehicle Formations" by Martin Saska, Martin Hess, and Klaus Schilling
- "Hybrid Laser and Vision Based Object Search and Localization" by Dorian Galvez Lopez, Kristoffer Sjo, Chandana Paul, and Patric Jensfelt

The Contingency Challenge required the contestants to solve a problem on the spot, with the tools and materials on hand.

ICRA participants interact with the robot.

- "Towards a Personal Robotics Development Platform: Rationale and Design of an Intrinsically Safe Personal Robot" by Keenan A. Wyrobek, Eric H. Berger, H. F. Machiel Van der Loos, and J. Kenneth Salisbury.

ICRA Space and HRI Challenges

The first ICRA Robotics Challenge presented a variety of problems, which the different teams were invited to solve using approaches developed in their ongoing research.

This approach was a fairly radical departure from the myriad of other robotics competitions, which generally impose a strict set of rules and require the team members to alter or even abandon their primary research objectives to meet the constraints of the competition.

This made comparisons of the different entries even more difficult for the judges, but the result was an amazing variety of creative and diverse solutions to the problems presented.

Space: Sandbox Results

All the teams that competed in the sandbox event successfully completed all the tasks they entered. Instead of making arbitrary rankings, awards were given for technical excellence in the event in which the teams performed well.

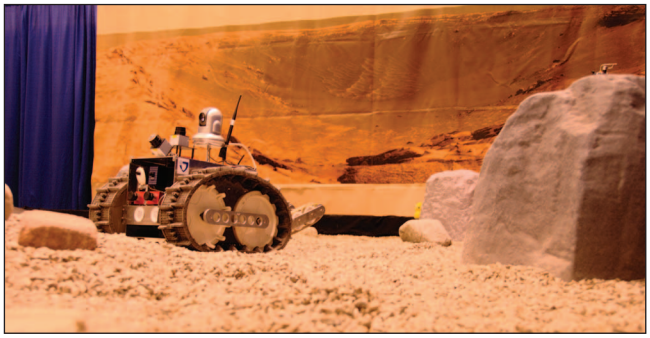

The robots in the Sandbox Challenge performed their tasks in a simulated Martian landscape. The competition took place the same week that the Phoenix Mars Lander began sending back pictures from the Red Planet.

- Jacobs University: Onto the surface, data collection, map the environment, and back on the lander
- Tohoku University: Onto the surface, data collection, map the environment, and back on the lander
- The University of Kansas: Onto the surface and map the environment.

Space: Contingency Results

Overall results:

- First place: Morpheus (USC/ISI)
- Second place: Diamond (MIT/CSAIL)
- Third place: SOSlab (University of Washington).

Special awards:

- Team Cornell (Cornell University)—Fastest Prototyping Team
- Odin (University of Southern Denmark)—Coolest Robot
- SOSLab (University of Washington)—Most Innovative Team
- Diamond (MIT/CSAIL)—Most Persistent in the Face of Life-Threatening Events.

HRI Challenge

The aim of the ICRA08 HRI Challenge was to demonstrate a number of state-of-the-art platforms in HRI, as well as to provide a realistic platform (the ICRA Conference) for evaluating the effectiveness of the interaction. A survey of human participants who interacted with the robots was used in the scoring.

- First place (TIE): KEEPON (NICT, Japan, and CMU, U.S.A.) and HOAP-3 (EPFL, Switzerland)
- Second place: Robot Weight Loss Coach, MIT, and Intuitive Automata, U.S.A.
- Third place: Kaspar, University of Hertfordshire, U.K.
- Fourth place: Robotvie, University of Osaka, Japan.

See the HRI Challenge Web page http://lasa.epfl.ch/icra08/hric.php for pictures of all the robots and teams.

RAS Society Awards Presented at ICRA 2008

The following individuals are the recipients of IEEE Robotics and Automation Society (RAS) Awards.

The ICRA HRI Challenge winning teams. From left: Humans: Eric Sauser (EPFL), Aude Billard (EPFL), Basilio Noris (EPFL), Sylvain Calinon (EPFL), Marino Alge (EPFL), Marek Michalowski (CMU), and Hideki Kozima (NICT). Robots: KEEPON (NICT, Japan, and CMU, USA) and HOAP-3 (EPFL, Switzerland). (Photo courtesy of EPFL.)

RAS 2008 Pioneer Award: Russ Taylor and Ari Requicha (holding certificates).

- Pioneer Award: Russell Taylor, Johns Hopkins University, and Aristides Requicha, University of Southern California
- Distinguished Service Award: Shigeki Sugano, Waseda University
- Early Industry/Government Career Award: Nicola Tomatis and Mike Tao Zhang
- Early Academic Career Award: Mike Montemerlo, Massachusetts Institute of Technology
- Inaba Award for Innovation Leading to Production: Rodney Brooks, Massachusetts Institute of Technology
- George Saridis Leadership Award: Georges Giralt, LAAS (emeritus)
- Chapter of the Year Award: Hong Kong (Dong Sun, Chair)
- Most Active TC: Rehabilitation and Assistive Robotics: Cochairs: Michelle Johnson, Medical College of Wisconsin/Marquette University; Takanori Shibata, AIST; and

Recipients of the IEEE 2008 Technical Field Award In Robotics and Automation. (From left: W.A. Gruver, TRA corecipients Larry Matthies, Eric Baumgartner, and Paul Backes; Awards Cochair David Orin and RAS President Bruno Siciliano.)

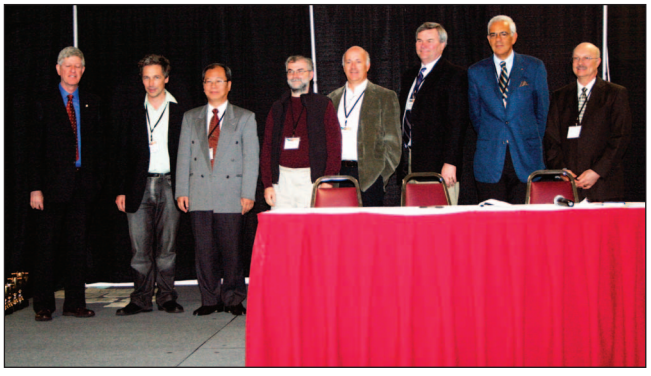

From left: W.A. Gruver; TRA corecipients Larry Matthies, Eric Baumgartner, and Paul Backes; RAS President Bruno Siciliano; and Awards Cochair David Orin.

Micera, Scuola Superiore Sant'Anna, ARTS Lab (Effective from January 2008, Eugenio Guglielmello is also a cochair)

- Most Active Distinguished Lecturer: Nancy Amato, Texas A&M University
- 2007 King-Sun Fu Memorial Best Transactions on Robotics Paper Award: Mitul Saha and Pekka Isto for "Manipulation Planning for Deformable Linear Objects," *IEEE Transactions on Robotics*, vol. 23, no. 6, pp. 1141–1150, Dec. 2007.

Descriptions of the awards, nomination, and evaluation criteria and the nomination forms are available on the RAS Web page.

IEEE TFA and 2008 RAS Fellows

At the 2008 ICRA Awards Ceremony Division X Director William Gruver presented the IEEE Technical Field Award in Robotics to corecipients: Paul G. Backes, Jet Propulsion Laboratory, Eric T. Baumgartner, Ohio Northern University, and Larry H. Matthies, Jet Propulsion Laboratory. The award was presented "for contributions to robotics enabling effective autonomous operations of science investigations under extreme conditions on the planet Mars."

Example of a state-of-the-art autonomous underwater robot. (Courtesy Autonomous Systems Laboratory, University of Hawaii.)

RAS 2008 IEEE Fellows who were present at ICRA were also recognized during the ceremony. The 14 RAS members of the 2008 IEEE Fellows class are Tianyou Chai, Fan-Tien Cheng, Peter Corke, Roy Featherstone, Vincent Hayward, Steven Holland, Zexiang Li, Max Meng, Roland Siegwart, Narahari Yadati, Alexander Zelinsky, Ju-Jang Lee, Dragan Nesic, and Karen Panetta.

New RAS TCS on Marine Robotics and Robot Learning

The RAS Administrative Committee (AdCom) has approved two new TCs. Organizers of the Marine Robotics TC include Gianluca Antonelli (antonelli@unicas.it), Corresponding and Membership Chair, Andrew Bennett, Hayato Kondo, Giacomo Marani, Richard Rikoski, Dan Stilwell, and Junku Yuh (http://webuser.unicas.it/antonelli/MarineRoboticsTC/).

Organizers of the Robot Learning TC (http://learning-robots.de) include Russ Tedrake, Morimoto, Jan Peters, Corresponding Cochair, and Nicholas Roy, Corresponding Cochair.

RAS TCs encourage research in specific areas, particularly those that are new and evolving. Membership is free and open to anyone. Further information about all the RAS TCs can be found on the Technical Activities Board Web page (http://www.ieee-ras.org/technical).

2008 RAS New Initiatives Grant Recipients

The IEEE RAS AdCom has approved the following applications for grants under the 2008 New Initiatives Program.

- Latin American Robotics Council (US$13,000)
- A Repository of Robotics Teaching Materials (Stage II) (US$12,500)
- Advancing Robotic Research and Education through an Open Source High-Fidelity Simulation Framework and Competition (US$15,000)
- The 2008 ICRA Robot Challenge (US$10,000)
- Ph.D. Fellowship for Women in Robotics and Automation (US$12,500).

The RASOR's ICRA 2008 gig featured vocalist Robin Murphy (RAS Parliamentarian), guitarist and vocalist Alessandro De Luca (IEEE T-Robotics EIC), Stefano Stramigioli (IEEE RA-Mag EIC) on drums, and Seth Hutchinson (RAS Conference Editorial Board EIC) on bass.

A call for proposals was issued in January 2008. The 19 proposals received were ranked by an evaluation committee, the RAS Financial Activities Board, and the ExCom and voted on by the AdCom. The Society was able to fund five of the proposals, for a total of US$63,000.

RAS Elections

We urge all RAS graduate student and higher-grade members to vote in the upcoming RAS elections for six new AdCom members. Members with valid e-mail addresses on record with IEEE will receive their electronic ballots by e-mail in a few weeks. Paper ballots will be sent on request. Members without a valid e-mail address or whose e-mails bounce will receive paper ballots, which they can return by fax or post. The paper ballots will include instructions for electronic voting.

Members should have already received your ballots for the IEEE election. Don't forget to return them!

The Lighter Side of Robotics and Automation

With two full days of workshops and tutorials and three days of 12 tracks of technical sessions and plenary speeches, ICRA is a pretty serious affair, but two special events in Pasadena revealed the startling diversity of hidden talents in the RAS community.

The RASOR Makes the Scene ICRA 2008 in Pasadena, California, featured a Student Party (oldies didn't get free drink tickets) with entertainment by the now legendary international rock band, RASOR! See the video at http://www.prisma.unina.it/ftp/TheRASOR_Videos.zip (>500 Mb) or clips on YouTube (http://www.youtube.com/watch?v=xW-8JlzK4yU). The band plans a repeat performance at Kobe, with more musicians including soundman and promoter Ken Goldberg and pianist Aude Billard and perhaps others. The Student Party followed the Gold Reception for graduate students and young professionals.

ICRA Robotics Comics Competition

A baker's dozen (13) of budding cartoonists or teams submitted entries to the First ICRA Comics Contest organized by Aude Billard and Jorge Cham. See the winning cartoon by LAAS-CNRS team:

The RASOR Cartoon—The RASOR—Seth Hutchinson, Robin Murphy, Stefano Stramigioli, Aude Billard, Alessandro De Luca, and Ken Goldberg (Artist: Costanzo Manes).

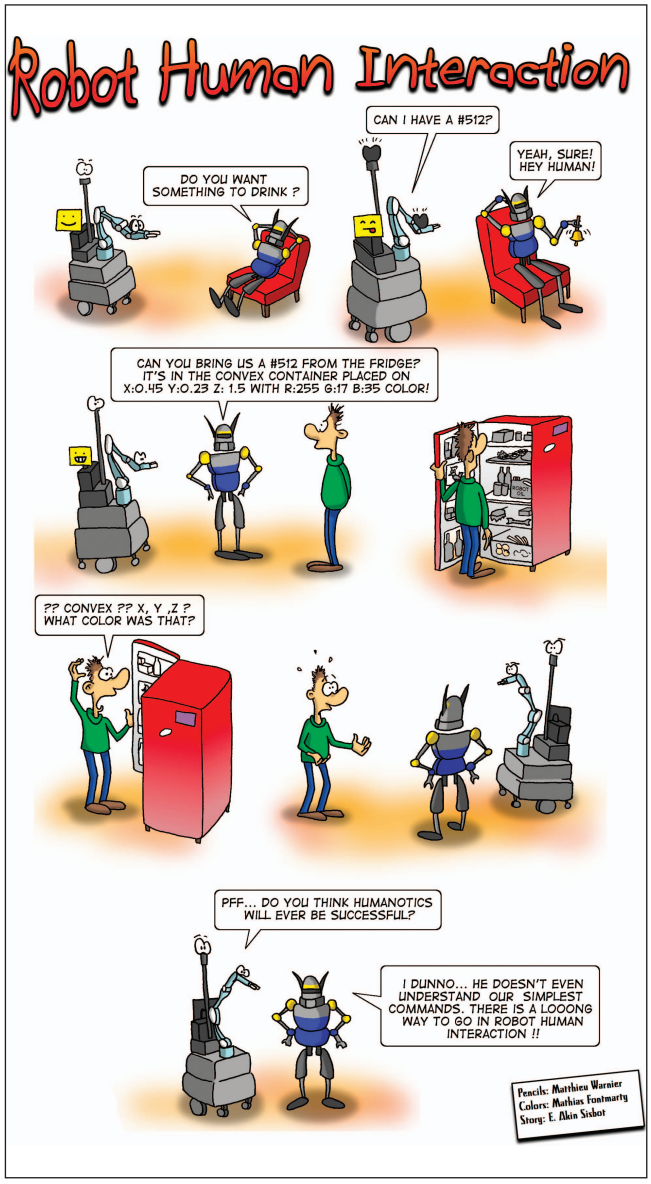

Matthieu Warnier, Mathias Fontmarty, and Akin Sisbot, and the other entries at http://lasa.epfl.ch/icra08/comics.html.

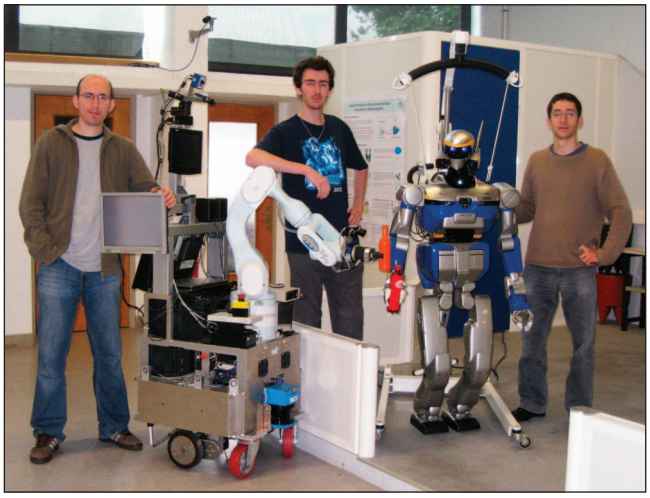

Three members of the winning team in the ICRA Comics Contest, Akin Sisbot, Matthias Warnier, and Matthias Fontmarty with the two robots pictured in the comic. Contrary to the impression given in the comic, the humans are still in control at LAAS.

Rehabilitation and Assistive Robotics

By Chairs Michelle J. Johnson (mjjohnso@mcw.edu), Medical College of Wisconsin; Silvestro Micera (micera@sssup.it), Scuola Superiore Sant'Anna; Takanori Shibata (shibata-takanori@aist.go.jp), AIST, Japan; and Eugenio Guglielmelli (e.guglielmelli@unicampus.it), Università Campus Bio-Medico

The goal of rehabilitation and assistive robotics is to investigate the application of robotics in therapeutic procedures for achieving the best possible motor and/or cognitive functional recovery for persons with impairments due to various diseases (e.g., stroke and other neuromotor disorders, brain and orthopedic traumas, cognitive diseases, etc.).

The goal of assistive robotics, instead, is to develop robotic aids for supporting independent living of persons who have chronic or degenerative limitations in motor and/or cognitive abilities, such as the elderly and persons with severe disabilities. Such robotic devices are typical key components of more general assistive systems, by integrating telematic, mechatronic, and other technological devices (e.g., advanced human–machine interfaces).

The recent advances of medical rehabilitation procedures, methodologies, and tools tend to include more cognitive aspects of motor control, also exploiting the new technologies for brain imaging, which close the loop from brain to action. This gives an important role to robotics, which can be fruitfully employed in the rehabilitation of neuromotor functions and motor capabilities, by providing tools that are flexible and programmable and that allow to set and assess procedures quantitatively. Robotic tools are being effectively applied not only to motor rehabilitation but also to promote the recovery of cognitive deficits and the psychological enrichment of the elderly.

At the same time, the development of assistive technology for the elderly and persons with disabilities, after a period of slow but steady scientific progress, seems to be mature for new research and application breakthroughs by combining human-centered design methodologies with integrated micromechatronic and robotic systems. New important research projects in this field have been recently launched both at academic and industrial level worldwide, e.g., in the United States, Europe, Japan, and Korea.

The growing interest in this area of robotics research worldwide is obvious from the success of focused publications and events, like the special issue on Rehabilitation Robotics of *Autonomous Robots* (2003), *Journal of Neuroengineering* (2006), *IEEE Engineering in Medicine and Biology Society (EMBS) Transactions on Neural Systems and Rehabilitation Engineering* (2007), International Conference on Rehabilitation Robotics (ICORR), held biannually, and the special sessions organized at the latest International Conference on Robotics and Automation (ICRA), International Conference on Intelligent Robots and Systems (IROS), and the International Conference on Advanced Robotics (ICAR).

Interactive robotic pets used in recreation therapy. (Image courtesy Takanori Shibata, AIST, Japan.)

The KineAssist robotic device helps retrain muscles and nerves after a stroke or accident. (Photo courtesy of the Rehabilitation Institute of Chicago.)

Digital Object Identifier 10.1109/MRA.2008.928304

(continued on page 110)

By George A. Bekey

Springer Handbook of Robotics

Bruno Siciliano and Oussama Khatib, Editors, Springer-Verlag 2008. ISBN: 978-3-540-23957-4.

Robotics has come of age. It is now clear that it is not a passing fancy but rather that robots in one form or another are finding their way into more and more aspects of society. Robots are in the factory, in the home, on the battlefield, and many more venues, performing an incredible array of tasks, many of which were inconceivable even 20 years ago. What is perhaps even more remarkable than the enormous range of applications is that the field has grown up with a solid foundation in physics and mathematics. This may be because most robots were born in university laboratories around the world, where thousands of students enabled them to perceive, process information, learn, move, manipulate, and perform a wide range of tasks before they became sufficiently robust and reliable to become commercial products. Now, theory and applications, fundamental work in universities, and technology developed in the industry are mature enough to attempt a consolidated view of the entire field. This handbook accomplishes this task beautifully, both in style and substance.

The handbook is a very large and truly encyclopedic work, covering all aspects of robotics, from fundamental principles to applications. The book's 1,600 pages are subdivided into seven parts: Part A: Robotics Foundations, Part B: Robot Structures, Part C: Sensing and Perception, Part D: Manipulation and Interfaces, Part E: Mobile and Distributed Robotics, Part F: Field and Service Robotics, and Part G: Human-Centered and Life-Like Robotics. Each of the seven parts is subdivided into multiple chapters, all written by experts in their fields throughout the world. This reviewer tried to find aspects of robotics not treated in the book, and he failed: it is indeed a remarkably complete view of the field. The book also has four forewords by leading contributors to robotics, including Hirochika Inoue from Japan, Georges Giralt from France, and Bernard Roth and Rodney Brooks from the United States. They provide a most valuable introduction to the handbook from their perspective and experience, as all of them are among the founders of the field.

One may view the contents in another way. The first two parts provide the mathematical and physical fundamentals of robotics, including not only kinematics and dynamics and an introduction to motion planning and system architectures but also treatments of the physical elements of robots, such as mechanisms, hands, legs, and wheels. The third part deals extensively with sensors. The next two parts concern basic and applied issues in manipulation, grasping, motion planning and control, and distributed systems. Part F deals with what we might call contemporary applications, in space, under water, in agriculture, medicine, rehabilitation, and others. These are the applications that many people view as representing the significant impact of robotics on society. In Part G, these areas are supplemented by problems that still present major research challenges, including humanoid robots, human-robot interaction, neurorobotics, and a discussion of robot ethics.

This amazing book does an incredible job of balancing theory and practice throughout. It should be an immensely valuable reference for students and practitioners of robotics for many years to come.

Digital Object Identifier 10.1109/MRA.2008.928399

TC SPOTLIGHT

(continued from page 16)

The new event promoted by the IEEE Robotics and Automation Society (RAS) jointly with the EMBS, the International Conference on Biomedical Robotics and Biomechatronics (BioRob conference), which took place in Pisa, Italy, 20–22 February 2006, explicitly included a dedicated track on rehabilitation and assistive robotics, which was very successful.

Both the rehabilitation and the assistive robotics fields have already produced several commercial spin-offs, which brought to the market advanced systems that are currently being validated in extensive clinical trials worldwide.

The Rehabilitation and Assistive Robotics Technical Committee (TC) was the recipient of the RAS 2008 Most Active TC award. The committee was established in 2001 as the Rehabilitation Robotics TC. The name was changed this year to reflect the scientific progress and maturity reached by this broad research area. The TC currently has about 450 registered members worldwide and welcomes new members. See the Web site at http://www-arts.sssup.it/IEEE_TC_RehaRob/.

Recent activities of the TC include workshops at ICRA 2007 in Rome, technical sponsorship of the First EURON Summer School on Rehabilitation Robotics, and special issue on Socially Assistive Robotics (*Autonomous Robots*, January 2007), Rehabilitation Robotics (*Journal of Neuroengineering and Rehabilitation*), and *IEEE Transactions on Neural Systems and Rehabilitation Engineering* (September 2006).

Robotic Manipulation Using an Open-Architecture Industrial Arm: A Pedagogical Overview

By Robert J. Wood

Robotics education at the undergraduate level is most effective as a coupling between theoretical concepts and tangible experiments. Making this connection effective requires a pragmatic way of applying the traditional robotic material to exciting laboratory exercises. A course recently offered in Harvard's School of Engineering and Applied Sciences, simply titled "Introduction to Robotics," utilizes an open-architecture robotic arm to give students hands-on experience with topics that they encounter in lecture. None of the experiments conducted in this course are wholly novel; however, the use of an open-architecture hardware or software system enables the instructor to rapidly prototype lab exercises with minimal effort. This column will give an overview of the apparatus and experiments used for this course.

Apparatus Overview

The majority of existing industrial arms are not conducive to education: the user interface (software or teach pendant) is typically oriented to repetition of precise tasks. Although the physical instantiation of the arm is not a primary concern, the software interface to the arm is of quintessential importance. Students should not spend an inordinate amount of time learning a proprietary motion description language specific to any given manufacturer. Instead, we settled on the six degrees of freedom (DoF) open-architecture robot from Quanser. This system consists of a 5 DoF CRS CataLyst-5 from Thermo Electron Corporation mounted to a linear track (for the sixth axis). The existing CRS controller is supplemented with a Quanser control board, allowing the user to switch between the industrial controller and an open-architecture controller in which the user has access to everything from high-level commands to individual joint signals. The open-architecture configuration uses a Matlab or Simulink interface that includes libraries for common functions such as kinematics and control. At the base of the workspace, a peg board was installed, which enabled the lab instructors to interchangeably place objects and obstacles for the latter labs. Additionally, an overhead camera, with its primary axis anti-parallel with the inertial z-axis, is used for vision.

Lab Overview

Prior to each lab, students write Matlab functions to solve tasks as prelab exercises. Each successive lab builds on tools that students developed for the previous exercise while maintaining a close connection to the material presented in class.

Digital Object Identifier 10.1109/MRA.2008.928281

Lab 1: Forward Kinematics

Given the Denavit-Hartenberg convention and the geometry of the arm (taken from data sheets), the students first write Matlab functions for the homogeneous transformations and a script to calculate position and orientation of the tool frame. During lab time, the students input various joint angles into both the arm controller and their script. They are then required to physically measure the location of the tool frame and compare to their predictions while using observations of the arm to debug any discrepancies. It is important that the scripts consider joint limitations, and thus some of the joint angles given to the students are outside the physical limits, so as to test the robustness of their code. Furthermore, the students use this script to evaluate the extent of the workspace by varying the joint angles through the configuration space.

Lab 2: Inverse Kinematics

The prelab requires students to write a function to calculate all solutions to the inverse kinematics when given the position and orientation of the tool frame. Furthermore, their code must check that each solution in the configuration space does not violate joint limits and discard erroneous solutions. During lab time, the students are given various position and orientation values for the tool frame. Using their inverse kinematics function, they first evaluate how many, if any, solutions exist. They must then implement all valid solutions for joint configurations on the arm and physically measure the difference between actual and desired tool frame position and orientation. As with the first lab, they use this comparison to iteratively debug their function.

Lab 3: Velocity Kinematics and Singularities

The third lab involves an exploration of the relationship between velocities in the workspace and velocities in the configuration space. To do this, students first construct the manipulator Jacobian using the forward kinematics module from the first lab. From their numerical Jacobian matrices, they predict the singularities of the arm. In lab, the students run the arm close to its singular configurations by choosing trajectories in the workspace appropriately. Simultaneously, they observe the joint velocities and watch where a finite workspace velocity corresponds to large joint velocities (limited by motor torque and current saturation). The purpose of observing singular configurations becomes apparent in the next lab where students must incorporate singularities as obstacles in the configuration space.

Lab 4: Path Planning and Obstacle Avoidance

The students write algorithms to generate safe way points in the configuration space when given physical descriptions of

This report on robotic teaching in academia addresses the important issues related to undergraduate courses. In this case, robotics is a very good tool to ground the theoretical concepts that students may be facing for the first time, to their physical and practical significance. As the author points out, there is no need of complete novelty in these courses, rather a clear pedagogical structure that can take students from theory to practice and vice versa, in preparation for the more challenging courses to come.

—Paolo Fiorini, RAS Education Committee Cochair

obstacles and a goal in the workspace. Students are told about the geometry of the peg board and that it would contain cylindrical obstacles within the workspace boundary. For path planning and obstacle avoidance, they could use any viable method; however, lectures covered the gradient descent and probabilistic road map methods. This is the first competitive lab; students were separated in teams and competed against each other based on speed (i.e., minimum number of way points) and number of obstacles hit (including singularities).

Teams were then told about the position and radius of obstacles in the workspace along with the start and goal positions. Once the teams generated safe way points, these were loaded into the arm controller, which interpolated the points and ran the trajectory while scoring each team.

Lab 5: Vision and Object Manipulation

The final lab entailed aspects of each of the preceding labs. In addition, students were given the position and orientation of an overhead video camera (with respect to the inertial frame). In class, vision algorithms were presented to segment an image and return the coordinates of objects (in the image plane). The students were told that the peg board would contain two objects: the smaller of the two is the object that is to be manipulated, and the larger object is the goal. Using the overhead camera, they were first required to determine the centroid of each object (by segmentation and a simple camera calibration) and their relative sizes. For this lab, the end effector from the previous lab was replaced with a simple bellows-actuated gripper. Students would generate way points in the configuration space that would bring the gripper over the smaller object while requiring an orientation of the gripper that will facilitate grasping. A close command is given to the gripper to pickup the object. The second set of way points should lift the object and move it to a safe position above the second object (goal) and release. In this lab, the goal object was a basket so that a successful trial is one that puts the smaller object in the basket.

Potential Additions

Once the open-architecture infrastructure is in place, multiple additional exercises could be readily developed into labs. For example, labs on individual joint control, visual servoing, force feedback for manipulation, and force versus position control would all be natural progressions of the previous labs.

Robert J. Wood is an assistant professor in Harvard School of Engineering and Applied Sciences. He completed his M.S. degree in 2001 and Ph.D. degree in 2004 in the Department of Electrical Engineering and Computer Sciences at the University of California, Berkeley. At Harvard, he founded the Harvard Microrobotics Lab and has demonstrated the world's first robotic insect capable of generating sufficient thrust to take off. His current research interests involve the creation of biologically inspired aerial and ambulatory microrobots, minimal control of underactuated, computationally limited, nonlinear dynamical systems, and decentralized control of multiagent systems. He is the winner of 2007 DARPA Young Faculty award, 2008 NSF CAREER award, 2008 ONR Young Investigator Program award, and many best paper and video awards.

Address for Correspondence: Robert J. Wood, School of Engineering and Applied Sciences, Harvard University, 33 Oxford St., Cambridge, MA 02138, USA. E-mail: rjwood@seas.harvard.edu.

Soft Robotics

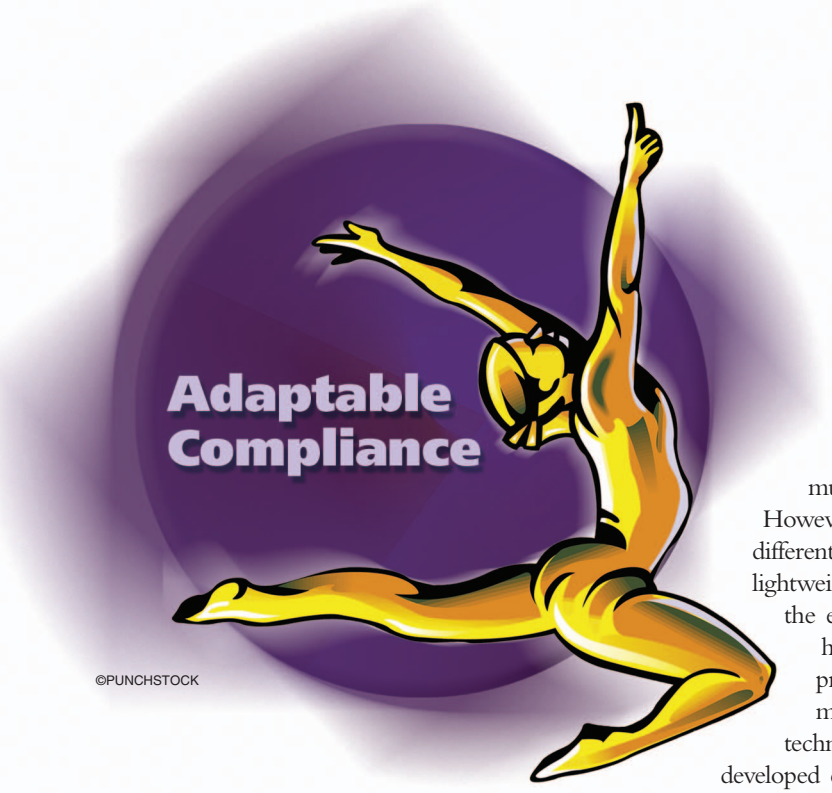

From Torque Feedback-Controlled Lightweight Robots to Intrinsically Compliant Systems

BY ALIN ALBU-SCHÄFFER, OLIVER EIBERGER, MARKUS GREBENSTEIN, SAMI HADDADIN, CHRISTIAN OTT, THOMAS WIMBÖCK, SEBASTIAN WOLF, AND GERD HIRZINGER

Digital Object Identifier 10.1109/MRA.2008.927979

After decades of intensive research, it seems that we are getting closer to the time when robots will finally leave the cages of industrial robotic workcells and start working in the vicinity of and together with humans. This opinion is not only shared by many robotics researchers but also by the leading automotive and IT companies and, of course, by some clear-sighted industrial robot manufacturers. Several technologies required for this new kind of robots reached the necessary level of performance, e.g., computing power, communication technologies, sensors, and electronics integration. However, it is clear that these human-friendly robots will look very different than today's industrial robots. Rich sensory information, lightweight design, and soft-robotic features are required to reach the expected performance and safety during interaction with humans or in unknown environments. In this article, we will present and compare two approaches for reaching the aforementioned soft-robotic features. The first one is the mature technology of torque-controlled lightweight robots (LWRs) developed during the past decade at the German Aerospace Center (DLR) (arms, hands, a humanoid upper body, and a crawler). Several products resulted from this research and are currently being commercialized through cooperations with different industrial partners (DLR-KUKA LWR, DLR-HIT-Schunk hand, DLR-Brainlab medical robot). The second technology, still a topic of worldwide ongoing research, is variable compliance actuation that implements the soft-robotic features mainly in hardware.

We start by reviewing the main design and control ideas of actively controlled compliant systems using the DLR arms, hands, and the humanoid manipulator Justin as examples. We take these robots as a performance reference, which we are currently trying to outperform with new variable stiffness actuators. This leads us to the motivation of the variable stiffness actuator design. We present the main design ideas and our first results with the new actuator prototypes. Some experimental examples providing first validation of the performance and safety gain of this design approach are presented finally.

Mechatronic Design of LWR with Joint Torque Sensing

In this section, a mechatronic design approach for obtaining the robots with the desired lightweight and performance properties is briefly described. The following aspects are of particular relevance.

- *Lightweight structures*: lightweight metals or composite materials are used for the robot links.
- *High-energy motors*: In contrast to industrial robots, motors with high torque at moderate speed, low energy loss, and fast dynamic response are of interest rather than high-velocity motors. For this purpose, special motors, namely, the DLR Robodrive, have been designed.
- *Gearing with high load to weight ratio*: Harmonic drive gears are used for the DLR robots.

1070-9932/08/$25.00©2008 IEEE

- *Integration of electronics into the joint, leading to a modular design*: This allows the design of robots of increasing kinematic complexity based on integrated joints as in the case of the DLR humanoid Justin. Moreover, one obtains a self-contained system, which is well suited for autonomous, mobile applications.
- *Full-state measurement in the joints*: As will be outlined in the "Compliance Control for Lightweight Arms" section, our robots use torque sensing in addition to position sensing to implement a compliant behavior and a smooth, vibration-free motion. The full-state measurement in all joints is performed at 3-kHz cycle using strain-gauge-based torque-sensors, motor position sensing based on magnetoresistive encoders, and link side position sensors based on potentiometers (used only as additional sensors for safety considerations).
- *Sensor redundancy for safety*: Positions, forces, and torques are redundantly measured.

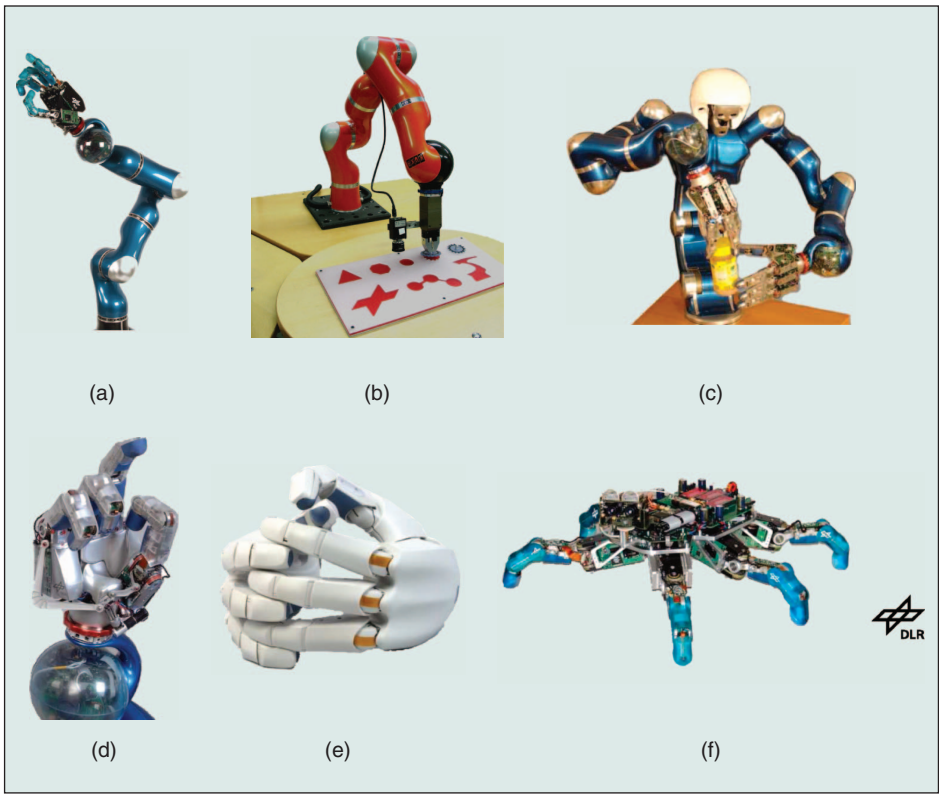

Figure 1. *Overview of the DLR Robots. (a) The DLR-LWR-III equipped with the DLR-Hand-II. (b) The DLR-KUKA-LWR-III that is based on the DLR-LWR-III. (c) The DLR humanoid manipulator Justin. (d) The DLR-Hand-II-b, a redesign of the DLR-Hand-II. (e) The DLR-HIT hand, a commercialized version of the DLR-Hand-II. (f) The DLR-Crawler, a walking robot based on the fingers of the DLR-Hand-II.*

These basic design ideas are used for the joints in the arms, hands, and torso of the upper body system Justin (Figure 1). Moreover, because the joints are self-contained, it is straightforward to combine these modules to obtain different kinematic configurations. For example, the fingers have been used to build up a crawler prototype. Figure 2 shows the exploded view of one LWR-III (DLR-LWR-III) joint.

Compliance Control for Lightweight Arms

In the next two sections, the framework used to implement active compliance control based on joint torque sensing is summarized. The lightweight design is obtained by using relatively high gear reduction ratios (typically 1:100 or 1:160), leading to joints that are hardly backdrivable and have already moderate intrinsic compliance. Therefore, we model the robot as a flexible joint system. Thus, measuring the torque after the gears is essential for implementing high-performance soft-robotic features. When implementing compliant control laws, the torque signal is used both for reducing the effects of joint friction and for damping the vibrations related to the joint compliance. Motor position feedback is used to impose the desired compliant behavior. The control framework is constructed from a passivity control perspective by giving a simple and intuitive physical interpretation in terms of energy shaping to the feedback of the different state vector components.

- A physical interpretation of the joint torque feedback loop is given as the shaping of the motor inertia.
- The feedback of the motor position can be regarded as shaping of the potential energy.

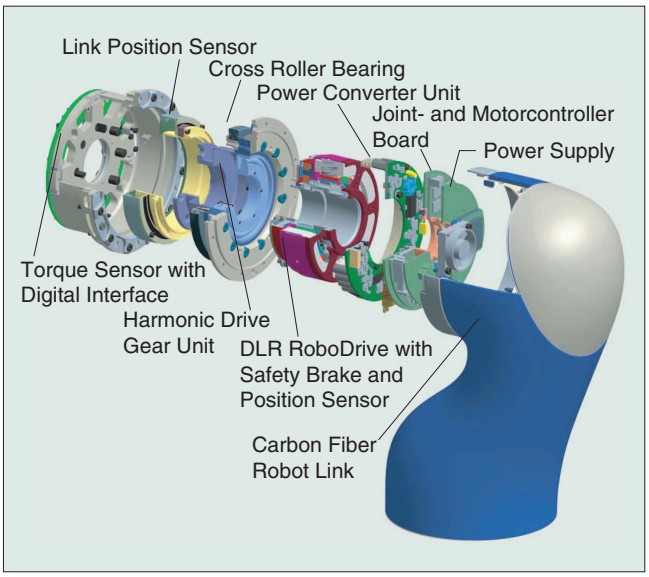

Figure 2. *The mechatronic joint design of the DLR-LWR-III, including actuation, electronics, and sensing.*

Joint Torque Control: Shaping the Actuator Kinetic Energy

To simplify the analysis and to be able to generalize the joint level approach also to Cartesian coordinates, the idea of interpreting the joint torque feedback as the shaping of the motor inertia plays a central role [1], [2]. It enables one to directly use the torque feedback within the passivity framework and conceptually divides the controller design into two steps. One is related to the torque feedback and the other to the position feedback (Figure 3). As sketched in the figure and presented in detail in [1] and [2], the torque control feedback reduces the motor inertia to a value $\boldsymbol{B}_\theta$, lower than the real value $\boldsymbol{B}$. (Although friction is not depicted in Figure 3, note that the frictional effect will be reduced by the same factor $\boldsymbol{B}_\theta^{-1}\boldsymbol{B}$.)

Motor Position-Based Feedback: Shaping the Potential Energy

Using motor position $\boldsymbol{\theta}$ for control, and not the link position $\boldsymbol{q}$, is essential for the passivity properties of the controller. However, the desired position and stiffness are usually formulated in terms of the link position. For the impedance controllers of the DLR LWRs, the position feedback has the form

$$\boldsymbol{u} = -\frac{\partial V_P(\bar{\boldsymbol{q}}(\boldsymbol{\theta}))}{\partial \boldsymbol{\theta}} - \boldsymbol{D}_\theta \dot{\boldsymbol{\theta}} + \boldsymbol{g}(\bar{\boldsymbol{q}}(\boldsymbol{\theta})), \tag{1}$$

with $\boldsymbol{u}$ being the input to the torque controller, V_P a positive definite potential function, and $\boldsymbol{D}_\theta$ a positive definite damping matrix chosen for a well-damped transient behavior [3]. This is the classical structure of a compliance controller for rigid robots, except for the fact that, instead of the link position $\boldsymbol{q}$, a position signal $\bar{\boldsymbol{q}}(\boldsymbol{\theta})$ is used, which is statically equivalent to $\boldsymbol{q}$, i.e., $\bar{\boldsymbol{q}}(\boldsymbol{\theta}) = \boldsymbol{q}$ if $\dot{\boldsymbol{q}} = \dot{\boldsymbol{\theta}} = \boldsymbol{0}$ and can be computed numerically [1], [2]. (In practice, we often use the trivial approximation $\bar{\boldsymbol{q}}(\boldsymbol{\theta}) = \boldsymbol{\theta}$ for applications in which high position accuracy is not required.)

Because now the position feedback is again only a function of $\boldsymbol{\theta}$, the passivity of the controlled robot is given with respect to the input-output pair $(\boldsymbol{\tau}_{\text{ext}}, \dot{\boldsymbol{q}})$ (Figure 3).

To obtain a joint level impedance controller, one can simply use $V_P(\bar{\boldsymbol{q}}) = \frac{1}{2}(\boldsymbol{q}_d - \bar{\boldsymbol{q}})^T K_J (\boldsymbol{q}_d - \bar{\boldsymbol{q}})$, whereas for Cartesian impedance control, V_P is defined as a function of the Cartesian coordinates $\boldsymbol{x}(\bar{\boldsymbol{q}})$, as detailed in the following section. The external torque $\boldsymbol{\tau}_{\text{ext}}$ is then replaced by the external force $\boldsymbol{F}_{\text{ext}}$. (The relation between the external tip force $\boldsymbol{F}_{\text{ext}}$ and the external joint torque $\boldsymbol{\tau}_{\text{ext}}$ is $\boldsymbol{\tau}_{\text{ext}} = \boldsymbol{J}(\boldsymbol{q})^T \boldsymbol{F}_{\text{ext}}$.) A Lyapunov function for the system is obtained by summing the kinetic and the gravity-potential energy of the rigid part of the robot dynamics with the kinetic energy of the scaled motor inertia and the potential energy of the controller [1], [2].

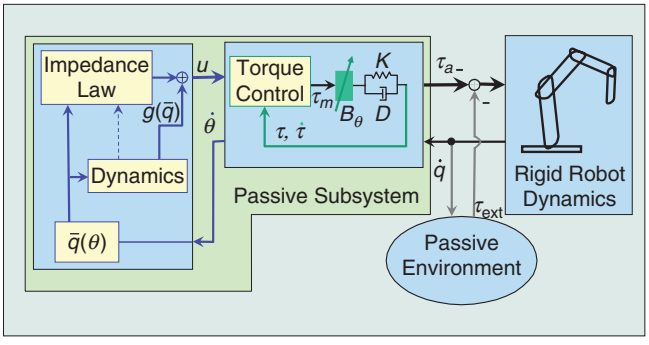

Figure 3. *Representation of the compliance-controlled robot as a connection of passive blocks. $\boldsymbol{\theta}$ is the motor position, and $\boldsymbol{q}$ the link position. B, K, and D are the motor inertia, joint stiffness, and damping matrices, respectively. τ is the elastic joint torque, τ_a the total (elastic and damping) joint torque, τ_{ext} the external torque, and g the gravity torque.*

Impedance Control for Complex Kinematic Chains

In this section, we show how to apply the impedance control concept from the previous section to kinematically more complex robot systems, like artificial hands and anthropomorphic two-handed manipulator systems.

The design of appropriate potential functions $V_P(\bar{\boldsymbol{q}})$ is discussed in this section. Furthermore, we will assume the potential function V_s of a virtual spatial spring, e.g., the ones designed in [4]–[6], as a basic building block. This potential function $V_s(\boldsymbol{H}_1, \boldsymbol{H}_2, \mathcal{K})$ depends on two frames $\boldsymbol{H}_1 \in SE(3)$ and $\boldsymbol{H}_2 \in SE(3)$, between which the spring is acting, and also on some configuration-independent internal parameters $\mathcal{K}$, like the stiffness values or the rest length.

Artificial Hands

Similar to the DLR lightweight arm, the DLR-Hand-II is equipped with joint torque sensors in addition to joint position measurements. Therefore, it is possible to apply the impedance control aspects as presented in the previous section to our anthropomorphic robot hand. The feedback of the torque sensors is used to increase the backdrivability, respectively the sensitivity, of the joints. Because of the small link masses and the high mechanical joint stiffness, vibration damping is not an issue here. Therefore, the approximation $\boldsymbol{q} = \boldsymbol{\theta} = \bar{\boldsymbol{q}}$ can be made. While joint and Cartesian impedance control are used for power grasp and independent fingertip motion, respectively, the most interesting case from a control point of view is the fine manipulation of a grasped object as all degrees of freedom (DoF) of the hand can contribute to its motion. In this case, the combined system containing arm, hand, and object represents a parallel robot (Figure 4). The task coordinates consist of two contributions. On the one hand, the Cartesian coordinates of the grasped object and, on the other hand, the coordinates that are related to internal forces.

In [7], we introduced a passivity-based object-level controller for a multifingered hand based on a virtual object similar to [8]. In contrast to the intrinsically passive controller (IPC) [8], the object frame is defined uniquely by the $i = 1 \ldots N$ Cartesian fingertip positions $\boldsymbol{p}_i(\bar{\boldsymbol{q}})$ by an appropriate kinematic relationship. The definition is such that it enables the spanning of the null space of the grasp matrix by internal forces generated by virtual elastic elements connecting the virtual object frame with the fingertips (Figure 4).

The definition of a potential function $V_P(\bar{\boldsymbol{q}})$ to derive at an object-level controller is then described by the superposition of two potentials: the potential of a spatial spring $V_s(\boldsymbol{H}_{ho}(\bar{\boldsymbol{q}}),$

$\boldsymbol{H}_{ho,d}, \mathcal{K}_{ho}$) between the virtual object frame $\boldsymbol{H}_{ho}(\bar{\boldsymbol{q}})$ and a virtual equilibrium frame $\boldsymbol{H}_{ho,d}$ and a potential $V_{hc}(\bar{\boldsymbol{q}}, \mathcal{K}_{hc})$ describing the ith spring connecting the virtual object with the ith frame of the fingertips $\boldsymbol{H}_{f,i}(\bar{\boldsymbol{q}})$ for $i = 1 \ldots N$ that are used to generate internal forces, i.e.,

$$V_P(\bar{\boldsymbol{q}}) = V_s(\boldsymbol{H}_{ho}(\bar{\boldsymbol{q}}), \boldsymbol{H}_{eq}, \mathcal{K}_{ho}) + V_{hc}(\bar{\boldsymbol{q}}, \mathcal{K}_{hc}). \tag{2}$$

The expressions $\mathcal{K}_{ho}$ and $\mathcal{K}_{hc}$ contain the stiffness matrix of the spatial spring and the coupling spring parameters, respectively. The potential for the coupling springs is different from the potentials for spatial springs and is chosen to be spherical for each fingertip i [7].

$$V_{hc}(\bar{\boldsymbol{q}}, \mathcal{K}_{hc}) = \frac{1}{2}\sum_{i=1}^{N} \mathcal{K}_{hc,i}[\|\Delta \boldsymbol{p}_i(\bar{\boldsymbol{q}})\| - \boldsymbol{l}_{i,d}]^2, \tag{3}$$

with $\Delta \boldsymbol{p}_i(\bar{\boldsymbol{q}}) = \boldsymbol{p}_i(\bar{\boldsymbol{q}}) - \boldsymbol{p}_{ho}(\bar{\boldsymbol{q}})$ being the distance from the position of the fingertip frame i to the virtual object frame position $\boldsymbol{p}_{ho}$, $l_{I,d}$ the desired rest length, and $K_{hc,i} > 0$ the corresponding coupling stiffness.

Employing Impedance Control for Two-Handed Manipulation

A natural extension of the impedance control approaches for the arms and hands allows one to formulate intuitive compliance behaviors also for more complex anthropomorphic manipulators like the humanoid manipulator Justin [Figure 1(c)]. This system was built at DLR as a test bed for studying two-handed manipulation tasks. It consists of two four-fingered artificial hands, two lightweight arms, and a sensor head mounted on a movable torso including the neck. Overall, Justin has 43 DoF.

Let us first consider the problem of controlling two arms. The end-effector frames of the right and left arm will be denoted as $\boldsymbol{H}_r(\bar{\boldsymbol{q}})$ and $\boldsymbol{H}_l(\bar{\boldsymbol{q}})$, respectively. Similar to multifingered hands, the compliance control of two arms has to handle the interaction forces between the two arms as well as the forces that the two arms exert cooperatively on the environment. The implementation, however, is even simpler in this case and can be done by combining two spatial springs. One spatial spring defines the relative compliance between the arms and can be described in a straightforward way by the potential function $V_s(\boldsymbol{H}_r(\bar{\boldsymbol{q}}), \boldsymbol{H}_l(\bar{\boldsymbol{q}}), \mathcal{K}_c)$. For implementing the cooperative action of the two arms, it is useful to rely on a virtual object frame $\boldsymbol{H}_o(\boldsymbol{H}_r(\bar{\boldsymbol{q}}), \boldsymbol{H}_l(\bar{\boldsymbol{q}}))$ depending on the two end-effector frames of the right and left arm. This object frame describes a relevant pose in between the arms (usually just the mean between the pose of the right and left arm) and thus represents the pose of a grasped object. This virtual object is then connected via a spatial spring $\mathcal{K}_o$ to a virtual equilibrium pose $\boldsymbol{H}_{o,d}$. In combination with the coupling stiffness, one can thus intuitively define an impedance behavior that is useful for grasping large objects with two arms. The resulting potential function is given by

$$\begin{aligned} V_P(\bar{\boldsymbol{q}}) = {} & V_s(\boldsymbol{H}_o(\boldsymbol{H}_r(\bar{\boldsymbol{q}}), \boldsymbol{H}_l(\bar{\boldsymbol{q}})), \boldsymbol{H}_{o,d}, \mathcal{K}_o) \\ & + V_s(\boldsymbol{H}_r(\bar{\boldsymbol{q}}), \boldsymbol{H}_l(\bar{\boldsymbol{q}}), \mathcal{K}_c). \end{aligned} \tag{4}$$

In case of a two-handed system, such a compliance behavior can easily be combined with the object-level compliance potentials designed for artificial hands. Therefore, the virtual viscoelastic springs are now attached to the virtual object frames $\boldsymbol{H}_{r,o}(\bar{\boldsymbol{q}})$ and $\boldsymbol{H}_{l,o}(\bar{\boldsymbol{q}})$ of the hands instead of attaching them directly to the end effectors of the arms (Figure 5). In combination with the interconnection potentials $V_{hcr}(\bar{\boldsymbol{q}}, \mathcal{K}_{hcr})$ and $V_{hcl}(\bar{\boldsymbol{q}}, \mathcal{K}_{hcl})$ for the right and left hand, the complete potential function is now given by

$$\begin{aligned} V_P(\bar{\boldsymbol{q}}) = {} & V_s(\boldsymbol{H}_o(\boldsymbol{H}_{r,o}(\bar{\boldsymbol{q}}), \boldsymbol{H}_{l,o}(\bar{\boldsymbol{q}})), \boldsymbol{H}_{o,d}, \mathcal{K}_o) \\ & + V_s(\boldsymbol{H}_{r,o}(\bar{\boldsymbol{q}}), \boldsymbol{H}_{l,o}(\bar{\boldsymbol{q}}), \mathcal{K}_c) \\ & + V_{hcr}(\bar{\boldsymbol{q}}, \mathcal{K}_{hcr}) + V_{hcl}(\bar{\boldsymbol{q}}, \mathcal{K}_{hcl}). \end{aligned} \tag{5}$$

Note that all spatial springs generate joint torques for the arms, hands, and torso by computing the total derivative of the potential function with respect to the generalized coordinates of the complete mechanism [c.f. (1)]. The presented control approach results in a passive closed-loop system by design, and it is therefore related to other intuitive passivity-based control approaches like the IPC

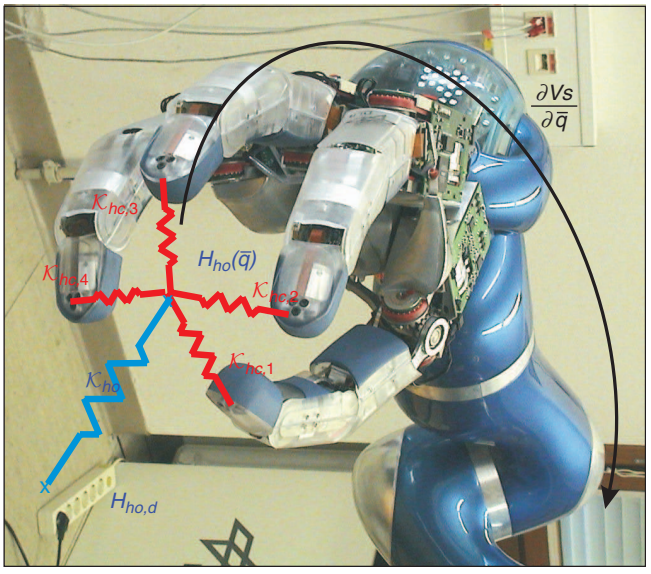

Figure 4. *DLR-Hand-II superimposed by the virtual springs defined by the potential functions in (2) and the virtual object.*

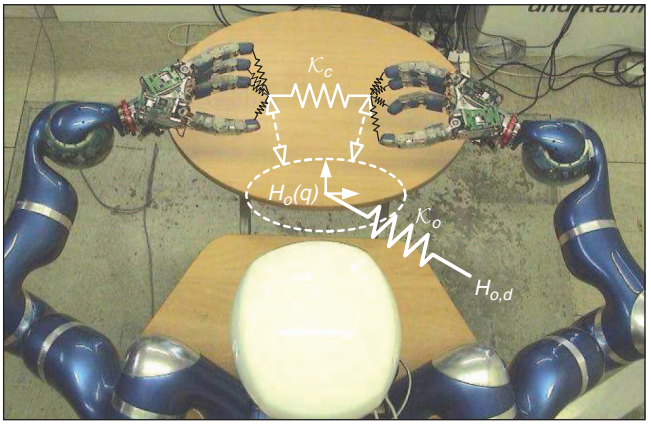

Figure 5. *Two-hand impedance behavior by combining the object-level impedances of the hands and the arms.*

[8]. Moreover, the chosen set of virtual spatial springs allows for a conceptually simple physical interpretation and consequently for an intuitive parametrization in any higher-level planning stage.

Adjusting the Mechanical Compliance: Motivation of the Variable Stiffness Actuator Design

From Actively Controlled to Passive Compliance

The paradigm of torque-controlled LWRs was presented in some detail up to now. Various robot examples and the underlying control concepts were introduced. On the basis of the experience gained with this successful approach, we were also trying to identify its limitations and recognize new directions of research for further increasing the performance and safety of robots.

The limitations of the achievable compliance by active control especially becomes an issue when considering the protection of the robot joint from external overload [9]–[11]. (This is due to the limited sensor precision, model accuracy, and sampling time as well as the motor saturation.) This threat can be diminished by deliberately introducing mechanical compliance into the joint. Furthermore, future robotic systems are supposed to execute tasks with similar speed and dexterity to humans. Extreme examples show that humans are capable of generating enormous joint speeds such as shoulder rotation of 6,900°–9,800°/s during a baseball pitch of a professional player [12]. This speed range is currently not realizable by robots if the torque range and the weight of the joint should also be compatible with human values. Therefore, new actuation concepts are sought for so as to approach such requirements. The concept of variable stiffness actuation (VSA), or its generalization of variable impedance actuation (VIA), seems to be a promising solution in this context, and its design and control was addressed in numerous publications [9], [13]–[16].

An elastic element in the joint serves as an energy storage mechanism, possibly decreasing the energy consumption of the entire system during the task execution, e.g., when playing drums or during running. Furthermore, the stored energy can be used to considerably increase the link speed as exemplified in the "Throwing" section. In contrast to the active compliance case, the robot remains compliant even in the case of deactivation or malfunction of the joint, thus potentially increasing the safety of humans interacting with the robot and protecting the robot joint from external impacts.

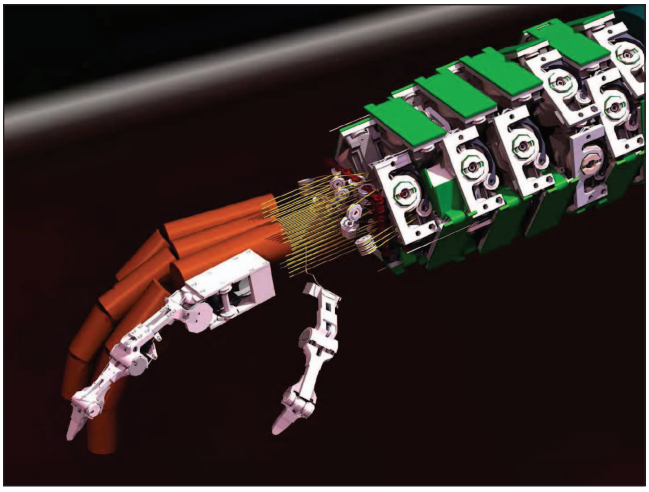

Figure 6. *The integrated DLR hand-arm system.*

Our goal is, based on our experience with torque-controlled LWRs, to built up a fully integrated VSA hand-arm system (Figure 6) for a close, safe, and performant interaction with humans while fulfilling the aforementioned requirements as close as possible.

Naturally, such a fundamental paradigm shift comes at a certain cost. The increased number of actuators and the small intrinsic damping are certainly some of the major challenges in controlling a variable compliance joint. (Introducing mechanical damping into the system would increase the open-loop performance at the cost of higher complexity, weight, and energy losses.) The expected reduction in absolute position accuracy because of the elasticity needs to be compensated for high precision tasks by external sensing, e.g., vision. Furthermore, a lower mechanical bandwidth will result from the generally lower joint stiffness. Regarding the realizable compliance, the first prototypes are expected to implement a diagonal joint stiffness matrix only. This is posing some limitations on the structure of the achievable Cartesian compliance [17]. However, if necessary, the couplings can still be obtained by active control as described in the "Compliance Control for Lightweight Arms" and "Impedance Control for Complex Kinematic Chains" sections.

To exemplify some possible advantages of the VSA design, a preliminary discussion of the influence of joint compliance on human and robot safety is presented before introducing the hardware design in the "New Hardware Design Concepts" section.

Protecting the Robot Joint and the Human by Variable Joint Stiffness

Rigid impacts at high speeds pose an enormous threat to the robot joint [11]. The exceedance of the maximum nominal joint torques is already shown at less than half of the maximum speed of the DLR-LWR-III. This problem necessitates fast collision detection and reaction schemes to prevent damage to the manipulator. (Results from [27] indicate that this is only possible up to a certain impact velocity that is far below the maximum velocity of the manipulator. Especially, the joint-torque sensor and the gears can be severely damaged.) In contrast, the VSA actuators limit in an intrinsic way the impact joint torques by elastically decoupling the link from gearbox and motor for the duration of the impact. To visualize this effect, a one-dimensional translational example (Figure 7) was simulated. In Figure 8, the joint force F_{Spring} during an impact with a human head at 2 m/s for a variable stiffness (VS) joint is depicted. One can see that it decreases dramatically for a joint stiffness reduced by one or two orders of magnitude compared with the DLR-LWR-III, thus substantially reducing the load of the joint. First experimental results confirming the aforementioned statements are shown in the "Experimental Validation of Joint Overload Protection" section.

The possible injury of the human during such rigid impacts is discussed in detail in [11] and [18]. It is shown there that the impact forces (which are mainly related to the impact velocity), and thus the potential injury of a human, do not depend on the joint stiffness already for link inertias and joint stiffness similar to the ones of the DLR-LWR-III. In Figure 8, the head injury criterion (HIC) and the impact forces F_{ext} are depicted, showing that even with reduced joint stiffness, they basically stay the same. This can be explained by the fact that rigid impacts are practically over before the joint force starts rising. In other words, it is only the link inertia involved in such hard and rigid impacts.

A case for which compliance of the robot does reduce the injury risk for humans is given by impacts with sharp tools at moderate velocity. This is exemplified by the experiment from Figure 9, in which the DLR-LWR holding a knife moves along a desired trajectory in position or joint impedance-controlled mode, penetrating a silicone block. Figure 10 shows that with very low joint stiffness, the force and penetration depth increase much slower. For this particular trajectory, one presumably could prevent damaging the human skin. (Already contact forces of <80 N are enough to penetrate the human skin and cause further injury with a knives in case of stabbing [18]. However, with appropriate collision detection strategies, we confirmed in pig experiments that the DLR-LWR can avoid injuries with such sharp tools as knives up to certain velocity [19]. The additional compliance of the actuator will increase the time available to react and thus enables higher maximal velocities.)

Apart from these benefits, the problem of impacting in a pretensioned state or at very high joint velocities caused by striking out is of major focus for future research. This problem is especially important in the context discussed in the "Throwing" section, which shows a vast performance increase concerning link velocity by using the stored potential energy of the joint spring to further accelerate the link inertia.

These two examples illustrate the benefit of VSA design from the robot safety and performance point of view, and the next section will introduce the DLR-VSA design and present some experimental evidence of the performance increase and robot protection. Increasing human safety by VIA design is also a major issue, which will constitute the topic of a separate publication.

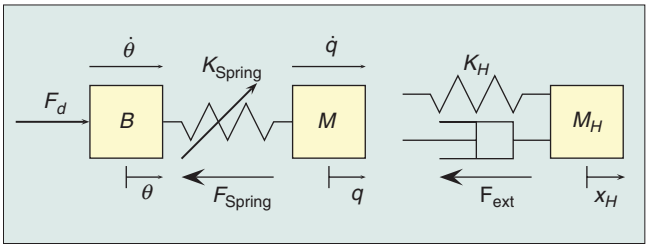

Figure 7. *1-DoF model of the impact between a VS robot and a human. The robot is modeled as a mass-spring-mass system, representing the motor mass, joint stiffness, and link mass. The human model is a Hunt-Crossley model harmonized with experimental crash test dummy data [11]. B, M were selected to be the reflected inertias in case of a typical stretched out collision configuration with the DLR-LWR-III, and K_{Spring} varied according to Figure 8.*

We are getting closer to the time when robots will finally leave the cages of industrial robotic workcells.

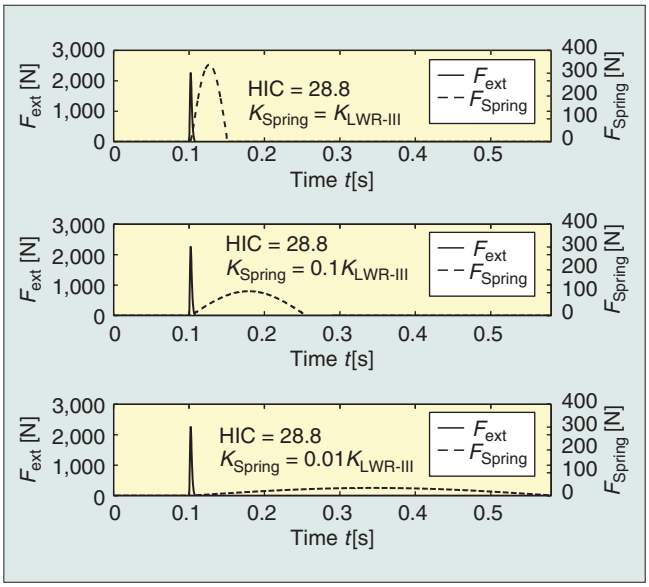

Figure 8. *Effect of joint stiffness reduction on impact force, HIC, and spring force during an impact with the human head at 2 m/s impact velocity. The spring force decreases in magnitude and increases in duration when lowering the spring stiffness. The joint stiffness K_{Spring} was chosen to be $K_{LWR-III}$, 0.1 $K_{LWR-III}$, and 0.01 $K_{LWR-III}$, i.e., 100%, 10%, and 1% of the reflected DLR-LWR-III joint stiffness.*

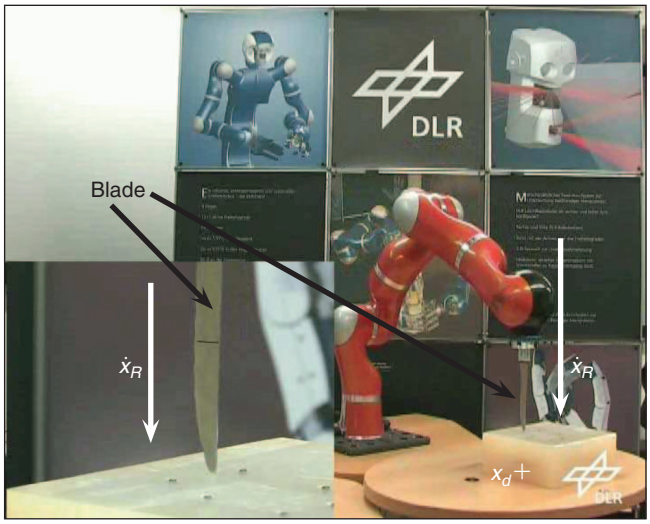

Figure 9. *The DLR-LWR-III equipped with a knife moves along a desired trajectory. The penetrated material is a silicone block. This experiment shows the benefit of intrinsic and controlled joint elasticity during impacts with sharp tools. The goal position x_d was approximately 7 cm inside the silicone block.*

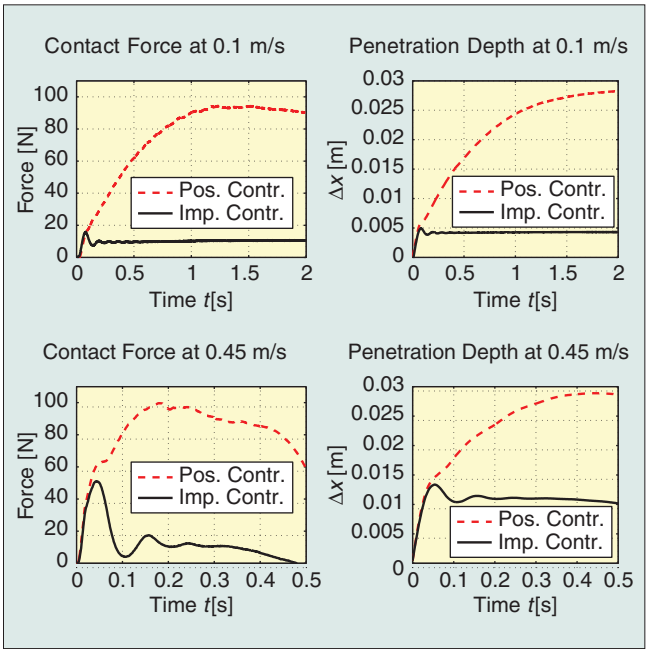

Figure 10. *Contact force and penetration depth for two different Cartesian velocities of 0.1 m/s and 0.45 m/s. Clearly, the benefit of the reduction of joint stiffness is apparent. The force level can be decreased even below levels that would potentially harm a human, whereas in position control, the force significantly exceeds this threshold. The goal position x_d was approximately 7 cm inside the silicone block.*

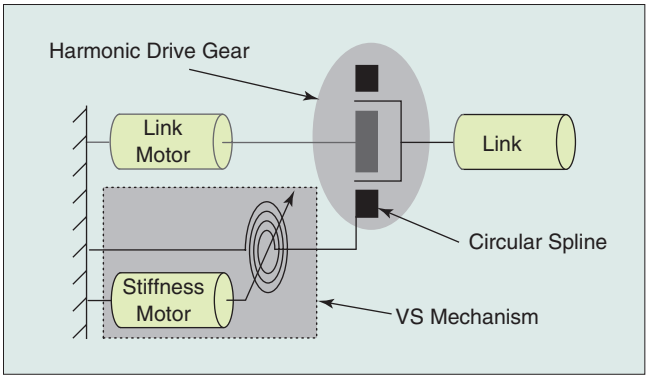

Figure 11. *Principle of joint mechanics. The circular spline of the harmonic drive gear is supported by the new mechanism.*

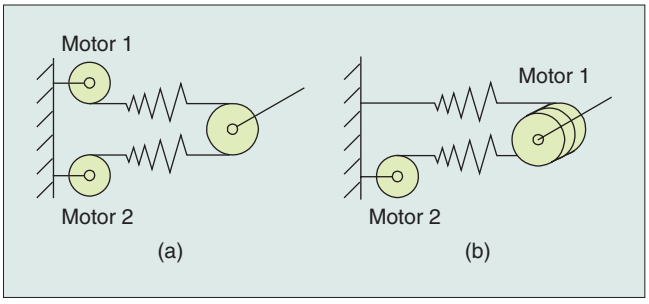

Figure 12. *VSA with nonlinear progressive springs in (a) antagonistic and (b) quasiantagonistic realization. In the later case, Motor 1 moves the joint, whereas Motor 2 is adjusting the stiffness.*

New Hardware Design Concepts

The simplest intrinsically compliant joint realization has a fixed spring behavior, usually with a constant or progressive stiffness characteristic. This results in a significant loss of link motion bandwidth and accuracy. To reduce this effect, the stiffness of the joint has to be adaptable to the desired task, requiring a second actuator. Several design approaches realizing robotic joints with variable mechanical stiffness are described in the literature [9], [13]–[16].

The biologically motivated concept of antagonistic actuation can already be found in some robotic systems [14], [20], [21]. In these realizations, two opposing actuators of similar size, each in combination with a series elastic element, were used. By running together in the same direction, the position is altered, and by moving in opposing direction, the link stiffness is adjusted [Figure 12(a)]. Unless nonbackdrivable gears are used, a high stiffness setting demands a constant torque of both actuators in opposing directions. This has some drawbacks in energy consumption. The approach in [22] aims at a reduction of these effects by motor cross coupling. As an advantage, the antagonistic principle provides in tendon driven joints an intrinsic robustness to kinematic errors. Furthermore, it is capable of completely distributing the power of both motors to stiffness changes or to the joint motion. The antagonistic principle is applied to the new tendon-controlled DLR hand.

Current work at DLR regarding robot arm joints is focused on a second option, in which one motor changes the link position and the other one the link stiffness almost independently [23]. This system leads to reduced dynamic losses and allows for stiffness adjustment independent from the link speed.

In our approach, the positioning motor is connected to the link via a harmonic drive gear. Mechanical compliance is introduced by a mechanism, which forms a flexible rotational support between the harmonic drive gear and the joint base (Figure 11). In case of a compliant deflection of the joint, the whole harmonic drive gear rotates relatively to the base, but the positioning motor is not moved. So, the link side inertia is altered only by the circular spline and some parts of the VS device. In contrast to that, the spring mechanism adds no inertia to the drive train between the positioning motor and the link. The link position is changed without moving the elasticity mechanism.

Two different mechanical compliant joint principles (patents pending) are derived from the previous considerations. A short overview of the principles is given in the following sections.

Quasiantagonistic Joint Mechanism

The elastic mechanism of the quasiantagonistic joint is derived from the antagonistic principle: two progressive elastic elements oppose each other, with a variable offset supporting the link with variable range of elastic motion (Figure 12).

The previously mentioned harmonic drive gear for link positioning is held in a bearing and has a cam bar attached to its normally fixed part (Figure 13). Two pairs of rocker arms act on different faces of this cam bar. External loads result in rotational displacement of the whole gear and force the rocker arms to spread against a linear spring, causing progressive restoring torque. The agonist rocker arms are fixed to the housing to save energy, whereas the antagonist part is positioned at a rotational

offset by a stiffness actuator, which can change the stiffness very quickly and independent from the link speed [Figure 12(b)].

The shape of the cam faces can be designed to provide the desired restoring torque characteristic. Superposition of agonist and antagonist forces with different offsets results in variable stiffness. In the nominal range, it has (close to) linear behavior and gets progressive toward the ends of the range for joint protection.

VS-Joint Mechanism

The concept of the VS joint as presented in [24] contains two motors of different size. The high-power motor changes the link position. The joint stiffness is adjusted by a much smaller and lighter motor, which changes the characteristic of the supporting mechanism (Figure 14). An unwound schematic of the principle is shown in Figure 15. A compliant link deflection results in a displacement of the cam disk and is counterbalanced by the roller pressed on it in axial direction by a spring. This generates a centering force resulting in the output torque of the link. To change the stiffness preset, the smaller motor moves the spring base axially to the cam disk and thus varies the spring force. The joint prototype can be equipped with different cam disks. The design of the cam disks specifies the torque/deflection characteristic of the joint. This permits an easy adaptation of the passive joint behavior to the desired application.

Control of Variable Impedance Actuators

Regarding the control of the VIA, the literature mostly deals with the problem of adjusting stiffness and position of the actuator in a decoupled manner by controlling the position or the torque of the two motors of the joint [13], [15], [16]. Moreover, in case of VSA structures with many DoF and cable actuation, the decoupling of the tendon control is treated [25], [26].

Our approach to the control of the VSA arms is to extend the passivity-based control framework developed for the torque-controlled LWRs to the VSA case. Some particular aspects compared with the controllers from the "Compliance Control for Lightweight Arms" and "Impedance Control for Complex Kinematic Chains" sections are summarized.

- Because of the high compliance of the joint, a separate torque sensor is not required any more, and the torque can be well estimated based on the motor and link position [24].
- An active compliance control will be used only for stiffness components that cannot be realized by the mechanical springs. Examples are zero stiffness or the joint coupling stiffness needed by arbitrary Cartesian stiffness matrices [17].
- The joints have very low intrinsic damping. While this is useful for cyclic movements involving energy storage (e.g., for running), the damping of the arm for fast, precise positioning tasks has to be realized by control. This is a challenging task regarding the strong variation of the inertia and the stiffness. Figure 16 shows the performance of the positioning for a very low as well as for a very high stiffness preset of the VS joint.

It is clear that these human-friendly robots will look very different from today's industrial robots.

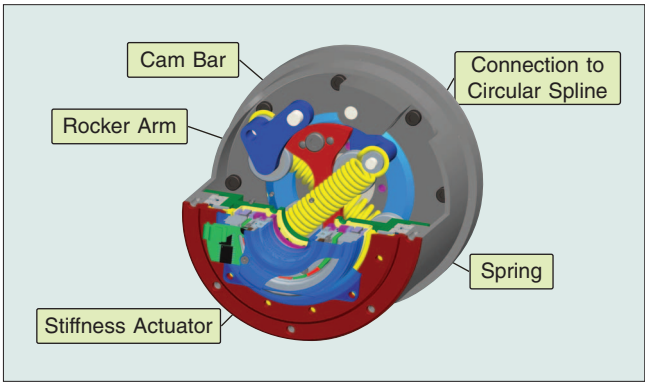

Figure 13. *Cross section of the quasiantagonistic joint design.*

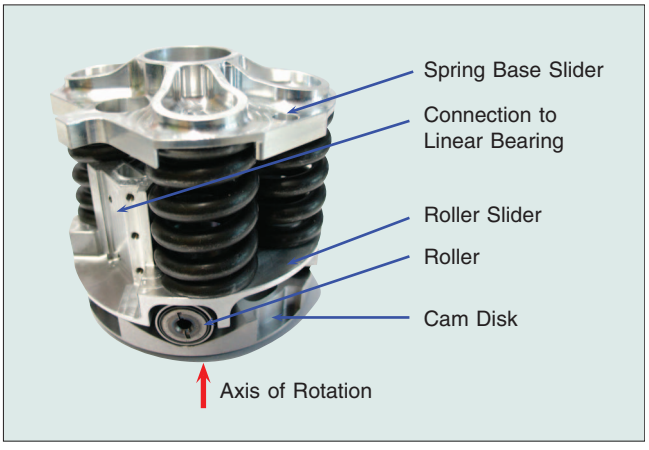

Figure 14. *VS-joint mechanism. The link axis is in the vertical direction. The cam disk rotates on a compliant link deflection.*

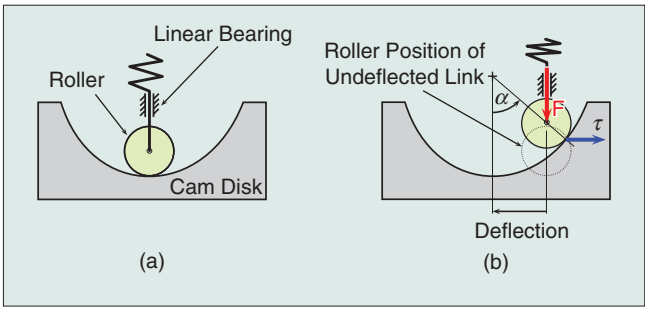

Figure 15. *Unwound schematic of the VS-joint principle in (a) centered and (b) deflected position. A deflection of the link results in a horizontal movement of the cam disk and a vertical displacement of the roller. The spring force generates a centering torque on the cam disk.*

- Absolute accuracy of precise manipulation has to be realized using additional external sensing at the tip.
- The antagonistically tendon-driven joints of the hand (Figure 6) require the extension to handle nonlinear coupled joints based on the tendon coupling matrix.
- The pulling constraint of the tendons has to be fulfilled strictly. Decoupling algorithms will be used to ensure the realization of the passive joint stiffness, whereas the active joint stiffness can be varied over a large domain. Furthermore, a quasistatic effective joint stiffness can be given as a set point.

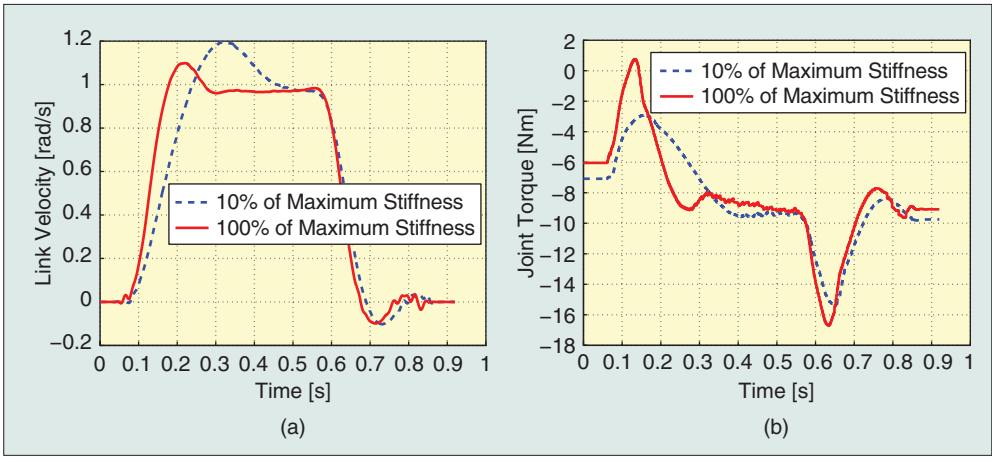

Figure 16. *Motion on a trajectory with rectangular velocity profile for small and maximal stiffness. (a) A critically damped velocity step response can be achieved independent from the stiffness and inertia value. (b) The effect of vibration damping is clearly observed in the torque signal, which contains only the acceleration peaks.*

Performance Validation

Along with the activity regarding the control of the joint, first experiments for validating the increase in performance were done.

Throwing

The application of throwing a ball is a good example to show the performance enhancement gained by the VS joint in terms of maximal velocity. For throwing a ball as far as possible, it has to be accelerated to the maximum achievable velocity and released at a 45° angle. The link velocity of a stiff link corresponds to the velocity of the driving motor. In a flexible joint, the potential energy stored in the system can be used to accelerate the link relatively to the driving motor. Additional energy can be inserted by the stiffness adjuster of the VS joint to gain an even faster motion.

A lacrosse stick head was mounted on the top of the link lever for the throwing tests. The ball is a 64-g rubber ball for school lacrosse. The distance between the link axis and the center of the ball when the ball leaves the lever is approximately 0.78 m.

A simple strikeout trajectory is used to gain high link velocity (Figure 17). It uses the resonance effect of the mass-spring system to maximize joint velocity. With the measured maximum link velocity of 572°/s, the throwing distance was approximately 6 m, corresponding well to the calculated distance of 6.18 m. The theoretical throwing distance with an inelastic link of the same setup with the same maximum motor velocity of 216°/s is 0.88 m, also confirmed experimentally. A speed gain of 265% for the link velocity between rigid and compliant joint was achieved in the test.

Compared with a human, the throwing range of the VS joint seems small, but one has to keep in mind that this was done by a single joint, whereas a human uses several DoF including the hip joints. A series arrangement of joints in a robot arm enlarges the achievable distance.

Stiffness Adjustment

A similar increase of velocity could also be realized by a series elastic actuator without adjustable stiffness. Figure 16 shows the advantage of the VSA design. Fast positioning can be

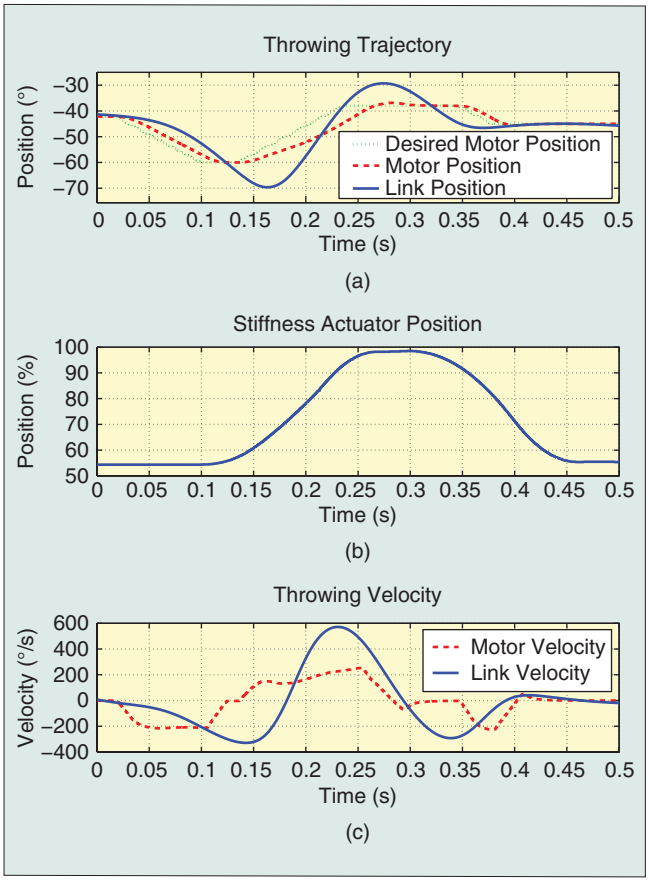

Figure 17. *(a) Throwing trajectory. (b) Stiffness motor position. (c) Joint velocities.*

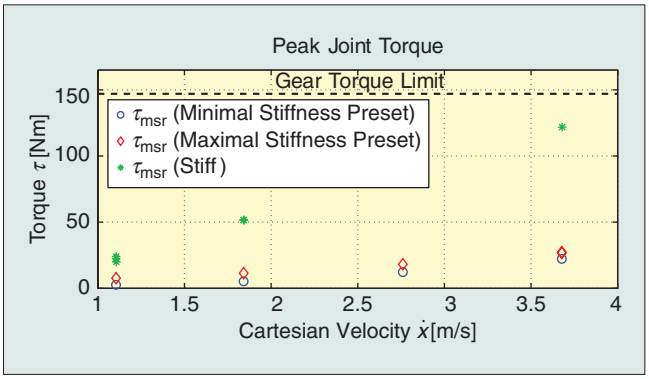

Figure 18. *Peak joint torque during impacts with the VS joint. The impact velocity ranges up to the maximum velocity of the KR500/Robocoaster on which the joint was mounted for the experiment.*

achieved by increasing the stiffness. On the other hand, lowering the stiffness can be used in certain situations for protecting the robot from external loads, as described in the "Protecting the Robot Joint and the Human by Variable Joint Stiffness" section, and validated by the following experiment. (An article with detailed discussion of the load reduction of the joint is currently in preparation.)

Experimental Validation of Joint Overload Protection

To validate the results from the "Protecting the Robot Joint and the Human by Variable Joint Stiffness" section, the impact of the joint at a predefined velocity with a test object was evaluated. Two stiffness setups are realized via the passively compliant VS joint. The most compliant as well as the stiffest configuration were chosen. In a third setup, a mechanical shortcut is inserted into the test bed instead of the VS joint mechanism such that a much stiffer joint is obtained (in the range of the DLR-LWR-III joint elasticity).

Both increasing impact speed and increasing joint stiffness result in higher peak joint torques as visualized in Figure 18. The maximum peak torque limit of the joint gear is almost reached with the stiff joint at an impact velocity of approximately 3.7 m/s, whereas the compliant VS joint is still far in the safe torque region.

Conclusions

In this article, we gave an overview on the DLR activities related to two approaches for the realization of soft robotics: actively torque-controlled LWRs and VSA. On the basis of our experience with torque-controlled robots, we presented an analysis on expected advantages and also disadvantages of VSA actuators. Furthermore, two VSA joint designs motivated by this analysis were presented.

Torque-controlled robots currently represent a technology mature enough for the market, but we believe that impressive research progress can be expected in the area of VSA-actuated robots in the next decade.

Keywords

Soft robotics, lightweight robot, joint torque control, variable compliance actuators.

References

[1] A. Albu-Schäffer, C. Ott, and G. Hirzinger, "A unified passivity based control framework for position, torque and impedance control of flexible joint robots," *Int. J. Robot. Res.*, vol. 26, no. 1, pp. 23–39, 2007.

[2] C. Ott, A. Albu-Schäffer, A. Kugi, and G. Hirzinger, "On the passivity based impedance control of flexible joint robots," *IEEE Trans. Robot. Automat.*, vol. 24, no. 2, pp. 416–429, 2008.

[3] A. Albu-Schäffer, C. Ott, and G. Hirzinger, "A passivity based cartesian impedance controller for flexible joint robots, Part II: Full state feedback, impedance design and experiments," in *Proc. IEEE Int. Conf. Robotics and Automation*, 2004, pp. 2666–2673.

[4] E. Fasse and J. Broenink, "A spatial impedance controller for robotic manipulation.," *IEEE Trans. Robot. Automat.*, vol. 13, no. 4, pp. 546–556, 1997.

[5] F. Caccavale, C. Natale, B. Siciliano, and L. Villani, "Six-dof impedance control based on angle/axis representations," *IEEE Trans. Robot. Automat.*, vol. 15, no. 2, pp. 289–299, 1999.

[6] S. Stramigioli and V. Duindam, "Variable spatial springs for robot control applications," in *Proc. IEEE/RSJ Int. Conf. Intelligent Robots and Systems*, 2001, pp. 1906–1911.

[7] T. Wimböck, Ch. Ott, and G. Hirzinger, "Passivity-based object-level impedance control for a multifingered hand," in *Proc. IEEE/RSJ Int. Conf. Intelligent Robots and Systems*, 2006, pp. 4621–4627.

[8] S. Stramigioli, *Modeling and IPC Control of Interactive Mechanical Systems: A Coordinate-Free Approach*, vol. 266, (Lecture Notes in Control and Information Sciences Series). New York: Springer-Verlag, 2001.

[9] T. Morita, H. Iwata, and S. Sugano, "Development of human symbiotic robot: Wendy," in *Proc. IEEE Int. Conf. Robotics and Automation*, 1999, pp. 3183–3188.

[10] S. Haddadin, T. Laue, U. Frese, and G. Hirzinger, "Foul 2050: Thoughts on physical interaction in human-robot soccer," in *Proc. IEEE/RSJ Int. Conf. Intelligent Robots and Systems*, San Diego, 2007, pp. 3243–3250.

[11] S. Haddadin, A. Albu-Schäffer, and G. Hirzinger, "Safety evaluation of physical human-robot interaction via crash-testing," in *Proc. Robotics: Science and Systems Conf. (RSS2007)*, Atlanta. [Online]. Available: http://www.roboticsproceedings.org

[12] I. P. Herman, *Physics of the Human Body.* New York: Springer-Verlag, 2007.

[13] A. Bicchi and G. Tonietti, "Fast and soft arm tactics: Dealing with the safety-performance trade-off in robot arms design and control," *IEEE Robot. Automat. Mag.*, vol. 11, no. 2, pp. 22–33, 2004.

[14] S. A. Migliore, E. A. Brown, and S. P. DeWeerth, "Biologically inspired joint stiffness control," in *Proc. IEEE Int. Conf. Robotics and Automation*, Barcelona, Spain, 2005, pp. 4519–4524.

[15] G. Palli, C. Melchiorri, T. Wimboeck, M. Grebenstein, and G. Hirzinger, "Feedback linearization and simultaneous stiffness-position control of robots with antagonistic actuated joints," in *Proc. IEEE Int. Conf. Robotics and Automation (ICRA2007)*, Rome, Italy, 2007, pp. 2928–2933.

[16] B. Vanderborght, B. Verrelst, R. V. Ham, M. V. Damme, D. Lefeber, B. M. Y. Duran, and P. Beyl, "Exploiting natural dynamics to reduce energy consumption by controlling the compliance of soft actuators," *Int. J. Robot. Res.*, vol. 25, no. 4, pp. 343–358, 2006.

[17] A. Albu-Schäffer, M. Fischer, G. Schreiber, F. Schoeppe, and G. Hirzinger, "Soft robotics: What cartesian stiffness can we obtain with passively compliant, uncoupled joints?" in *Proc. IEEE Int. Conf. Intelligent Robotic Systems*, 2004, pp. 3295–3301.

[18] S. Haddadin, A. Albu-Schäffer, and G. Hirzinger, "Safe physical human-robot interaction: Measurements, analysis and new insights," in *Proc. Int. Symp. Robotics Research*, Hiroshima, Japan, 2007.

[19] S. Haddadin, A. Albu-Schäffer, A. De Luca, and G. Hirzinger, "Evaluation of collision detection and reaction for a human-friendly robot on biological tissues," in *Proc. IARP Int. Workshop on Technical Challenges and for Dependable Robots in Human environments*, Pasadena, 2008. [Online]. Available: http://www.robotic.de/fileadmin/robotic/haddadin/haddadin_et_al_iarp2008.pdf

[20] K. Koganezawa, "Mechanical stiffness control for antagonistically driven joints," in *Proc. IEEE/RSJ Int. Conf. Intelligent Robots and Systems*, Aug. 2005, pp. 2512–2519.
[21] C. English and D. Russell, "Implementation of variable joint stiffness through antagonistic actuation using rolamite springs," *Mech. Mach. Theory*, vol. 34, no. 1, pp. 27–40, 1999.
[22] G. Tonietti, "Variable impedance actuation," Ph.D. dissertation, University of Pisa, 2005.
[23] T. Morita and S. Sugano, "Development and evaluation of seven-d.o.f. mia arm," in *Proc. 1997 IEEE Int. Conf. Robotics and Automation*, Sept. 1997, pp. 462–467.
[24] S. Wolf and G. Hirzinger, "A new variable stiffness design: Matching requirements of the next robot generation," in *Proc. IEEE Int. Conf. Robotics and Automation*, Pasadena, CA, 2008, pp. 1741–1746.
[25] H. Kobayashi and R. Ozawa, "Adaptive neural network control of tendon-driven mechanisms with elastic tendons," *Automatica*, vol. 39, pp. 1509–1519, 2003.
[26] K. Tahara, Z.-W. Luo, R. Ozawa, J.-H. Bae, and S. Arimoto, "Biomimetic study on pinching motions of a dual-finger model with synergistic actuation of antagonist muscles," in *Proc. IEEE Int. Conf. Robotics and Automation*, 2006, pp. 994–999.
[27] S. Haddadin, A. Albu-Sch, A. De Luca, and G. Hirzinger, "Collision detection and reaction: A contribution to safe physical human-robot interaction," in *Proc. IEEE/RSJ Int. Conf. on Intelligent Robots and Systems*, Nice, France, 2008.

Alin Albu-Schäffer received the Dip.-Ing. degree in electrical engineering from the Technical University of Timisoara, Romania in 1993 and the Ph.D. degree in control systems from the Technical University of Munich (TUM), Germany, in 2002. Since 1995, he has been working with the German Aerospace Center (DLR), Institute of Robotics and Mechatronics, Wessling, Germany, where he is currently coordinating the control and advanced manipulation activities. His current research interests include robot modeling and control, nonlinear control, flexible joint robots, impedance and force control, physical human-robot interaction, and variable impedance actuation.

Oliver Eiberger received his Dipl.-Ing. degree in mechanical engineering from TUM in 2000 and joined DLR in the same year. He is working on DLR Robot arm designs and the quasiantagonistic joint concept.

Markus Grebenstein received his diploma in mechanical engineering in 1996 from TUM. Since 1996, he has been with the DLR, Institute of Robotics and Mechatronics. Since May 2000, he has been leading the mechanical design group. His main research focus is the design of anthropomorphic multifingered robot hands and the design of lightweight robot joints. He published 24 papers on these topics, holds more than eight patents, and has about five patents pending.

Sami Haddadin received his Dipl.-Ing. degree in electrical engineering in 2006 from TUM and holds an honors degree in technology management from TUM and the Ludwig Maximilian University in Munich. He currently works at the DLR as a research engineer. His main research topics are physical human-robot interaction, robot control, and safety and dependability in robotics.

Christian Ott received his Dipl.-Ing. degree in mechatronics from the Johannes Kepler University (JKU), Linz, Austria, in 2001, and the Dr.-Ing. degree in control engineering from Saarland University, Saarbrücken, Germany, in 2005. From March 2001 to April 2007, he was with the DLR, Institute of Robotics and Mechatronics, Wessling, Germany. Since May 2007, he has been a project assistant professor in the Department of Mechano-Informatics, University of Tokyo, Japan. His current research interests include nonlinear control of robotic systems, flexible joint robots, impedance control, and two-armed humanoid manipulation.

Thomas Wimböck studied electrical engineering at the Rensslaer Polytechnic Institute, Troy, and at the Ecole Polytechique Fédérale de Lausanne, Switzerland. He received his B.Sc. and M.Sc. (in 2004) degrees in electrical engineering from TUM. In 2004, he joined the DLR, Institute of Robotics and Mechatronics, as a Ph.D. student. His main research interests include nonlinear control, dexterous robot hands, impedance control, VS control, two-handed (humanoid) manipulation, and kinematic redundancy.

Sebastian Wolf received his Dipl.-Ing. degree in mechanical engineering in 2004 from TUM, Germany. He joined the Institute fur Feingeratebau und Mikrotechnik at TUM, Germany, as a research associate in 2004. Since 2005, he has been a research engineer at the DLR, Institute of Robotics and Mechatronics. His main research interest is in VS actuation.

Gerd Hirzinger received the Dipl.-Ing. and Ph.D. degrees from TUM, Germany, in 1969 and 1974, respectively. Since 1992, he has been the director at the DLR, Institute of Robotics and Mechatronics, Wessling, Germany. In 1991, he received a joint professorship from TUM and in 2003, an honorary professorship at the Harbin Institute of Technology, China. He was a prime investigator of the first remote control space robot ROTEX, which flew onboard the shuttle Columbia in April 1993. He is the recipient of numerous national and international awards, including the Joseph-Engelberger-Award for achievements in robotic science in 1994, the Leibniz-Award, in 1995, the Japan Robotics Association (JARA) Award, the Karl-Heinz-Beckurts-Award in 1996, and the IEEE Fellow Award in 1997. In 2004, he received the order of merit of the Federal Republic of Germany and became a member of the Wall of Fame of the Heinz Nixdorf Computer Museum. He is also the recipient of the IEEE Pioneer Award of the Robotics and Automation Society, the 2005 Honorary Citizenship of Budapest Tech, and the IEEE Field Award Robotics and Automation in 2007.

Address for Correspondence: Alin Albu-Schäffer, DLR-German Aerospace Center, P.O. Box 1116, 82230 Wessling, Germany. E-mail: alin.albu-schaeffer@dlr.de.

Toward Soft Robots You Can Depend On

©PUNCHSTOCK

A Study of Antagonistic Actuation

BY ROBERTO FILIPPINI, SOUMEN SEN, AND ANTONIO BICCHI

Digital Object Identifier 10.1109/MRA.2008.927696

Physical human–robot interaction (pHRI) represents one of the most motivating, challenging, and ambitious research topics in robotics. Many of the future and emerging applications of robotics, be they in service [14], assistance and care [23], rehabilitation [34], or in more traditional working contexts [34], will indeed require robots to work in close vicinity if not in direct contact with humans.

A robot for pHRI applications must be regarded in all aspects as a safety-critical system, as it has been unfortunately proven several times in the past that conventional robots can be dangerous or even deadly machines [33]. Since the very beginning of industrial robotics, a great deal of attention has been paid to robot safety, the first line of defense having always been to take all measures to enforce segregation between robots and people [5], [40]. As market pressures together with ethical concerns are about to topple some of the barriers separating robots and people, safety standards are evolving. The 2006 revision of the ISO10218-1 standard [21], for instance, introduces more advanced concepts than in the past, such as the idea of a collaborative operation between humans and robots, and the replacement (albeit to a very limited, conservative extent) of fixed rules with risk assessment procedures. More generally, for applications involving pHRI, analysis tools are needed that are classical in the literature on critical systems [2], [38] but are still rather new in robotics [9], [10], [13], [42]. These tools focus on the attributes of 1) safety, i.e., the absence of damages and injuries; 2) reliability, the continuity of service; and 3) availability, the readiness of service; in a word, the comprehensive attribute of 4) dependability. The goal of this article is to begin an in-depth study of the dependability of robots for pHRI, starting with the analysis of an elementary, yet critical, robot component, i.e., the joint-level actuation subsystem.

As an answer to the need to build robots that can provide useful performance while guaranteeing safety against all odds, engineers have proposed several innovative solutions to overcome the classical paradigm "rigidity by design, safety by sensors and control," which is more suited for conventional industrial robotics, and are shifting toward a "safety by design, performance by control" philosophy [1], [14], [18]. In our own previous work [3], [4], variable stiffness actuation (VSA) and its generalization in variable impedance actuation (VIA) have been demonstrated to be effective in obtaining a safe yet performing robot motion by swiftly alternating stiff-and-slow and fast-and-soft motion modes. Indeed, in high-velocity impacts, low-joint impedance can effectively decouple the link's inertia from the actuator's reflected inertia, which is typically large due to the transmission gear ratio. Although the investigation of VIA, including variable damping [11], [25], [29], [31] and/or gear ratio, is a very promising research direction, as of today there are only very few examples of general VIA systems for robotics applications. On the contrary, a number of different prototypes exist that can vary the transmission stiffness [8], [22], [32], [43]. Among these, we focus on VSA mechanisms whereby joint stiffness values can be continuously varied as a function of joint velocities. This is

1070-9932/08/$25.00©2008 IEEE

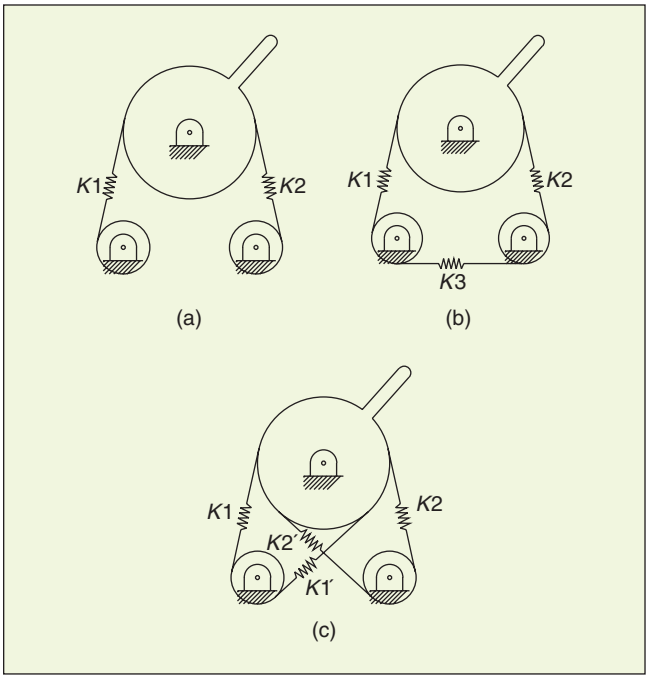

Figure 1. *Three possible arrangements for AA: (a) simple, (b) cross coupled, and (c) bidirectional.*

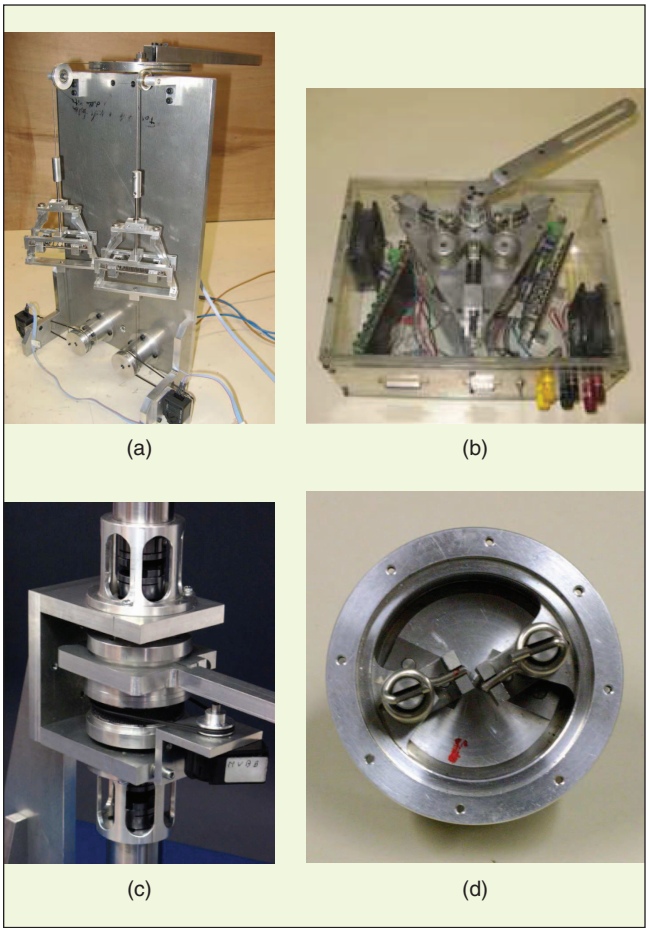

Figure 2. *Laboratory prototypes of three AA arrangements: (a) simple AA with exponential springs, (b) cross-coupled arrangement of the VSA-I, (c) bidirectional arrangement of the VSA-II, and (d) one half of the VSA-II opened up.*

contrasted to other methods that adapt compliance only once for each different task and implies that implementation of VSA requires hardware capable of changing stiffness with a time-constant comparable to that of the mechanics of the rigid robot (i.e., of the order of milliseconds). Furthermore, among several possible solutions to implement the VSA idea, we focus our attention here on the notable class of antagonistic actuation (AA) systems. Agonist-antagonist actuator pairs are commonly seen in nature and have been studied in biomechanics as well as robotics for a long time [15]. Artificial AA systems are more complex in design, construction, and operation when compared with conventional rigid robot joints. This increase in design complexity, while useful for achieving a safer system in nominal conditions, might affect the dependability attributes and the performance in the presence of faults.

This article describes possible implementations of the VSA concept via three different arrangements of the agonist-antagonist actuation scheme. A detailed comparative dependability analysis of possible specific failure modes is conducted, whose results provide insights on the design of the actuation mechanism and of fault management (FM) layers, including fault detection and identification (FDI), system reconfiguration, and fail-safe emergency stops, to provide the ability of tolerating faults and continuing safe operations.

AA Arrangements

In its simplest implementation, an AA arrangement consists of two prime movers connected to the moving element (link) through two nonlinear elastic elements [see Figure 1(a)]. Rotation of the motors in the same sense generates a net torque to the joint, while rotations in the opposite sense set different levels of effective compliance at the joint. Depending on the implementation, prime movers can be regarded as either torque or position sources, and elastic transmissions can have different characteristics. We assume that motors have much higher reflected inertia at the joint axis than the link itself, due to the fact that in robotic applications high gear ratios are often used (gears are included in the prime-mover element in our analysis). We also consider unidirectional (tendon-like) transmission elements. A laboratory implementation of a simple AA arrangement is depicted in Figure 2(a).

A closer inspection of the musculoskeletal system in humans shows that not all articulations are actuated by an arrangement of agonistic–antagonistic muscles analogous to this simple case: indeed, more muscles are involved, and couplings exist between the actuation of different joints. From an engineering viewpoint, simple AA arrangements might not be optimal as well. For instance, if pull-only tendons are considered, the maximum torque available at the joint cannot be more than that of each single motor, and no net torque is available at the joint when stiffness is at the maximum. To overcome this limitation, a possible modification is to introduce a third elastic element (possibly different from the two antagonists) to cross couple the two prime movers [see Figure 1(b)]. Cross coupling allows setting preload forces in the system to tune it to nominal working conditions and using (a fraction of) each motor's torque in both directions. The VSA-I prototype introduced in [37] and depicted in Figure 2(b) is an implementation of this concept.

One further variation of the basic AA arrangement, which addresses the issues of unidirectional actuation not using cross coupling, consists of connecting each actuator to the link via two elastic elements (not necessarily symmetric) in the push-pull configuration [see Figure 1(c)]. The VSA-II prototype introduced in [35] and depicted in Figure 2(c) implements such a bidirectional AA arrangement. Figure 2(d) is a view of one half of the VSA-II mechanism. One motor is connected to the inner pulley (marked in red), while the link is fixed to the outer shells of the two halves. Two elastically preloaded four-bar mechanisms are visible, which are used to connect bidirectionally the motor to the outer shell.

Mechanics and Control Codesign

We chose to design the actuation arrangements considered in this article by the mechanical/control codesign approach that was illustrated in [3]. The basic idea is to select the mechanical elements (springs and motors) and design the nominal (open-loop) input functions so as to optimize performance while guaranteeing that a given risk threshold is never exceeded during the robot motion. This is a variational optimization problem (the so-called safe brachistochrone), which can be solved numerically. The evaluation of the safety threshold is done through extensive simulation runs of impacts of the moving link with a human, occurring at different velocities and for different values of joint stiffness. The impact effects were quantified using the head injury coefficient (HIC) [41]. It should be noted that the HIC criterion is not a completely satisfactory index for pHRI if the same metrics are used to measure the injury risk as in car crash tests, as discussed, e.g., in [12]. If HIC values evaluated for robotic impacts are mapped to risks by abbreviated injury scales developed for automotive applications, the results underestimate the consequences. Although other safety metrics are being actively investigated, we, in this study, use the HIC index, assuming that pHRI risks are proportional to HIC by a scaling factor still to be evaluated empirically. Confusion may occur about the units of measure for HIC. In SI units, HIC is measured in $m^{2.5}/s^4$. If acceleration is measured in $g = 9.81\ m/s^2$, instead, then HIC is measured in seconds. A factor of $g^{5/2} \approx 300$ applies between HIC values in different units. Automotive crash test literature typically uses the latter units. We use SI units in this article.

A substantial difference between the safe brachistochrone characterization in [3] and its application to the AA arrangements considered is that here the variation of stiffness cannot be achieved instantaneously (as it was in the ideal model in [31]), and its rate is limited by the available actuator torque and inertia. Furthermore, we take into account the dissipative effect of back electromotive force.

Interestingly enough, the basic result of the safe brachistochrone study remains valid in these more realistic conditions and for the different design configurations encountered in the AA implementations described here: the minimum-time control of a VSA under strict safety constraints consists of alternating stiff-and-slow and soft-and-fast motion modes. As an illustrative example, the numerical results for the safe brachistochrone optimization of the cross-coupled AA arrangement are shown in Figure 3.

Modeling for Dependability Assessment

The behavior of a system under unexpected conditions or failures is the main subject of dependability engineering. A system is said to be dependable when its service can be justifiably

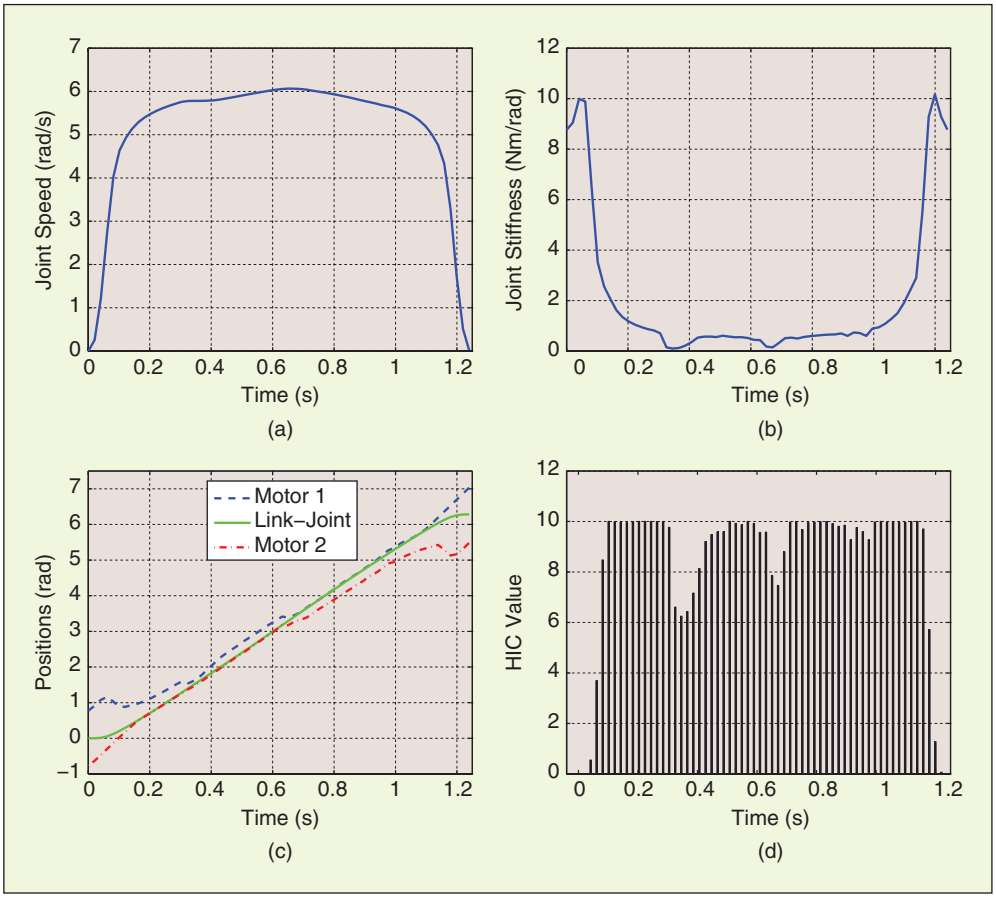

Figure 3. *Numerical optimization results for the codesign of a cross-coupled AA arrangement implementing joint variable stiffness. (a) The link goes through an approximately trapezoidal velocity profile. (b) Stiffness is correspondingly high in the initial and final phases of motion, and low in between. (c) Agonist and antagonist actuators are shown in action in the different phases. (d) The optimized HIC values during motion tend to the acceptable limit (here set to 10 $m^{2.5}/s^4$).*

trusted over well-stated operational conditions and a given time interval. This general definition specializes into several attributes [24]. The most important ones include

1) safety or the absence of catastrophic effects of failures
2) reliability or the continuity of service
3) availability or the readiness of service.

A dependability assessment study typically starts with the failure modes and effects analysis (FMEA) and returns a random variable for the dependability attribute, with its distribution and statistics (e.g., average and variance). For instance, the mean time to failure (MTTF) and the mean time between failure (MTBF) are often used as statistic indicators for reliability and availability, respectively.

Methods for dependability assessment (modeling and analysis) are basically split into 1) combinatorial (e.g., fault trees, reliability block diagrams) and 2) state based (e.g., Markov chains, Petri nets). Combinatorial approaches typically return the probability of an event, e.g., the overall system failure, in a rather computationally efficient way, which is useful for the analysis of complex systems. State-based approaches instead return a richer description of the whole failure process, from the fault-free state to the system failure state, including the transitional states. When this description is required, state-based approaches prove to be more powerful and lend themselves to the evaluation of more detailed failure scenarios, including the effect of fault tolerant design and periodical inspections. In this article, we will adopt the state-based approach to analyze the dependability of rather simple joint actuation arrangements introduced previously.

Failure Modes and Fault Management

The FMEA is a tool for identifying the failure modes in a system and for reporting the causes on the basis of their occurrence and the general effects on the delivered function [16]. While FMEA analysis can be very detailed, we use it here only to establish a principled but reasonably simple failure model of the three AA arrangements under consideration (see Figure 1).

To this purpose, the following assumptions are made:

- Faults are statistically independent random processes.
- The occurrence of a fault in a component causes the sudden transition from a fully functional to a failed state.
- Faults are permanent. Slow performance drifts and transient and systematic failure modes are not considered.

To further limit the complexity of an FMEA for the three AA arrangements under consideration, we restrict our consideration to only two elementary components, i.e., motors and elastic transmission elements (referred to as springs, although they might not be realized as such in practice). The control and electronic power amplifier system is included in the motor FMEA model.

Motors are assumed to fail either by a controller fault (whereby in the worst case the shaft torque defaults to its maximum value) or by a mechanical gear breakdown, with the axis getting stuck at a fixed position or breaking loose. Springs breakage causes zero torque to be transmitted through the corresponding elastic element.

For a critical system such as a pHRI robot joint, some measures of FM should be taken to minimize the effects of faults. In our examples, we postulate a simple FM control layer, which consists of a series of three independent modules: sensors, internal logic, and recovery actions. Sensors pick up motor current and position signals, which are processed by the FDI logic, whose role is to track state changes in the joint actuation mechanism. Recovery actions are issued accordingly, either by system reconfiguration or fail-safe emergency stop.

Because we assume that VSA joints are controlled to track optimal safe velocity-stiffness references (planned, e.g., by the safe brachistochrone method), an FM action is necessary to restore the system to a functioning state or to stop it safely [27], [42]. For example, a spring failure in the bidirectional arrangement alters the mechanism stiffness and the effective impacting inertia at the link. To avoid risks in the subsequent operations, the system should be reconfigured to reset its internal stiffness value according to the optimal VSA solution in the new conditions.

Three types of reconfigurations are considered to restore the functioning of the system automatically, before repair intervention. A reconfiguration of the R1 type copes with the failure scenarios by which it is possible to recover control of both the link motion and stiffness, albeit at the cost of some performance loss (e.g., due to a reduced stiffness variation range). The breakage of the preloading spring in the cross-coupled AA and of one of the springs in the bidirectional AA are such scenarios. A second type of reconfiguration (R2) is applied when the steering of the link is not compromised, although stiffness cannot be controlled any longer. Controls are switched into the non-VSA mode in order that the system may continue to operate safely at a reduced velocity. Finally, a reconfiguration of the third type (R3) simply uses the residual functioning elements of the system to reduce the elastic energy stored in the system, before shutting down to a fail-safe stop. This fail-safe operation abort by emergency stop is issued if the detected failure is critical for safety or reconfiguration has failed.

The list of failure modes for the three arrangements illustrated in Figure 1 is shown in Table 1. Each component is assigned a failure mode, the effect is provoked at the system level, and the type of coverage action is provided by an FM system. The reported effects correspond to each fault occurring singularly.

State-Based Model

The last changes caused by the occurrence of single faults and sequences of faults with the respective recovery actions are accommodated in a state transition diagram, evolving as a discrete event system [6].

In total, the following five states are identified:

1) *Fault free*: The system functions normally.
2) *Recovered with VSA*: After successful reconfiguration, the system controls both the link motion and stiffness.
3) *Recovered without VSA*: After successful partial reconfiguration, the system controls the link position but not its stiffness.
4) *Fail-safe stop*: The system has been detected as failed and the operation stops.
5) *System failure*: The system has failed in operation.

The last state is reached in worst-case situations where a reconfiguration or fail-safe stop action may itself fail.

System dependability attributes are defined on subsets of the state space X. Thus, reliability is the probability of conserving the VSA function, namely of being in states $X_R =$

$\{$*fault free*, *recovered with VSA*$\}$. We introduce the term *steerability* to indicate a partial reliability attribute, for the system conserving the steering function possibly without stiffness (VSA) control. In other words, steerability is the probability of being in $X_{S_T} = X_R \cup \{$*Recovered without VSA*$\}$. The system is expected to be safe in the reliable states, in the *recovered without VSA* state and in the fail-safe stop state, namely $X_S = X_{S_T} \cup \{$*Fail-safe stop*$\}$ (compare later simulation results in the "Safety" section).

The state-based dependability models for the three AA arrangements are shown in Figure 4(a)–(c). The definitions of the states are described in Table 2. Cases where one motor axis gets stuck due to gear-box breakage lead immediately to failure (possibly through the R3 reconfiguration) and are not further discussed here. A 0 in a motor column, hence, indicates a loose joint, while 1 indicates correct functioning. Symmetric failure conditions in the considered systems are aggregated in a single state in the diagrams. A label with the names of the destination or source states is used in place of arcs to keep the description as compact as possible. For example, in Figure 4(c), the state X_3 has two labeled output transitions to states X_6 and X_7 and one labeled input transition from state X_0. Each state is also described by two entries spaced by the symbol || indicating for each motor whether it can apply bidirectional torques to the link (value 2), unidirectional (value 1), or no torque at all (value 0).

For all models, the actions issued by FM are successfully accomplished with a certain probability that depends on the correct execution of the fault-handling process, i.e., the sequence of detection, identification, and recovery [7], [20]. This probabilistic model is represented by a coverage factor C, which is a number that ranges between 1, in case the fault is certainly covered, and 0, if that fault is certainly not covered [39]. The noncoverage fraction $1 - C$ accounts for missed detections and/or improper reconfigurations, which lead to the *system failure* state.

Failures and recovery actions draw stochastic processes in X which, in our consideration, can be modeled by a continuous time Markov chain (CTMC) [39]. A CTMC is described by a state probability vector $p(t) = [p_0(t), \ldots \; p_{N-1}(t)]$, $p_i(t) \geq 0$, $\forall i = 0 \ldots \; N-1$, and $\sum p_i(t) = 1$. Here $p_k(t)$ is the probability that the system is in state X_k at time t. The probability distribution $p(t)$ evolves according to Kolmogorov's equation

$$\frac{d}{dt}p(t) = p(t)Q, \tag{1}$$

for $t \geq 0$, with initial conditions $p(0)$. The transition rate matrix Q, corresponding to the Laplacian of the transition graph, is specified for the three different models as follows.

1) Simple AA $Q_{\text{Simple}} =$

$$\begin{pmatrix} -\lambda_0 & \lambda_{01} & \lambda_{02} \\ 0 & 0 & 0 \\ 0 & 0 & 0 \end{pmatrix}. \tag{2}$$

2) Cross-coupled AA $Q_{\text{CC}} =$

$$\begin{pmatrix} -\lambda_0 & \lambda_{01} & \lambda_{02} & \lambda_{03} & \lambda_{04} \\ 0 & -\lambda_1 & 0 & \lambda_{13} & \lambda_{14} \\ 0 & 0 & -\lambda_2 & \lambda_{23} & \lambda_{24} \\ 0 & 0 & 0 & 0 & 0 \\ 0 & 0 & 0 & 0 & 0 \end{pmatrix}. \tag{3}$$

3) Bidirectional AA $Q_{\text{Bid}} =$

$$\begin{pmatrix} -\lambda_0 & \lambda_{01} & 0 & \lambda_{03} & \lambda_{04} & 0 & 0 & \lambda_{07} \\ 0 & -\lambda_1 & \lambda_{12} & 0 & \lambda_{14} & 0 & \lambda_{16} & \lambda_{17} \\ 0 & 0 & -\lambda_2 & 0 & \lambda_{24} & 0 & \lambda_{26} & \lambda_{27} \\ 0 & 0 & 0 & -\lambda_3 & \lambda_{34} & \lambda_{35} & \lambda_{36} & \lambda_{37} \\ 0 & 0 & 0 & 0 & -\lambda_4 & 0 & \lambda_{46} & \lambda_{47} \\ 0 & 0 & 0 & 0 & 0 & -\lambda_5 & \lambda_{56} & \lambda_{57} \\ 0 & 0 & 0 & 0 & 0 & 0 & 0 & 0 \\ 0 & 0 & 0 & 0 & 0 & 0 & 0 & 0 \end{pmatrix}. \tag{4}$$

The diagonal elements of Q are the sum of the elements in the row, according to the balance of rates entering and leaving each state k, i.e., $\lambda_k = -\sum_{j=0,\neq k}^{N-1} \lambda_{kj}$.

The transition rates of Q are expressions of the component failure rates and of the reconfiguration coverage factors.

Let $\lambda_{M_i^+}$ and $\lambda_{M_i^0}$ denote the number of failures per hour of motor M_i defaulting to maximum torque and to zero torque, respectively, and $\lambda_{M_i} = \lambda_{M_i^+} + \lambda_{M_i^0}$. Let also λ_{K_i} be the failure rate of the nonlinear spring K_i, and $\lambda_{K_i'}$ be the failure rate of the linear spring K_i'.

In the analysis, we have assumed identical motors and symmetrical springs, so that $\lambda_{M_i^+} = \lambda_{M^+}$, $\lambda_{M_i^0} = \lambda_{M^0}$, $\lambda_{M_i} = \lambda_M$, $\lambda_{K_i} = \lambda_K$, and $\lambda_{K_i'} = \lambda_{K'}$. When only one motor or spring among the symmetrical ones is valid, the subscript is omitted.

For example, transition $X1 \longrightarrow X3$ from *recovered with VSA* to *fail-safe stop* for the cross-coupled arrangement is:

$$\lambda_{13} = C_3(\lambda_{K_1} + \lambda_{K_2} + \lambda_{M_1} + \lambda_{M_2}), \tag{5}$$

Table 1. FMEA of the three AA arrangements.

Component	Failure Mode	Effect	Action
Simple AA			
Motor 1 $\wedge$ 2	Maximum torque	Uncontrolled motion	Fail-safe stop
Motor 1 $\wedge$ 2	No torque	Uncontrolled motion	Fail-safe stop
Motor 1 $\wedge$ 2	Stuck	Uncontrolled stiffness	R3
Springs $K1 \wedge K2$	Breakage	Uncontrolled motion	Fail-safe stop
Cross-coupled AA			
Motor 1 $\wedge$ 2	Maximum torque	Uncontrolled motion	Fail-safe stop
Motor 1 $\wedge$ 2	No torque	Uncontrolled motion	R2
Motor 1 $\wedge$ 2	Stuck	Link stuck	R3
Springs $K1 \wedge K2$	Breakage	Uncontrolled motion	Fail-safe stop
Spring $K3$	Breakage	Uncontrolled motion	R2
Bidirectional AA			
Motor 1 $\wedge$ 2	Maximum torque	Uncontrolled motion	R3
Motor 1 $\wedge$ 2	No torque	Uncontrolled motion	R2
Motor 1 $\wedge$ 2	Stuck	Link stuck	R3
Springs $K1 \wedge K2$	Breakage	Uncontrolled stiffness	R1
Springs $K1' \wedge K2'$	Breakage	Uncontrolled stiffness	R1

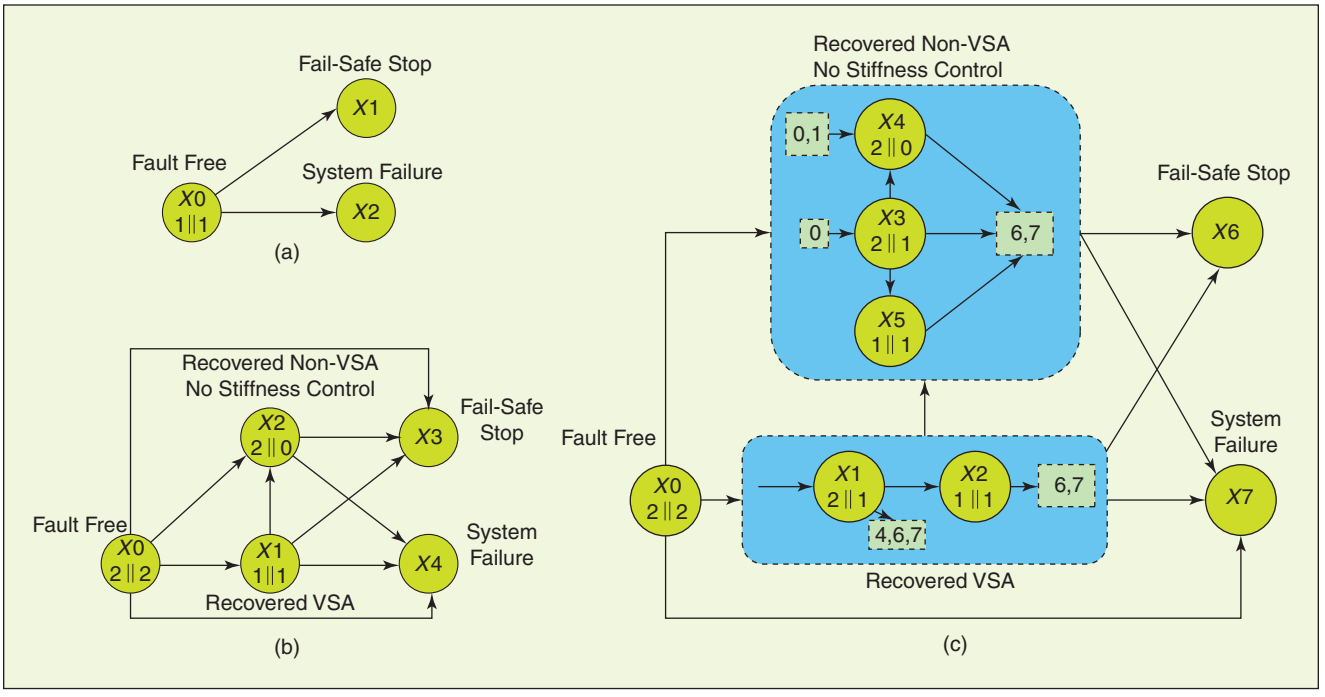

Figure 4. *State-based dependability models of the (a) simple, (b) cross-coupled, and (c) bidirectional AA arrangements.*

Table 2. Description of the functional states.

State	M1	K1	K1′	M2	K2	K2′	K3
Simple AA							
X0	1	1	N/A	1	1	N/A	N/A
X1 and X2	Failure of any further component from state X0						
Cross-coupled AA							
X0	1	1	N/A	1	1	N/A	1
X1	1	1	N/A	1	1	N/A	0
X2	1	1	N/A	0	1	N/A	1
X2(sym.)	0	1	N/A	1	1	N/A	1
X3 and X4	Failure of any further component from states X1 and X2						
Bidirectional AA							
X0	1	1	1	1	1	1	N/A
X1	1	1	1	1	1	0	N/A
X1(sym.)	1	1	0	1	1	1	N/A
X2	1	1	0	1	1	0	N/A
X3	1	1	1	1	0	1	N/A
X3(sym.)	1	0	1	1	1	1	N/A
X4	1	1	1	1	0	0	N/A
X4(sym.)	1	0	0	1	1	1	N/A
X4	1	1	1	0	1/0	1/0	N/A
X4(sym.)	0	1/0	1/0	1	1	1	N/A
X5	1	0	1	1	0	1	N/A
X6 and X7	Failure of any further component from states X2, X3, X4, and X5						

where the coverage factor C_3 accounts for reconfiguration R3 in case of failure of one component among two nonlinear springs and two motors, given spring $K3$ has already failed. Transition $X0 \longrightarrow X1$ from *fault free* to *recovered with VSA* for the bidirectional arrangement is:

$$\lambda_{01} = C_1(\lambda_{K_1'} + \lambda_{K_2'}), \tag{6}$$

where the coverage factor C_1 accounts for reconfiguration R1 in case of failure of one of the two linear springs. An example is also given for transitions that lead to the *system failure* state. Transition $X0 \longrightarrow X2$ from *fault free* to *system failure* for the simple arrangement is:

$$\lambda_{02} = (1 - C_3)(\lambda_{M_1} + \lambda_{M_2} + \lambda_{K_1} + \lambda_{K_2}), \tag{7}$$

where $1 - C_3$ accounts for the missed coverage in case of failure of one component among two motors and two springs.

Failure rates in the expressions are added up because of their assumed statistical independence.

Results

Dependability Analysis Results

The dependability attributes of interest, reliability R, and steerability S_T are defined for the three AA mechanisms as the stochastic variables $R(t)$ and $S_T(t)$, where

- simple: $R(t) = S_T(t) = p_0(t)$
- cross coupled: $R(t) = p_0(t) + p_1(t)$; $S_T(t) = R(t) + p_2(t)$
- bidirectional: $R(t) = p_0(t) + p_1(t) + p_2(t)$; $S_T(t) = R(t) + p_3(t) + p_4(t) + p_5(t)$.

A numerical evaluation of reliability and steerability is conducted under the following assumptions for all models:

1) The component failure rates are constant and equal to 10^{-5} failures per hour.
2) Systems are assumed to be working correctly at the start. Hence, the initial probability vector is $p(0) = [1, 0, \ldots, 0]$.
3) An indefinitely long mission time is specified so that operations only end when the system fails.

In these conditions, the transient analysis of $p(t)$ can be replaced by average statistics [39], in particular MTTF for reliability and mean time to steering failure (MTTSF) for steerability. These quantities can be calculated by applying the final value theorem of the Laplace transform, i.e.,

$$\mathrm{MTTF} = \lim_{t\to\infty} \int_0^t R(\tau)d\tau = \lim_{s\to 0} R(s) \tag{8}$$

$$\mathrm{MTTSF} = \lim_{t\to\infty} \int_0^t S_T(\tau)d\tau = \lim_{s\to 0} S_T(s) \tag{9}$$

where

$$\begin{aligned} R(s) &= p(0)(sI - Q)^{-1}\nu_r \\ S_T(s) &= p(0)(sI - Q)^{-1}\nu_s \end{aligned}$$

with ν_r and ν_s suitably defined according to the above discussion: for instance, for the cross-coupled AA, one has

$$\begin{aligned} \nu_r^T &= [1 \quad 1 \quad 0 \quad 0 \quad 0] \\ \nu_s^T &= [1 \quad 1 \quad 1 \quad 0 \quad 0]. \end{aligned}$$

Three operational scenarios are considered, namely, OP I, OP II, and OP III, which correspond to three different settings of coverage factors $C1$, $C2$, and $C3$. In the first scenario, recovery actions R1, R2, and fail-safe stop always occur when needed ($C1 = C2 = C3 = 1$). In the second scenario, reconfiguration R2 is not available ($C2 = 0$, $C1 = C3 = 1$), while in the third case no reconfiguration is operational, and only the fail-safe stop action is available ($C1 = C2 = 0$, $C3 = 1$). Numerical results for MTTF and MTTSF are reported in Table 3 and illustrated in Figure 5. With the only fail-safe emergency stop and no reconfiguration (OP III), the simple AA is the most reliable arrangement with MTTF = 2.8 years, while the bidirectional AA and the cross-coupled AA are 1.9 and 2.3 years, respectively. The result can be explained by considering that without reconfigurations, the complexity in the design of the bidirectional and cross-coupled arrangements turns out to be a source of unreliability for the system. For example, the breakage of a linear spring affects the trajectory of the link and lowers the reliability. If reconfiguration R1 is performed (OP II), MTTF (as well as MTTSF) becomes 2.8 years for the three AA arrangements. Reconfiguration R2 in scenario OP I ensures an MTTSF of six years for the bidirectional, against four years for the cross-coupled and 2.8 years for the simple arrangement.

Safety

As mentioned earlier, the design of the three VSA actuators has been conducted so that an impact occurring in any phase of their motion would not exceed a given injury risk. However, this guarantee only holds in case the systems are fully functioning. To assess the safety of the mechanism in case of possible faults, the effects of impacts occurring in coincidence with some of the possible mechanical faults must be considered.

As reasonable coverage of all possible cases by actual impact experiments is not feasible, a rather extensive simulation campaign has been conducted. In each simulation run, faults are injected in the system according to the model described in the sections discussing FMEA and reliability analysis. We consider faults consisting of the failure of a single component, occurring at an arbitrary time instant in the course of task execution by the VSA system. Representative fault timing is considered to be in the acceleration, intermediate, and deceleration phases. No FM strategy is used in the simulations. For comparison purposes, the dynamical models of three AA arrangements for VSA are considered. The model parameters (inertias, spring constants, and actuator torques) are chosen so that they would perform equally well under nominal fault-free conditions. Specifically, they accomplish the reference task (a rest-to-rest motion of 2π rad) under equal safety bounds in the same time.

An example simulation with a fault injected in the acceleration phase for the three different arrangements is reported in Figure 6, showing that this type of fault can actually become

Table 3. MTTF and MTTSF (in years) for the actuation arrangements versus different settings of the FM system (three OP scenarios).

	OP III		OP II		OP I	
	MTTF	MTTSF	MTTF	MTTSF	MTTF	MTTSF
Simple	2.8	2.8	2.8	2.8	2.8	2.8
Cross coupled	2.3	2.3	2.8	2.8	2.8	4.0
Bidirectional	1.9	1.9	2.8	2.8	2.8	6.0

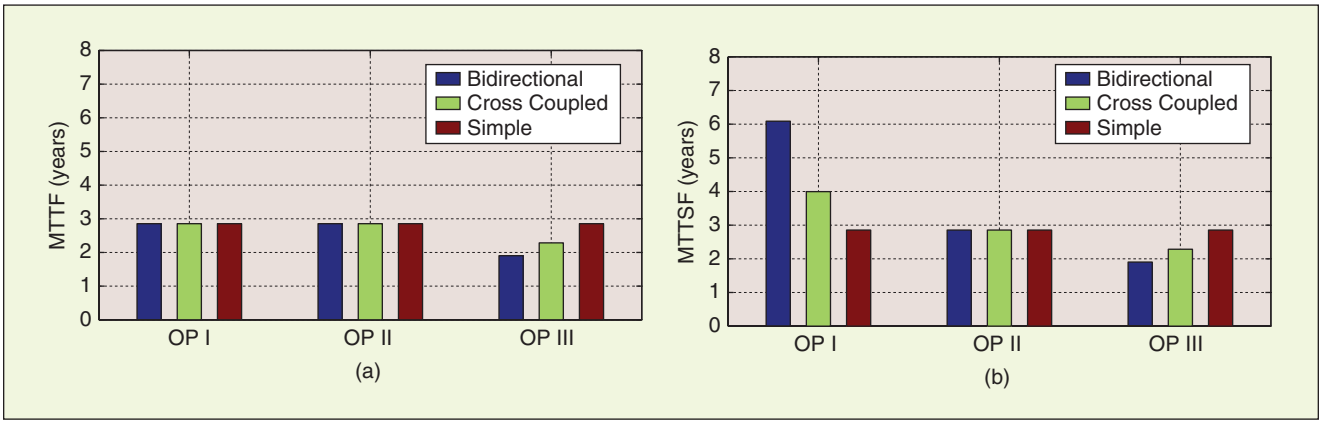

Figure 5. *(a) Reliability (MTTF) and (b) steerability (MTTSF) of the actuation systems versus the FM coverage (three OP scenarios).*

dangerous. As another representative example, the effects of failure of the coupling elastic element in a cross-coupled actuator is shown in Figure 7. It can be observed that the system maintains the ability of adapting stiffness in this case. Accordingly, safety margin violations are only marginal. Similar results are found for the bidirectional arrangement, thus confirming the expectation (discussed in the "State-Based Model" section) that reliable states are safe.

Table 4 describes a summary of the consequences of the various failures in the three arrangements as obtained through simulations. Note that simulations evaluate the worst-case consequence of an impact occurring at any time between the start and end of motion, in the presence of a given type of failure occurring in one of the three phases. Thus, for instance, the first line in Table 4 means that, if in a simple AA arrangement, motor 1 fails defaulting to maximum torque in the acceleration phase, then at some subsequent time an impact will overcome the safety limits.

It should be further noted that a conventional joint, rigidly connected to the motor, and dimensioned to achieve the same performance in the reference task, would result to be unsafe for impacts even in the fault-free case (the only countermeasure

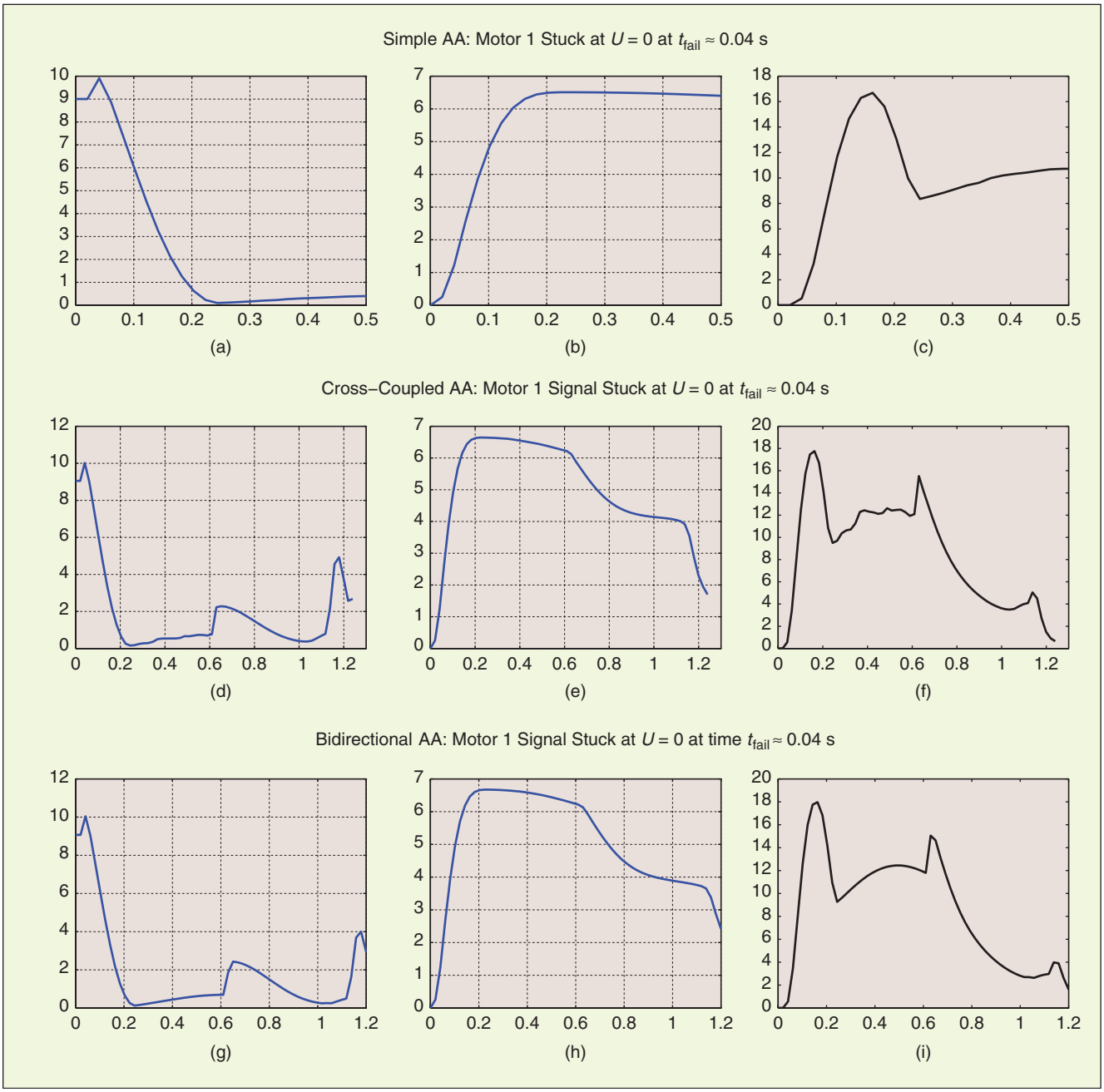

Figure 6. *An example of a safety-verification simulation test, showing runs for each of the three arrangements with a failure of motor 1, defaulting to zero torque in the acceleration phase. The effects of the fault are shown on the (a), (d), and (g) joint stiffness (in Nm/rad); (b), (e), and (h) velocity (in rad/s); and (c), (f), and (i) resulting HIC for impacts potentially occurring thereafter (in $m^{2.5}/s^4$). Time is reported in seconds on the abscissae.*

here would be to lower the velocity and hence the performance).

Conclusions

In this article, we performed an analysis of the dependability of an elementary yet critical robot component, i.e., the joint-level actuation subsystem. We consider robot actuators that implement the VSA paradigm, i.e., ability to change the effective transmission stiffness during motion to achieve high performance while constantly keeping injury risks by accidental impacts with humans below a given threshold.

Without attempting a comprehensive review of different existing design approaches to VSA, we focused on the analysis of three different arrangements of agonistic/antagonistic actuation mechanisms for pHRI applications. Several aspects of their performance, safety, and dependability have been considered to get an indicative, though certainly not exhaustive, comparison of these alternatives.

According to our results, the simple AA arrangement is more reliable (due to the simplicity of its mechanical implementation) if FM is not used. Proper FM actions can make other designs perform equally well as the simple AA concerning reliability and can perform better for steerability. Simulations of impacts in failed states (where FM is not used by a worst-case assumption) also show that the different designs have comparable safety properties.

Although overall results for the bidirectional arrangements are somewhat superior, especially in terms of steerability (if FM is applied), we do not extrapolate any general claim in this regard. Indeed, many factors influence the results of similar studies, and each case should be considered in detail and very carefully.

The scope of the study can become quite broad, and many of the theoretical and technical issues presented here (e.g., fault detection, supervisory control, and safety-related systems) will require further separated investigations. One of the purposes of this work was to explore and further promote dependability studies in robotics, as a means of addressing concerns in safety-critical robotic systems for physical interactions with humans. In this sense, a robot for pHRI applications is a

Table 4. Single component failures during acceleration, intermediate, and deceleration phases for the particular nominal task execution.

Component	Failure Mode	Consequence
Simple AA		
Motor 1	Maximum torque	Acceleration → Unsafe Intermediate → Unsafe Deceleration → Safe
Motor 1	No torque	Acceleration → Unsafe Intermediate → Safe Deceleration → Safe
Motor 2	Maximum torque	Acceleration → Safe Intermediate → Safe Deceleration → Safe
Motor 2	No torque	Acceleration → Unsafe Intermediate → Unsafe Deceleration → Safe
Spring $K1$	Breakage	Acceleration → Safe Intermediate → Safe Deceleration → Safe
Spring $K2$	Breakage	Acceleration → Marginally unsafe Intermediate → Safe Deceleration → Safe
Cross-coupled AA		
Motor 1	Maximum torque	Acceleration → Unsafe Intermediate → Unsafe Deceleration → Safe
Motor 1	No torque	Acceleration → Unsafe Intermediate → Safe Deceleration → Safe
Motor 2	Maximum torque	Acceleration → Safe Intermediate → Safe Deceleration → Safe
Motor 2	No torque	Acceleration → Unsafe Intermediate → Unsafe Deceleration → Safe
Spring $K1$	Breakage	Acceleration → Safe Intermediate → Safe Deceleration → Safe
Spring $K2$	Breakage	Acceleration → Marginally unsafe Intermediate → Safe Deceleration → Safe
Spring $K3$	Breakage	Acceleration → Marginally unsafe Intermediate → Marginally unsafe Deceleration → Safe
Bidirectional AA		
Motor 1	Maximum torque	Acceleration → Unsafe Intermediate → Unsafe Deceleration → Safe
Motor 1	No torque	Acceleration → Unsafe Intermediate → Safe Deceleration → Safe
Motor 2	Maximum torque	Acceleration → Safe Intermediate → Safe Deceleration → Safe
Motor 2	No torque	Acceleration → Unsafe Intermediate → Unsafe Deceleration → Safe
Spring $K1$	Breakage	Acceleration → Safe Intermediate → Safe Deceleration → Safe
Spring $K2$	Breakage	Acceleration → Marginally unsafe Intermediate → Safe Deceleration → Safe
Spring $K1' \wedge K2'$ (preloading linear springs)	Breakage	Acceleration → Safe Intermediate → Safe Deceleration → Safe

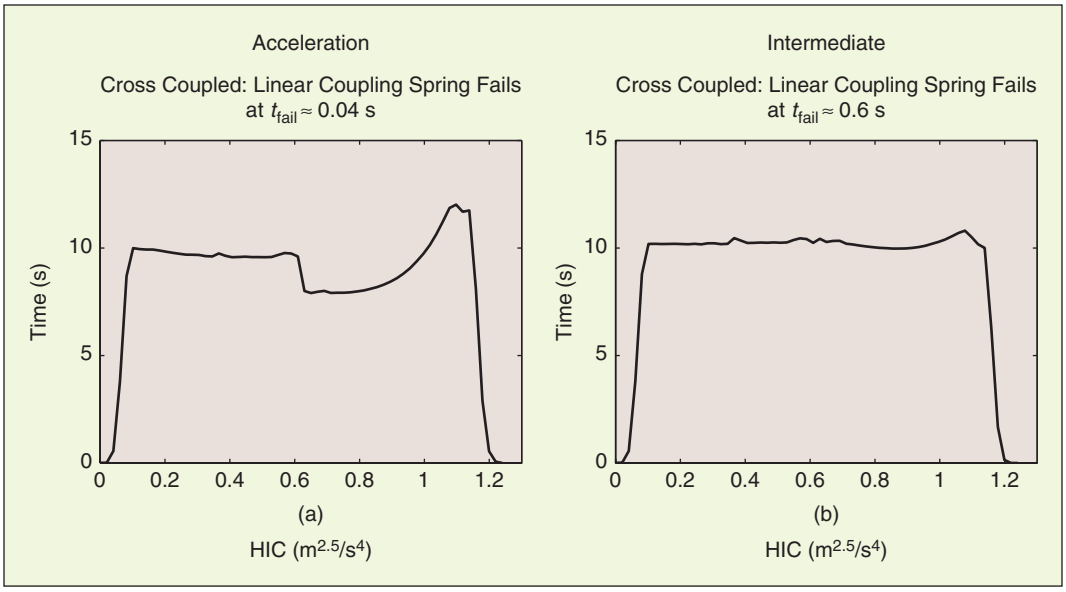

Figure 7. *Simulation results corresponding to failures of the coupling elements in a cross-coupled AA arrangement. HIC values developed with faults injected during (a) acceleration and (b) intermediate phases are shown, indicating a marginal violation of the set value (10 $m^{2.5}/s^4$), which can be tolerated if a suitable safety margin is used.*

unique benchmark for improving the state of art of fault tolerant design as well as in developing tools to master performance, dependability, and safety issues of a robotic structure.

Acknowledgments

We thank Riccardo Schiavi, Giorgio Grioli, Gianluca Boccadamo, Marco Piccigallo, and Giovanni Tonietti for their work on different aspects of the development of VSA actuators. This work was supported by the PHRIENDS Specific Targeted Research Project, funded under the Sixth Framework Programme of the European Community under Contract IST-045359. We are solely responsible for its content. It does not represent the opinion of the European Community and the community is not responsible for any use that might be made of the information contained therein.

Keywords

pHRI, safety, VSA, AA, mechanism, control, FMEA, dependability, reliability, steerability.

References

[1] A. Albu-Schäffer, A. Bicchi, G. Boccadamo, R. Chatila, A. D. Luca, A. D. Santis, G. Giralt, G. Hirzinger, V. Lippiello, R. Mattone, R. Schiavi, B. Siciliano, G. Tonietti, and L. Villani, "Physical human-robot interaction in anthropic domains: Safety and dependability," presented at the 4th IARP/IEEE-EURON Workshop on Technical Challenges for Dependable Robots in Human Environments, Nagoya, Japan, 2005.

[2] A. Avizienis, J. Laprie, B. Randell, and C. Landwehr, "Basic concepts and taxonomy of dependable and secure computing," *IEEE Trans. Depend. Secure Comput.*, vol. 1, no. 1, pp. 11–33, Jan./Mar. 2004.

[3] A. Bicchi and G. Tonietti, "Fast and soft arm tactics: Dealing with the safety–performance tradeoff in robot arms design and control," *IEEE Robot. Automat. Mag.*, vol. 11, no. 2, pp. 22–33, June 2004.

[4] A. Bicchi, S. L. Rizzini, and G. Tonietti, "Compliant design for intrinsic safety: General issues and preliminary design," in *Proc. Int. Conf. Robotic Systems (IROS 2001)*, Maui, HI, 2001, pp. 1864–1869.

[5] A. Bicchi, E. Colgate, and M. Peshkin, "Physical human-robot interaction," in *Springer Handbook of Robotics*, O. Khatib and B. Siciliano, Eds. New York: Springer-Verlag, 2008, ch. 57, pp. 1335–1348.

[6] C. G. Cassandras and S. Lafortune, *Introduction to Discrete Events Systems*. Norwell, MA: Kluwer, 1999.

[7] J. B. Dugan and K. S. Trivedi, "Coverage modeling for dependability analysis of fault tolerant systems," *IEEE Trans. Comput.*, vol. 38, no. 6, pp. 775–787, June 1989.

[8] C. English and D. Russell, "Implementation of variable joint stiffness through antagonistic actuation using rolamite springs," in *Mechanism and Machine Theory*, vol. 34. New York: Pergamon, 1999, pp. 27–40.

[9] R. Filippini, S. Sen, G. Tonietti, and A. Bicchi, "A comparative dependability analysis of antagonistic actuation arrangements for enhanced robotic safety," in *Proc. Int. Conf. Robotics and Automation (ICRA 2007)*, Rome, 2007, pp. 4349–4354.

[10] G. Giralt and P. Corke, Eds., "Technical challenge for dependable robots in human environments," presented at the IARP/IEEE Workshop, Seoul, Korea, 2001.

[11] A. H. C. Goslin and V. Hayward, "Time-domain passivity control of haptic interfaces with tunable damping hardware," in *Proc. World Haptics Conf. 2007*, pp. 164–169.

[12] S. Haddadin, A. Albu-Schäffer, and G. Hirzinger, "Safety evaluation of physical human-robot interaction via crash-testing," presented at the Robotics: Science and Systems Conf. (RSS 2007), Atlanta, 2007.

[13] D. L. Hamilton, I. D. Walker, and J. K. Bennett, "Fault tolerance versus performance metrics for robot systems," in *Proc. IEEE Int. Conf. Robotics and Automation*, 1996, pp. 3073–3080.

[14] J. Heinzmann and A. Zelinsky, "The safe control of human friendly robots," in *Proc. IEEE/RSJ Int. Conf. Intelligent Robots and Systems (IROS'99)*, pp. 1020–1025.

[15] N. Hogan, "Adaptive control of mechanical impedance by coactivation of antagonist muscles," *IEEE Trans. Automat. Control*, vol. 29, no. 8, pp. 681–690, 1984.

[16] A. Hoyland and M. Rausand, *System Reliability Theory: Models and Statistical Methods*, 2nd ed. New York: Wiley, 2005.

[17] J. W. Hurst, J. E. Chestnutt, and A. A. Rizzi, "An actuator with physically variable stiffness for highly dynamic legged locomotion," in *Proc. IEEE Int. Conf. Robotics and Automation*, New Orleans, 2004, pp. 4662–4667.

[18] K. Ikuta, H. Ishii, and M. Nokata, "Safety evaluation method of design and control for human-care robots," *Int. J. Robot. Res.*, vol. 22, no. 5, pp. 281–297, May 2003.

[19] *Functional Safety of Electrical-Electronic-Programmable Electronic Safety Related Systems*, IEC Standard 61508, 1998.
[20] R. Iserman, *Fault-Diagnosis Systems: An Introduction from Fault Detection to Fault Tolerance*. Berlin, Germany: Springer-Verlag, 2006.
[21] *Robots for Industrial Environments—Safety Requirements. Part 1: Robot*, ISO10218-1, 2006.
[22] K. Koganezawa, T. Nakazawa, and T. Inaba, "Antagonistic control of multi-DOF joint by using the actuator with non-linear elasticity," in *Proc. IEEE Int. Conf. Robotics and Automation*, Orlando, May 2006, pp. 2201–2207.
[23] Y. Hirata, A. Hara, and K. Kosuge, "Motion control of passive intelligent walker using servo brakes," *IEEE Trans. Robot.*, vol. 23, no. 5, pp. 981–990, Oct. 2007.
[24] J. Laprie, "Dependability: Its attributes, impairments and means," in *Predictably Dependable Computing Systems*, B. Randell et al. Eds. New York: Springer Verlag, 1995, pp. 3–24.
[25] K. F. Laurin-Kovitz, J. E. Colgate, and S. D. R. Carnes, "Design of components for programmable passive impedance," in *Proc. IEEE Int. Conf. Robotics and Automation*, Sacramento, Apr. 1991, pp. 1476–1481.
[26] D. Logothesis, A. Puliafito, and K. S. Trivedi, "Markov regenerative models," in *Proc. Int. Computer Performance and Dependability Symp.*, Erlangen, Germany, 1995, pp. 134–143.
[27] B. Lussier, R. Chatila, F. Ingrand, M. O Killijian, and D. Powell, "On fault tolerance and robustness in autonomous systems," presented at the 3rd IARP-IEEE/RAS-EURON Joint Workshop on Technical Challenges for Dependable Robots in Human Environments, Manchester, U.K., Sept. 7-9, 2004.
[28] J. McDermid, "Issues in the development of safety critical systems," *Safety-Critical Systems: Current Issues, Techniques and Standards*, F. Redmill and T. Anderson, Eds. London, U.K.: Chapman Hall, 1990, pp. 16–42.
[29] J. S. Mehling, J. E. Colgate, and M. A. Peshkin, "Increasing the impedance range of a haptic display by adding electrical damping," in *Proc. 1st Joint Eurohaptics Conf. Symp. Haptic Interfaces for Virtual Environment and Teleoperator Systems*, 2005, pp. 257–262.
[30] H. J. Merly, P. Prasad, and G. Nusholtz, "Head injury risk assessment for forehead impacts," *SAE Trans.*, vol. 15, no. 6, pp. 26–46, 1996.
[31] T. Morita and S. Sugano, "Robot arm equipped with mechanical impedance adjuster," in *Proc. IEEE/RSJ Int. Conf. Intelligent Robots and Systems*, 1995, vol. 1. pp. 407–412.
[32] M. Okada, Y. Nakamura, and S. Ban, "Design of programmable passive compliance shoulder mechanism," in *Proc. IEEE Int. Conf. Robotics and Automation*, Seoul, Korea, 2001, pp. 348–353.
[33] OSHA Technical Manual. *Industrial Robots and Robot System Safety* [Online]. Available: http://www.osha.gov/dts/osta/otm/otm_iv/otm_iv_4.html
[34] *Draft Standard for Trial Use for Intelligent Assist Devices—Personnel Safety Requirements*, Robotic Industries Association, T15.1, 2002.
[35] R. Schiavi, G. Grioli, S. Sen, and A. Bicchi, "VSA-II: A novel prototype of variable stiffness actuator for safe and performing robots interacting with humans," presented at the IEEE Int. Conf. on Robotics and Automation, Pasadena, CA, May 2008.
[36] K. W. Hollander and T. G. Sugar, "Design of lightweight lead screw actuators for wearable robotic applications," *ASME J. Mech. Des.*, vol. 128, no. 5, pp. 644–648, 2006.
[37] G. Tonietti, R. Schiavi, and A. Bicchi, "Design and control of a variable stiffness actuator for safe and fast physical human/robot interaction," in *Proc. IEEE Int. Conf. Robotics and Automation (ICRA 2005)*, pp. 528–533.
[38] K. S. Trivedi, G. Ciardo, M. Malhotra, and R. Sahner, "Dependability and performability analysis," in *Performance Evaluation of Computer and Communication Systems* (Lecture Notes in Computer Science), L. Donatiella and R. Nelson, Eds. New York: Springer-Verlag, 1993, pp. 587–612.
[39] K. S. Trivedi, *Probability and Statistics with Reliability, Queuing and Computer Science Applications*, 2nd ed. New York: Wiley, 2002.
[40] K. T. Ulrich, T. T. Tuttle, J. P. Donoghue, and W. T. Townsend, "Intrinsically safer robots," Barrett Technology Inc., Final Report NASA Contract NAS10-12178, 1995.
[41] J. Versace, "A review of the severity index," presented at the Stapp Car Crash Conf., 1971, Paper SAE 710881.
[42] M. L. Visinsky, J. R Cavallaro, and I. D. Walker, "A dynamic fault tolerance framework for remote robots," *IEEE Trans. Robot. Automat.*, vol. 11, no. 4, pp. 477–490, Aug. 1995.
[43] J. Yamaguchi, S. Inoue, D. Nishino, and A. Takanishi, "Development of a bipedal humanoid robot having antagonistic driven joints and 3-DOF trunk," in *Proc. IEEE/RSJ Int. Conf. Intelligent Robots and Systems*, Victoria, Canada, 1998, pp. 96–101.

Roberto Filippini received the Laurea degree in computer engineering in 2000 and his Ph.D. degree in automatics, robotics, and bioengineering from the University of Pisa in 2006. He worked in the Centro Interdipartimentale di Ricerca E. Piaggio, Pisa, and CERN, Geneva, where he contributed to the dependability analysis of the Large Hadron Collider machine protection system. Currently, he is at the Paul Scherrer Institut in Switzerland. His research interests include dependability modeling and probabilistic safety assessment of safety-critical systems.

Soumen Sen received his bachelor's degree in mechanical engineering from the National Institute of Technology, Durgapur, India, in 1992 and his master's degree in production technology and robotics from Jadavpur University, Kolkata, India, in 1994. He worked with the Department of Atomic Energy, Government of India, for more than nine years. He served in the Centre for Advanced Technology, Indore, where he was involved in the design activities for development of a large particle accelerator, and, subsequently, in Bhabha Atomic Research Centre, Mumbai, where he worked on robotics for nuclear applications and multifingered grasping and manipulation. In August 2005, he joined the Centro Interdipartimentale di Ricerca E. Piaggio, Pisa, Italy. Currently, he is pursuing a Ph.D. program in automation, robotics, and bioengineering at the University of Pisa. His research activity concerns pHRI and its associated design and the development of robots and robot components.

Antonio Bicchi is a professor of automatic control and robotics at the University of Pisa. He graduated from the University of Bologna in 1988 and was a postdoctoral scholar at the Artificial Intelligence Lab, Massachusetts Institute of Technology, from 1988–1990. His main areas of research include dynamics, kinematics, and control of complex mechanical systems including robots, autonomous vehicles, and automotive systems; haptics and dexterous manipulation; theory and control of nonlinear systems, in particular, hybrid (logic-dynamic, symbol-signal) systems. He has edited and published more than 200 papers in international journals, books, and refereed conferences. Currently, he serves as the director of the Interdepartmental Research Center E. Piaggio of the University of Pisa. He is a Fellow of the IEEE and chair of the conference editorial board for the IEEE Robotics and Automation Society (RAS). He has served as past vice-president for Member Activities, IEEE RAS, Distinguished Lecturer, and editor for several scientific journals including *IEEE Transactions on Robotics and Automation*. He chaired the First World Haptics Conference in 2005 and the Hybrid Systems: Computation and Control Conference in 2007.

Address for Correspondence: Antonio Bicchi, Interdepartmental Research Centre E. Piaggio, University of Pisa, 56126 Pisa, Italy. E-mail: bicchi@ing.unipi.it.

Series Compliance for an Efficient Running Gait

©PUNCHSTOCK

Lessons Learned from the Electric Cable Differential Leg

BY JONATHAN W. HURST AND ALFRED A. RIZZI

Digital Object Identifier 10.1109/MRA.2008.927693

Many robots excel at precise positioning and trajectory tracking using software control, and most successful robotic applications use this ability—examples include computer numeric control (CNC) machining, robotic welding, painting, and pick-and-place circuit board assembly. The mechanical design of these robots focuses on rigid transmissions and minimizing compliance in the structure so that the software controller can accurately track a desired position as a function of time, regardless of any disturbance forces. However, there is a class of tasks for which rigid actuation is not ideal: physical interaction with the world, especially interaction that involves an impact or kinetic energy transfer. Animals tend to excel at these tasks and far outperform the best robots. Examples include walking, running, catching a ball, gripping a piece of fruit firmly but without causing damage, and many types of assembly tasks.

For dynamic behaviors such as running, the performance limitations of a robot are often due to limitations of the mechanical design. A robot is an integrated system of electronics, software, and mechanisms, and each part of the system limits or enables the behavior of the whole. While some behaviors can easily be implemented through simple actuators and direct software control, a running machine requires a mechanical design that is specialized for the task. Among other things, physical springs are essential for a robust and efficient running gait, to store energy, provide high mechanical power, and overcome bandwidth limitations of traditional actuators. An ideal kinematic design, where the joints and links are perfectly sized and placed for the desired task, and motors that exceed the force and speed requirements of the task are not sufficient for successful dynamic interactions. Inertia, transmission friction, and other dynamic effects have a significant role on the behavior of a running robot.

We are building running and walking machines with a focus on the mechanical design to enable efficient and robust gaits. The defining characteristic of a running gait is spring-like behavior; all running animals, from small insects to large mammals, exhibit a center-of-mass motion that resembles a bouncing ball or a pogo stick. The spring-like behavior is implemented with the assistance of physical springy elements, such as tendons, and not entirely through software or neural control. Energy cycles back and forth between the ballistic trajectory of the body and the compression of the leg spring. To exhibit this behavior, our robots incorporate a mechanical spring that is tuned to absorb and release the energy of a running gait at the appropriate frequency. Electric motors act in series with this spring to add or remove energy from the cycle to modify or control the running gait.

Our first prototype machine is a single actuator mounted to a bench, called the actuator with mechanically adjustable series compliance (AMASC). The stiffness and the no-load position of the joint are mechanical configurations that can be independently adjusted using two separate motors, and it is a test platform to

1070-9932/08/$25.00©2008 IEEE

verify and refine several design ideas for leg joints of running and walking robots. After significant testing and design revision, we incorporated the ideas behind the AMASC into the design of a full bipedal robot, the biped with mechanically adjustable series compliance (BiMASC). A single leg prototype of the BiMASC was constructed and tested, and after some final revisions, we have built the electric cable differential (ECD) leg (Figure 1). The ECD leg derives its name from the construction—using electric motors, cable drives, and mechanical differentials to actuate the system. One ECD leg, named Thumper, was assembled as a monopod and installed in our laboratory at the Robotics Institute to study the role of compliance in running gaits. Two ECD legs were assembled as a biped named MABEL, which is installed in Prof. Jessy Grizzle's laboratory at the University of Michigan and will serve as a platform to explore an advanced feedback control theory for legged locomotion [31].

In this article, we discuss some earlier legged machines, explain some of the limitations of traditional actuation systems, and explain why mechanical springs are essential for a running gait. Not any arbitrary spring will help; the spring must be designed specifically for the task, and the "Tuned Spring: Stiffness Adjustment" section provides further details about the methods for creating a specific desired spring behavior that can be tuned as the environment changes. Finally, we discuss the lessons learned from the construction and testing of AMASC and BiMASC and explain the revisions to the final ECD leg, which eliminate the mechanically adjustable compliance.

We are building running and walking machines with a focus on the mechanical design to enable efficient and robust gaits.

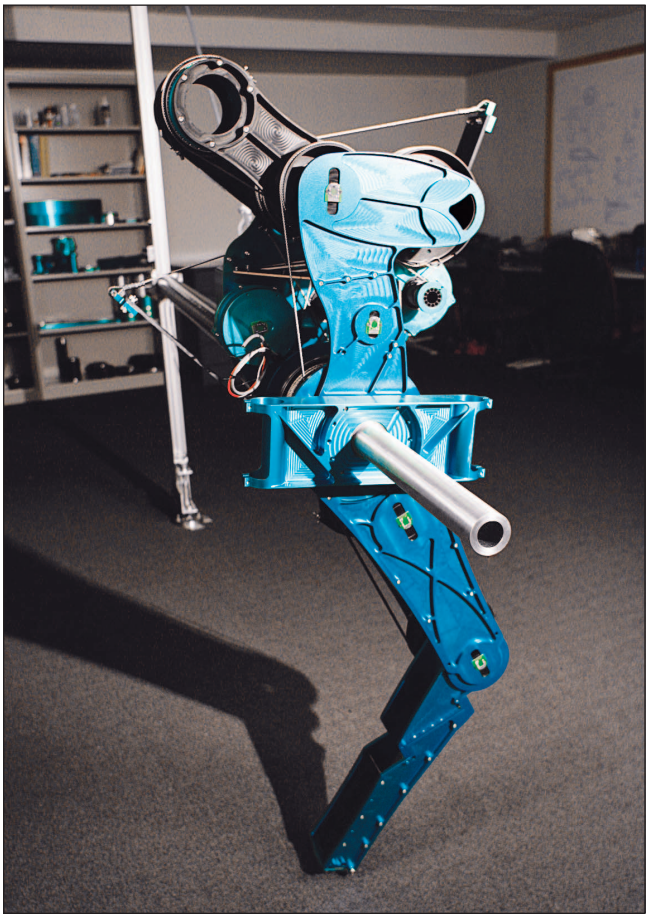

Figure 1. *Thumper, the monopod ECD leg. Fiberglass bar springs are at the front and back of the body, but they act in series between the leg length motor and the actual leg length. A bipedal version, MABEL, is installed in Prof. Jessy Grizzle's laboratory at the University of Michigan.*

Background and Previous Work

A common theme among all runners is spring-like behavior. Runners follow an approximate center-of-mass motion similar to that of a bouncing ball. Spring-mass models such as the spring-loaded inverted pendulum (SLIP) model have been developed as a tool to describe this center-of-mass motion [1]–[3]. Our spring-mass model is shown in Figure 2.

All running animals, and most running robots, store mechanical spring energy during a running gait [4]–[7]. The basic definition of running is linked to the use of leg springs, as depicted in the SLIP model—energy is transferred from kinetic energy in the flight phase to spring energy in the stance phase and vice versa [8].

Many robots have been built for the purpose of walking and running. There are generally two classes: robots that use mechanical springs to store and release kinetic energy during

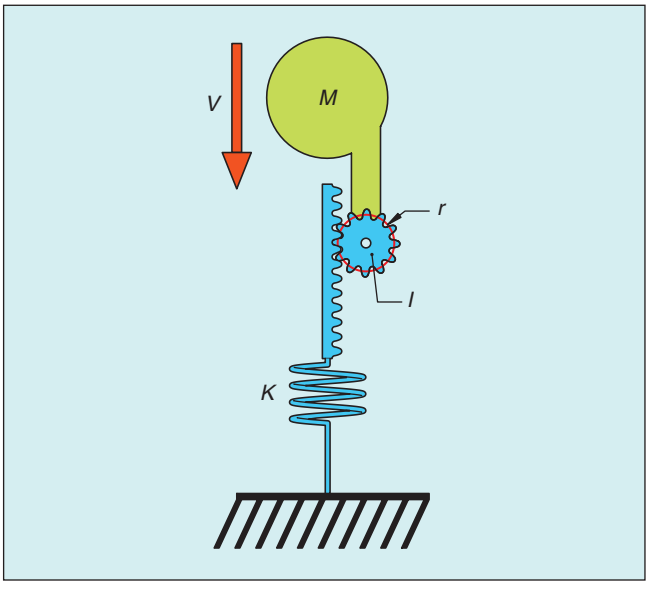

Figure 2. *Our spring-mass model for running, similar to the SLIP model, but incorporating physically realistic actuator dynamics such as motor inertia. The motor, with inertia I and speed reduction r, can actuate the spring to excite a regular vertical oscillation to hop off the ground, much like a person on a pogo stick.*

Runners follow an approximate center-of-mass motion similar to that of a bouncing ball.

a running gait, much like animals, and robots that rely on software control to implement all behaviors. The planar biped, built at the Leg Laboratory during its Carnegie Mellon days, is an example of a spring-mass robot, using air springs for energy storage [9]. This robot could also adjust the preload of air pressure in the cylinder that affects the leg stiffness. [Marc Raibert founded the Leg Laboratory at Carnegie Mellon University in 1979–1980. Raibert and the Leg Laboratory moved to Massachusetts Institute of Technology (MIT) in 1986.] The planar biped was capable of high-performance behavior such as front flips, because it was tethered to a large hydraulic compressor and air compressor. In contrast to the high power of many of the Leg Laboratory machines, both the Bowleg Hopper from Carnegie Mellon University and the ARL Monopod II from McGill University have defensible claims to being the most efficient running robots [10], [11]. Both gain their efficiency by using leg springs to effectively store and release energy during each stride, and so the electric motors do relatively little work during a normal running gait.

The MIT Leg Laboratory's Spring Flamingo does use springs but not for energy storage. The springs on the MIT-series elastic actuator (MIT-SEA) are primarily for force sensing and mechanical filtering purposes [12], [13]. The springs of an MIT-SEA are essentially a soft load cell, acting as a force sensor for the low-level controller. At low frequencies, the MIT-SEA acts as a more sensitive and robust force actuator than a gear motor and a load cell.

Recent bipeds that can change the stiffness of their joints have also been constructed [14], [15]. They have successfully walked, but they are not designed for running and are similar to the MIT-SEA in that they do not store significant amounts of energy in their springs. Additionally, when using pneumatic actuators for the joint stiffness control [15], the resulting system can be difficult to model and control precisely.

Robots with rigid transmissions, such as RABBIT and Asimo, do not use springs and are examples of machines that attempt to create all dynamics through software control [16], [17]. This is an important difference. If these robots are capable of an aerial phase, it is only at the expense of great motor power output and high energetic cost, with relatively unpredictable dynamic behavior at ground impact. Furthermore, the response of such machines to a disturbance, such as a slightly raised or lowered ground surface, will vary dramatically from that of an animal due to the fundamental mechanical differences.

Actuators for Running

While a general-purpose actuator would provide ideal flexibility for software controller development on a running robot, all actuators have natural dynamics that can limit the authority of the software controller. The mechanical system, unlike the software controller, cannot be easily modified and changed once it is built. Therefore, the best approach is to begin the robot design with a specification for the dynamic behavior of the machine. In other words, many aspects of the control should be designed before any mechanical system is created so that the natural dynamics of the actuator can assist and enable the behavior of the machine rather than impose hard limits.

Although several successful running and walking machines have used pneumatic and hydraulic power, most designers opt for the simplicity and robustness of electric motors [18], [19]. Pneumatics have limitations on the control rate due to small tubes and valves and limitations on the power supply, especially for untethered machines. However, we do not discuss the details of pneumatic actuators. Hydraulic actuators have many limitations similar to that of electric gearmotors, and also power supply limitations similar to that of the pneumatic actuators. Most of the discussion in this article can be applied to hydraulic actuators, but we discuss electric motors primarily.

Electric Gearmotors and Inelastic Collisions

A simple design for a legged robot would involve the use of an electric gear motor at each joint. Several groups have built bipedal robots using this design, and some intended to make the robots run as well as walk. The problem with this approach to running is that most of the kinetic and potential gait energy is lost, with each hop, to an inelastic collision with the ground.

A spring-free, gear motor–actuated running robot is represented in Figure 3(a). Because there is no physical spring, all behaviors of the leg must be exhibited by the software through the motor. The entire mass of the robot (including the mass of the motor) is represented by M, and the leg is assumed to be massless. However, the rotational inertia of the motor cannot be lumped into the overall mass of the robot; it is represented by the variable I, and after the rotational inertia of the motor is converted to linear inertia by the conversion ratio r, the overall reflected inertia at the joint of the robot is $\frac{I}{r^2}$. For a typical harmonic-drive gear motor on a humanoid robot, the resulting reflected motor inertia can approach that of the robot mass, M.

Because the rotor inertia and the robot mass are uncoupled, the robot leg may be moved to the ground without affecting the model, as shown in Figure 3(b). The rotor begins at rest, and after collision, acquires some speed that matches that of the mass. If the kinetic energy just prior to impact is represented as T_0, the rotor inertia is represented as I, the conversion from rotational to linear motion is represented by a fictional pulley radius r, and M is the robot's total mass, then the energy lost to an impact is

$$T_{\text{loss}} = \frac{I}{Mr^2+I}\,T_0$$

and the remaining energy, stored in the downward motion of the robot and the rotation of the motor is

$$T_{\text{final}} = \frac{Mr^2}{Mr^2 + I} T_0.$$

If the effective inertia of the motor rotor (I/r^2) is the same as the robot's mass, then half the kinetic energy from flight will be lost to the inelastic collision. This estimate is in the best of situations, assuming absolutely no friction or losses in the transmission. For a realistic system, any energy remaining after the collision must be converted through the motor and transmission inefficiencies, which are compounded when energy must pass into the system and then out. In effect, very little energy can be recovered.

Adding Series Springs

Minimizing the reflected inertia of the motor can reduce the energy lost to inelastic collisions, but it is difficult to create a motor with sufficiently low reflected inertia that can still apply sufficient torque. Alternatively, a series spring can be used to decouple the motor inertia and the load inertia, eliminating the inelastic collision and the associated energy loss during impacts. Both methods are used in force-control applications [20]–[23], which are similar in many ways to the implementation of a spring rate.

An SEA may be much more effective than a standard gear motor at creating spring-like behavior, even when the physical spring is of a different stiffness than that of the desired behavior. In this case, the software must control the motor so that the overall system exhibits the desired total spring rate. In the ideal scenario of an inertia-free rotor, a proportional controller will behave like a spring, creating two springs in series—a software spring and a physical spring, as shown in Figure 4(a). This is relatively simple to analyze and provides a conservative estimate of energy use and power output due to the assumption of no inertia. Therefore, for the sake of argument, further analysis will assume perfect force control of a massless rotor, providing an ideal software spring in series with a physical spring.

Power Density of a Series Spring System

In a cyclical system, such as a hopping spring-mass system, energy is transferred from external sources (kinetic energy of motion or potential energy of height) to internal sources (physical spring energy or chemical battery energy) and vice versa, repeatedly. This transfer of energy is represented in Figure 4(b), where the energy may go into and out of the physical spring as an energy storage element (compression and extension) or through the physical spring merely as a power-transmission element (the spring translating with no deflection). The power output will be divided between the software spring and the physical spring, depending on their stiffnesses.

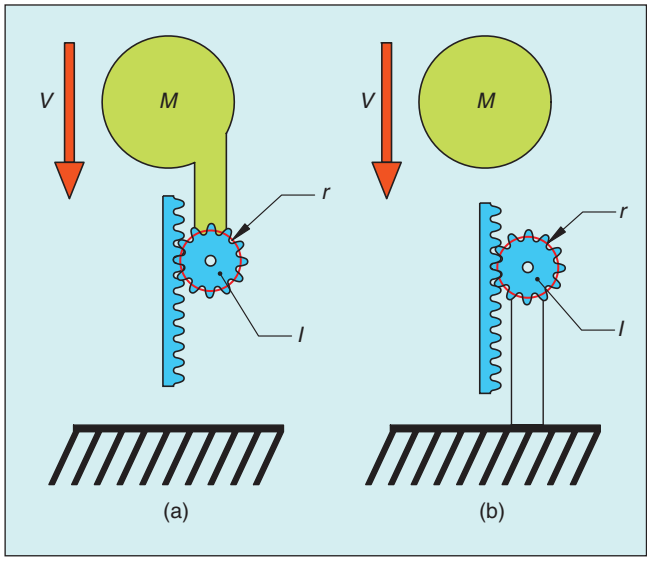

Figure 3. *Figures representing the mass-spring model, with the physical spring removed. The inertia of the motor is represented by I, the mass of the robot by M, the conversion from motor angular velocity to linear velocity by a fictional pulley radius r, and the velocity of the robot just before collision by V. (a) Mass-spring model without a spring. (b) The inertias separated but still in the same collision model.*

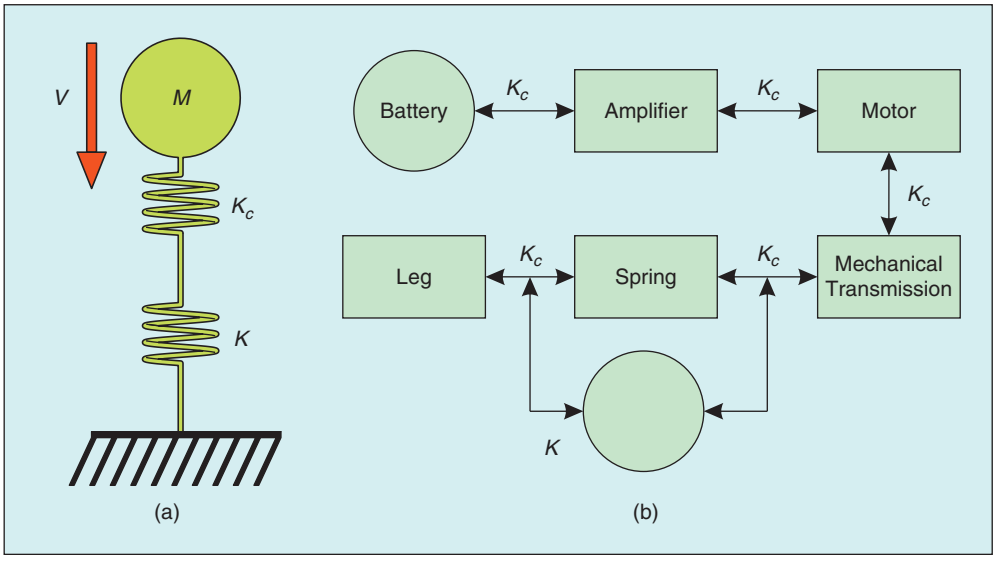

Figure 4. *Assuming an inertia-free actuator, the software controller can simulate a spring K_c. Acting in series with the physical spring K, the energy will flow into one or the other depending on the ratio of the stiffnesses. (a) Our spring-mass model, with software spring rate K_c and hardware spring rate K. (b) Energy flow diagram: K_c represents the energy path of the stiffness behavior implemented through software control; K represents the mechanical spring stiffness.*

A robot is a unified dynamic system comprising electronics, software, and mechanical components.

If the series spring system is deflecting at some rate, the power output attributed to the software spring, P_{K_c}, is

$$P_{K_c} = \frac{K}{K_c + K} P(t),$$

where $P(t)$ is the total power output of both springs in series, K_c is the proportional gain of the computer controller, and K is the physical spring constant. If the physical spring is perfectly tuned to match the desired stiffness, the software spring K_c becomes infinitely stiff, and it can be seen from the equation that the motor (exhibiting the software spring) exerts zero shaft power.

Because springs have higher power density than electric motors, it makes sense to design a system such that the physical spring transfers as high a proportion of the power as possible. A physical spring can have nearly infinite power density, depending on its stiffness; therefore, a comparison between the power density of a spring and that of a motor must be made in the context of an application. Choosing reasonable values for a hopping robot of leg stiffness $K = 5{,}000$ N/m, hopping height of $h = 0.25$ m, and robot mass of $m = 30$ kg, the highest power output during stance is approximately 1 kW (root mean square power is 680 W) and the maximum work stored is about 75 J. With an efficient fiberglass spring, such as those used on archery bows that have an energy capacity of around 1,000 J/kg, a 75-g spring can store the required energy and output the desired power. In contrast, a brushless motor that can output 600 W of continuous power (such as the Emoteq Quantum series 3401 [32]) weighs approximately 2.2 kg, almost 30 times the mass of the spring. Adding the necessary electronics and batteries would add to the mass considerably.

Based on this analysis, even ignoring the inertia of the rotor and the inefficiencies of the motor, it is clear that a spring has much higher power density than an electric motor in a cyclic system. This effect has been noticed in the biomechanics community, where experiments have shown that animals use their springy tendons to amplify the power output of their muscles for jumping and running [24], [25]. Recent work also uses the effect of tuned springs to amplify the power output of actuators for prosthetic limb designs [26].

Energy Efficiency of a Series Spring System

Although avoidance of inelastic collisions and power requirements are compelling reasons to use physical springs, the energetic efficiency of a cyclic system is also improved through the use of tuned physical springs. Again referring to Figure 4(b), energy can be stored and returned through the mechanical spring or through the batteries, which must first convert the mechanical energy to electrical, electrical to chemical, and back again. Assuming an overall efficiency of the spring energy storage e_k and an overall efficiency of energy storage through the motors and batteries of e_c, and given the previous assumptions of a perfect software spring K_c and an inertia-free rotor, spring constant K, and leg deflection x, the equation for energy returned is

$$E_{\text{ret}} = \frac{K_c}{2(K + K_c)} K x^2 e_k + \frac{K}{2(K + K_c)} K_c x^2 e_c.$$

Because springs can store and return energy more efficiently than an electric motor system, it makes sense for the physical spring stiffness to be as close to the desired spring stiffness as possible. If our assumption of zero rotor inertia is false, as in any real system, then the motor must transmit power to change the momentum of the rotor, and it will expend more energy than in this idealized example.

Tuned Spring: Stiffness Adjustment

For an oscillating mass-spring system, such as a running machine, matching the natural frequency of the mechanical system to the desired stride frequency will minimize the required motor power. In other words, a robot or animal of a particular size may have an optimal leg stiffness to minimize the amount of effort required to run. However, the optimal leg stiffness will change as the desired gait changes or as the environment changes. Observations from nature tell us that animals do adjust their leg stiffness in various situations, but we do not have a conclusive answer as to the specific strategy they use or how they do it.

There are a variety of ways to create stiffness behavior in robotic systems, and a variety of ways to adjust the stiffness on the fly. The most common approach is to simulate spring behavior using an actuator and a feedback sensor, such as an electric motor or a hydraulic actuator with a force sensor. As discussed, this method has drawbacks with bandwidth limitations, power limitations, and energy efficiency for realistic actuators. In the absence of a perfect actuator free of all dynamics or limitations, the best way to create spring-like behavior is to use a physical spring in some way.

When designing an actuator that incorporates physical springs, there are several ways to adjust or tune the spring stiffness to suit a particular task. There are a range of mechanical solutions, which use linkages, transmissions, or clutches to adjust stiffness. Cocontraction of antagonistic springs is a biologically inspired approach and the basis for the AMASC and BiMASC designs. After extensive experimentation, we found that this method of stiffness adjustment has significant drawbacks for running gaits, mostly due to the additional mechanical complexity and the reduced energy storage capacity of the springs. More promising for this particular application is a hybrid active-passive approach, where a physical spring is tuned for the standard running gait, and a series motor actively adjusts the spring forces for gait changes or other nonstandard behaviors.

Cocontraction of Antagonistic Nonlinear Springs

A popular method of stiffness adjustment is the cocontraction of antagonistic springs as shown in Figure 5. Animals have this capability, and most robotic devices with variable stiffness use this method [9], [27], [28]. With two springs opposed across a single joint, the deflection of the joint, x, compresses one spring while relaxing the other. Cocontraction of the springs, p, compresses both springs. For the cocontraction to affect the joint stiffness, the springs must be nonlinear. For the simple example of quadratic springs, the force on each spring is

$$F_1 = K(p + x)^2$$
$$F_2 = K(p - x)^2,$$

and the combined force on the joint is

$$F = F_1 - F_2 = 4Kpx,$$

where the cocontraction can be considered as part of the spring constant that determines the resultant forces of a joint deflection x.

The obvious drawback for cocontraction is that two actuators are required for a single joint, and they must apply forces to hold a particular stiffness even if no work is done by the joint. This drawback can be minimized by using nonbackdrivable transmissions, mechanical differentials, brakes, and other mechanisms, such that joint work can be done by a large motor, and stiffness adjustment may be accomplished by a small motor with a holding brake. This is the idea behind our first prototype actuation system, the AMASC.

Adjusting Stiffness Behavior: Alternative Methods

Apart from cocontraction of antagonistic springs, the stiffness of a single spring can be adjusted by varying its effective length through some mechanical means. For example, a torsion bar can have a rigid base that rolls up and down the length, immobilizing a variable portion of the spring. A helical spring could have a rigid base that threads up and down the spring, immobilizing more or less of the coil [29], or many springs in parallel can be clutched in and out of the system in some way.

Because stiffness is essentially an energetically conservative force-distance relationship, a continually variable transmission (CVT) in series with a spring would be ideal; the forces could be changed arbitrarily for a particular energy transfer. The knee joint

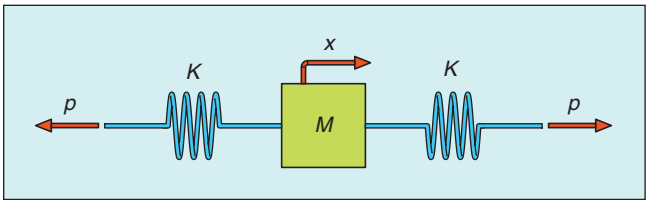

Figure 5. *Two opposing springs in cocontraction across a single linear joint. Spring constant K, joint deflection x, joint load mass M, and cocontraction p.*

One goal of a tuned leg stiffness is to minimize the amount of energy that the motor must use to maintain a constant gait cycle.

in a robot or animal leg can act as a constrained CVT, because the angle of the knee affects the mechanical advantage between the toe forces and the spring deflection. In effect, different knee angles can modify the force profile of the spring. It is not an ideal CVT, because the mechanical advantage cannot be changed arbitrarily, but mechanisms such as a knee can potentially be used to the advantage of a running gait or other dynamic behavior.

In many cases, the stiffness behavior of an actuator with series springs can be modified through active software control. In the example of a spring-mass running robot with a spring and motor in series, the spring undergoes a predictable trajectory based on the body mass and the leg stiffness, and so a preplanned motor trajectory or an other simple controller can be used to modify the overall leg stiffness. In the instance of an unexpected impact, only the passive behavior of the spring will contribute to the toe force, because the inertia of the motor prevents instantaneous acceleration. After the motor begins to accelerate and move, either relaxing or compressing the spring, it can add or remove energy and modify the force profile of the spring, effectively altering its stiffness. The force profile will not be a perfect simulation of a spring due to the inertia of the motor, but this may be of little consequence; it is certainly less problematic than the inelastic collision that exists with no physical spring in series with the motor. More importantly, any active modification of the natural spring oscillation will result in wasted energy by the gearmotor, and so this is a tradeoff to be considered.

Experimental Prototypes: AMASC and BiMASC

The AMASC, shown in Figure 6, was developed as a prototype leg for a running robot [30]. It is a single compliant joint, with two adjustable parameters and two corresponding

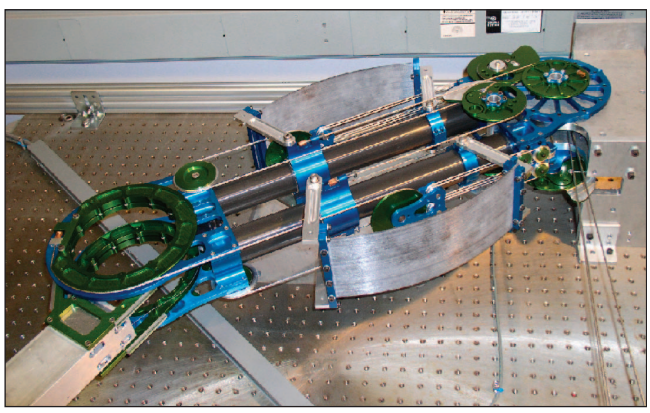

Figure 6. *The AMASC is a prototype leg joint for a running robot.*

motors: joint stiffness and no-load joint position. Two fiberglass springs act as an antagonistic pair, and a mechanical differential allows one small motor to adjust pretension, which corresponds to stiffness, and one large motor to control the no-load joint position. The mechanical system was designed specifically to behave in a dynamically simple manner, such that a basic mathematical model could predict the behavior of the AMASC. After testing through a range of frequencies and forces, the simulated model of the AMASC closely matched the dynamic behavior of the real device.

Based on ideas developed through the construction and simulation of the AMASC, we designed and built a single prototype leg of the BiMASC shown in Figure 7. The design has three degrees of freedom (DoF) per leg: the leg length, leg angle, and leg stiffness. The legs end in small hooves, and the motors are placed in the body to minimize leg mass and more closely emulate a simple SLIP running system. Similar to the AMASC prototype actuator, the BiMASC uses two antagonistic springs and a small braked motor to allow for joint stiffness adjustment. The springs act in series with a large motor, which controls the length of the leg. Another large motor controls the leg angle relative to the body.

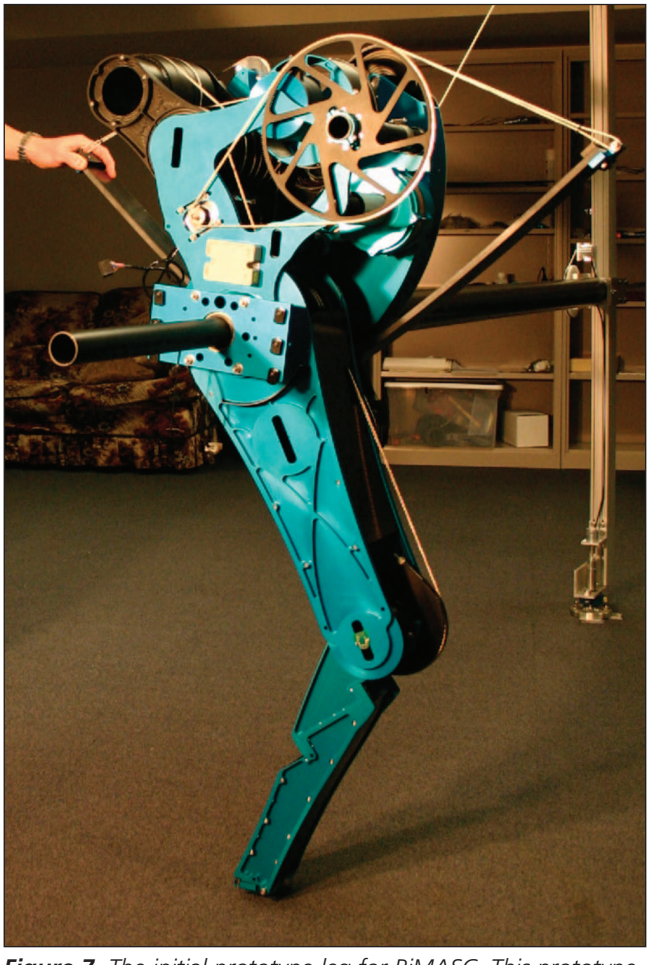

Figure 7. *The initial prototype leg for BiMASC. This prototype used many of the same ideas from the AMASC, including cocontraction of antagonistic springs for stiffness adjustment. Based on the testing of BiMASC, the choice was made to eliminate the mechanically adjustable stiffness and instead use active methods for on-the-fly adjustment of the leg spring behavior on the ECD leg.*

After initial construction of the prototype BiMASC leg, we tested some of the basic functionality. We moved all of the joints through their entire range of motion to verify whether there was any mechanical interference. We tested the robustness of the safety harness and the robot hard stops by lifting the machine in the air and throwing it toward the ground. We locked the motor shafts and manually bounced the robot in place. While most of the test results were encouraging and informative, it became apparent that antagonistic springs have significant tradeoffs. The springs, although physically large and capable of storing significant energy, did not store enough energy as an antagonistic pair to convincingly bounce the robot in the air.

As illustrated in our experiment, there are several effects that can reduce the energy storage capacity of antagonistic springs by nearly an order of magnitude over a single spring of the same size. First, only one of the springs is actually compressing when the joint compresses, halving the potential energy storage, and the other spring is actually relaxing and releasing energy into the compressing spring rather than into the joint. This effect accounts for approximately a factor of three. Additionally, the individual spring deflections are the sum of both the cocontraction and the joint deflection $(p + x)$, and so increasing the cocontraction will reduce the maximum allowable joint deflection if we assume an upper and lower limit on the spring deflection. If the joint stiffness is to be adjusted by a factor of three, for example, then the maximum joint deflection will be three times lower than the case where no stiffness adjustment is required. Combining these two effects, the energy storage capacity of the springs for this example is reduced by a factor of nine. Apart from the reduction in energy storage capacity, using antagonistic pairs of springs increases internal forces beyond the applied joint forces, which increases friction and requires stronger parts. There is also an extra actuator for stiffness adjustment and other additional parts, which add mass and complexity to the system.

There are several ways to affect the stiffness behavior of a running machine, and cocontraction of antagonistic springs is only one method. After implementing the mechanical adjustment with sufficient energy storage for a running gait and observing the complexities of the real system, the costs seem to be higher than the benefits. Although improvements could certainly be made to the mechanical design, the fundamental issues of high internal forces and reduced spring energy storage cannot be overcome but present a useful piece of information for the design of variable stiffness mechanisms.

The ECD Leg

The ECD leg is the final revision of the BiMASC design. We created three copies of the ECD leg: the monopod named Thumper and the biped named MABEL. Similar to the earlier prototypes, the ECD leg uses electric motors, a

cable drive transmission, and mechanical differentials to implement the desired relationships between motors and joints. However, the online stiffness adjustment can be achieved through active software control during the toe's ground contact time and through changes to the knee angle upon landing. The ECD leg has no antagonistic springs and cannot adjust its stiffness mechanically as do the BiMASC or AMASC. For experiments to determine the energy efficiency, the fiberglass springs were swapped between runs. The ECD leg has a lower mass and is mechanically simpler than the BiMASC, which we believe is a worthwhile tradeoff.

Table 1. Parameters for Thumper.

Leg length, fully extended	1 m
Leg length, fully retracted	0.5 m
Leg angle range	±45° from vertical
Robot mass	38 kg
Knee stiffness	512–585 Nm/rad
Motor peak torque	30 Nm
Speed reduction factor between motor and knee	31.5

The ECD leg is designed to behave in a dynamic manner similar to that of the spring-mass model shown in Figure 1 so that the dynamic behaviors can be quantified and controlled. There are two motors—one to control the leg angle and another to control the leg length, with a large spring placed in series between the leg length motor and the actual leg length. The ECD leg has a knee joint, partly to enable human-like walking and partly to incorporate the CVT aspect of an adjustable mechanical advantage during running. The leg ends in a simple rounded hoof, with no articulation or actuation. Parameters and dimensions for the ECD leg are provided in Table 1. Thumper, the single ECD leg at Carnegie Mellon, can sustain a stable hopping gait as shown in Figure 8. We have tested the ability of varying the leg stiffness by actively controlling the set position of the spring as a function of its deflection or by changing leg length on touchdown to increase the mechanical advantage of the knee. Figure 9 shows the change in duty factor or the percent of the gait that the robot spends in the stance phase, as a function of physical leg stiffness or actively modified leg stiffness.

One goal of a tuned leg stiffness is to minimize the amount of energy that the motor must use to maintain a constant gait cycle. We measured the amount of mechanical steady-state work that must be inserted with each vertical hop and found that there is a leg stiffness that minimizes this motor work. In other words, the energetically optimal stiffness maximizes the spring restitution of the machine, as shown in Figure 10. We speculate that this is caused by a balance between energy losses from the inelastic collision of the toe, and energy losses from internal friction of the transmission. Stiffer springs will result in a more forceful impact on the ground and increased losses, whereas softer springs will result in greater spring deflection and correspondingly higher frictional losses through the mechanical transmission.

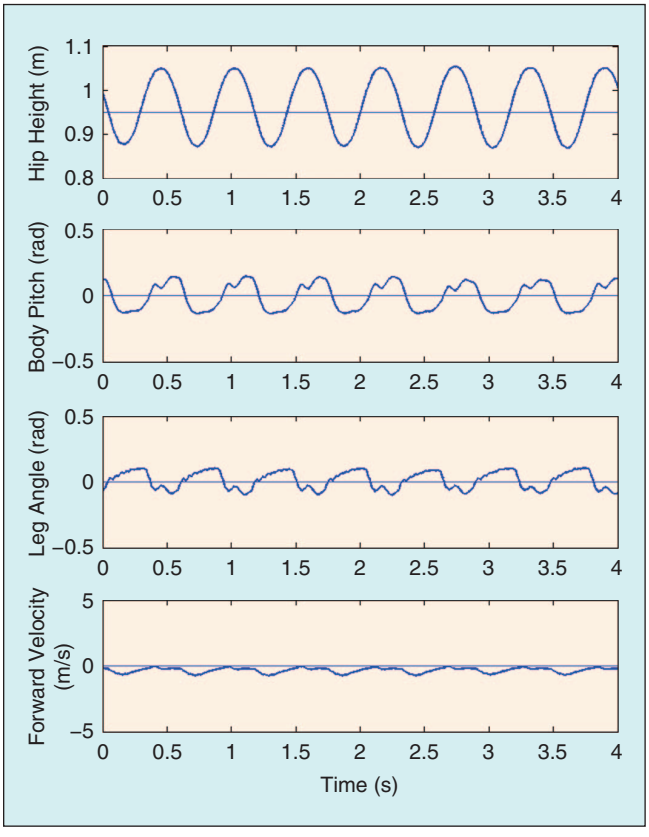

Figure 8. *Data recorded from Thumper, hopping with approximately zero forward velocity. A small time-section of the data has been plotted so that details of the motion are visible, but the rest of the dataset is similar. The length of the leg at full extension is 1 m, but the leg length at touchdown is held at 0.95 m for this experiment. Any values above 0.95 m are an aerial phase of running, while values below 0.95 m are stance phases. The knee stiffness in this experiment was 524 Nm/rad.*

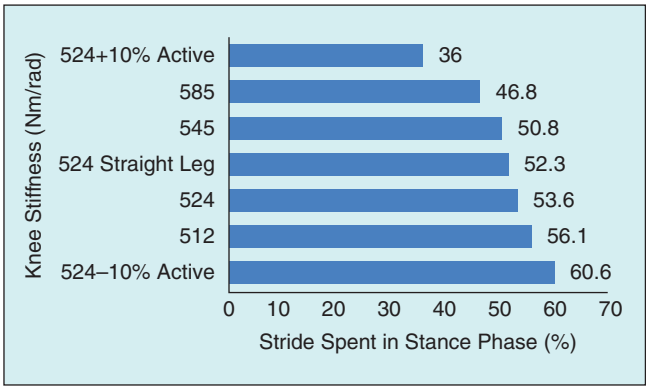

Figure 9. *The duty factor, or percent of gait cycle spent on the ground, as a function of knee stiffness. Although the physical spring acts in the direction of the leg length and is not strictly acting at the knee joint, it is a reasonable simplification. We have chosen to report stiffness in terms of the linear torsional knee spring, because the leg spring is affected by the mechanical advantage of the knee joint and becomes nonlinear.*

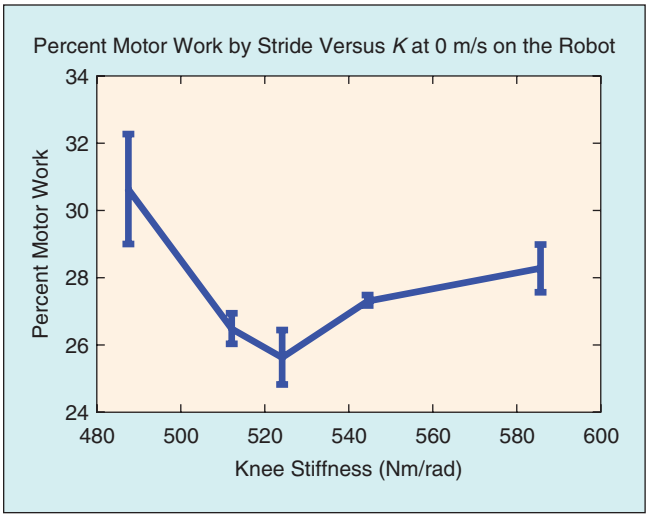

Figure 10. *The percent of mechanical work done by the electric motor during a stance phase, as a function of leg stiffness, while hopping in place. The goal is to minimize this value, which means that the spring is doing the maximum amount of work. Data points in this plot are calculated from ten averaged hops for each knee stiffness, with the standard deviation shown by error bars.*

Discussion

In choosing to remove the adjustable stiffness capability of the BiMASC and the AMASC for the ECD leg revision, we made a subjective engineering decision. The internal forces of the antagonistic springs, along with the additional mechanism associated with our implementation, seemed to have greater costs than the benefits could warrant. Because different engineering implementations may achieve better performance than ours, we cannot conclude that the variable stiffness mechanism is not worthwhile. Our experiments have illustrated some energetic effects of different leg stiffnesses in a real system, and future work could show greater effects for running at speed.

When choosing the leg springs for testing the energy use on Thumper, we first calculated the necessary energy storage capacity based on the mass and the hopping height and verified whether our springs would be physically large enough. After construction of the robot, we tried various different springs to find the one that provided the best subjective running gait. We then ran experiments with springs that were slightly softer and slightly stiffer. The very soft springs resulted in long leg deflections that neared the limits of leg deflection, while very stiff springs resulted in harsh ground impacts that destabilized the gait. We do not believe that it is coincidental that the subjective best leg stiffness also resulted in the best spring restitution for the robot, although the influence of leg stiffness on spring restitution was somewhat weak. The curve in Figure 10 might be much more pronounced for significant forward velocities.

The energy insertion is calculated by measuring the deflection of the motor at each millisecond, and the deflection of the spring at that point in time, which corresponds to the applied force at the motor shaft. By measuring only the mechanical work, we avoid the effects of the motor technology, such as inertia or stall inefficiencies, and the results of our experiments can be compared more easily to robots using other actuation technologies. We also avoid the consideration of a software controller in the calculation of work insertion; the energy can be inserted in a way that is electrically inefficient, using high torques and accelerations, without affecting the results of our experiment. This way, we are certain that the energy savings come from some mechanical effect, such as collision losses or frictional losses.

Thumper has an unexpected preference for running backwards, assuming that the forward direction is a human-like knee bend. In addition, Thumper has some difficulty running very fast, because the leg swing causes a significant body pitch, which destabilizes the machine. In recent experiments, we have added a long bar to increase the rotational inertia of the torso. This modification dramatically improved the Thumper's running performance, allowing as forward running speed of approximately 1.5 m/s. It is our hope that MABEL will be better suited for running without an added torso inertia bar, because the two legs can counter each other's inertia and keep the body relatively stable.

Conclusions

The important message to take from this article is that a robot is a unified dynamic system comprising electronics, software, and mechanical components, and for certain tasks such as running, a significant portion of the behavior is best exhibited through natural dynamics of the mechanism. Therefore, the mechanical system must be specialized for the task and designed with the same care for dynamic control as the software control system.

In constructing the ECD leg, we have attempted to follow this philosophy and design the mechanical system for the specific tasks of walking and running. The prototype actuator, with dynamics verified by testing, exhibited behavior that enabled running in simulation. The ECD leg builds on design revisions from the BiMASC prototype, and the successful experiments with Thumper hopping around the laboratory have proven the ideas and engineering behind the design. Prof. Grizzle's group at the University of Michigan has already demonstrated tentative walking with MABEL, and we expect to demonstrate robust and efficient walking and running gaits in the near future.

Acknowledgments

This work was supported in part by the National Science Foundation (NSF) grant 0413251, through Profs. Matt Mason and Al Rizzi; by NSF grants ECS-0322395 and ECS-0600869, through Prof. Jessy Grizzle at the University of Michigan; and by the Robotics Institute of Carnegie Mellon University.

Keywords

Legged locomotion, actuation, series compliance.

References

[1] W. J. Schwind and D. E. Koditschek, "Characterization of monopod equilibrium gaits," in *Proc. IEEE Int. Conf. Robotics and Automation*, 1997, pp. 1986–1992.

[2] R. J. Full and C. T. Farley, "Musculoskeletal dynamics in rhythmic systems—A comparative approach to legged locomotion," *Biomechanics and Neural Control of Posture and Movement*, J. M. Winters and P. E. Crago, Eds. New York: Springer-Verlag, 2000.

[3] R. Blickhan and R. J. Full, "Similarity in multilegged locomotion: Bouncing like a monopode," *J. Compar. Physiol.*, vol. 173, no. 509, pp. 509–517, 1993.

[4] G. A. Cavagna, H. Thys, and A. Zamboni, "The sources of external work in level walking and running," *J. Physiol.*, vol. 262, no. 3, pp. 639–657, 1976.

[5] G. A. Cavagna, "Elastic bounce of the body," *J. Appl. Physiol.*, vol. 29, no. 3, pp. 279–282, 1970.

[6] G. A. Cavagna, N. C. Heglund, and C. R. Taylor, "Mechanical work in terrestrial locomotion: Two basic mechanisms for minimizing energy expenditure," *Am. J. Physiol.*, vol. 233, no. 5, pp. R243–R261, 1977.

[7] T. A. McMahon, "Mechanics of locomotion," *Int. J. Robot. Res.*, vol. 3, no. 2, pp. 4–28, 1984.

[8] J. R. Hutchinson, D. Famini, R. Lair, and R. Kram, "Are fast-moving elephants really running?" *Nature*, vol. 422, no. 6931, pp. 493–494, 2003.

[9] J. K. Hodgins and M. H. Raibert, "Adjusting step length for rough terrain," in *Proc. IEEE Trans. Robot. Automat.*, vol. 7, no. 3, pp. 289–298, 1991.

[10] M. Ahmadi and M. Buehler, "The ARL monopod II running robot: Control and energetics," in *Proc. IEEE Int. Conf. Robotics and Automation*, 1999, pp. 1689–1694.

[11] G. Zeglin and H. B. Brown, "Control of a bow leg hopping robot," in *Proc. IEEE Int. Conf. Robotics and Automation*, 1998, pp. 793–798.

[12] J. Pratt and G. Pratt, "Exploiting natural dynamics in the control of a planar bipedal walking robot," in *Proc. 36th Annu. Allerton Conf. Communication, Control, and Computing*, 1998.

[13] D. W. Robinson, J. E. Pratt, D. J. Paluska, and G. A. Pratt, "Series elastic actuator development for a biomimetic walking robot," in *Proc. IEEE/ASME Int. Conf. Advanced Intelligent Mechatronics*, 1999, pp. 561–568.

[14] R. V. Ham, B. Vanderborght, B. Verrelst, M. V. Damme, and D. Lefeber, "MACCEPA: The mechanically adjustable compliance and controllable equilibrium position actuator used in the controlled passive walking biped Veronica," in *Proc. 15th Int. Symp. Measurement and Control in Robotics*, 2005.

[15] B. Vanderborght, B. Verrelst, R. Van Ham, M. Van Damme, D. Lefeber, B. M. Y. Duran, and P. Beyl, "Exploiting natural dynamics to reduce energy consumption by controlling the compliance of soft actuators," *Int. J. Robot. Res.*, vol. 25, no. 4, pp. 343–358, 2006.

[16] C. Chevallereau, G. Abba, Y. Aoustin, F. Plestan, E. R. Westervelt, C. C. de Wit, and J. W. Grizzle, "RABBIT: A testbed for advanced control theory," *IEEE Control Syst. Mag.*, vol. 23, no. 5, pp. 57–79, June 2003.

[17] Honda Humanoid Robot ASIMO. (2008). [Online]. Available: http://world.honda.com/ASIMO

[18] M. Raibert, *Legged Robots That Balance*. Cambridge, MA: MIT Press, 1986.

[19] M. Ahmadi and M. Buehler, "A control strategy for stable passive running," in *Proc. IEEE Conf. Intelligent Systems and Robots*, 1995, pp. 152–157.

[20] W. T. Townsend and J. K. Salisbury, "Mechanical bandwidth as a guideline to high-performance manipulator design," in *Proc. IEEE Int. Conf. Robotics and Automation*, 1989, vol. 3, pp. 1390–1395.

[21] T. Kanade and D. Schmitz, "Development of CMU direct-drive arm II," Robotics Inst., Carnegie Mellon Univ., Pittsburgh, PA, Tech. Rep. CMU-RI-TR-85-05, Mar. 1985.

[22] J. D. Schutter, "A study of active compliant motion control methods for rigid manipulators based on a generic control scheme," in *Proc. IEEE Int. Conf. Robotics and Automation*, 1987, pp. 1060–1065.

[23] G. A. Pratt and M. M. Williamson, "Series elastic actuators," in *Proc. IEEE Int. Conf. Intelligent Robots and Systems*, 1995, vol. 1. pp. 399–406.

[24] T. J. Roberts, "The integrated function of muscles and tendons during locomotion," *Compar. Biochem. Physiol. A*, vol. 133, no. 4, pp. 1087–1099, 2002.

[25] A. Seyfarth, R. Blickhan, and J. L. V Leeuwen, "Optimum takeoff techniques and muscle design for long jump," *J. Exp. Biol.*, vol. 203, no. 4, pp. 741–750, 2000.

[26] K. W Hollander, R. Ilg, T. G. Sugar, and D. Herring, "An efficient robotic tendon for gait assistance," *J. Biomech. Eng.*, vol. 128, no. 5, pp. 788–791, 2006.

[27] G. Tonietti, R. Schiavi, and A. Bicchi, "Design and control of a variable stiffness actuator for safe and fast physical human/robot interaction," in *Proc. IEEE Int. Conf. Robotics and Automation*, 2005, pp. 526–531.

[28] J. Yamaguchi and A. Takanishi, "Development of a biped walking robot having antagonistic driven joints using nonlinear spring mechanism," in *Proc. IEEE Int. Conf. Robotics and Automation*, 1997, pp. 185–192.

[29] K. W Hollander, T. G. Sugar, and D. E. Herring, "Adjustable robotic tendon using a jack spring," in *Proc. IEEE Conf. Rehabilitation Robotics*, 2005, pp. 113–118.

[30] J. W. Hurst, J. E. Chestnutt, and A. A. Rizzi, "An actuator with physically adjustable compliance for highly dynamic legged locomotion," in *Proc. IEEE Int. Conf. Robotics and Automation*, 2004, pp. 4662–4667.

[31] E. Westervelt, J. Grizzle, C. Chevallereau, J. Choi, and B. Morris, *Feedback Control of Dynamic Bipedal Robot Locomotion* (Control and Automation Series). Boca Raton, FL: CRC, 2007.

[32] Emoteg Corporation. (2008). [Online]. Available: www.emoteq.com

Jonathan W. Hurst is an assistant professor of mechanical engineering at Oregon State University. He received the B.S. degree in mechanical engineering, the M.S. degree in robotics, and the Ph.D. degree in robotics from Carnegie Mellon University, Pittsburgh, Pennsylvania, in 2001, 2004, and 2008, respectively. His research interests include legged locomotion, natural dynamics, and robot actuation.

Alfred A. Rizzi is a lead robotics scientist at Boston Dynamics, Cambridge, Massachusetts. He is responsible for real-time embedded software development and is an expert in robot control, distributed systems, and system integration. Before joining Boston Dynamics, in 2006, he served as an associate research professor at the Robotics Institute at Carnegie Mellon University, where he directed research on hybrid sensor-based control. He is a corecipient of the Nakamura Prize for the best paper at the IROS 2001 and serves on the editorial board of the International Journal of Robotics Research.

Address for Correspondence: Jonathan W. Hurst, School of Mechanical, Industrial, and Manufacturing Engineering, Oregon State University, 204 Rogers Hall, Corvallis, OR 97331-6001. E-mail: jhurst@cmu.edu.

Powered Ankle-Foot Prosthesis

©PUNCHSTOCK

The Importance of Series and Parallel Motor Elasticity

BY SAMUEL K. AU
AND HUGH M. HERR

Digital Object Identifier 10.1109/MRA.2008.927697

The loss of a limb is a major disability. Unfortunately, today's prosthetic technology is a long way from realizing fully functioning artificial limb replacements. Although lower-extremity prostheses are currently better able to provide assistance than their upper-extremity counterparts, very basic locomotory problems still remain. For example, compared with intact persons, walking amputees require 10–60% more metabolic energy depending on walking speed, physical fitness level, cause of amputation, amputation level, and prosthetic intervention characteristics. Additionally, amputees walk at 11–40% slower self-selected gait speeds than do persons with intact limbs [1]–[7]. Such clinical problems may, in part, be attributed to today's prosthetic ankle-foot designs. Commercially available prostheses comprise spring structures that store and release elastic energy throughout each walking stance period [8], [9]. Because of their passive nature, such prostheses cannot generate more mechanical energy than is stored during each walking step. In distinction, the human ankle performs positive net work and has a greater peak power over the stance period, especially at moderate to fast walking speeds [10]–[14].

A transtibial amputee overcomes these energetic deficiencies by using hamstring muscles to aggressively extend the hip throughout early stance [15]. Hyperactivity in this muscle group causes an excessive flexor moment about the knee, which then has to be canceled by cocontracting knee extensors. Winter and Sienko [15] hypothesized that this increase in muscle cocontraction results in a relatively higher gait metabolism. Another mechanism for the increased metabolic rate of walking amputees may be due to the inability of conventional prostheses to provide sufficient positive power at terminal stance to limit heel strike losses of the adjacent leg [14]–[16].

Several engineering challenges hinder the development of a powered ankle-foot prosthesis [15], [19], [20]. With current actuator technology, it is challenging to build an ankle-foot prosthesis that matches the size and weight of the human ankle-foot complex but still provides sufficient stance-period work and instantaneous power output to propel an amputee. Ankle-foot mechanisms for humanoid robots are often too heavy or not sufficiently powerful to meet the human-like specifications required for a powered prosthesis [21], [22]. Furthermore, a powered prosthesis must be position- and impedance-controllable. Often, robotic ankle controllers follow preplanned kinematic trajectories during walking [21], [22], whereas the human ankle is believed to operate in impedance control mode during stance and position control mode during swing [12]–[14].

A critical objective in the field of prosthetic leg design is to advance a powered ankle prosthesis capable of mimicking the dynamics of the human ankle. Some recent work has focused on the development of quasipassive ankle-foot prostheses. Researchers have built prostheses that use active damping or spring-clutch mechanisms to allow automatic ankle angle adjustment for distinct ground surfaces [8],

1070-9932/08/$25.00©2008 IEEE

[23], [25], [26] or to allow for an improved metabolic walking economy [24]. As these devices do not include an actuator to actively plantar flex the ankle at the terminal stance, no net work is performed throughout each walking step, as is the case with the human ankle [10]–[14].

In 1998, Klute and colleagues [27] were the first to build a powered ankle-foot prosthesis capable of performing net positive work. Their device employed a pneumatic actuation strategy with an off-board power supply. More recent work has focused on the design of energetically autonomous powered systems [28]–[36]. In this article, we review and further develop the ankle-foot design described in [28]–[35]. The article is organized as follows. In the next section, we present biomimetic design goals for the ankle-foot prosthesis, including prosthesis mass, torque, speed, bandwidth, net work, and stiffness. In subsequent sections, we discuss the importance of series and parallel motor elasticity in prosthesis shock tolerance, joint bandwidth, and energy economy. We conclude the article with the physical implementation of our design, including preliminary clinical data addressing the system's capacity to improve amputee gait.

Biomimetic Design Goals

We seek an ankle-foot prosthesis design that is capable of human-like ankle dynamics while still matching the shape and mass of the missing biological limb. Specifically, a biomimetic ankle-foot prosthesis should satisfy the following design specifications.

- *Size and mass*: Prosthesis height should be equal to or less than the nominal height of a conventional high-profile ankle-foot prosthesis, which is 18 cm from the ground to the proximal prosthetic adapter [8], [9]. The desired prosthesis mass should be 2.5% of the total body mass, which is equal to the percent mass of the missing biological limb at a point 18 cm from the ground surface [37].
- *Torque and speed*: The prosthesis should capture the entire torque-speed behavior of the human ankle in walking. The measured peak velocity, torque, and power of the human ankle during the stance period of walking can be as high as 3.6 ± 0.2 rad/s, 1.6 ± 0.2 Nm/kg, and 3 ± 1 W/kg, respectively. Here, both peak torque and power are normalized by body mass. These data are from [11], replotted in Figure 1 in the manner of [20].
- *Torque bandwidth*: The torque bandwidth requirement of the prosthesis was estimated based on the power spectrum of the human ankle torque data during the stance period of walking. The torque bandwidth was defined at that frequency range over which 70% of the total signal power was captured. Analyzing human ankle data from [11], the torque bandwidth was found to be approximately 3.5 Hz, at which the ankle torque varied between 50 and 140 Nm. The torque controller for the prosthesis should therefore be capable of outputting any torque level between 50 and 140 Nm at 3.5 Hz. This goal requires that the torque bandwidth of the open-loop system be significantly larger than 3.5 Hz, otherwise the inherent dynamics of the prosthesis may inhibit the controller's ability to specify the desired dynamics. Thus, an open-loop bandwidth is sought that is at least fivefold larger than the closed-loop bandwidth of 3.5 Hz.
- *Net positive work*: The prosthesis should also be capable of generating net positive work during stance. The average net positive work done at the human ankle per unit body mass for self-selected speed is 0.21 ± 0.05 J/kg [11].
- *Controlled dorsiflexion stiffness*: For the stance phase control, instead of simply tracking human ankle kinematics, it is commonly believed that a powered prosthesis should mimic the human ankle's quasistatic stiffness or the slope of the measured torque-angle curve during stance [12], [13]. Most critically, the prosthesis should output a human-like quasistatic stiffness during controlled dorsiflexion (or from point 2 to point 3 in Figure 1). A target stiffness value was obtained by estimating the slope of the measured human ankle torque-angle curve from the zero torque-angle point to the torque at maximum dorsiflexion (or point 3 in Figure 1). The average human ankle stiffness per unit body mass at a self-selected walking speed is 8 ± 1 Nm/rad/kg.

In this article, we design an ankle-foot prosthesis for a nominal male subject, walking at a self-selected speed of 1.25 m/s, whose body mass, height, and foot length are 78 kg, 175 cm, and 27 cm, respectively [40]. Table 1 lists the parameter values corresponding to the aforementioned design goals.

Shock Tolerance

Designing a motorized leg prosthesis that is robust to shock loads is a critical design challenge, especially at the most distal joint, or the ankle, where impact loads at foot strike have to be carefully managed. Series motor compliance [41]–[43] has been used in humanoid leg design [43] and leg exoskeletal applications [44]–[46] to effectively lower shock loads and protect the motor transmission from damage.

For a prosthetic ankle-foot device, how much series compliance is necessary to protect the transmission from excessive shock loads at heel strike? To answer this question, we employ a linear model of an ankle-foot prosthesis with a series elastic actuator (SEA) (see Figure 2). In the model, the effective mass M_e, linear motor force F_e, and damping b_e are defined as follows: $M_e = I_m R^2$; $F_e = T_m R$; and $b_e = b_m R$. The motor is modeled as a torque source T_m with a rotary internal inertia I_m, applying a force to the series spring k_s through a transmission R. State variables x and θ_m denote the linear and rotary motor displacements, respectively, where $x = \theta_m / R$. The damping term b_m represents motor friction from bearings and brushes. In the model, we assume that the foot is a rigid body of negligible mass, as foot mass is relatively small compared with the effective motor inertia. The equation of motion becomes

$$M_e \ddot{x} + b_e \dot{x} + k_s(x - \mathrm{r}\theta) = F_e. \tag{1}$$

This equation is the standard dynamic equation for an SEA [42], which ignores amplifier dynamics, nonlinear friction, and internal resonances. The series spring force $F_s = k_s(x - r\theta)$ acts at a perpendicular distance $\mathbf{r}$ from the ankle joint. Thus, ankle torque T_{ext} is equal to rF_s.

During the double support phase of nonamputee human walking, the trailing leg performs mostly positive external work on the body's center of mass, whereas the leading leg performs predominantly negative external work. In the human walking study of [47], the negative external work performed during double support was found to increase from 6.5 J at 0.75 m/s to 26.8 J at the maximum walking speed of 2.00 m/s. To determine the series stiffness k_s that adequately protects the transmission, we assume that the prosthesis worn on the leading leg has to absorb all 27 J of energy during ankle-controlled plantar flexion (see Figure 1). (This is a worst case condition since other joint motions are likely to contribute to negative external work production, such as early-stance knee flexion and subtalar joint inversion and eversion.) We simulate this condition by assuming that half the amputee's body mass (0.5 × 78 kg body mass) falls a distance of 7 cm from rest onto the linear SEA prosthesis of Figure 2(b). For this simulated heel strike, the amputee's body mass has 27 J of kinetic energy when the SEA ankle first begins to absorb energy at the instant of touch down. For this simulation, the peak shock load applied to the transmission is determined for each series stiffness value k_s. We assume that the ground reaction force acts at a point 3 cm posterior to the ankle rotational axis, as this is the approximate position of the center of pressure at heel strike [48]. Additionally, in the simulation, a 200-W dc brushless motor (Maxon EC-Powermax 30) is assumed, with rotor inertia $I_m = 30.4\,\mathrm{g/cm^2}$. Motor damping b_e is set equal to 8,250 Ns/m based on experimental measurements in [31]. Furthermore, a ballscrew transmission (Nook ECN-10030-LG, 10 mm × 3 mm) is assumed ($R = 3{,}560$), specifically sized for a nominal male foot size of 27 cm, with a maximum transmission load rating of 5 kN. Thus, the design goal is to select a series spring constant such that the peak shock load applied to the transmission is equal to or less than the maximum transmission load rating of 5 kN.

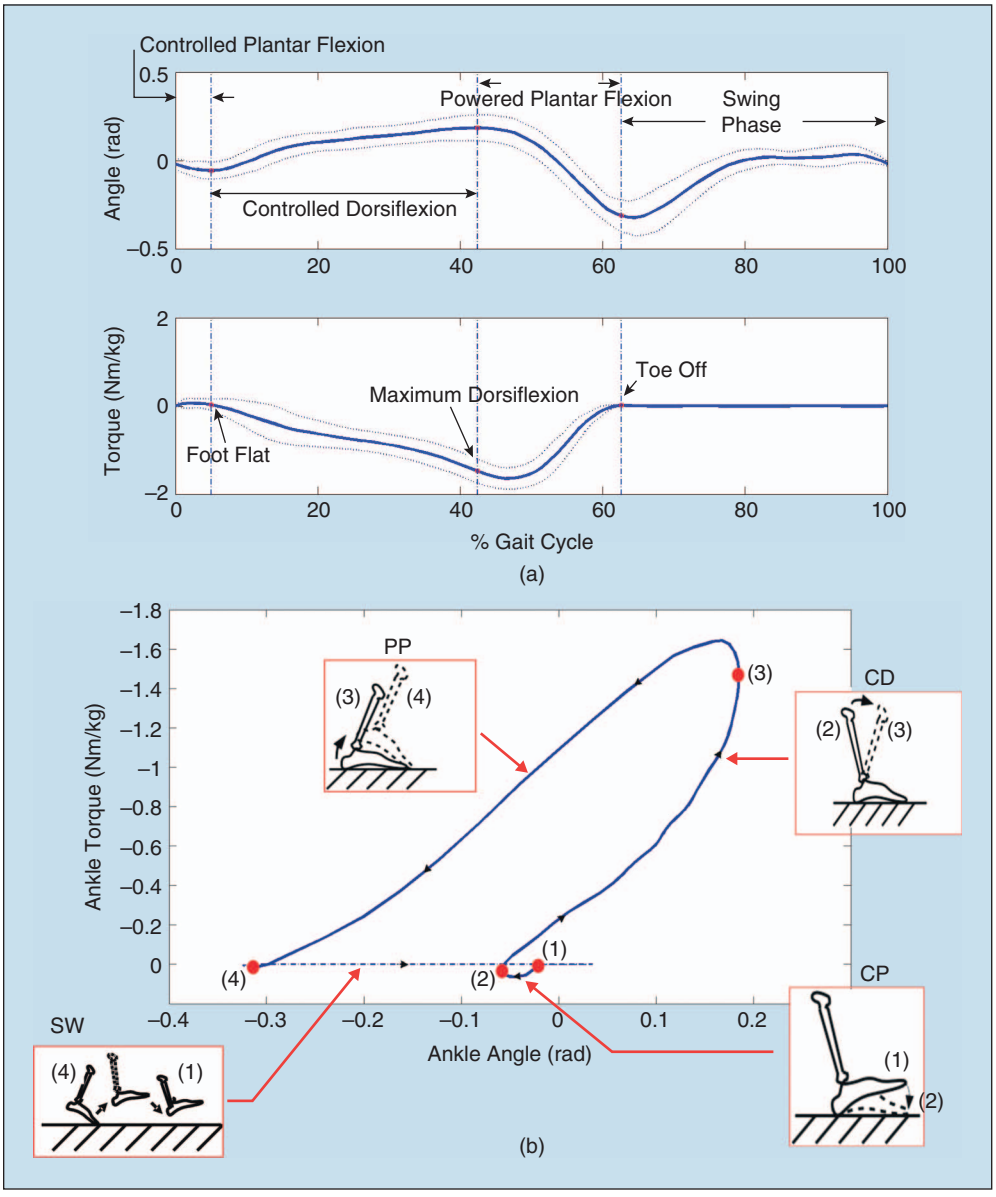

Figure 1. *Human ankle kinematics and kinetics at a self-selected walking speed [9]. (a) Average ankle angle and torque data for 16 study participants are plotted versus percent gait cycle. The dotted lines represent the first standard deviations of the ankle angle and torque data over one gait cycle. One complete walking cycle is shown [from heel strike (0%) to heel strike (100%) of the same leg]. (b) Ankle torque is plotted versus ankle angle. The solid line shows the ankle torque-angle behavior during stance, whereas the dashed line shows the swing phase. Points (1), (2), (3), and (4) denote the gait events of heel strike, foot flat, maximum dorsiflexion, and toe off, respectively. The segments (1)–(2), (2)–(3), (3)–(4), and (4)–(1) represent the ankle torque-angle behaviors during gait phases of controlled plantar flexion (indicated by CP), controlled dorsiflexion (indicated by CD), powered plantar flexion (indicated by PP), and swing phase (indicated by SW), respectively. The area enclosed by points (1), (2), (3), and (4) is the net work done at the joint during stance (or 0.21 J/kg).*

The results are plotted in Figure 3. The gray region indicates the estimated peak shock load applied to the transmission for different series spring constants under different active motor impedances. The

upper boundary denotes the peak load when the motor shaft is held fixed or when linear motor force F_e of (1) is sufficiently large to hold the effective mass M_e at a fixed position. In distinction, the lower boundary is simulated under the condition that the motor moves freely with F_e equal to zero. From Figure 3, we see that a series stiffness value of 600 kN/m results in a peak transmission force approximately equal to the 5-kN load limit of the ball-screw transmission.

Force Bandwidth

When designing a controller, one needs to guarantee that the actuator system does not saturate within the desired operating range of torque and speed. A critical actuator performance metric is the open-loop force bandwidth. As highlighted in the previous section, series compliance improves shock tolerance by limiting shock loads applied to the transmission. However, this advantage comes with a price. Although shock tolerance is improved, because of motor saturation, the open-loop force bandwidth is reduced when a spring is placed in series with the motor and transmission. Thus, when designing a motorized ankle-foot prosthesis, series spring stiffness has to be carefully selected so as to provide adequate actuator shock tolerance and force bandwidth.

In the section "Biomimetic Design Goals," a 17-Hz open-loop torque bandwidth was specified as the lower limit to still allow a prosthetic controller to capture the torque-velocity behavior of the human ankle in walking. For a prosthetic ankle-foot device, what series compliance is necessary to produce at least that bandwidth? To answer this question, we set the ankle angle θ equal to zero, making the equation of motion (1) for this model equivalent to a standard second-order differential equation for a spring-mass-damper system.

With the series spring force F_s considered as the system output, the transfer function that describes the force bandwidth due to the maximum input motor force F_{sat} is

$$\frac{F_s^{\max}}{F_{\text{sat}}} = \frac{k_s}{M_e s^2 + (b_e + \frac{F_{\text{sat}}}{V_{\text{sat}}})s + k_s}, \tag{2}$$

where $F_s^{\max}$ and V_{sat} are the maximum output spring force and linear velocity, respectively. An additional linear damping term, $F_{\text{sat}}/V_{\text{sat}}$, was included in (2) to model the effect of back-electromotive force (EMF) to the motor [42]. This term describes the inability of the amplifier to produce high force (or a loss in motor force) because of the back-emf of the motor. We set $F_{\text{sat}} = RT_{\text{motor}}^{\max}$ and $V_{\text{sat}} = \omega^{\max}/R$, where $T_{\text{motor}}^{\max}$ and $\omega^{\max}$ are the stall torque and maximum angular velocity of the motor, respectively. As can be seen in (2), the

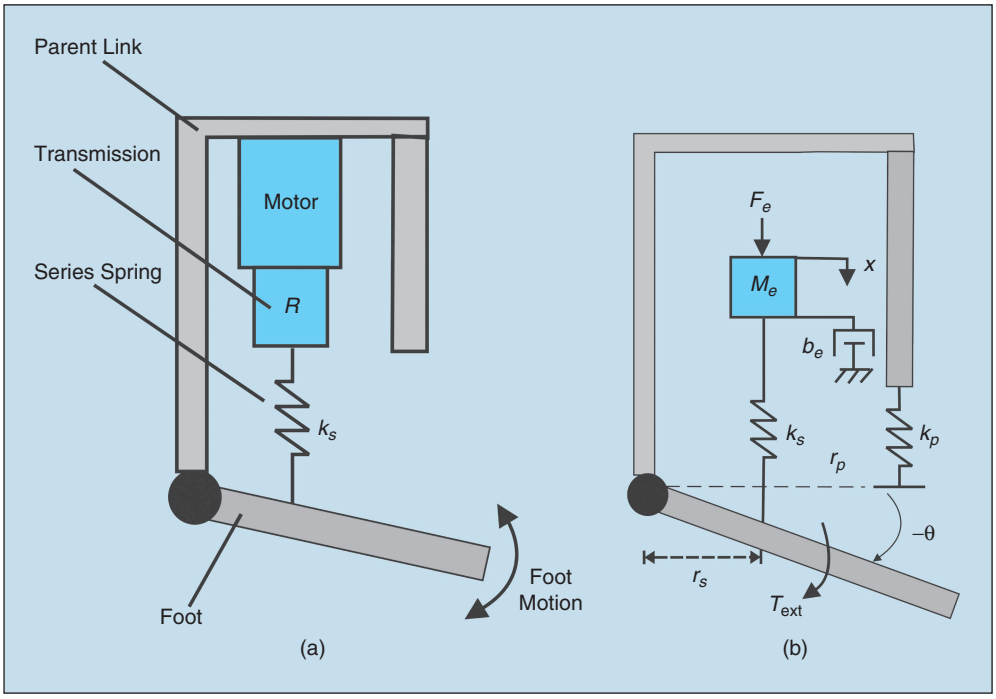

Figure 2. *A powered prosthesis with series elasticity: (a) schematic model and (b) linear model.*

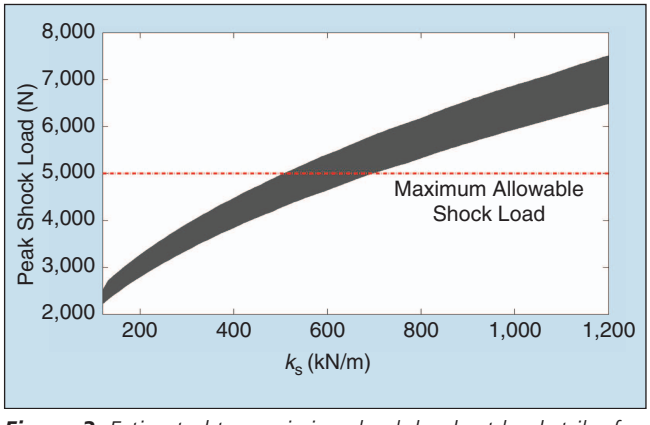

Figure 3. *Estimated transmission shock loads at heel strike for different series spring stiffnesses and active motor impedance levels.*

Table 1. Design specifications for a nominal male subject.

Total prosthetic mass (kg)	2.0
Peak torque (Nm)	125.0
Peak velocity (rad/s)	3.6
Peak power (W)	234.0
Open-loop torque bandwidth (Hz)	17.0
Net work done (J)	16.0
Controlled dorsiflexion stiffness (Nm/rad)	630.0

open-loop bandwidth depends on the intrinsic system behavior determined by the motor, transmission, and series spring. Using the same motor (EC-Powermax 30) and ball-screw transmission ($R = 3{,}560$) employed in the shock tolerance simulations of the previous section, the bandwidth simulation results are plotted in Figure 4. At the peak actuator force (horizontal line at $F_s^{\max}/F_{\text{sat}} = 0.18$), the force bandwidth for three distinct series motor spring stiffnesses, or 120, 600, and 1,200 kN/m, is 0.8, 4, and 8 Hz, respectively. Thus, the greatest series stiffness that offers adequate shock tolerance, or 600 kN/m, fails to provide sufficient bandwidth (bandwidth specification of 17 Hz, see Table 1).

As a resolution to this difficulty, we introduce parallel motor elasticity to the prosthetic architecture. As shown in Figure 5, the parallel spring is unidirectional, meaning that the spring engages only for ankle angles less than zero degrees (ankle dorsiflexed). Parallel elasticity increases the open-loop force bandwidth because force levels borne by the SEA are effectively lowered. By setting the parallel spring stiffness equal to the human-controlled dorsiflexion stiffness (see Table 1, $K_p = 630$ Nm/rad), the peak SEA force becomes $F_s^{\max}/F_{\text{sat}} = 0.023$, increasing the bandwidth to 20 Hz (see Figure 4).

In summary, the maximum level of series stiffness that adequately protects the transmission from damage during heel strike fails to satisfy bandwidth requirements. As a resolution to this difficulty, parallel motor elasticity is used to lower the forces borne by the SEA, increasing force bandwidth to an acceptable level for biomimetic ankle-foot behavior.

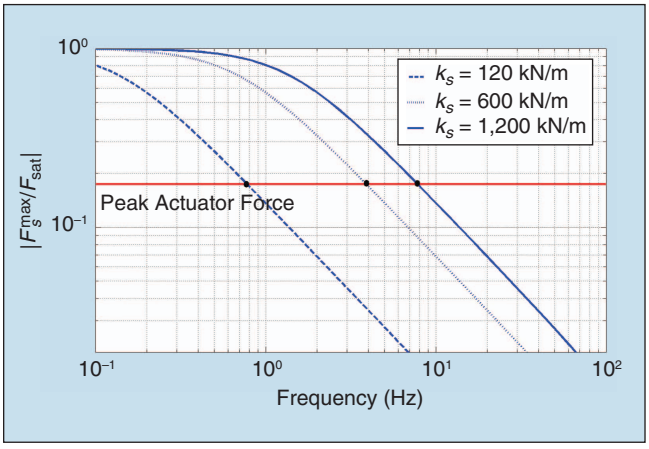

Figure 4. *Force bandwidth due to motor saturation.*

Energy Economy

A powered prosthesis must operate for at least one full day on a single battery charge. Prosthesis energy economy is therefore of critical importance, especially when one considers the requirement that the prosthesis must be lightweight. We define energy economy as an energetic cost of transport (COT) or the electrical energy required to transport unit body weight (amputee + prosthesis) in unit distance. We normalize the electrical energy consumption by body weight times distance traveled given the fact that a greater amount of ankle net work, and therefore a greater amount of electrical energy to pay for that net work, is required to transport a heavier amputee.

What are the stiffness values for the series and parallel springs that minimize prosthesis COT? To answer this question, we use a standard dc motor model to estimate the electrical energy consumption of the prosthesis. The equations are as follows:

$$I = I_{nl}\text{sgn}(\dot{\theta}_m) + \frac{T_m}{K_t}, \quad (3)$$

$$V = \frac{\dot{\theta}_m}{K_e} + R_m I, \quad (4)$$

$$P_m = IV, \quad (5)$$

where I, V, and P_m are the motor current, voltage, and electrical power consumption, respectively. Furthermore, K_e, K_t, I_{nl}, and R_m are the speed constant, torque constant, no load current, and motor resistance, respectively.

Using the reference human ankle angle and torque trajectories in Figure 1(a), we estimate the required linear motor movement and its derivatives $(x, \dot{x}, \ddot{x})$ and also the required motor torque T_m. We then

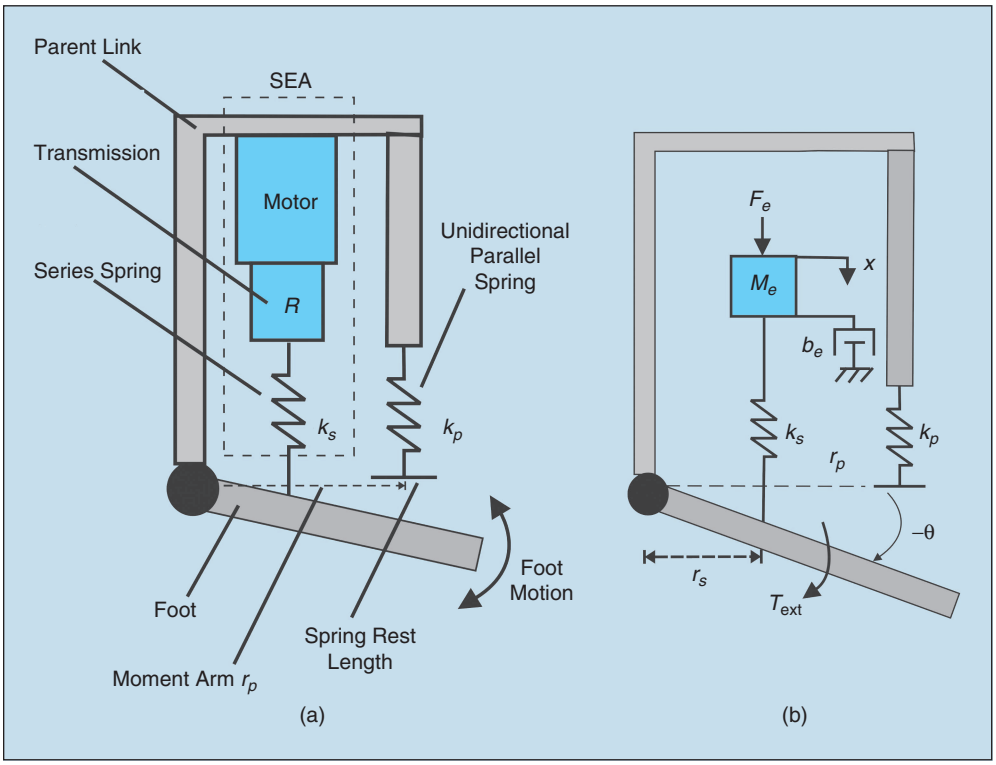

Figure 5. *A powered prosthesis with both series and parallel elasticity: (a) schematic model and (b) linear model.*

compute the electrical motor power consumption using (3)–(5) and obtain the electrical energy consumption of the motor by integrating electrical power (5) over one gait cycle. When computing energy consumption, we assume that only 30% of the negative electrical energy can be stored and reused to provide the energy for ankle-powered plantar flexion. Figure 6 shows the simulation results of the prosthesis COT for different total reduction ratios and stiffness values of series and parallel springs. Parallel stiffness, normalized by the human-controlled dorsiflexion stiffness of 630 Nm/rad (see Table 1), is noted as $\hat{K}_p$ on the upper portion of each graph. Without parallel stiffness ($\hat{K}_p = 0$), the energy consumption of the prosthesis is minimal at a total reduction ratio greater than 400 and a series spring stiffness greater than 400 kN/m. As parallel spring stiffness increases ($\hat{K}_p > 0$), the prosthesis COT can attain a lower minimum value while also requiring a smaller total reduction ratio and series spring stiffness. Using a lower reduction ratio allows the system to have a larger bandwidth and a faster intermittent response.

Using step-count monitoring systems, researchers have determined that active transtibial amputees walk 3,060 ± 1,890 steps per day [49]. Assuming the case of a nominal male amputee walking for 5,000 steps at a moderate walking speed, how large would the onboard battery have to be? Using a parallel spring stiffness equal to the human ankle stiffness ($\hat{K}_p = 1$), and the shock-tolerant series stiffness of 600 kN/m, the optimized prosthesis COT is 0.05 (see Figure 6) at an optimal total reduction ratio greater than, or equal to, 200. For a nominal male of 78 kg walking at a self-selected speed of 1.25 m/s, with a cycle time of 1.1 s (see Figure 1), this COT value converts to 26 J per walking cycle. Using a Li-Polymer battery [energy density 165 W/h/kg (e.g., www.thunderpowerrc.-com)], a 0.22-kg battery would enable 5,000 steps of powered walking. This battery mass is reasonable as it is the same size as the required battery for the Össur's Proprio Foot [8] now being sold commercially.

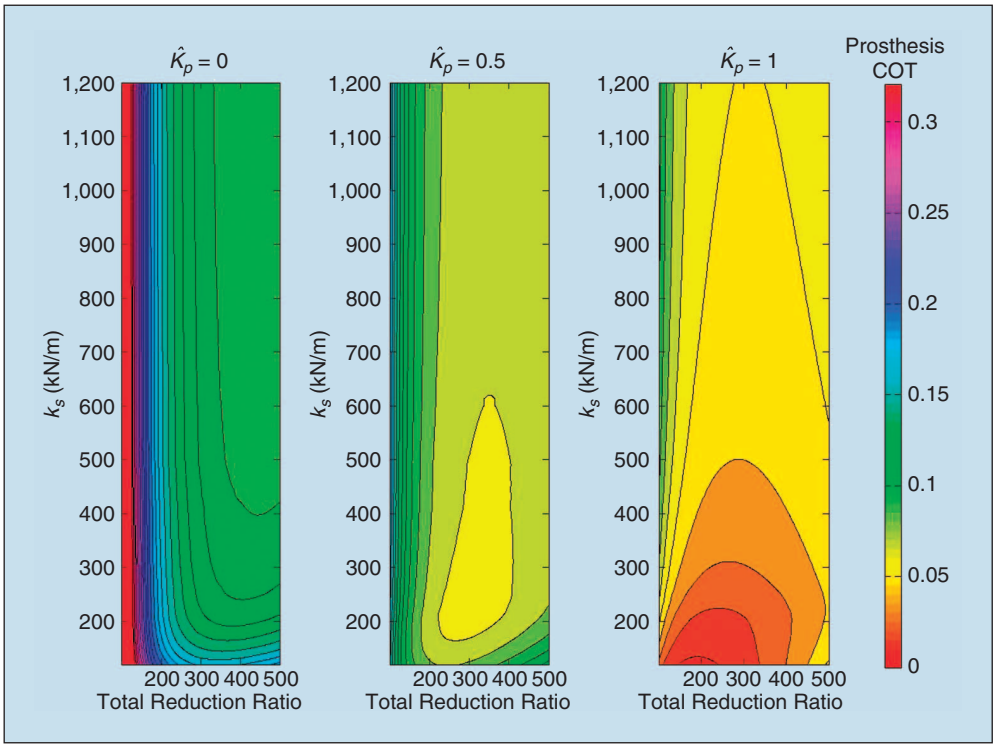

Figure 6. *The effect of total reduction ratio, series stiffness, and parallel stiffness on prosthesis COT. The total reduction ratio is equal to the SEA moment arm r multiplied by transmission ratio R. The prosthesis COT is equal to the amount of electrical energy consumed in one walking cycle divided by half body weight (0.5 × 78 kg × 9.8 m/s^2) and the distance traveled during one walking cycle (1.25 m/s × 1.1 s cycle time = 1.4 m).*

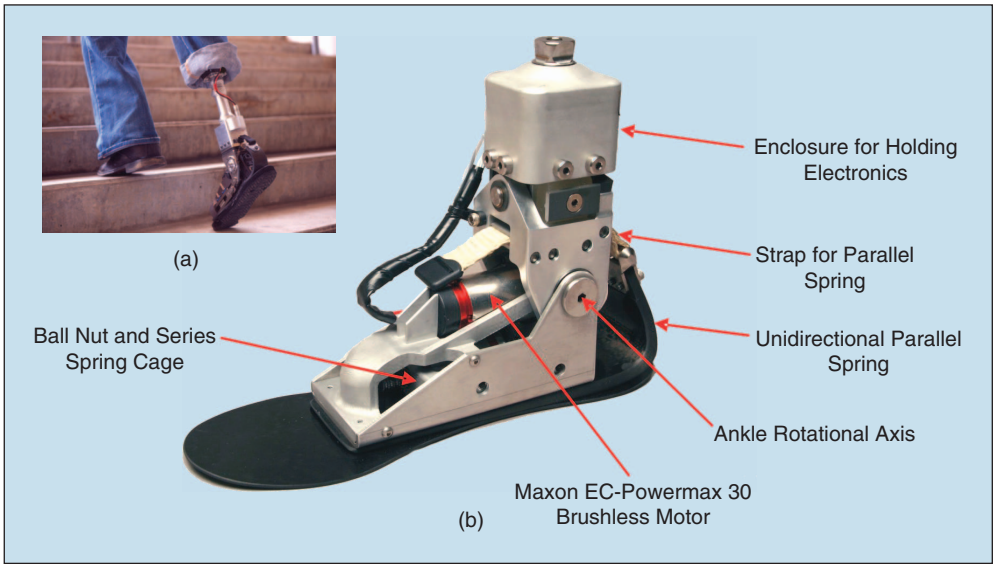

Figure 7. *Powered ankle-foot prosthesis with series and parallel elasticity. (a) The prosthesis is shown powering an amputee up a flight of stairs. (b) The powered prosthesis is shown including all components except for the battery.*

Prosthesis Implementation and Assessment

The ankle-foot prosthesis is shown in Figure 7. The prosthesis weighs 2 kg, which includes a 0.22-Kg battery. The battery attaches to the prosthetic socket (not shown in Figure 7). The unidirectional parallel spring is a leaf spring made from carbon composite material, having a rotary stiffness of 630 Nm/rad. The series spring is formed by polyurethane material positioned in series with a ball-screw transmission (Nook ECN-10030-LG, 10 mm $\times$ 3 mm), having a linear stiffness of 600 kN/m. The total reduction ratio is 170. The EC-Powermax 30 motor from Maxon was selected because of its small size and weight. Although the control system design for the prosthesis is not described here, an interested reader can see [34], [35].

During system evaluations, we found that for a 76-kg walking transtibial amputee, the powered ankle-foot prosthesis delivered a peak ankle velocity, torque, and power equal to 2.1 $\pm$ 0.1 rad/s, 141 $\pm$ 2 Nm, and 230 $\pm$ 10 W, respectively ($N = 8$ walking trials at 1.3 m/s). Furthermore, the powered prosthesis provided a net positive stance work and controlled dorsiflexion stiffness of 12.6 $\pm$ 0.2 J and 576 $\pm$ 5 Nm/rad, respectively. These prosthetic values agree reasonably well with the target human ankle values listed earlier in the section "Biomimetic Design Goals." Furthermore, the prosthesis required 30 J per step of electrical energy at a 1.3 m/s walking speed and a cycle distance equal to 1.4 m. Thus, the prosthesis COT was 0.06, similar to the predicted value in Figure 6.

The prosthesis is shown to deliver similar ankle dynamics in walking compared with a biological ankle, but does it have the capability to improve amputee gait? In a preliminary investigation on the clinical efficacy of the powered prosthesis [32]–[35], we measured the rate of oxygen consumption and carbon dioxide production as a determinant of metabolic rate on three unilateral transtibial amputees walking at self-selected speeds. With only a modest accommodation period of approximately two hours, we found that the powered prosthesis improved amputee metabolic economy on average by 14% compared with the conventional passive-elastic prostheses evaluated (Flex-Foot Ceterus and Freedom Innovations Sierra), highlighting the clinical importance of prosthetic interventions that closely mimic the mass distribution, kinetics, and kinematics of the missing limb. [Metabolic economy is defined as the amount of metabolic energy required to transport unit amputee weight (unit distance). For a detailed experimental methodology, see [32]–[35].]

Conclusions

The minimum level of series compliance that adequately protects the transmission from damage during foot collision fails to satisfy bandwidth requirements. As a resolution to this difficulty, parallel motor elasticity is used to lower the forces borne by the SEA, enhancing system force bandwidth. To minimize prosthesis COT and motor or transmission size, we select a parallel stiffness that supplies the necessary ankle stiffness during early stance period dorsiflexion, eliminating the need for SEA during that gait phase. In future investigations, we hope to apply the ankle-foot design to robotic, orthotic, and exoskeletal applications. In the design of biomimetic ankle-foot systems, we feel both series and parallel motor elasticity are of paramount importance.

Acknowledgments

This research was supported by the U.S. Veterans Administration under grant VA241-P-0026 and by the Army Telemedicine and Advanced Technology Division under grant W81XWH-07-1-0343. We would like to acknowledge the contributions of Manta Designs and Massachusetts Institute of Technology (MIT) researchers Chris Barnhart, Bruce Deffenbaugh, and Jeff Weber for their invaluable electromechanical design work.

Keywords

Powered ankle-foot prosthesis, amputee gait, series elasticity, parallel elasticity, impedance control.

References

[1] N. H. Molen, "Energy/speed relation of below-knee amputees walking on motor-driven treadmill," *Eur. J. Appl. Physiol.*, vol. 31, no. 3, pp. 173–185, 1973.

[2] E. G. Gonzalez, P. J. Corcoran, and R. L. Reyes, "Energy expenditure in B/K amputees: Correlation with stump length," *Arch. Phys. Med. Rehabil.*, vol. 55, no. 3, pp. 111–119, 1974.

[3] G. R. Colborne, S. Naumann, P. E. Longmuir, and D. Berbrayer, "Analysis of mechanical and metabolic factors in the gait of congenital below knee amputees: A comparison of the SACH and Seattle Feet," *Am. J. Phys. Med. Rehabil.*, vol. 71, no. 5, pp. 272–278, 1992.

[4] D. J. Sanderson and P. E. Martin, "Lower extremity kinematic and kinetic adaptations in unilateral below-knee amputees during walking," *Gait Posture*, vol. 6, no. 2, pp. 126–136, 1997.

[5] A. Esquenazi and R. DiGiacomo, "Rehabilitation after amputation," *J. Am. Podiatr. Med. Assoc.*, vol. 91, no. 1, pp. 13–22, 2001.

[6] L. Torburn, C. M. Powers, R. Guiterrez, and J. Perry, "Energy expenditure during ambulation in dysvascular and traumatic below-knee amputees: A comparison of five prosthetic feet," *J. Rehabil. Res. Dev.*, vol. 32, no. 2, pp. 111–119, 1995.

[7] M. J. Hsu, D. H. Nielsen, S.-J. L. Chan, and D. Shurr, "The effects of prosthetic foot design on physiologic measurements, self-selected walking velocity, and physical activity in people with transtibial amputation," *Arch. Phys. Med. Rehabil.*, vol. 87, no. 1, pp. 123–129, 2006.

[8] Össur, Inc. (2008). [Online]. Available: www.ossur.com

[9] S. Ron, *Prosthetics and Orthotics: Lower Limb and Spinal*. Baltimore, MD: Lippincott Williams & Wilkins, 2002.

[10] A. L. Hof, B. A. Geelen, and J. W. Van Den Berg, "Calf muscle moment, work and efficiency in level walking; role of series elasticity," *J. Biomech.*, vol. 16, no. 7, pp. 523–537, 1983.

[11] D. A. Winter, "Biomechanical motor pattern in normal walking," *J. Mot. Behav.*, vol. 15, no. 4, pp. 302–330, 1983.

[12] M. Palmer, "Sagittal plane characterization of normal human ankle function across a range of walking gait speeds," M.S. thesis, Dept. Mech. Eng., MIT, Cambridge, MA, 2002.

[13] D. H. Gates, "Characterizing ankle function during stair ascent, descent, and level walking for ankle prosthesis and orthosis design," M.S. thesis, Dept. Biomed. Eng., Boston Univ., MA, 2004.

[14] A. Hansen, D. Childress, S. Miff, S. Gard, and K. Mesplay, "The human ankle during walking: Implication for the design of biomimetric ankle prosthesis," *J. Biomech.*, vol. 37, no. 10, pp. 1467–1474, 2004.

[15] D. A. Winter and S. E. Sienko, "Biomechanics of below-knee amputee gait," *J. Biomech.*, vol. 21, no. 5, pp. 361–367, 1988.

[16] A. D. Kuo, "Energetics of actively powered locomotion using the simplest walking model," *J. Biomech. Eng.*, vol. 124, no. 1, pp. 113–120, 2002.

[17] A. D. Kuo, J. M. Donelan, and A. Ruina, "Energetic consequences of walking like an inverted pendulum: Step-to-step transitions," *Exerc. Sport Sci. Rev.*, vol. 33, no. 2, pp. 88–97, 2005.

[18] A. Ruina, J. E. Bertram, and M. Srinivasan, "A collisional model of the energetic cost of support work qualitatively explains leg sequencing in

walking and galloping, pseudo-elastic leg behavior in running and the walk-to-run transition," *J. Theor. Biol.*, vol. 237, no. 2, pp. 170–192, 2005.
[19] K. Koganezawa and I. Kato, "Control aspects of artificial leg," in *Proc. IFAC Symp. Control Aspects of Biomedical Engineering*, 1987, pp. 71–85.
[20] S. Au, P. Dilworth, and H. Herr, "An ankle-foot emulation system for the study of human walking biomechanics," in *Proc. IEEE Int. Conf. Robotics and Automation*, Orlando, FL, May 2006, pp. 2939–2945.
[21] K. Hirai, M. Hirose, Y. Haikawa, and T. Takenaka, "The development of Honda humanoid robot," in *Proc. IEEE/RSJ Int. Conf. Intelligent Robots and Systems*, Leuven, Belgium, May 1998, pp. 1321–1326.
[22] K. Kaneko, F. Kanehiro, S. Kajita, H. Hirukawa, T. Kawasaki, M. Hirata, K. Akachi, and T. Isozumi, "Humanoid robot HRP-2," in *Proc. IEEE Int. Conf. Robotics and Automation*, New Orleans, LA, April 2004, pp. 1083–1090.
[23] "Self-adjusting prosthetic ankle apparatus," U.S. Patent 6 443 993, Sept. 3, 2002.
[24] S. H. Collins and A. D. Kuo, "Controlled energy storage and return prosthesis reduces metabolic cost of walking," in *Proc. ISB 20th Congr. and the American Society of Biomechanics Annu. Meeting*, Cleveland, Ohio, 2003, p. 804.
[25] C. Li, M. Tokuda, J. Furusho, K. Koyanagi, S. Morimoto, Y. Hashimoto, A. Nakagawa, and Y. Akazawa, "Research and development of the intelligently controlled prosthetic ankle joint," in *Proc. IEEE Int. Conf. Mechatronics and Automation*, Luoyang, China, 2006, pp. 1114–1119.
[26] A. H. Hansen, S. A. Gard, D. S. Childress, B. Ruhe, and R. Williams, "Automatically adapting ankle-foot prosthesis concept," in *12th World Congr. Int. Society for Prosthetics and Orthotics*, Vancouver, Canada, 2007.
[27] G. K. Klute, J. Czerniecki, and B. Hannaford, "Development of powered prosthetic lower limb," in *Proc. 1st Nat. Meeting, Veterans Affairs Rehabilitation R&D Service*, Washington, DC, Oct. 1998.
[28] H. Herr, D. Paluska, P. Dilworth, and S. Kwau, "A hybrid actuator comprising motor, spring and variable-damper elements," Patent Provisional F-51 SN 60/666,876, Mar. 31, 2005.
[29] S. Au, P. Bonato, and H. Herr, "An EMG-position controlled system for an active ankle-foot prosthesis: An initial experimental study," in *Proc. IEEE 9th Int. Conf. Rehabilitation Robotics (ICORR)*, Chicago, IL, June 2005, pp. 375–379.
[30] S. Au and H. Herr, "Initial experimental study on dynamic interaction between an amputee and a powered ankle-foot prosthesis," presented at the Workshop on Dynamic Walking: Mechanics and Control of Human and Robot Locomotion, Ann Arbor, MI, May 2006.
[31] S. K. Au, J. Weber, and H. Herr, "Biomechanical design of a powered ankle-foot prosthesis," in *Proc. IEEE Int. Conf. Rehabilitation Robotics*, Noordwijk, The Netherlands, June 2007, pp. 298–303.
[32] S. Au, J. Weber, E. Martinez-Villapando, and H. Herr, "Powered ankle-foot prosthesis for the improvement of amputee ambulation," in *Proc. 29th Annu. Int. Conf. IEEE Engineering in Medicine and Biology Society*, Lyon, France, 2007, pp. 3020–3026.
[33] H. Herr, J. Weber, and S. Au, "Powered ankle-foot prosthesis," in *Proc. Int. Conf. Biomechanics of the Lower Limb in Health, Disease and Rehabilitation*, Manchester, England, Sept. 3–5 2007, pp. 72–74.
[34] S. K. Au, "Powered ankle-foot prosthesis for the improvement of amputee walking economy," Ph.D. dissertation, Dept. Mech. Eng., MIT, Cambridge, MA, 2007.
[35] S. Au, J. Weber, and H. Herr, "Powered ankle-foot prosthesis improves walking metabolic economy," *IEEE Trans. Robot.*, to be published.
[36] J. Hitt, R. Bellman, M. Holgate, T. Sugar, and K. Hollander, "The SPARKy (spring ankle with regenerative kinetics) projects: Design and analysis of a robotic transtibial prosthesis with regenerative kinetics," in *Proc. ASME Int. Design Engineering Tech. Conf.*, CD-ROM, 2007, pp. 1–10.
[37] D. A. Winter, *Biomechanics and Motor Control of Human Movement*, 2nd ed. New York: Wiley, 1990.
[38] V. T. Inman, H. J. Ralston, and F. Todd, *Human Walking*. Baltimore: Williams and Wilkins, 1981.
[39] J. Perry, *Gait Analysis: Normal and Pathological Function*. Thorofare, New Jersey: SLACK Inc., 1992.
[40] A. R. Tilley, H. Dreyfuss, and S. B. Wilcox, *The Measure of Man and Woman: Human Factors in Design*, rev. ed. New York: Wiley, 2001.
[41] G. A. Pratt and M. M. Williamson, "Series elastic actuators," in *Proc. IEEE/RSJ Int. Conf. on Intelligent Robots and Systems*, Pittsburgh, 1995, pp. 399–406.
[42] D. Robinson, "Design and an analysis of series elasticity in closedloop actuator force control," Ph.D. dissertation, Dept. Mech. Eng., MIT, Cambridge, MA, 2000.
[43] J. Pratt, A. Torres, P. Dilworth, and G. Pratt, "Virtual actuator control," in *Proc. IEEE Int. Conf. Intelligent Robots and Systems (IROS '96)*, Osaka, Japan, 1996, pp. 1219–1226.
[44] J. Blaya and H. Herr, "Adaptive control of a variable-impedance ankle-foot orthosis to assist drop foot gait," *IEEE Trans. Neural. Syst. Rehabil. Eng.*, vol. 12, no. 1, pp. 24–31, 2004.
[45] C. Walsh, K. Pasch, and H. Herr, "An autonomous, underactuated exoskeleton for load-carrying augmentation," in *Proc. IEEE/RSJ Int. Conf. Intelligent Robots and Systems (IROS)*, Beijing, China, October 9–16, 2006, pp. 1410–1415.
[46] C. Walsh, D. Paluska, K. Pasch, W. Grand, A. Valiente, and H. Herr, "Development of a lightweight, underactuated exoskeleton for load-carrying augmentation," in *Proc. IEEE Int. Conf. Robotics and Automation*, Orlando, FL, May 2006, pp. 2939–2945.
[47] J. M. Donelan, R. Kram, and A. D. Kuo, "Simultaneous positive and negative external mechanical work in human walking," *J. Biomech.*, vol. 35, no. 1, pp. 117–124, 2002.
[48] M. Popovic, A. Goswami, and H. Herr, "Ground reference points in legged locomotion: Definitions, biological trajectories and control implications," *Int. J. Robot Res.*, vol. 24, no. 12, pp. 1013–1032, 2005.
[49] J. M. Stepien, S. Cavenett, L. Taylor, and M. Crotty, "Activity levels among lower-limb amputees: Self-report versus step activity monitor," *Arch. Phys. Med. Rehabil.*, vol. 88, no. 7, pp. 896–900, 2007.

Samuel K. Au received his B.S. and M.S. degrees from the Department of Automation and Computer-Aided Engineering at the Chinese University of Hong Kong and his Ph.D. degree from the Mechanical Engineering Department at MIT. He is currently a postdoctoral associate working in the Biomechatronics Group within the MIT Media Lab. His research interests include system dynamics, system identification, biomedical signal processing, control, biomechanics, artificial intelligence, robotics, and prosthetics.

Hugh M. Herr received the B.A. degree in physics from the Millersville University of Pennsylvania in 1990, the M.S. degree in mechanical engineering from MIT, and the Ph.D. degree in biophysics from Harvard University in 1998. He is an associate professor within MIT's Program of Media Arts and Sciences and the Harvard-MIT Division of Health Sciences and Technology. His primary research objective is to apply the principles of biomechanics and neural control to guide the designs of prostheses, orthoses, and exoskeletons. He is the author of more than 60 technical publications in biomechanics and wearable robotics and is an active Member of the IEEE. He is the recipient of the 2007 Heinz Award for Technology, the Economy, and Employment.

Address for Correspondence: Hugh M. Herr, Biomechatronics Group, MIT Media Lab, E15-424, Cambridge, MA 02139, USA. E-mail: hherr@media.mit.edu.

Compliant Actuation of Rehabilitation Robots

©PUNCHSTOCK

Benefits and Limitations of Series Elastic Actuators

BY HEIKE VALLERY, JAN VENEMAN, EDWIN VAN ASSELDONK, RALF EKKELENKAMP, MARTIN BUSS, AND HERMAN VAN DER KOOIJ

Digital Object Identifier 10.1109/MRA.2008.927689

Development of robotic devices for gait rehabilitation of stroke patients is motivated by the need for a both intensive and task-specific training, which are key factors in recovery [1], [2], and by the need for therapist-friendly training. Evaluations of the first-generation commercial devices have shown that gait training using these devices is at least as effective as manual therapy [3], [4]. First-generation devices are characterized by the approach of enforcing gait upon a patient by rigidly moving the legs through a prescribed pattern, so that the patient can hardly influence these motions. The training effect may be extendable by increasing active participation of patients, e.g., by letting the patient walk on own effort and only offer robotic assistance as needed (AAN). The potential of AAN algorithms in promoting neural recovery has not yet been shown in gait training of humans, but it was assessed in gait training of mice [5] and in arm training of stroke patients [6], [7]. AAN strategies require interaction control [8], meaning that the apparent mechanical impedance of the device is programmable to desired values (within limits), so that the behavior of the robot can be varied from very stiff to very compliant. Compared with general haptic devices, low apparent stiffness and mass are demanded from a gait trainer, and gait motions are slow. We opted for a combination of compliant actuation and impedance control [9], [10], which provides means to minimize undesired interaction torques.

This article describes and discusses the general advantages and limitations of a compliant actuation concept for rehabilitation robots on the example of our realization called the lower extremity powered exoskeleton (LOPES). The major focus is on the limitations: stiffness and bandwidth constraints as well as the influence of uncompensated exoskeleton dynamics. The stability analysis provides an interesting new result. If the rendered stiffness of an elastically actuated joint is increased beyond the intrinsic stiffness of the elastic element, stability of the coupled system human-robot cannot be guaranteed, at least not in the conservative terms of passivity. Finally, the experimental results with subjects walking with the device are presented. These results show that the limitations, in the given application, become secondary to the gain of compliant actuation.

LOPES: A Low-Weight Exoskeleton with Series Elastic Actuated Joints

Mechanical Design

Impedance control implies that the actuators should be high-precision force sources. Mass and inertia of the actuated construction (the exoskeleton) should be minimized, as the means to reduce the apparent mass by control are limited. Our gait rehabilitation robot LOPES is characterized by 1) the choice of degrees of freedom (DoF) that are actuated or left free to allow kinematically natural walking patterns and 2) the possibility

1070-9932/08/$25.00©2008 IEEE

of low impedance control of these DoF to allow unhindered and thus kinetically natural walking. Both horizontal pelvis translations are actuated [1 and 2 in Figure 1(a)]; the vertical motion of the pelvis is left free with passive weight compensation [3 in Figure 1(a)]. There are three rotational joints per leg: hip adduction [4 in Figure 1(a)], hip flexion [5 in Figure 1(a)], and knee flexion [6 in Figure 1(a)]. With these nine DoF, LOPES allows more versatile motion than just forward stepping (as also provided by commercial devices such as the Lokomat [11]). Maintaining the fundamental instability of a standing or walking human, LOPES allows balance training, which has been recognized as an important aspect of gait training [12], [13]. Pelvis motion is also increasingly integrated into other new robotic devices such as ALEX [14] or KineAssist [15].

In contrast to the aforementioned devices, which use stiff actuators, LOPES is intrinsically compliant, similar to PAM and POGO presented in [8]. The joints of the robot are actuated with series elastic actuators (SEAs), an actuation principle introduced by Robinson and colleagues [16]. Bowden cables are used to realize a flexible transmission, so that the motors are detached from the exoskeleton, reducing its weight [see Figure 1(a)]. For the rotary joints, two compression springs are connected to the actuator disk with a cable, so that a torsion spring is created between the actuator disk and the load side segment [see Figure 1(b)]. Both springs are pretensioned with the maximum desired force, so that the cables are always under tension during operation. The concept, construction, and functionality of these joints are described extensively in [9]. The sideways pelvis translation is equipped with a linear SEA.

Table 1 provides the geometric and inertial specifications of the exoskeleton part. For each segment of the exoskeleton, the length L, the center of mass location with respect to the proximal joint L_{CoM}, the mass m, and the moment of inertia around the center of mass J_{s1} and around the proximal joint J_{s2} are listed for an average configuration (the segment lengths are adaptable to the patient). Table 2 gives the specifications of components used in the actuation part. Motor and gear inertial properties and transmission ratio i determine the reflected inertia J_A or m_A of the drives in the exoskeleton coordinate system. For the sideways direction, the reflected mass m_A of the drive is 1.2 kg, much less

To lower undesired interaction torques, it is crucial to minimize the reflected mass of the device.

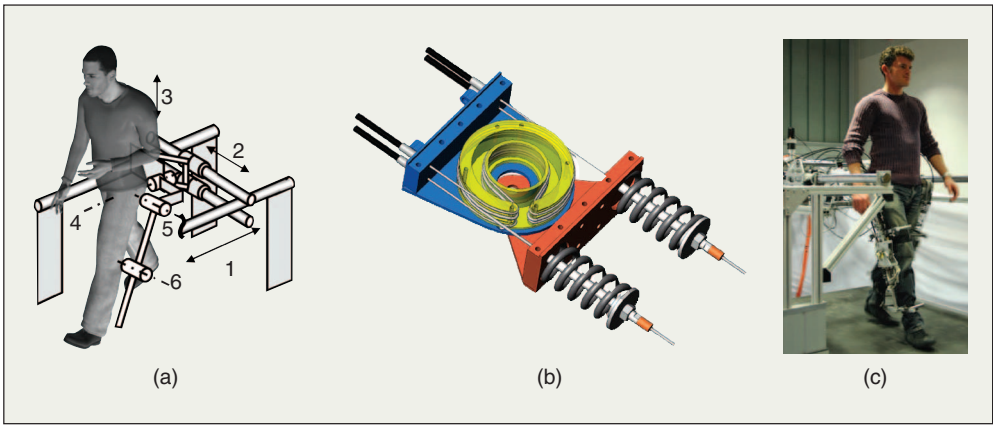

Figure 1. *Design of the LOPES robot. (a) DoF of the pelvis and leg segments of the LOPES gait rehabilitation robot: (1) forward linear guides, (2) sideways linear guides, (3) vertical motion, passively weight compensated by a spring parallelogram between frame and pelvis segment, (4) hip frontal rotation (adduction), (5) hip sagittal rotation (flexion/extension), (6) knee sagittal rotation. Except for (3), all DoFs are actuated. (b) Design of the SEAs: Bowden cables connect the springs to EM motors, which are detached from the exoskeleton. (c) Photographic impression of LOPES in operation.*

Table 1. Dimensions and mass properties of the LOPES exoskeleton.

	L (m)	L_{CoM} (m)	m (kg)	J_{s1} (kg·m²)	J_{s2} (kg·m²)
Upper limb	0.43	0.27	2.9	0.088	0.30
Lower limb	0.37	0.17	2.25	0.064	0.13
Pelvis B/F			35		
Pelvis L/R			27		

Table 2. Actuator specifications of the LOPES.

DoF	Motor Type	Power	Torque/ Force	Motor Inertia	Gear Inertia	i	Refl. Inertia J_A, m_A	r_d	k_s
Flex/ext hip	Kollmorgen	567 W	2.73 Nm	1.6e-5 kg · m²	1.6e-5 kg · m²	64	0.13 kg · m²	0.047 m	35.10 kN/m
Flex/ext knee	Kollmorgen	567 W	2.73 Nm	1.6e-5 kg · m²	1.6e-5 kg · m²	64	0.13 kg · m²	0.047 m	35.10 kN/m
Ab/ad hip	Kollmorgen	567 W	2.73 Nm	1.6e-5 kg · m²	1.6e-5 kg · m²	64	0.13 kg · m²	0.047 m	57.20 kN/m
Left/right	Berger-Lahr	690 W	2.2 Nm	1.6e-4 kg · m²	1.8e-5 kg · m²	$8/r_d$	1.2 kg	0.098 m	3.98 kN/m
Back/forward	Linmot	250 W	204 N	1.8e-5 kg · m²	2.3 kg		2.3 kg		

The SEA cannot display a higher pure stiffness than the spring stiffness, if passivity is desired.

than the mass of the pelvis segment (27 kg). In contrast, the reflected moment of inertia J_A of the drives actuating the rotational joints is $0.13\ \mathrm{kg}\cdot\mathrm{m}^2$, which is in the same order of magnitude as the moment of inertia J_{s2} of the exoskeleton segments. However, as the motor mass is decoupled from the exoskeleton by the springs, the actuator mass is not felt by the subject, and the reflected mass of the device is reduced to the exoskeleton mass only. The disk radius r_d and the spring constant k_s in Table 2 define the intrinsic rotational stiffness K of the SEA; for hip and knee, K is given by $2k_s r_d^2 = 155$ Nm/rad.

Control Scheme

The control strategy is multilayered. On the outermost layer, references for the desired interaction with the patient are defined. Two different strategies have been implemented on the LOPES: complementary limb motion estimation (CLME) [17], [18] and virtual model control (VMC) [19], [20]. The control schemes differ in their conceptual background, yet they both aim at improved patient cooperativeness and do not prescribe fixed trajectories to be tracked. This article describes only VMC. The low-level control deals with the SEA unit used to generate and measure the interaction forces. First, this underlying low-level SEA control is described as a single-input single-output (SISO) system, and then, the VMC is outlined.

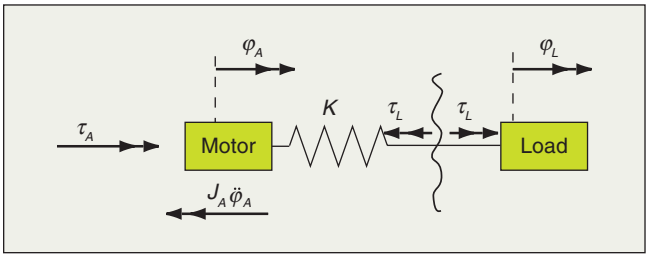

Figure 2. *SEA: The drive is connected to the load via a compliant element (a torsion spring with spring constant K). The drive dynamics are represented by the inertia J_A, and the motor torque is τ_A. The spring torque τ_L acting on the load is proportional to the difference between motor angle φ_A and joint angle φ_L, which makes the spring length a direct measure of the torque acting on the load.*

Control of the SEA

In a SEA, the load is coupled to the drive via a compliant element, in this case, a spring with linear characteristic [see Figure 1(b)]. A relative displacement of load and actuator provokes a spring torque τ_L. This principle is schematically illustrated in Figure 2. The simplifying assumptions made here neglect several important aspects of the actuator side that are relevant in the specific mechanical realization, such as friction and elasticity in the Bowden cable transmission. We justify this by the purpose of the investigations in the later analysis, which is to show some generic parameter and performance limitations of SEAs.

Figure 3 shows the block chart of the SEA embedded in a SISO impedance control loop. The concept of a cascaded force control loop with proportional-integral (PI) controllers was chosen because of its reported effectiveness [21], [22]. In our setup, the innermost motor velocity loop is realized by the pulse-width modulation. The force control has been described and evaluated in [23]. The outer impedance controller sets the desired impedance, whereby we consider only the case of a rendered stiffness P.

Selective and Partial Support of Gait Functions with Virtual Model Control

The observation of manual physical therapy of stroke survivors shows that in case of severely impaired subjects, two or three therapists are needed. Depending on the individual impairment, the therapist assists only in certain gait subtasks. The idea of the LOPES control is that the therapist still decides how to assist the patient but that the strenuous labor is taken over by the robot. Following this concept, LOPES should assist a patient only when it is needed. For example, in case of deficient foot clearance during the swing phase, LOPES should help in lifting up the foot. We have divided the control of human gait into different functional units, which can be partially and selectively supported by LOPES, depending on the patient's individual needs:

1) balance control in the sagittal/frontal plane
2) control of walking speed
3) foot placement in the sagittal and frontal plane

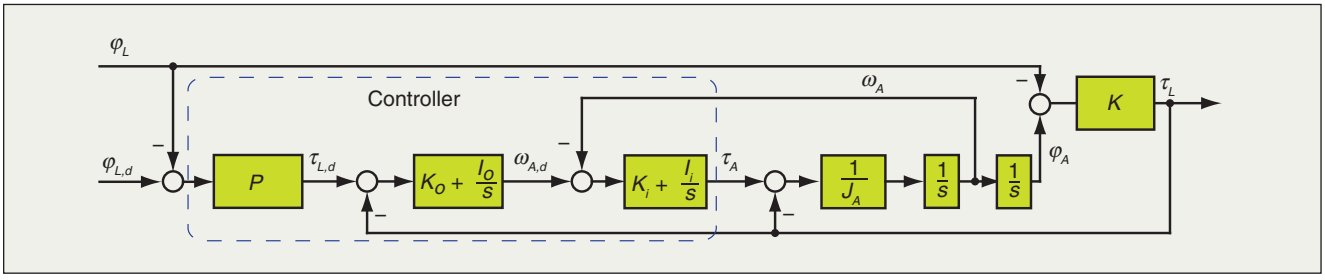

Figure 3. *Impedance control with cascaded torque control. The plant (SEA, on the right) is characterized by actuator inertia J_A and spring constant K. The torque controller is cascaded, with inner (index i) loop on motor velocity ω_A and outer (index o) loop on torque τ_L, both PI-controlled with gains K and I. Outside, an impedance control loop is closed on the joint angle φ_L, here rendering a pure virtual stiffness P. The subscript d denotes reference signals.*

4) foot clearance during swing phase to prevent stumbling
5) weight bearing.

The reason behind the division of subfunctions is given in [24]. To support these gait functions, we use VMC, which is a motion control framework that uses virtual mechanical components to generate desired interaction forces and torques. With components such as springs and dampers, it is possible to simulate almost any interaction that a therapist would have with a patient. Usual therapist interaction forces have been quantified in [25]. VMC has been implemented in several two- and three-dimensional walking robot models [26].

The supportive forces for balance control and walking speed control are realized by the drives actuating the pelvis in the horizontal plane [1 and 2 in Figure 1(a)]. All other DoF are rotational, such that the virtual forces in Cartesian space need to be mapped to joint torques. These torques create the illusion that the simulated components are connected to the robot.

Balance control, control of walking speed, and weight bearing are described elsewhere. In this article, we consider only the case of a healthy subject walking in LOPES while the step length and height are modified by VMC. Each of these two virtual models consists of a spring attached to the ankle of LOPES either horizontally or vertically. The desired virtual force acting on the ankle is given by

$$\boldsymbol{F}^{\mathrm{VMC}} = \mathbf{K}_x^{\mathrm{VMC}}(\boldsymbol{x} - \boldsymbol{x}_{\mathrm{ref}}), \tag{1}$$

where $\boldsymbol{K}_x^{\mathrm{VMC}}$ is the Cartesian virtual stiffness matrix, $\boldsymbol{x}$ contains the Cartesian coordinates of LOPES' ankle position, and $\boldsymbol{x}_{\mathrm{ref}}$ is the ankle position reference trajectory. This reference trajectory is tailored to each patient's individual needs, by scaling his/her normal, unassisted ankle trajectory during swing phase in the vertical and horizontal direction to increase foot clearance and/or step length.

The virtual force $\boldsymbol{F}^{\mathrm{VMC}}$ is mapped to joint torque by

$$\tau^{\mathrm{VMC}} = \mathbf{J}^T(\boldsymbol{\theta})\boldsymbol{F}, \tag{2}$$

where $\boldsymbol{\theta}$ is the joint angle and $\mathbf{J}(\boldsymbol{\theta})$ is the Jacobian relating joint velocities to Cartesian ankle velocities. Security measures are taken to avoid knee hyperextension. For step height modification, the ankle height reference is defined with respect to the horizontal ankle-hip distance. Thus, it is not predefined in time. For step length control, the horizontal ankle reference is defined in time, and it is triggered at toe off. Toe off and heel contact are sensed by force transducers on the treadmill.

Advantages of the SEA

Table 3 lists the advantages and drawbacks of SEA. One important advantage is that it allows treating the force control loop as a position control, because the spring length can be considered proportional to the force output. As has previously been demonstrated, a higher compliance in the force control loop allows for higher control gains [16]. This way, better force tracking performance can be achieved. Higher gains allow the realization of proper feedback-controlled torque actuators for LOPES despite substantial adverse effects of high friction and stick-slip in the Bowden cables, as well as play in the transmission. The low realizable impedance of the LOPES robot in the presence of these heavy nonlinear effects has been demonstrated in practical experiments, for example in [23]. Another important advantage of a SEA, as mentioned earlier, is that the spring decouples the motor inertia from the exoskeleton. The Bowden cables also locally decouple the motors from the exoskeleton, further reducing the reflected mass of the device. This reduction is important given that the endpoint mass is an uncontrollable element, i.e., no causal controller can affect its value [27].

A compliantly actuated robot will give way at impact. This is advantageous in terms of safety issues and actuator impact resistance, as well as for realistic stepping experience and training efficacy during impact-type events such as heel strike.

There is a tradeoff between achievable stiffness and low undesired interaction torques.

Performance Limitations

The SEA gains easier and robust force control without depending on expensive (high-speed, high-precision) mechatronic components, yet there is a price to pay. The following analysis will first illustrate the well-known drawback of bandwidth limitations in a compliant actuator [28]. Then, a new result will be presented: the rendered stiffness of the device cannot be increased beyond the stiffness of the elastic element, if conservative demands for stability (in terms of passivity) are to be met. The analysis concludes with the influence of these limitations, as well as the influence of uncompensated exoskeleton mass, on the VMC performance.

Bandwidth Limitations

Bandwidth limitations will be illustrated on the example of the LOPES actuators, first for the SEA alone and then for the more realistic case, in which there is an extra end-effector mass (an exoskeleton) between the patient and the elastic element.

Bandwidth of the SEA with Massless End-Effector

For haptic systems, the impedance Z is generally defined as the transfer of function from the input velocity to the opposing

Table 3. Advantages and disadvantages of SEA.

Pros	Cons
Decoupled actuator inertia	Limited stiffness
Reduction of friction effects	Limited bandwidth
Inherent safety and impact resistance	Extra mechanical element
Energy storage	High power requirements

The employed VMC, which attempts to separately modify the selected gait characteristics, proved to be effective.

torque. This definition is used here because it allows to assess stability in terms of passivity. Using the notation of II-B1, $Z(s)$ is

$$Z(s) = \frac{\tau_L}{-\varphi_L s}. \tag{3}$$

With the simplified model of Figure 2, which neglects friction and elasticity of the Bowden cables, and with the parameters given in Figure 3, the impedance transfer function value is

$$Z(s) = \frac{K(J_A s^4 + K_i s^3 + (K_i K_o P + I_i)s^2 + aPs + I_i I_o P)}{(J_A s^4 + K_i s^3 + (K_i K_o K + K + I_i)s^2 + aKs + I_i I_o K)s}, \tag{4}$$

with $a = (I_i K_o + I_o K_i)$.

Replacing the complex variable s in (4) by $j\omega$, the frequency response $Z(j\omega)$ is obtained. A look at the asymptotic behavior of $Z(j\omega)$ is useful for an intuitive understanding of the SEA behavior; for frequencies below the bandwidth ($\omega \to 0$), the programmed impedance can be achieved, which is that of a virtual spring with stiffness P. For high frequencies ($\omega \to \infty$), however, the impedance of the haptic display will approach the impedance of the SEA's mechanical spring with stiffness K.

The integrators show considerable influence only for low frequencies, and thus, the bandwidth analysis can be simplified by considering only the case where both integrator gains are zero. This makes major effects more obvious, as it reduces (4) to

$$Z_s(s) = K\frac{J_A s^2 + K_i s + K_i K_o P}{(J_A s^2 + K_i s + K_i K_o K + K)s}. \tag{5}$$

The actually displayed stiffness value K_{disp} deviates from the value of P if no integrators are employed:

$$K_{\text{disp}} = \lim_{s\to 0} s\ Z_s(s) = \frac{PK_oK_i}{1 + K_oK_i}, \tag{6}$$

and a desired stiffness must be mapped to a higher P.

Figure 4(a) illustrates the bandwidth limitations; for low frequencies, the desired impedance is successfully rendered, whereas for frequencies above the bandwidth, the system behaves like the (stiffer) mechanical spring. For frequencies in between, the behavior approaches a spring-damper, the damping parameter of which depends only on the control parameters (given in the figure legend). The intersection of asymptotes of damper and rendered spring in Figure 4(a) shows that the bandwidth, i.e., the maximum frequency until which rendering of the pure desired stiffness is possible, is bounded by $\omega = PK_o$. This implies that the control gain K_o has a dominant influence on bandwidth. A high value of K_o lowers the damping characteristics of the second-order low-pass in (5), and to counteract this, the motor velocity loop gain value K_i needs to be increased as well. Practical considerations such as motor saturation, however, put bounds on the realizable gains.

Influence of Exoskeleton Mass on Bandwidth

In a realistic rehabilitation robot, there will always be some mass between the actuator and the patient, generally connection elements like an exoskeleton. The exoskeleton LOPES is

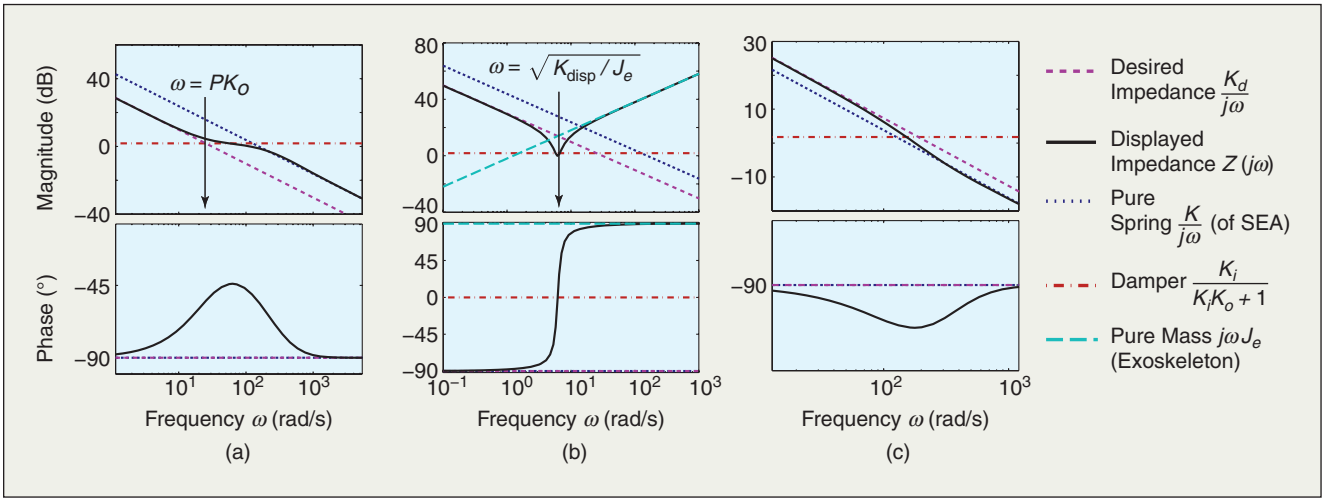

Figure 4. *Bandwidth and stiffness limitations. (a) Bandwidth with massless end effector: At high frequencies, the displayed impedance (black solid line) matches the intrinsic elasticity (green dotted line) of the SEA. The achievable bandwidth depends on the torque control gain K_o. (b) With an additional mass at the load side of the SEA (e.g., an exoskeleton), further bandwidth limitations are introduced. (c) Impedance control with too high desired stiffness (above the natural spring stiffness): The phase of the impedance frequency response has values below −90°, and thus the system is not passive.*

constituted of several coupled segments, such that a multi-input multi-output (MIMO) system results. For schematic purposes, i.e., to illustrate the general influence of this extra mass on bandwidth, however, we will consider only the simplified case where a rigid body with inertia J_e is introduced on the load side of the SEA model of Figure 2, which could be interpreted as a 1-DoF exoskeleton. This extra mass augments the impedance transfer function (4) by the extra summand $J_e s$. The system will no longer behave like a spring at high frequencies, and its behavior will then be dominated by the added mass, as displayed in Figure 4(b). Depending on its value, such an additional mass can also lower the bandwidth even further. Another upper bound for the bandwidth is indicated at the intersection of the asymptotes in Figure 4(b), with a value of $\omega = \sqrt{K_{\text{disp}}/J_e}$.

Stiffness Limitations Due to Passivity Concerns

Now, passivity conditions for the impedance control of Figure 3 will be investigated with similar methods as in [23], resulting in bounds for the control gains (with integrators).

Passivity is ensured if the impedance (3) is positive real. Necessary and sufficient conditions for this are as follows [27]:

- $Z(s)$ must be stable
- The real part of $Z(j\omega)$ must be nonnegative for all ω for which $j\omega$ is not a pole of $Z(s)$.

First, we look at the stability condition. As the system poles are independent of the impedance parameters, stability depends only on the inner force control loop. Checking the Hurwitz determinants gives a necessary and sufficient condition:

$$K_i K_o I_i^2 + K K_i (1 + K_o K_i) a - K J_A a^2 > 0. \tag{7}$$

For example, this can be achieved conservatively by following the simple rules in [23], which is to select a velocity loop gain higher than the motor inertia, and constraining both integrator gains to half of the respective proportional gain values.

For passivity, the real part of

$$Z(j\omega) =: A(j\omega)/B(j\omega) \tag{8}$$

has to be nonnegative for all $\omega \in (-\infty, \infty)$ that are not roots of the denominator. For nonzero denominator B, the real part of the complex fraction can be nonnegative only if

$$R(\omega) = \text{Re}(A)\text{Re}(B) + \text{Im}(A)\text{Im}(B) = \sum_{i=1}^{8} d_i \omega^i \tag{9}$$

is nonnegative for all $\omega \in (-\infty, \infty)$. All coefficients d_i of the polynomial in ω are zero, except for

$$d_6 = K\left[(K_i^2 K_o - a J_A)(K - P) + K_i K\right],$$
$$d_4 = K\left[I_i^2 K_o (K - P) - a K P\right].$$

The requirement that both coefficients have to be nonnegative bounds the achievable stiffness. With positive integrator gains, the coefficient d_4 is only nonnegative for

$$P \le K \frac{I_i^2 K_o}{I_i^2 K_o + a K} < K. \tag{10}$$

With zero integrator gains, (9) simplifies to

$$R(\omega) = \omega^6 K(-K_i^2 K_o P + K_i^2 K_o K + K_i K) \ge 0. \tag{11}$$

The controller gain P may thus exceed the value of K. However, without integrators, the stiffness displayed at low frequencies deviates from the value of P, as given in (6), and the actually displayed stiffness K_{disp} equals K for the maximum value of P allowed in (11). This implies that the SEA cannot display a higher pure stiffness than the spring stiffness, if passivity is desired.

It is important to note that the real part of the impedance and thus passivity is independent of the presence of additional end-effector mass J_e, because this simply adds the imaginary term $j\omega J_e$ to the frequency response.

Figure 4(a) and (b) features a desired stiffness lower than the allowed value. The phase never leaves the range of $+90°$ to $-90°$, which is equivalent to a positive real part, and thus the system is passive. In contrast, Figure 4(c) illustrates the case of an excessive desired stiffness; the phase falls below $-90°$. This implies that the haptic display is not passive, and the coupled system will only be stable with a certain number of environments, for example with a pure spring (a differentiator, which shifts the phase up). However, coupled to a pure mass (an integrator), the open-loop frequency response will invariably have a phase below $-180°$ for all frequencies, and thus the closed-loop system is unstable.

Limitations for the VMC

As indicated in the preceding section, both the bandwidth and the maximum value of the rendered stiffness are constrained because of the compliant actuator. Further performance limitations originate from undesired interaction forces due to exoskeleton dynamics. The influence of these effects on the achievable performance of the VMC will now be analyzed.

Performance Limitations Due to Limited Stiffness

To meet passivity requirements, the maximal joint stiffness that can be realized by joint-space impedance control is limited by the spring stiffness of the series elastic element, as was shown in the previous section. This results in boundaries for the maximum displayed Cartesian stiffness, whereby the relation between the Cartesian stiffness matrix $\mathbf{K}_x$ and the joint stiffness matrix $\mathbf{K}_\theta$ is defined by the Jacobian [29]:

$$\mathbf{K}_x = \mathbf{J}^{-T} \mathbf{K}_\theta \mathbf{J}^{-1}. \tag{12}$$

The mapped Cartesian stiffness ellipse, with $\mathbf{K}_\theta$ as the identity matrix and specifications given in Table 1, is displayed in Figure 5. Its shape and orientation are determined by the eigenvalues and vectors of $\mathbf{K}_x$, whereby it can be seen that the smallest eigenvalue depends on the knee angle.

When the exoskeleton has 90° knee flexion, the smallest eigenvalue of $\mathbf{K}_x$ is 2.53, and it is 1.3 with 10° knee flexion. The worst case is when the knee is fully extended and when the Cartesian stiffness ellipse is aligned with one of the virtual models. In this worst case scenario, the Cartesian stiffness is only 200 N/m given the maximal joint stiffness of the hip and knee of 155 Nm/rad, as given in the "Mechanical Design" section.

Performance Limitations Due to Manipulator Dynamics

The VMC does not compensate for the open-loop impedance of the exoskeleton. As a consequence, in free space, the human operator will always feel the full inertia and friction of the manipulator [30], and thus not only the virtual model.

The undesired additional interaction torque τ in the swing phase given by the equation of motion of the exoskeleton:

$$\tau = \mathbf{M}(\boldsymbol{\theta})\ddot{\boldsymbol{\theta}} + \mathbf{v}(\boldsymbol{\theta}, \dot{\boldsymbol{\theta}}) + \boldsymbol{g}(\boldsymbol{\theta}), \tag{13}$$

where $\boldsymbol{\theta}$ is the vector of joint angles, $\mathbf{M}(\boldsymbol{\theta})$ is the mass matrix, $\boldsymbol{v}(\boldsymbol{\theta}, \dot{\boldsymbol{\theta}})$ are Coriolis and centrifugal torques, and $\boldsymbol{g}(\boldsymbol{\theta})$ are gravitational torques. To give an idea of the inertia of the device reflected at LOPES's ankle, these unwanted torques can be mapped to forces in Cartesian space with ankle position $\boldsymbol{x}$:

$$\boldsymbol{F} = \mathbf{M}_x(\boldsymbol{\theta})\ddot{\boldsymbol{x}} + \boldsymbol{v}_x(\boldsymbol{\theta}, \dot{\boldsymbol{\theta}}) + \boldsymbol{g}_x(\boldsymbol{\theta}), \tag{14}$$

whereby the relation between joint space and Cartesian space matrices can be derived using the Jacobian [29].

To compensate the components $\boldsymbol{v}_x(\boldsymbol{\theta}, \dot{\boldsymbol{\theta}})$ and $\boldsymbol{g}_x(\boldsymbol{\theta})$, the VMC could be modified, since as terms depend only on joint angles and velocities. However, in our application, we compensate neither of these forces. First, centrifugal and Coriolis forces in $\boldsymbol{v}_x$ are negligibly small. Second, subjects walking with compensated exoskeleton gravitational forces $\boldsymbol{g}_x$ reported that it felt unnatural, and compensating for $\boldsymbol{g}_x$ with constant $\mathbf{M}_x$ increases the natural frequency. (As stated before, $\mathbf{M}_x$ can not be reduced by any causal controller.)

Especially at high frequencies, the behavior of the device is dominated by the reflected mass $\mathbf{M}_x$ of the exoskeleton. With respect to the ankle, this reflected mass is related to the joint space mass matrix by

$$\mathbf{M}_x = \mathbf{J}^{-T}\mathbf{M}\mathbf{J}^{-1}. \tag{15}$$

Using the specifications given in Table 1, this reflected mass is visualized by the inertia ellipse of Figure 5. Its shape and orientation are determined by the eigenvalues and vectors of $\mathbf{M}_x$. The orientation of the ellipse is always perpendicular to the lower segment of the exoskeleton, which means that the reflected mass is minimal in perpendicular direction and maximal in the parallel direction of the most distal segment of the exoskeleton. The eigenvalues of $\mathbf{M}_x$ depend only on the knee angle of the exoskeleton. The smallest eigenvalue remains fairly constant around 0.95 kg. The largest eigenvalue is minimal (3.9 kg) when the knee is 90° flexed and increases when the knee is extended. Note that the reflected mass of the device would be much higher if the motors were not detached from the exoskeleton and if the motor mass was not decoupled from the device by the series elastic element.

Experimental Results

The remarkable capabilities of the SEA in terms of force tracking and backdrivability (i.e., the inner control loop) have been evaluated experimentally and are described in [23]. These practical experiments also showed a very good agreement between the theoretically predicted and actually achieved force tracking bandwidth, with a value of approximately 16 Hz. The experimental results presented in this article are limited to the performance of the outer impedance control loop.

For the control of an individual joint of the exoskeleton alone (without human subject), the maximum achievable stiffness before undesired oscillations occurred is almost equal to the spring stiffness (±10%, depending on gain variations in the torque control loop), as predicted by the theoretical analysis. In contrast, the maximum achievable Cartesian stiffness in practical experiments with healthy subjects walking under the influence of VMC resulted to be 1,500 N/m in vertical direction (step height control) and 700 N/m in horizontal direction (step length control), which is considerably higher than the theoretic worst-case bound. With the angle data from the experiment and (12), the Cartesian stiffness in horizontal direction should be limited to 200 Nm and in vertical direction to 355 Nm.

The reflected mass of the exoskeleton constrains the achievable bandwidth, as illustrated in the "Bandwidth Limitations" section for the SISO case. The limit is given by the square root of the desired stiffness of the virtual component

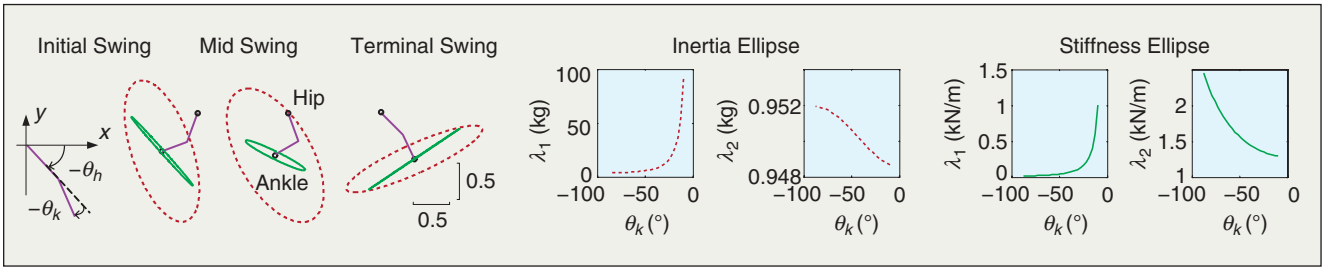

Figure 5. Reflected mass and stiffness at the ankle: The mass (red and dashed) and stiffness (green and solid) ellipses that reflect the inertia of the exoskeleton and hip and knee joint stiffnesses of 1 Nm/rad at the ankle for different kinematic configurations. The principal axes of the stiffness ellipses are the inverse of the Cartesian stiffness matrix eigenvalues λ_1 and λ_2; the axes of the inertia ellipses are the inverse of the square root of the respective eigenvalues. Thus, the larger the ellipses, the less mass or stiffness is reflected.

divided by the reflected exoskeleton mass. Below this frequency, the virtual spring is felt, whereas above, the reflected device mass is felt. In the case where the reflected mass is minimal (0.95 kg), this frequency is 4.3 and 6.3 Hz for the stiffnesses of 700 and 1,500 N/m, respectively. For a desired stiffness of 700 N/m and using a worst-case approach, it reduces to 2.14, 1.93, 1.21, and 0.44 Hz for 90°, 60°, 30°, and 10° knee flexion, respectively.

Despite these heavy bandwidth limitations, the combination of the mechanical designs of LOPES and VMC was well able to modify the step height and step length of healthy subjects [20]. Each of the two parameters could be lengthened or shortened by VMC, simply by scaling the reference path. The change in each specific gait parameter left the other parts of the gait cycle almost unaffected, and the modification was not perceived awkward until it got excessively large. In experiments with varying stiffness, we found that the subjects perceived stiffer controllers as less comfortable; they preferred more compliant virtual springs. Adjustment of the reference parameters beyond the desired value in combination with a softer controller (equivalent to additional feedforward torques, which is not unique to VMC) also achieved the desired modification and was perceived as more comfortable than a stiff control. The selective modification of average ankle trajectories is shown in Figure 6 for the maximum stiffness. However, the figure also shows that the step length was not exactly modified by the desired 20% due to the compliant interface. The experiments are described in detail in [31].

Discussion

A comparison of the theoretical predictions and the experimental outcome shows good agreement for joint-space impedance control without human subject, but it also shows that the Cartesian stiffness used in the VMC can be higher than the theoretically derived worst-case bound. The fact that this higher stiffness is rendered without stability problems can be explained by several factors. First, the worst case in terms of kinematic configuration hardly occurred in the practical experiments, or at least, the system never remained in this state for long, such that the instable effects might have been transient. Second, passivity is a conservative means of ensuring stability of coupled systems, and a less conservative, explicit MIMO stability analysis could replace it (requiring the exoskeleton, the patient's impedance, the compliant coupling between human and exoskeleton, and the environment to be modeled reliably, which is difficult). Nevertheless, without a human subject, the theoretical and practical results coincided well. Therefore, a probable reason is that the healthy subjects did not behave like pure masses, the worst environment discussed in the section "Stiffness Limitations Due to Passivity Concerns," but formed stabilizing elements in the control loop. This positive contribution might stem from intrinsic and neuronally coordinated stiffness and damping, and it is for example exploited for the control of BLEEX [32]. Although it seemed possible to render higher stiffness for healthy subjects than theoretically derived, we decided not to rely on this effect when working with patients. Instead, we increased the stiffness of the SEA by a factor of 2.5. Equipped with these stiffer springs, LOPES can operate with sufficiently stiff VMC and still remain within the conservative limits resulting from the passivity analysis. Generally, there is a tradeoff between achievable stiffness on the one hand and low undesired interaction torques on the other. One possibility would be to use an adaptive compliance, as suggested by [33], to meet the individual patient's needs.

Conclusion

This article discusses the pros and cons of compliant actuation for rehabilitation robots on the example of LOPES, focusing on the cons. After illustrating the bandwidth limitations, a new result has been derived: if stability in terms of passivity of the haptic device is desired, the renderable stiffness is bounded by the stiffness of the SEA's elastic component.

In practical experiments with the VMC, the aforementioned limitations affected the control performance. Desired gait modifications were not tracked exactly, because the subjects were able to deviate from the prescribed pattern even in the stiffest possible configuration. Despite the limitations, the practical experiments also demonstrated the general effectiveness of the realization. Manipulation of selected gait parameters is possible, whereby other parameters are left unaffected. This high selectivity is made possible by the low level of undesired interaction torques, which is

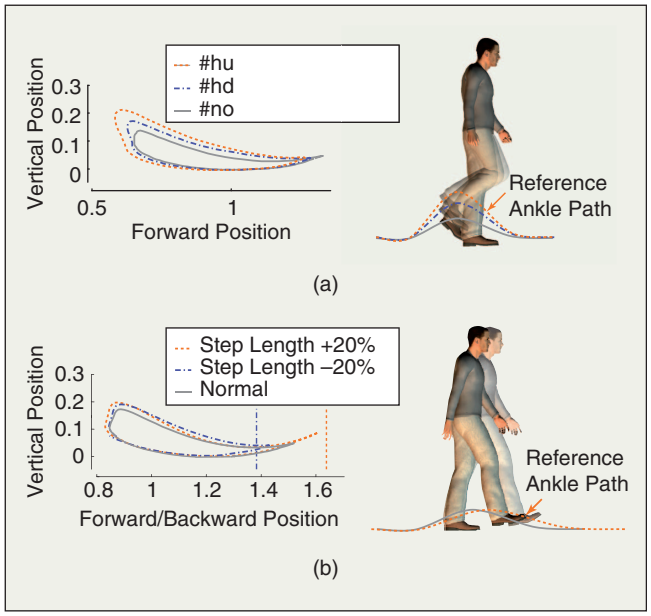

Figure 6. *Modification of the (a) step height and (b) length. The normal ankle trajectories are scaled to obtain a reference trajectory for the ankle. With a virtual spring attached at the ankle, the differences between the true and desired ankle position are mapped to a (a) vertical or (b) horizontal virtual force at the ankle. Typical example of a subject's modified ankle trajectories (a) for the case that the maximal foot clearance is increased to 17 or 22 cm, and (b) for the case that the step length is increased or decreased by 20%.*

achieved by elastic decoupling of motor mass and a lightweight exoskeleton.

The discrepancy between theoretical bounds and rendered stiffness indicated that healthy subjects might represent a stabilizing component of the coupled system, which could be different for patients. In light of the theoretical stability analysis and with the focus on patients, the LOPES actuation was slightly modified. The robot was equipped with stiffer springs to obtain sufficient stiffness and to ensure stability without relying on stabilizing effects of the human.

For this application, the disadvantages of compliant actuation can thus be tolerated or dealt with, and they are small compared with the advantages. Given that a rehabilitation robot, in the first place, is supposed to imitate therapist action, the limitations of bandwidth and stiffness do not pose severe problems. In contrast, safety and backdrivability are highly relevant, and they can be ensured easier with a compliant actuator. Therefore, we conclude that compliant actuation and a lightweight exoskeleton provide effective means to accomplish the desired AAN behavior of a rehabilitation robot. The next step is to evaluate the robot behavior, control performance, and therapeutic effectiveness in patient studies.

Acknowledgments

H. Vallery was supported by the Studienstiftung des Deutschen Volkes. All authors from the University of Twente were supported by the Netherlands Organisation for Scientific research (Vernieuwings-impuls 2001, 22016027011, granted to Dr. H. van der Kooij) and by the Institute for Biomedical Technology.

Keywords

Series elastic actuators, gait training, passivity-based control, stroke, compliance, rehabilitation robots.

References

[1] G. Kwakkel, R. C. Wagenaar, T. W. Koelman, G. J. Lankhorst, and J. C. Koetsier, "Effects of intensity of rehabilitation after stroke. A research synthesis," *Stroke*, vol. 28, no. 8, pp. 1550–1556, 1997.

[2] R. Teasell, J. Bitensky, K. Salter, and N. A. Bayona, "The role of timing and intensity of rehabilitation therapies," *Top. Stroke Rehabil.*, vol. 12, no. 3, pp. 46–57, 2005.

[3] B. Husemann, F. Muller, C. Krewer, S. Heller, and E. Koenig, "Effects of locomotion training with assistance of a robot-driven gait orthosis in hemiparetic patients after stroke: A randomized controlled pilot study," *Stroke*, vol. 38, no. 2, pp. 349–354, 2007.

[4] M. Pohl, C. Werner, M. Holzgraefe, G. Kroczek, J. Mehrholz, I. Wingendorf, G. Hoolig, R. Koch, and S. Hesse, "Repetitive locomotor training and physiotherapy improve walking and basic activities of daily living after stroke: A single-blind, randomized multicentre trial (DEutsche GAngtrainerStudie, DEGAS)," *Clin. Rehabil.*, vol. 21, pp. 17–27, 2007.

[5] L. L. Cai, A. J. Fong, C. K. Otoshi, Y. Liang, J. W. Burdick, R. R. Roy, and V. R. Edgerton, "Implications of assist-as-needed robotic step training after a complete spinal cord injury on intrinsic strategies of motor learning," *J. Neurosci.*, vol. 26, no. 41, pp. 10564–10568, 2006.

[6] M. Ferraro, J. J. Palazzolo, J. Krol, H. I. Krebs, N. Hogan, and B. T. Volpe, "Robot-aided sensorimotor arm training improves outcome in patients with chronic stroke," *Neurology*, vol. 61, no. 11, pp. 1604–1607, 2003.

[7] N. Hogan, H. I. Krebs, B. Rohrer, J. J. Palazzolo, L. Dipietro, S. E. Fasoli, J. Stein, R. Hughes, W. R. Frontera, D. Lynch, and B. T. Volpe, "Motions or muscles? Some behavioral factors underlying robotic assistance of motor recovery" *J. Rehabil. Res. Dev.*, vol. 43, no. 5, pp. 605–618, 2006.

[8] D. Aoyagi, W. E. Ichinose, S. J. Harkema, D. J. Reinkensmeyer, and J. E. Bobrow, "A robot and control algorithm that can synchronously assist in naturalistic motion during body-weight-supported gait training following neurologic injury," *IEEE Trans. Neural Syst. Rehab. Eng.*, vol. 15, no. 3, pp. 387–400, 2007.

[9] J. F. Veneman, R. Ekkelenkamp, R. Kruidhof, F. C. T. van der Helm, and H. van der Kooij, "A series elastic- and Bowden-cable-based actuation system for use as torque actuator in exoskeleton-type robots," *Int. J. Robot. Res.*, vol. 25, no. 3, pp. 261–281, 2006.

[10] J. F. Veneman, R. Kruidhof, E. E. G. Hekman, R. Ekkelenkamp, E. H. F. Van Asseldonk, and H. Van der Kooij, "Design and evaluation of the LOPES exoskeleton robot for interactive gait rehabilitation," *IEEE Trans. Neural. Syst. Rehabil. Eng.*, vol. 15, no. 3, pp. 379–386, 2007.

[11] G. Colombo, M. Joerg, R. Schreier, and V. Dietz, "Treadmill training of paraplegic patients using a robotic orthosis," *J. Rehabil. Res. Dev.*, vol. 37, no. 6, pp. 693–700, 2000.

[12] J. F. Israel, D. D. Campbell, J. H. Kahn, and T. G. Hornby, "Metabolic costs and muscle activity patterns during robotic- and therapist-assisted treadmill walking in individuals with incomplete spinal cord injury," *Phys. Ther.*, vol. 86, no. 11, pp. 1466–1478, 2006.

[13] D. J. Reinkensmeyer, D. Aoyagi, J. L. Emken, J. A. Galvez, W. Ichinose, G. Kerdanyan, S. Maneekobkunwong, K. Minakata, J. A. Nessler, R. Weber, R. R. Roy, R. de Leon, J. E. Bobrow, S. J. Harkema, and V. R. Edgerton, "Tools for understanding and optimizing robotic gait training," *J. Rehabil. Res. Dev.*, vol. 43, no. 5, pp. 657–670, 2006.

[14] S. K. Banala, S. K. Agrawal, and J. P. Scholz, "Active leg exoskeleton (ALEX) for gait rehabilitation of motor-impaired patients," in *Proc. IEEE ICORR 2007*, pp. 401–407.

[15] M. Peshkin, D. A. Brown, J. J. Santos-Munné, A. Makhlin, E. Lewis, J. E. Colgate, J. Patton, and D. Schwandt, "KineAssist: A robotic overground gait and balance training device," in *Proc. IEEE ICORR 2005*, Chicago, pp. 241–246.

[16] D. W. Robinson, "Design and analysis of series elasticity in closed-loop actuator force control," Ph.D. thesis, Dept. Mech. Eng., MIT, Cambridge, MA, 2000.

[17] H. Vallery and M. Buss, "Bewegungsintentionsschätzung auf Basis von Gelenkkoordination," *at-Automatisierungstechnik*, vol. 55, no. 10, pp. 503–510, 2007.

[18] H. Vallery, R. Ekkelenkamp, H. van der Kooij, and M. Buss, "Complementary limb motion estimation based on interjoint coordination: experimental evaluation," in *Proc. IEEE ICORR 2007*, pp. 798–803.

[19] R. Ekkelenkamp, J. Veneman, and H. van der Kooij, "LOPES: Selective control of gait functions during the gait rehabilitation of CVA patients," in *Proc. IEEE ICORR 2005*, pp. 361–364.

[20] E. H. F. Van Asseldonk, R. Ekkelenkamp, J. F. Veneman, F. C. T. van der Helm, and H. van der Kooij, "Selective control of a subtask of walking in a robotic gait trainer(LOPES)," in *Proc. IEEE ICORR 2007*, pp. 841–848.

[21] G. Wyeth, "Control issues for velocity sourced series elastic actuators," in *Proc. Australasian Conf. Robotics and Automation*, 2006.

[22] G. A. Pratt, P. Willisson, C. Bolton, and A. Hofman, "Late motor processing in low-impedance robots: Impedance control of series-elastic actuators," in *Proc. 2004 ACC*, pp. 3245–3251.

[23] H. Vallery, R. Ekkelenkamp, H. van der Kooij, and M. Buss, "Passive and accurate torque control of series elastic actuators," in *Proc. IEEE IROS 2007*, San Diego, CA, pp. 3534–3538.

[24] H. van der Kooij, R. Jacobs, B. Koopman, and F. van der Helm, "An alternative approach to synthesizing bipedal walking," *Biol. Cybern.*, vol. 88, no. 1, pp. 46–59, 2003.

[25] J. A. Galvez, G. Kerdanyan, S. Maneekobkunwong, R. Weber, M. Scott, S. J. Harkema, and D. J. Reinkensmeyer, "Measuring human trainers' skill for the design of better robot control algorithms for gait training after spinal cord injury," in *Proc. IEEE ICORR 2005*, pp. 231–234.

[26] J. E. Pratt, C. M. Chew, A. Torres, P. Dilworth, and G. Pratt, "An intuitive approach for bipedal locomotion," *Int. J. Robot. Res.*, vol. 20, no. 2, pp. 129–143, 2001.

[27] J. E. Colgate, "The control of dynamically interacting systems," Ph.D. thesis, Dept. Mech. Eng., MIT, Cambridge, MA, 1988.

[28] S. D. Eppinger and W. P. Seering, "Understanding bandwidth limitations in robot force control," in *Proc. ICRA 1987*, pp. 904–909.

[29] J. J. Craig, *Introduction to Robototics: Mechanics and Control*, 2nd ed. Reading, MA: Addison-Wesley, 1989.

[30] R. W. Adams and B. Hannaford, "Control Law Design for Haptic Interfaces to Virtual Reality," *IEEE Trans. Contr. Syst. Technol.*, vol. 10, no. 1, pp. 3–13, 2002.

[31] R. Ekkelenkamp, E.H.F. van Asseldonk, B. Koopman, P. H. Veltink, S. Stramigioli, and H. van der Kooij, "Swing phase adaptation during walking by virtual model control of a powered exoskeleton," submitted for publication.

[32] H. Kazerooni, Jean-Louis Racine, Lihua Huang, and Ryan Steger, "On the control of the berkeley lower extremity exoskeleton (BLEEX)," in *Proc. IEEE ICRA 2005*, pp. 4364–4371.

[33] K. W. Hollander, T. G. Sugar, and D. E. Herring, "Adjustable robotic tendon using a 'Jack Spring'," in *Proc. IEEE ICORR 2005*, pp. 113–118.

Heike Vallery received her diploma (with honors) in mechanical engineering from RWTH Aachen University in Germany in 2004. She is about to finish her Ph.D. degree at the Institute of Automatic Control Engineering at the Technische Universität München, Germany, where she worked on patient-cooperative control strategies for rehabilitation robots. In May 2008, she joined the Sensory-Motor Systems Laboratory at the ETH Zürich, Switzerland. Her research interests include haptics, human motor control, and robotics. She is a Student Member of the IEEE.

Jan Veneman received M.Sc. degrees in mechanical engineering and philosophy of science, technology and society in 1998 and 2001, respectively, and the Ph.D. degree in biomechanical engineering in 2007, all from the University of Twente, Enschede, The Netherlands. His research project was on the design and evaluation of a prototype gait rehabilitation robot. His principal research interests are haptics, man–machine interaction, and robotics.

Edwin van Asseldonk received his M.Sc. degree (honors) in human movement sciences from the Free University, Amsterdam, The Netherlands and his Ph.D. degree in biomechanical engineering from the University of Twente in 2008. Currently, he is an assistant professor at the University of Twente. His field of research includes balance control, motor control in stroke patients and rehabilitation robotics.

Ralf Ekkelenkamp received his M.Sc. degree in electrical engineering at the University of Twente in 2003. From 2003 until 2007, he was working as a Ph.D. candidate on the advanced control of a gait rehabilitation robot, also at the University of Twente. Currently, he is a design engineer at Sensata Technologies.

Martin Buss received the diploma engineer degree in electrical engineering in 1990 from the Technical University Darmstadt, Germany, and the doctor of engineering degree in electrical engineering from the University of Tokyo, Japan, in 1994. In 2000, he finished his habilitation in the Department of Electrical Engineering and Information Technology, Technische Universität München, Germany. In 1988, he was a research student at the Science University of Tokyo, Japan, for one year. As a postdoctoral researcher, he worked at the Department of Systems Engineering, Australian National University, Canberra, Australia, in 1994–1995. From 1995 to 2000, he has been senior research assistant and lecturer at the Institute of Automatic Control Engineering, Department of Electrical Engineering and Information Technology, Technische Universität München, Germany. He has been appointed full professor, head of the control systems group, and deputy director of the Institute of Energy and Automation Technology, Faculty IV—Electrical Engineering and Computer Science, Technical University Berlin, Germany, from 2000–2003. Since 2003, he has been full professor (chair) at the Institute of Automatic Control Engineering, Technische Universität München, Germany. Since 2006, he has been the coordinator of the DFG Excellence Research Cluster Cognition for Technical Systems—CoTeSys. His research interests include automatic control, mechatronics, multimodal human–system interfaces, optimization, nonlinear, and hybrid discrete-continuous systems. He is a Member of the IEEE.

Herman van der Kooij received his Ph.D. degree with honors (cum laude) in 2000 and is an associate professor at the Department of Biomechanical Engineering at the University of Twente (0.8 fte), and Delft University of Technology (0.2 fte), The Netherlands. His expertise and interests are in the field of human motor control, adaptation, and learning, rehabilitation robots, diagnostic robotics, virtual reality, rehabilitation medicine, and neurocomputational modeling. He is a Member of the IEEE Engineering in Medicine and Biology Society Technical Committee of Biorobots and was a member of several scientific program committees in the field of rehabilitation robotics, biorobotics, and assistive devices. He is the founder and head of the Rehabilitation Robotics Laboratory, at the University of Twente, which developed powered exoskeletons for the rehabilitation of upper and lower extremities. He is also the founder and head of the Virtual Reality Human Performance Lab that combines robotic devices, motion capturing, and virtual environments to assess and train human balance, walking, and hand–eye coordination. He is a recipient of the VIDI award.

Address for Correspondence: Heike Vallery, Sensory Motor Systems Lab, ETH Zürich, 8008 Zürich, Switzerland. E-mail: heike.vallery@mavt.ethz.ch.

Pulling Your Strings

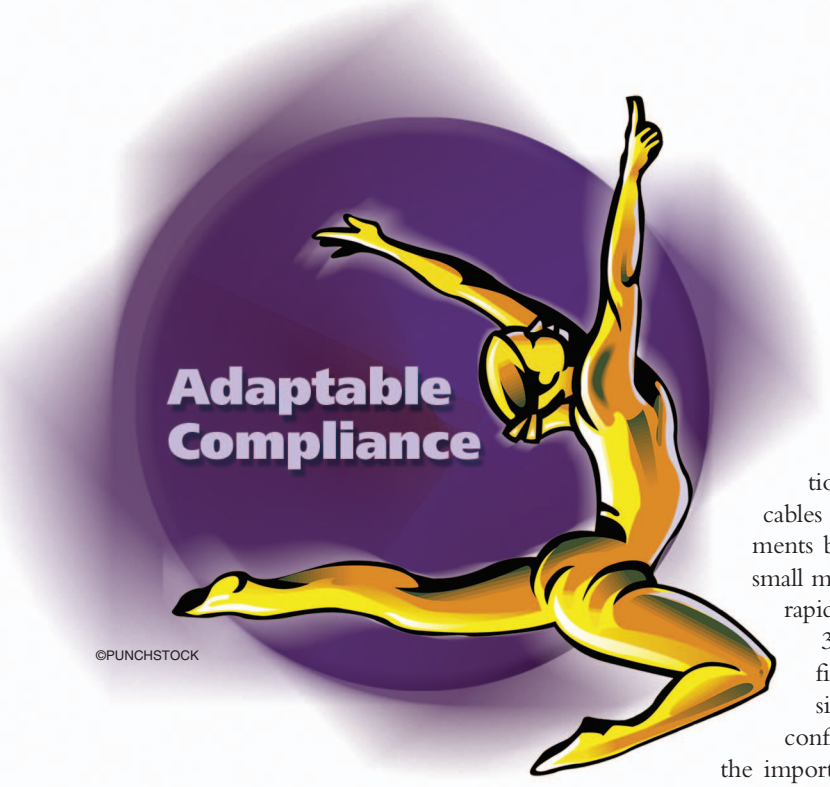

©PUNCHSTOCK

Cable Moment Arm Manipulation as a Modality of Joint Actuation

BY JAMES S. SULZER, MICHAEL A. PESHKIN, AND JAMES L. PATTON

Digital Object Identifier 10.1109/MRA.2008.927692

Recently, there has been an exciting array of new robotic devices especially designed for human-machine interaction. Consequently, a new field related to haptics has flourished: development of simple and often inexpensive devices that provide force feedback or positioning of a human operator as controlled by customized computer programs. One method, which seems to be less explored, is the use of cable actuators for such a robot.

Cables are advantageous because of remote actuation, flexibility, and low weight. Tendons are examples of cables used in nature. The body uses these natural tension elements by keeping them close to the joints, which generates a small moment arm that limits torque but allows large and often rapid movement. For example, forearm muscles only contract 30% of their rest length but use tendons to span across the fingers, enhancing range of motion and dexterity while simultaneously reducing arm inertia. Studies of the joint configuration-based changes in muscle leverage have revealed the importance of both tension and moment arms in generating force, motion, and impedance [1]. In robotics, the Utah/MIT hand is a robotic analog to the human hand's use of cables [2]. This robot hand uses cables passing over pulleys, which for humans would be represented by tendon sheaths, for low-friction remote actuation.

Cable-actuated mechanisms have been used by human beings in the past. The whole arm manipulator uses a novel, differential cable transmission system to reduce high cable tension, increase backdrivability, and reduce cable failure in an articulating arm [3]. The PHANTOM by SensAble uses a low backlash cable-driven transmission to create a multipurpose haptic interface [4]. A number of human-interactive experiments have used cables to successfully actuate human joints, either directly at the joint [5], through a parallel configuration [6], [7], or through series elastic elements [8].

The concept of series elastic actuation, first published by Pratt and Williamson, controls the equilibrium point of a linear spring in series with a gearmotor [9]. This creates a lightweight, low-cost, simple, and compliant interface fit for human applications. Veneman et al. take this concept a step further, using cables to remotely actuate the elastic joints on a lower body exoskeleton for gait rehabilitation [8]. They consider this device, known as LOwer-extremity Powered ExoSkeleton (LOPES), to be a more beneficial method of assisting gait because of its inherent compliance and lower apparent inertia than position-controlled robotic gait trainers such as the Lokomat [10].

Our key motivation is the rehabilitation of individuals recovering from stroke or other neurological insult. This area needs constant development because of an expanding aged population and improved rates of survival from injuries. Recent research strongly supports rehabilitation by prolonged practice of functional activities of the upper limb, even though professionally supervised therapy is quite limited by the current medical economic system. Although robotic therapy has

1070-9932/08/$25.00©2008 IEEE

been thought to be able to fill this gap, performance and cost have been a difficult optimization. Lower-cost, lighter-weight gearmotors lack the ability to provide the forgiving torque-controlled output that human therapists deliver. Although passive, compliant training devices are now becoming available for home rehabilitation [11], few, if any, active training devices exist that are inexpensive, compliant, safe, and capable of home use. In this article, we summarize research that introduces a novel modality of joint actuation based on previous work [12]–[14], one that can potentially lead to a low-cost, human-friendly home rehabilitation system. This method manipulates both the tension and the moment arm in a cable-driven joint to create a variable compliant interface.

The torque exerted by a cable-driven joint is the cross product of the line of action of the cable, known as the moment arm, and its tension. The subject of this article delves into this latter, less-studied quantity associated with torque. The concept of moment arm manipulation of a cable-driven joint is introduced, developed, formalized, and then examined with experiments on a physical, single-joint device. This method of moment arm manipulation, referred to as the moment arm manipulation for remote induction of net effective torque (MARIONET), is found to have distinct advantages that make it feasible for home rehabilitation as well as potential outside of the field.

Concept Development

The key to this investigation is how the moment arm is manipulated. Figure 1(a) is a schematic of a single cable-driven joint, with parameters given in polar coordinates. A fictional hand changes the line of action of the cable under constant tension, and the moment arm path can vary in an infinite number of ways. Ultimately, a single degree-of-freedom (DoF) path variation can be broken down into two archetypes: linear and rotational. Figure 1(b) provides four basic examples of path variation using these two archetypes, of which either may be centered at the joint or located some offset distance away. At any joint position, there exists a maximum and minimum torque (referred to as a torque envelope) that can be exerted on the joint, given the constraint of the moment arm path and constant tension. Figure 2 displays a normalized envelope resulting from a 1-m link length and a unit cable tension showing how torque varies for different moment arm paths across joint positions. Because a linear path does not reflect the movement of the joint, its torque envelope will be nonlinear. As Figure 2(a) illustrates, a linear path through the joint center can produce the largest possible torque at a few certain joint positions, but it is incapable of producing torque in the opposite direction at those same points. Furthermore, the maximum attainable torque in this design varies with joint position. As a result of this behavior, the endpoint stiffness, which is the partial derivative of the torque according to joint position, is also highly nonlinear, reducing the system effectiveness for perturbations. In short, a linear moment arm path is not globally controllable, but it does have high torque capability.

One example of an application of a linear path is a leg rehabilitation robot by Homma et al. [5]. Traveler cars riding on rails 2 m above a prone subject pull on cables that directly manipulate the lower extremities. With such a large offset, the

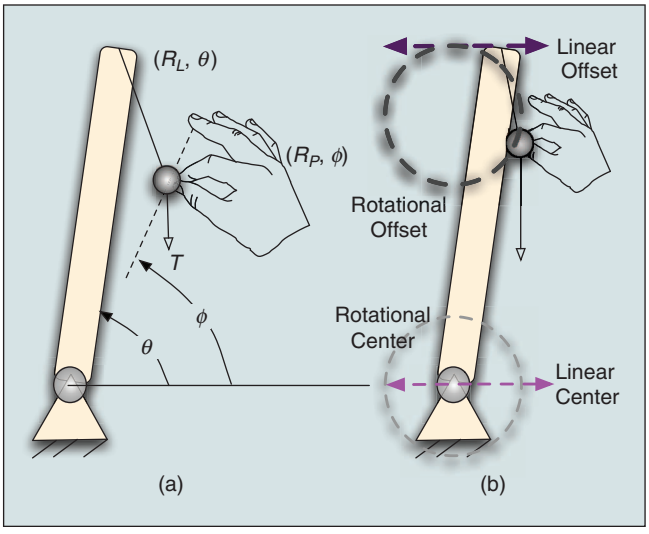

Figure 1. *(a) Fictional hand can move the cable's line of action in any manner. Variable definitions are given for this simple cable-driven joint in polar coordinates. (b) Four different candidate moment arm paths are shown for subsequent analysis.*

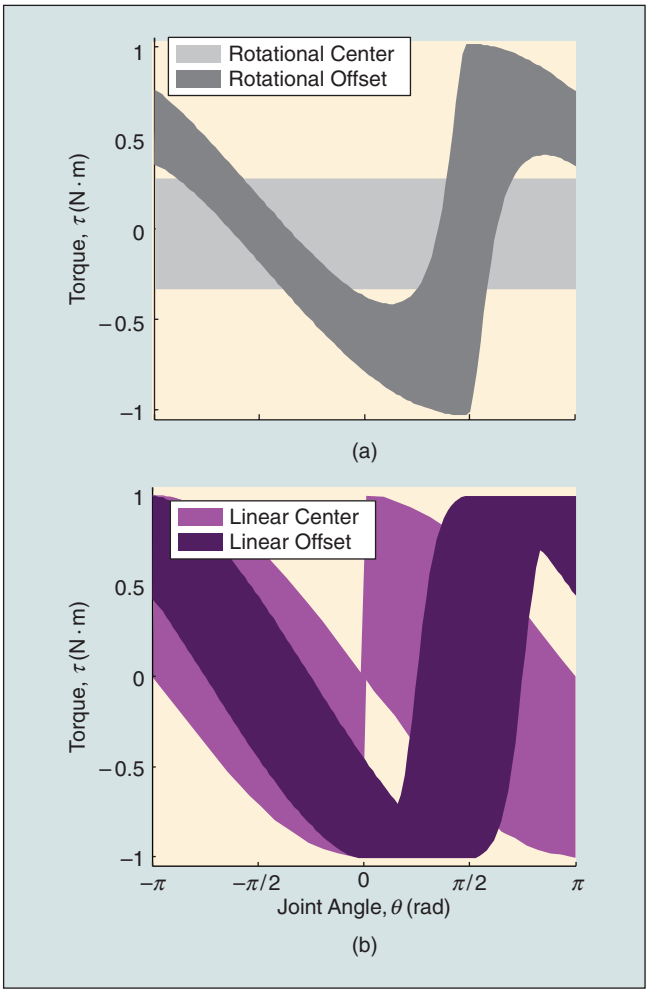

Figure 2. *Shaded areas display the range of achievable torques (torque envelopes) at each joint angle. (a) Rotational path. (b) Linear path. Since the rotational center path is constant and easily controllable, it was chosen for our initial implementation of the MARIONET.*

This method manipulates both the tension and moment arm in a cable-driven joint to create a variable compliant interface.

structure takes advantage of the high moment arm that can be achieved for the limited range of motion of the leg. Controllability is restored by using gravity to return the leg to its initial position.

The candidate rotational paths show a larger difference in comparison. Figure 2(b) shows that, while the offset rotational path also has a nonlinear relationship with joint position, the rotational path centered at the joint produces a constant torque envelope in both directions. Maximum torque increases with radius, and endpoint stiffness is locally positive, definite, smooth, and symmetric, making it robust to perturbations. These properties make this rotational path appropriate for the general application outlined in this article.

A schematic using this rotational moment arm path version of the MARIONET is shown in Figure 3. There are a few basic components in this system. The end effector rotates about a center with a cable connected to it at point (R_L, Θ). The cable then passes through a pulley on the rotator at point (R_P, Φ), which, as its name implies, can only rotate, creating

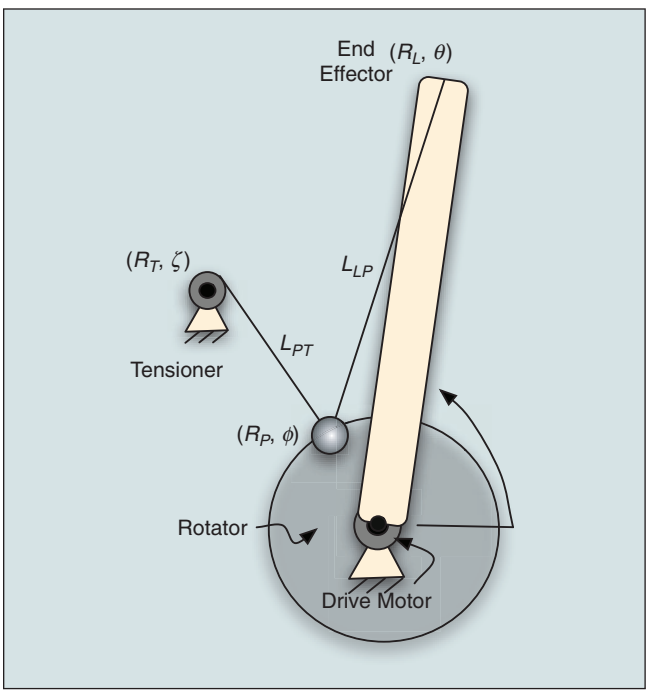

Figure 3. *Schematic and definitions of variables used throughout the analysis. The drive motor rigidly controls the position of the rotator and the tensioner creates cable tension, which couples the free-rotating end effector to the motion of the rotator. Both have the same center of rotation. All angles are measured relative to the horizontal datum, and all coordinates are in polar notation.*

the desired moment arm constraint. The length of cable from end effector to rotator is denoted as L_{LP}. The cable then travels from the pulley on the rotator to a motor at point (R_T, ζ), known as the tensioner, which supplies cable tension, and for the purpose of this article, it maintains a constant value. The length of cable from (R_P, Φ) to (R_T, ζ) is denoted as L_{PT}. The end effector and rotator have the same center of rotation. Although the end effector is left free to rotate, it is pulled along by the cable that passes through the rotator, whose position is rigidly controlled by the drive motor.

The energy, torque, and stiffness of the system are a function of the length of the cable and its tension. The system will settle at equilibrium, or in other words, its minimum potential energy, where the cable is at its minimum length. The work, W, that the system does on its environment may be expressed in terms of the tension, T, and the change in length of the cable, otherwise known as cable excursion, dx,

$$W = \int T dx. \tag{1}$$

The sum of the lengths of the cable is calculated as segments separated at the pulley:

$$dx = L_{PT}(\Phi) + L_{LP}(\Phi, \Theta) - l_0, \tag{2}$$

where l_0 is the length of the cable at minimum energy. Using the law of cosines to solve for the terms mentioned earlier,

$$L_{PT}(\Phi)^2 = R_P^2 + R_T^2 - 2R_P R_T \cos(\Phi - \zeta) \text{ and} \tag{3a}$$

$$L_{LP}(\Phi, \Theta)^2 = R_L^2 + R_P^2 - 2R_L R_P \cos(\Theta - \Phi). \tag{3b}$$

With a constant cable tension, the work is the product of the length of cable and tension and can be stated in terms of joint torque τ,

$$W = \int T\, dx = \int \tau\, d\Theta. \tag{4}$$

This equation can be simplified to

$$\frac{\tau}{T} = \frac{dx}{d\Theta}. \tag{5}$$

Therefore, the torque per unit tension (moment arm) is equivalent to the change in the amount of cable excursion according to the end effector position. In other words, a small amount of excursion that causes a large change in joint position, as does in the fingers, indicates a small moment arm. Carrying out the math,

$$\frac{\tau}{T} = R_L \frac{R_P}{L_{LP}(\Psi)} \sin(\Psi), \tag{6}$$

where $\Psi = \Theta - \Phi$ is the relative angle between the rotator and the end effector. The endpoint stiffness, k, can be found in a similar manner, since

$$\frac{k}{T} = \frac{d\tau}{d\Theta} = \frac{d^2x}{d\Theta^2}, \tag{7}$$

which means that the amount the moment arm changes with joint position is the endpoint stiffness. This provides a basis for the configuration-dependent stiffness of human limbs. Carrying out the math,

$$\frac{k}{T} = R_L \frac{R_P}{L_{LP}(\Psi)} \cos(\Psi) - R_L^2 \frac{R_P^2}{L_{LP}(\Psi)^3} \sin^2(\Psi). \tag{8}$$

If an elastic element is placed in series with the cable, as will be examined in the following example, the torque equation now becomes

$$\tau = R_L R_P \sin(\Psi) k_s L_{LP0}, \tag{9}$$

where k_s is the stiffness of the linear spring, and L_{LP0} is the controlled equilibrium position of the spring. Therefore, both torque and endpoint stiffness can be manipulated using the relative angle, Ψ. Moreover, one can linearly modify torque and stiffness by varying the tension.

The general concept of the MARIONET is to vary moment arm along any path while in some way maintaining tension in the cable. Other paths may be desirable in specific applications, such as where workspace is limited or where specific torques are required. A practical application is the mechanically adjustable compliance and controllable equilibrium position actuator (MACCEPA) design that uses a nonbackdrivable motor to control a rotational moment arm path and also controls the length of a linear spring between the end effector and the rotator using another nonbackdrivable motor [15]. This has been used to control both equilibrium position and stiffness to actuate gait in a bipedal robot [16].

Some of the differences between using a spring and using a constant tension are illustrated in Figure 4. The torque-deflection relationship varies with both tension and geometrical parameters. Producing constant cable tension (gray gradient) and linear spring cable tension (green gradient) results in different possible ranges of torques. Increasing pretension amplifies the torque-deflection relationship in both curves in Figure 4(a). At low pretension, the linear spring case needs more deflection than constant tension to reach higher torques, but this aspect could be useful for filtering out disturbances. An increase in the pretension for both cases makes a more responsive system. Differences between the two cases become more pronounced when changing the relationship between the rotator radius (R_P) and the end effector length (R_L), shown in Figure 4(b). A very small rotator compared with the end effector could not create a large moment arm, and therefore in both cases, very little torque can be produced. However, as the rotator radius approaches the end effector, the greatest possible moment arm occurs as the relative angle between them approaches zero. In the case of the linear spring, the greatest amount of torque is produced when there is the optimum combination of both spring deflection and moment arm. From the standpoint of achieving high torque production, these plots suggest that constant force impedance, achieved perhaps by a constant force spring, would be more advantageous than a linear spring in situations with small rotator excursion and vice versa. A final item to note is that that the torque-angle relationship in Figure 4(a) closely resembles the way the force-length characteristic of mammalian muscle [17] and how it acts to smoothly and stably generate torque over a range of angles.

Our key motivation is the rehabilitation of individuals recovering from stroke or other neurological insult.

In fact, knowing such stability characteristics of this nonlinear system is essential for human use. The system indeed

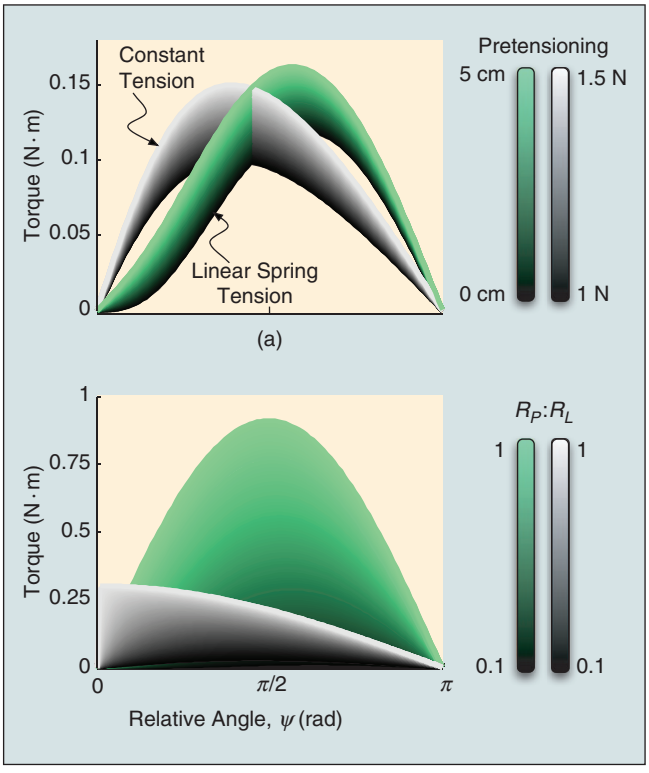

Figure 4. *The effect of (a) tension and (b) geometry are presented for two cases: one with constant tension on the cable (gray) and one with a linear spring inducing tension (green). Color bars on the right represent cable pretension in (a), and in (b), the ratio of rotator radius (R_P) to end effector length (R_L). Spring stiffness used was 10 N/m, and in (a), R_L and R_P were 0.3 and 0.1 m, respectively. Both figures show that higher torques can be reached with less rotator movement with constant tension, but linear spring tension can be useful for damping out disturbances.*

Cables are advantageous because of remote actuation, flexibility, and low weight.

has a concave energy surface, where the system settles to an equilibrium point of minimum potential energy (Figure 5). Assuming the system starts at rest, Figure 6 uses specific parameters to provide a more intuitive example of stability. A more generalized analysis of stability is detailed in another work [13]. The energy corresponds to the system's geometry, with the picture on Figure 5(a) showing the MARIONET at maximum energy state on the user's elbow (magenta), and minimum energy (cyan). These colors correspond to the potential energy surface to the bottom, where the magenta hills are the positions of highest energy, and the cyan valley is at the lowest. The maximum torque occurs at the highest slope of this plot, in this case, just inside the two peaks. This region represents the workspace of the MARIONET and comprises the region of convergence defined as the region where difference between the link angle and the pulley angle (Ψ) converges to zero, therefore, an attractor region of stability. The shallow bowl shape of the surface comes from the small amount of energy stored in L_{PT}, the length of cable from the tensioner to the rotator pulley.

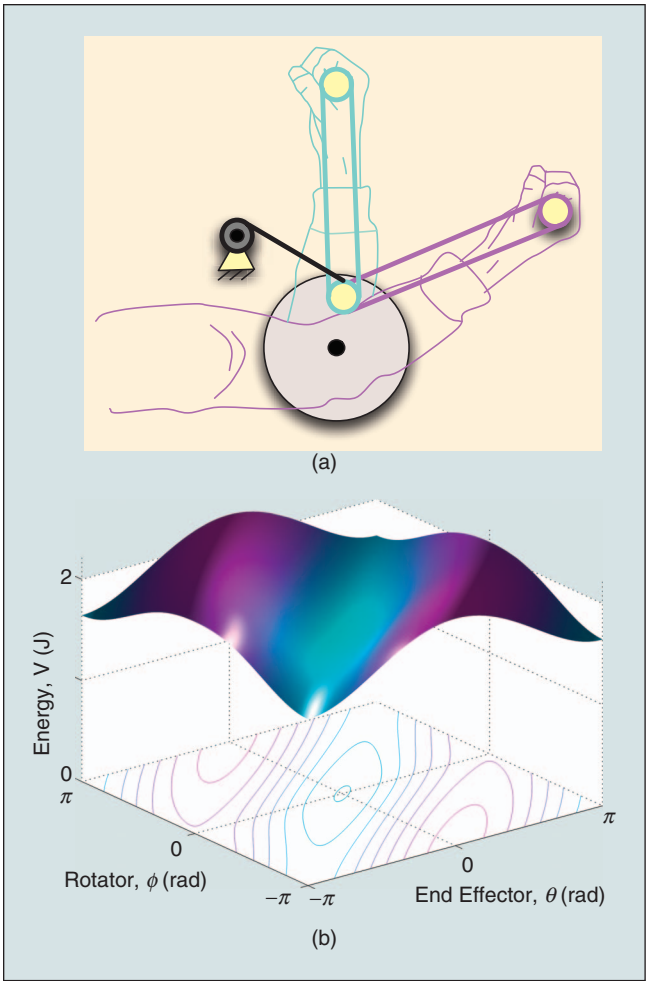

Figure 5. *As the rotator is aligned with the (a) arm (cyan), this corresponds to the minimum on the (b) energy surface below (cyan). As the moment arm increases (magenta), the energy reaches a maximum. In this case, the rotator is not fixed, and the slight bowl shape comes from the force of the tensioner, and the block and tackle between the hand and the rotator (4:1 reduction), as used in the proof-of-concept. The parameters used in this specific example are also taken from the proof-of-concept,* $R_L = 0.43$ m, $R_P = 0.07$ m, and $R_T = 0.15$ m.

Proof of Concept

We designed and built a proof of concept to actuate the human elbow. This version of the MARIONET, shown in Figure 6, has been designed to exert a light amount of torque (5 N · m) on the elbow within its range of motion (135°). The rotator is driven remotely using a 200-W servomotor through a 10:1 roller chain transmission. This drive motor can control the rotator position to the nearest 0.016° (0.0003 rad) and exert a

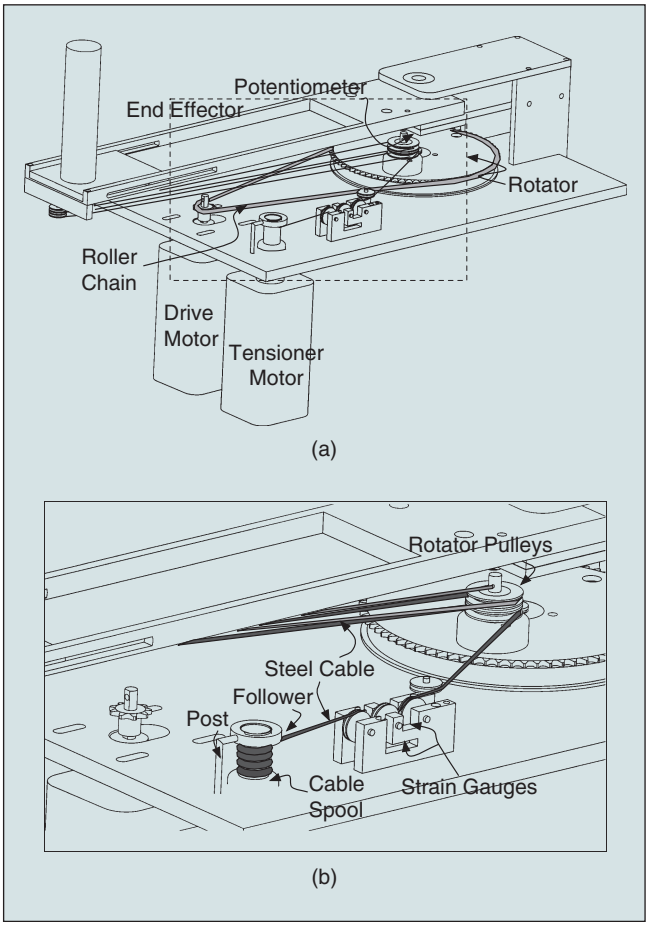

Figure 6. *(a) Proof-of-concept drawing shows the basic elements of the MARIONET. (b) A detailed view of the cable routing and tension measurement system. Note that the cable between the rotator and end effector is organized in a block and tackle.*

maximum continuous torque of 6 N·m. The rotator has two pulleys mounted concentrically near its outer diameter for cable routing. A steel aircraft cable, with a diameter of 1/32 in (0.79 mm), is tensioned by a second 200-W servomotor, known as the tensioner, through a cable spool. The spool is composed of three parts: the spool itself, a follower, and a post. The spool is a threaded cylinder to guide cable wrapping. The threads alone are not sufficient to make sure that the cable does not overlap or skip threads, so a follower with the same thread pitch moves up and down the spool, guiding the cable into the threads. The post keeps the follower in the same orientation as it guides the cable into and out of the spool. This type of cable guidance is common in fishing reels.

As the cable leaves the spool, it passes through a mounting composed of a set of pulleys. The mounting ensures that the cable leaves at a constant height and measures cable tension with the help of two strain gauges. The cable passes through another set of pulleys on the rotator and then forms a block and tackle with a third set of pulleys on the end effector (4:1 reduction).

The end effector, built with an adjustable handle, rotates about the same center as the rotator. The position of the end effector is measured by a conductive plastic potentiometer with a resolution of 0.03° (0.0005 rad).

Torque on the elbow is controlled by regulating the position of the rotator relative to the end effector. The drive motor is operated in torque mode, with a PID controlling for position. In addition to control of the moment arm by the drive, the tensioner controls torque operating in an open-loop torque mode. Data are sampled at 2 kHz using a real-time operating system (QNX RTOS 2.0).

There are a number of safety precautions taken. Two mechanical stops prevent the end effector from leaving the workspace of the elbow. An emergency stop switch is available to both the user and the operator. Software stops shut off the motors if they move too fast for a given duration. A chain guard prevents anyone from touching the roller chain during operation.

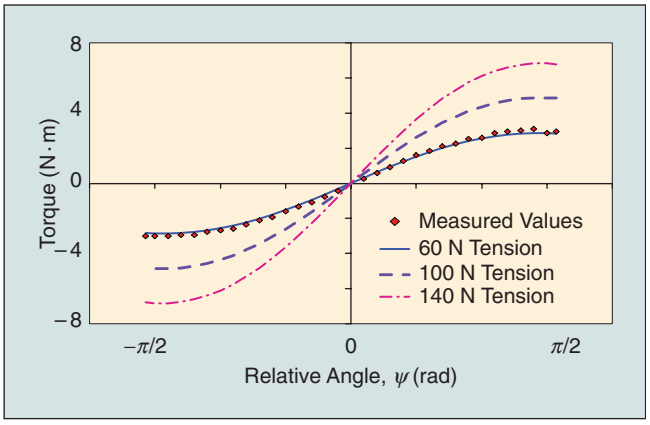

Figure 7. *Mathematical analysis accurately predicts torque of MARIONET. Because of high friction at low speeds of the tensioner, we used a hanging mass to supply constant torque.*

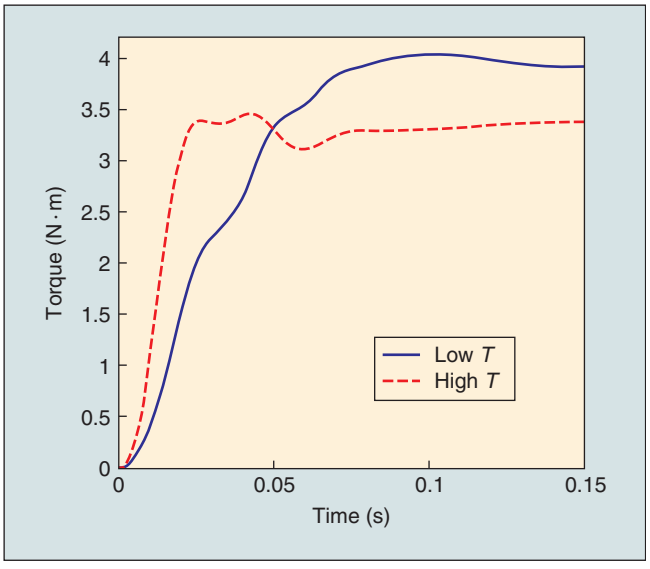

Figure 8. *Step responses at low (70 N) and high (300 N) tensions show quick response times.*

Performance

We evaluated the performance of the device based on its intended tasks. Given the application of rehabilitation and motor control experiments, we measured how quickly the MARIONET could exert accurate torque.

When the tensioner operates at slow speeds, friction develops between the poles of the motor, making torque measurement difficult. Instead, we substituted a mass for the motor and calculated the resulting

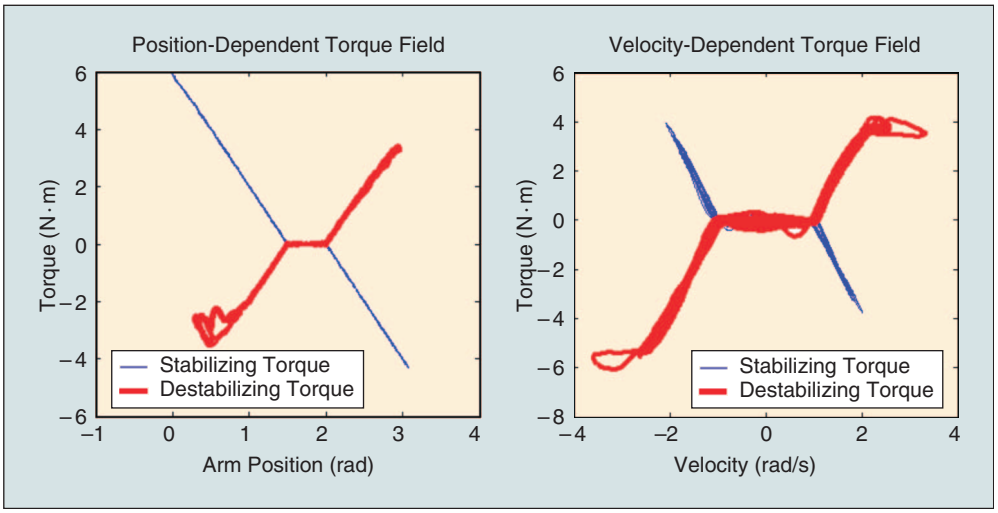

Figure 9. *The MARIONET is capable of producing torque fields of any shape. This case shows position and velocity-dependent linear torque fields for both stabilizing and destabilizing modes limited by motor saturation.*

The compliant and safe aspects of the MARIONET make it a strong candidate for home rehabilitation.

torque from the given weight and relative position of end effector and rotator. This value was compared with an empirical value obtained from a load cell that kept the end effector fixed. The calculated torque matches with the experimentally determined torque (Figure 7). The sinusoidal relationship between relative angle and torque continued as increasing the tension proportionally increased the amplitude.

A torque step response test (Figure 8) showed how fast the actuator could exert a substantial torque under either high or low cable tension. To accomplish this, the rotator had to move as quickly as possible to a new appropriate position to step up to the desired torque. In the low cable tension case (70 N of tension through the block and tackle), the 5% rise time was 65 ms, much faster than human reactions in voluntary movement of about 150 ms [18]. In the high cable tension case (300 N), the rise time was 21 ms, much faster than human reflex of about 30 ms [18]. Consequently, the cable tension can be adjusted to a level appropriate to the requirements of the human motor task.

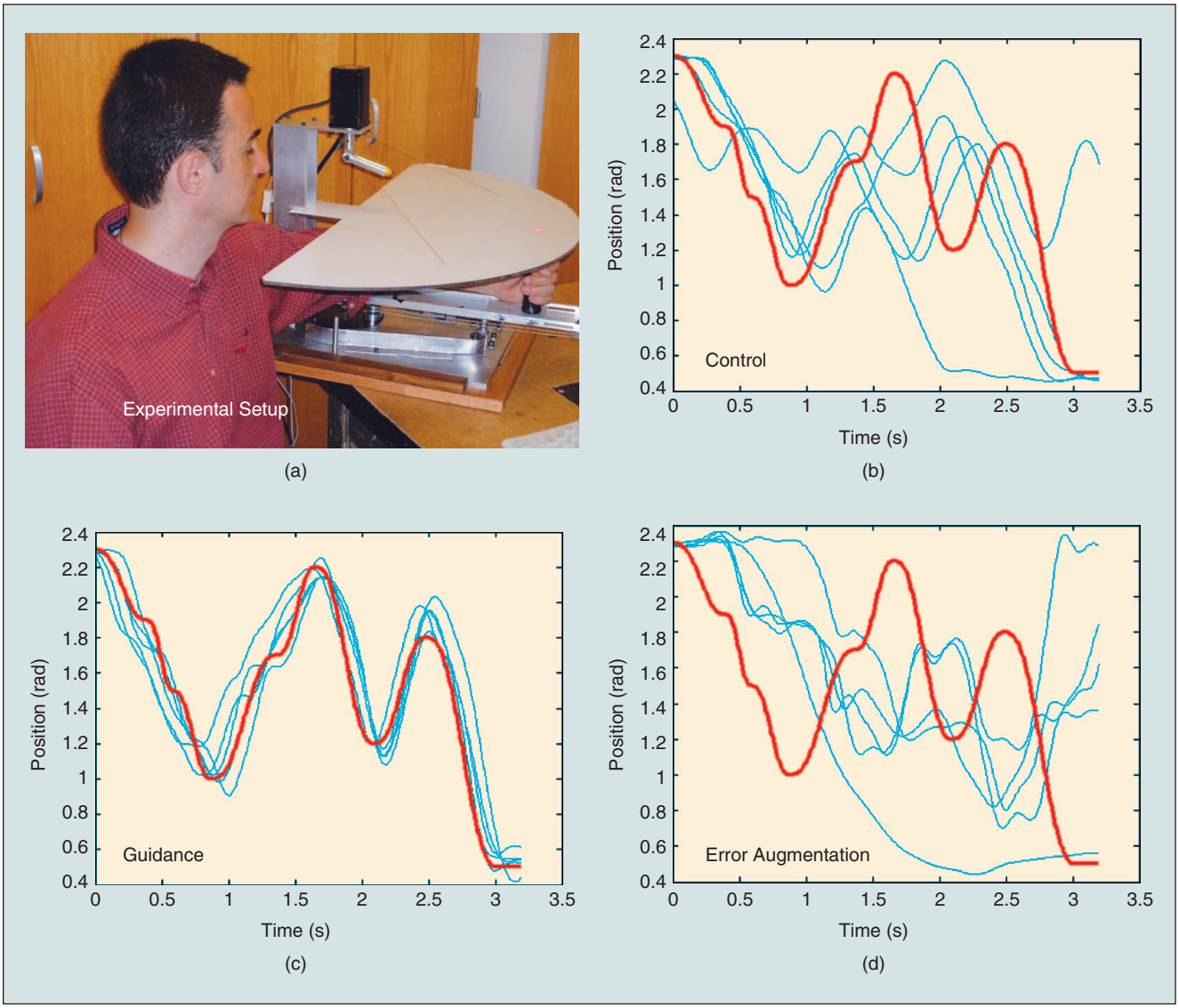

Figure 10. *(a) Experimental setup showing user following laser-dictated trajectory with MARIONET. (b)–(d) The desired trajectory (red) and the individual trials (blue) indicate that the single-DoF MARIONET is capable of producing error augmentation and guidance force fields. The control subject experiences the difficulty of mimicking a trajectory with no force feedback. The guidance subject has a much easier time, allowing the robot to push him toward the desired trajectory, while the error-augmentation subject has a difficult time mimicking the trajectory, often being pushed to opposite ends of the workspace.*

Although the system was capable of producing fast and accurate torque, robotic training, rehabilitation, and haptic applications often require state-dependent force fields. In a final performance test, we created a linear torque field that depended on either position or velocity with a user-defined deadband. The MARIONET was capable of rendering a linear force field within a given range of output torques before the drive motor saturated (Figure 9). Both stabilizing (guidance) and destabilizing (error augmentation) fields were rendered, indicating a wide range of modes of control that might be possible with appropriate software.

Human Pilot Study of Robotic Training

Two of the many possible training paradigms currently used in robotic teaching and rehabilitation are forces that guide the user toward a desired trajectory (guidance) compared with nonintuitive, yet promising, approach of pushing the user away from a desired trajectory (error augmentation). For this preliminary study, six healthy, institutional review board-approved subjects (four male) were separated into three groups that differed in the type of torques they received: error augmentation (two subjects), guidance (two subjects), and a control group that experienced no torques (two subjects). Both error-augmentation and guidance torques pushed the arm 3 $(N \cdot m)/rad$ of error. Each subject was asked to move his or her elbow to mimic a complex movement of a dot projected on a platform above the arm by a laser. This ideal movement lasted 3.2 s and ranged between 0.5 and 2.3 rad. The experimental setup is shown in Figure 10(a).

The results of this basic pilot show that the MARIONET was capable of altering its user's trajectories. In the control group, the subjects' individual movements [Figure 10(b), blue] were similar to the desired trajectory [Figure 10(b), red], but the timing was different. In the guidance group [Figure 10(c)], users' trajectories were attracted to the desired trajectory, but in the error augmentation group [Figure 10(d)], the users' trajectories seem to be opposite to the desired trajectory. The data here demonstrate the MARIONET's effectiveness as a programmable experimental device for human training.

Discussion and Conclusions

While performing to expectations, the proof-of-concept MARIONET, like all robotic devices, is limited by the power of its actuators and its geometry. The concept allows both moment arm manipulation and tension control to produce torque and impedance at a joint. In addition, the moment arm path can be altered to fit the application's requirements. For instance, a linear path may be more advantageous than a rotational path. Weight and cost can be reduced by using a highly geared drive motor and further by implementing an elastic element in series with a highly geared tensioner or even completely substituting the tensioner for a passive element. When using an active tensioner, regardless of configuration, the variable control of stiffness and equilibrium position make the MARIONET act like a variable compliant series elastic actuator. As a result, it shares many of the same advantages such as low weight, low cost, and compliance. In addition, by adding remote actuation, inertia is further reduced, the effect being amplified as the number of joints increase. This concept is illustrated in detail in previous work [14].

The torque-deflection relationship varies with both tension and geometrical parameters.

The technology has great potential in several areas, but one growing area that should make positive use of MARIONET transmission is in neurorehabilitation training, in which a patient learns to move correctly with repetitive training that is facilitated by interactions with a robot. For example, the financial costs of recovery from injuries such as stroke are staggering, with a projected total of US$2 trillion over the next 45 years [19]. Although a sizeable fraction (9%) of that total comes from rehabilitation costs, additional cost comes from informal care such as assistance from a family member. The compliant and safe aspects of the MARIONET make it a strong candidate for home rehabilitation, which has been shown to be comparably effective in the therapy in the clinic [20]–[22]. Although home rehabilitation is more stressful for caregivers [20], a tireless home robotic system could become a part of the standard of care.

Besides rehabilitation, the MARIONET concept has potential in any application where remote actuation and mechanical compliance is desired and a high torque rate of change is not required. Such a unique device that imitates the variable moment arms of muscle and tendons may be used in teleoperation, surgery, mobile robots, micromanipulation, or hazardous material handling. Whether the application is in orthoses or in bridges, the variable compliance, lightweight, and remote actuation characteristics of the MARIONET have a promising future.

Keywords

Rehabilitation, cable, moment arm, variable impedance, exotendon.

References

[1] W. M. Murray, S. L. Delp, and T. S. Buchanan, "Variation of muscle moment arms with elbow and forearm position," *J. Biomech.*, vol. 28, no. 5, pp. 513–526, 1995.

[2] S. Jacobsen, E. K. Iversen, D. F. Knutti, R. T. Johnson, and K. B. Biggers, "Design of the Utah/MIT dextrous hand," in *Proc. IEEE Int. Conf. Robotics and Automation (ICRA)*, San Francisco, 1986, pp. 1520–1532.

[3] W. Townsend and J. Guertin, "Teleoperator slave-WAM design methodology," *Ind. Robot*, vol. 26, no. 3, pp. 167–177, 1999.

[4] T. H. Massie and J. K. Salisbury, "The PHANTOM haptic interface: A device for probing virtual objects," in *Proc. ASME Winter Annu. Meeting, Symp. Haptic Interfaces Virtual Environment and Teleoperator Systems*, Chicago, IL, 1994, pp. 295–301.

[5] K. Homma, O. Fukuda, Y. Nagata, and M. Usuba, "Study of a wire-driven leg rehabilitation system," in *Proc. Int. Conf. Intelligent Robots and Systems*, Sendai, Japan, 2004, vol. 2, pp. 1451–1456.
[6] D. Surdilovic, R. Bernhardt, T. Schmidt, and J. Zhang, "STRING-MAN: A new wire robotic system for gait rehabilitation," in *Proc. 8th Int. Conf. Rehabiliation Robotics*, Korea, 2003, pp. 64–66.
[7] D. Mayhew, B. Bachrach, W. Z. Rymer, and R. F. Beer, "Development of the MACARM—A novel cable robot for upper limb neurorehabilitation," in *Proc. IEEE 9th Int. Conf. Rehabilitation Robotics*, Chicago, IL, 2005, pp. 299–302.
[8] J. Veneman, R. Ekkelenkamp, R. Kruidhof, F. C. T. van der Helm, and H. van der Kooij, "Design of a series elastic and bowden cable-based actuation system for use as torque-actuator in exoskeleton-type training," in *Proc. Int. Conf. Rehabilitation Robotics (ICORR)*, Chicago, IL, 2005, pp. 496–499.
[9] G. A. Pratt and M. M. Williamson, "Series elastic actuators," in *Proc. Int. Conf. Intelligent Robots and Systems (IROS)*, 1995, pp. 399–406.
[10] G. Colombo, M. Joerg, R. Schreier, and V. Dietz, "Treadmill training of paraplegic patients using a robotic orthosis," *J. Rehabil. Res. Dev.*, vol. 37, no. 6, pp. 693–700, 2000.
[11] D. J. Reinkensmeyer and S. J. Housman, "If I can't do it once, why do it a hundred times?": Connecting volition to movement success in a virtual environment motivates people to exercise the arm after stroke," *Virt. Rehabil.*, pp. 44–48, 2007.
[12] J. S. Sulzer, M. A. Peshkin, and J. L. Patton, "MARIONET: An exotendon-driven series elastic actuator for exerting joint torque," in *Proc. Int. Conf. Rehabilitation Robotics (ICORR)*, Chicago, IL, 2005, pp. 103–108.
[13] J. S. Sulzer, M. A. Peshkin, and J. L. Patton, "Catastrophe and stability analysis of a cable-driven joint," in *Proc. IEEE Int. Conf. Engineering Medicine and Biology Society*, New York, 2006, pp. 2429–2433.
[14] J. S. Sulzer, M. A. Peshkin, and J. L. Patton, "Design of a mobile, inexpensive device for upper extremity rehabilitation at home," in *Proc. Int. Conf. Rehabilitation Robotics (ICORR)*, Noordwijk, Netherlands, 2007, pp. 933–937.
[15] R. Van Ham, M. Van Damme, B. Vanderborght, B. Verrelst, and D. Lefeber, "MACCEPA: The mechanically adjustable compliance and controllable equilibrium position actuator," in *Proc. 9th Int. Conf. Climbing and Walking Robots*, Belgium, 2006, pp. 196–203.
[16] R. Van Ham, B. Vanderborght, M. Van Damme, B. Verrelst, and D. Lefeber, "MACCEPA, the mechanically adjustable compliance and controllable equilibrium position actuator: Design and implementation in a biped robot," *Robot. Autonom. Syst.*, vol. 55, no. 10, pp. 761–768, 2007.
[17] A. F. Gordon, A. F. Huxley, and F. J. Julian, "Variation in isometric tension with sarcomere length in vertebrate muscle fibers," *J. Physiol.*, vol. 184, no. 1, pp. 170–192, 1966.
[18] D. A. Winter, *Biomechanics and Motor Control of Human Movement*. Hoboken, NJ: Wiley, 1990.
[19] D. L. Brown, B. Boden-Albala, K. M. Langa, L. D. Lisabeth, M. Fair, M. A. Smith, R. L. Sacco, and L. B. Morgenstern, "Projected costs of ischemic stroke in the United States," *Neurology*, vol. 67, no. 8, pp. 1390–1395, 2006.
[20] C. Anderson, S. Rubenach, C. N. Mhurchu, M. Clark, C. Spencer, and A. Winsor, "Home or hospital for stroke rehabilitation? Results of a randomized controlled trial. I. Health outcomes at 6 months," *Stroke*, vol. 31, no. 5, pp. 1024–1031, 2000.
[21] L. Widén Holmqvist, L. von Koch, V. Kostulas, M. Holm, G. Widsell, H. Tegler, K. Johansson, J. Almazán, and J. de Pedro-Cuesta, "A randomized controlled trial of rehabilitation at home after stroke in southwest Stockholm," *Stroke*, vol. 29, no. 3, pp. 591–597, 1998.
[22] C. Anderson, S. Rubenach, C. N. Mhurchu, M. Clark, C. Spencer, and A. Winsor, "Home or hospital for stroke rehabilitation? Results of a randomized controlled trial. II. Cost minimization analysis at 6 months," *Stroke*, vol. 31, no. 5, pp. 1032–1037, 2000.

James S. Sulzer received his B.S. degree from Ohio State University in 2002 and his M.S. degree from Northwestern University in 2006, both in mechanical engineering. He is currently a Ph.D. candidate at Northwestern and the Rehabilitation Institute of Chicago. His current research involves developing robotic mechanisms for understanding gait in stroke.

Michael A. Peshkin received his Ph.D. degree from Carnegie Mellon University, Pittsburgh, Pennsylvania, in 1988. He is a professor of mechanical engineering at Northwestern University, Evanston, Illinois. He is an inventor of cobots (collaborative robots, with J. Edward Colgate) and has been working in human-interactive aspects of robotics for many years. He is the founder of three companies: Mako Surgical (image-guided surgery), Cobotics (materials handling), and Kinea Design (rehabilitation robotics). His other research interests include exercise robotics, haptic communication between people, and electromagnetic sensors.

James L. Patton received B.S. degrees in mechanical engineering and engineering science/bioengineering from the University of Michigan at Ann Arbor in 1989, an M.S. degree in theoretical mechanics from Michigan State University at Lansing in 1993, and the Ph.D. degree in biomedical engineering from Northwestern University at Evanston in 1988. Currently, he is the associate director of the Center for Rehabilitation Robotics at the Rehabilitation Institute of Chicago (RIC) and an associate professor of bioengineering at the University of Illinois at Chicago. His work has focused on haptics, modeling the human–machine interface, robotic teaching, and robotic facilitation of recovery from a brain injury. He is a member of the IEEE Robotics and Automation Society (RAS) and the IEEE Engineering in Medicine and Biology Society (EMBS). He is a reviewer for *IEEE Transactions on Biomedical Engineering*, *IEEE Engineering in Medicine Biology Magazine*, and *IEEE Transactions on Robotics and Automation*. He also chairs the EMBS Technical Committee on Biomedical Robotics.

Address for Correspondence: James S. Sulzer, Northwestern University, Department of Mechanical Engineering, Sensory Motor Performance Program, Rehabilitation Institute of Chicago, 345 E. Superior Suite 1406, Chicago, IL 60611. E-mail: sulzer@northwestern.edu.

A Manipulator Plays Jenga

Applying Multisensor Integration in Industrial Manipulation Control

BY TORSTEN KRÖGER, BERND FINKEMEYER, SIMON WINKELBACH, LARS-OLIVER EBLE, SVEN MOLKENSTRUCK, AND FRIEDRICH M. WAHL

One reason why industrial manipulators are mainly used for trajectory-following operations, i.e., pure position control, is that today commercial control units are rarely open for sensor integration. Research institutions often replace the existing control units with their own to perform experiments in control engineering. On the other hand, when studying literature, we get the impression that problems of force control, visual servoing, distance control, manipulator dynamics, and control software architectures are solved sufficiently. In concrete cases, this is correct. Problems appear when merging all these fields together. Developers should be encouraged to have a better view of the overall manipulation control system. When considering any kind and any number of sensors (force/torque, distance, vision, pressure, light barriers, etc.), how can even nonexperienced programmers implement guarded and guided motion commands with respect to any reference coordinate system? What could such a hybrid control architecture look like? How can sensor signals be consistently mapped to stable, unambiguous, and deterministic manipulator motions? Questions such as these are supposed to be answered by the research community to bring existing control approaches into industrial practice.

JENGA® & 2008 HASBRO, INC. Used with permission

The application described in this article, which plays Jenga [1], is not an industrial one. Nevertheless, it is well suited to show the potential of multisensor integration and to demonstrate the possibilities when concepts of the aforementioned fields are combined. Jenga is a parlor game that consists of 54 wooden rectangular blocks. All blocks are set up together as a tower with three blocks on each level. The aim of the game is to find a loose block in the tower, take it out, and put it back onto the top of the tower. With each move, the tower gets more unstable. Even for human players, this is a task requiring a very high tactile sensitivity. The manipulator plays against itself with the aim of building a tower as high as possible. The setup of the manipulator work cell is shown in Figure 1. Sensor feedback is given by a six-dimensional (6-D) force/torque sensor, a 6-D acceleration sensor, and a laser triangulation distance sensor. To get visual feedback, two charge-coupled device (CCD) cameras observe the tower. To reduce the demands on the image-

Digital Object Identifier 10.1109/MRA.2008.921547

How can even nonexperienced programmers implement guarded and guided motion commands with respect to any reference coordinate system?

processing system, each block was colored black and has two white lines and two dots (see Figure 1).

Related Work

There has been a multitude of research in each specific aspect of this manipulation problem (force/torque control, sensor fusion, task specification, vision, and robot programming). Each area has been developed independently without considering how they can be integrated together.

Whitney [2], Mason [3], and Raibert and Craig [4] published initial works on force control concepts and compliant motion control. Today, literature provides basically three different approaches for force control: 1) impedance control [5], which uses relationships between acting forces and manipulator position to adjust the mechanical impedance of the end effector with external forces; 2) parallel control [6], which enables control of both force and position along the same task space direction; and 3) force/position control, which controls force and position in two orthogonal subspaces [8]. (The problem of orthogonality has to be taken into account here as stated by Duffy [7], who extended the approach such that it is consistent, independent of units, and independent of any origin coordinate system.) The third approach, force/position control, is used within this work, and selection matrices are used here to address the concerns mentioned previously [9].

When applying force/torque control, in practice, it is very helpful to separate forces and torques caused by inertia and those caused by environmental contacts. A recently published approach for force/torque and acceleration sensor data fusion is based on observer techniques to estimate noncontact forces [10]. A more traditional approach that is based on inertia tensor identification, measured forces, and accelerations to calculate the desired contact forces and torques was presented by Kozłowski [11].

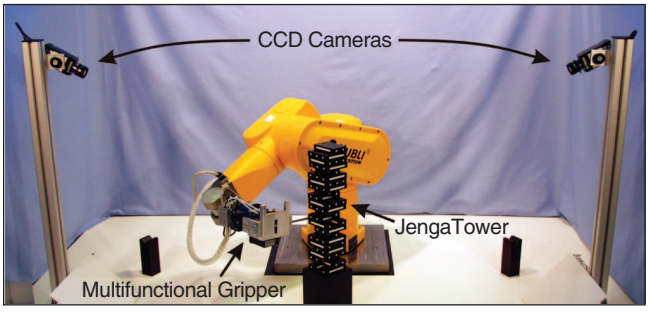

Figure 1. *Work cell setup for the Jenga-playing manipulator.*

Khatib published the operational space approach in 1987 [12], which has been one of the most significant frameworks to realize sensor-guided manipulator motions. De Schutter, Van Brussels, and Bruyninckx published significant articles on compliant motion specification [13], [14] and compliant motion control [15]. Schimmels and Huang wrote about force-guided assembly in a very theoretical manner [16]. The Ph.D. thesis of Natale [17] constitutes the objective in clear theoretical expressions as well as in good practical experiments.

For the realization of visual servoing, Baeten presents a good overview in theory and practice [18]. To achieve advanced vision integration, robust and fast image-processing algorithms have to be implemented [19] for applications in this field.

Considering any kind and any number of sensors in a manipulation work cell, the question of programming concepts or even automated programming arises. Approaches on task specifications can be found in [14], [20], and [21]. Since the complexity and the demands on manipulation control systems have been continuously growing during the last decades, the development of suitable software control architectures gains importance. Two widely known approaches are the Open Robot Control Software (OROCOS) project [22] and the Open System Architecture for Controls Within Automation Systems (OSACA) [23].

Our recent works address task-level programming [24], force/torque control [25], [26], sensor data fusion [27], multisensor integration [28], [29], online trajectory generation [30], and control software architectures [9]. The following sections briefly present the respective approaches and describe the Jenga-playing manipulator. The experiments were also published as a video sequence [31]. In comparison with all the works mentioned previously, this article gives an overview of a concrete implementation and contains parts of all the mentioned fields.

Technical Realization

The hardware and software setup is explained in the subsequent sections, which is then followed by a brief introduction on manipulation primitives (MP) that constitute the interface between the underlaying control levels and the user application. Finally, the underlying control architecture and the user application for playing Jenga are outlined.

Hardware

The robot used for all experiments in this context is a Stäubli RX60 industrial manipulator. Its original controller has been replaced as described in [9], and only the original power electronics has been retained. Depending on the experiment or application, the control system consists of several PC nodes, and, here, we use four PCs. With the high-level hybrid controller, we achieve a control rate of 2 kHz, whereas the low-level joint controller runs at rate of up to 20 kHz. Figure 2 illustrates the developed gripper, which is mounted to the end effector of the manipulator. The gripper is equipped with a 6-D force/torque sensor, a 6-D acceleration sensor, and a laser triangulation distance sensor. The acceleration sensor can be used for the application of a 6-D sensor data fusion approach

to compute forces and torques established by environmental contacts [10], [27].

Software Architecture

One of the overall aims has been to provide a manipulation control system that is open for any kind and any number of sensor systems while offering a unique and intuitive programming interface (the so-called MPs) to the user. One important requirement was to develop a scalable real-time hardware and software system. Middleware for robotics and process control applications (MiRPA) constitutes the communication base [9]. It is a distributed real-time middleware, which runs on several PC nodes, with QNX running as the real-time operating system. Every software process in the system has only one communication partner: MiRPA. As a result, a very high modularity is achieved, as can be seen in Figure 3, which depicts the global software architecture for all PC nodes.

The software modules MP Interface and MP Execution form the core of the adaptive hybrid control system and feed the joint control module. The user application robot task is programmed by means of MP nets and sends single MPs to the MP interface module. All software modules on the right of Figure 3 are drivers for actuators, drivers for sensors, or controllers (open or closed loop), which are triggered by the MP execution module. For example, the modules `Force_Ctrl`, `Distance_Ctrl`, and `Vision_Ctrl` are closed-loop controllers, whereas all trajectory-generating modules like `Position_Ctrl` and `Velocity_Ctrl` are feed-forward controllers, which are addressed in the next two sections. The Gripper module is the only actuator in this concrete setup. All the modules mentioned on the right of Figure 3 use the same communication profile so that they can be added and exchanged very easily.

MPs

MPs constitute the interface from the control level to the user application. They are used to specify sensor-guided and sensor-guarded motion commands. A hybrid motion command enables the user to assign set points of any physical magnitude to each degree of freedom (sensor-guided motion). Here, the manipulator motion is generated directly on the base of the respective sensor signal(s). To obtain the universality as demanded in the introduction, any sensor signal can principally be addressed here.

Additionally, a boolean expression called the stop condition, which can contain any sensor signal in any coordinate frame, can be set up to determine the end of a single MP (sensor-guarded motion). As soon as this expression becomes true, the execution of a single MP is finished. For

How can sensor signals be consistently mapped to stable, unambiguous, and deterministic manipulator motions?

instance, one can specify a hybrid motion command such that the manipulator performs force control in x-direction, distance control in y-direction, vision-based control in z-direction, and trajectory-following control in all rotational degrees of freedom (DoF). The execution ends, if, for example, the force in x-direction exceeds a certain value or a position in y-direction gets under a certain minimum value.

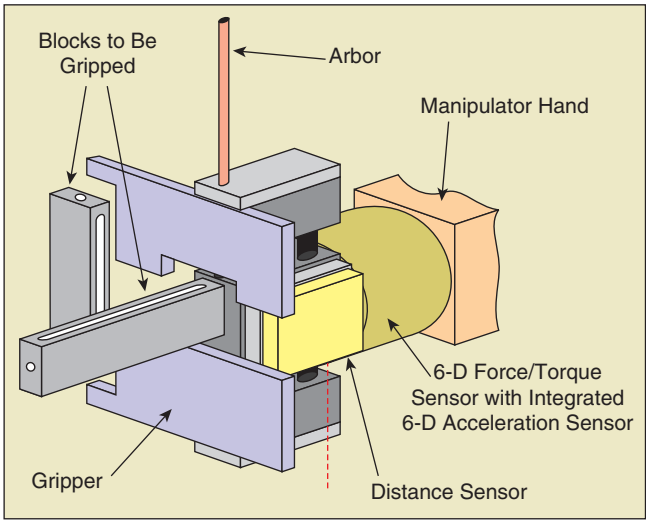

Figure 2. *Multifunctional gripper with sensor devices. Blocks of the game can be gripped in two different configurations. The arbor is used to push single blocks out of the Jenga tower.*

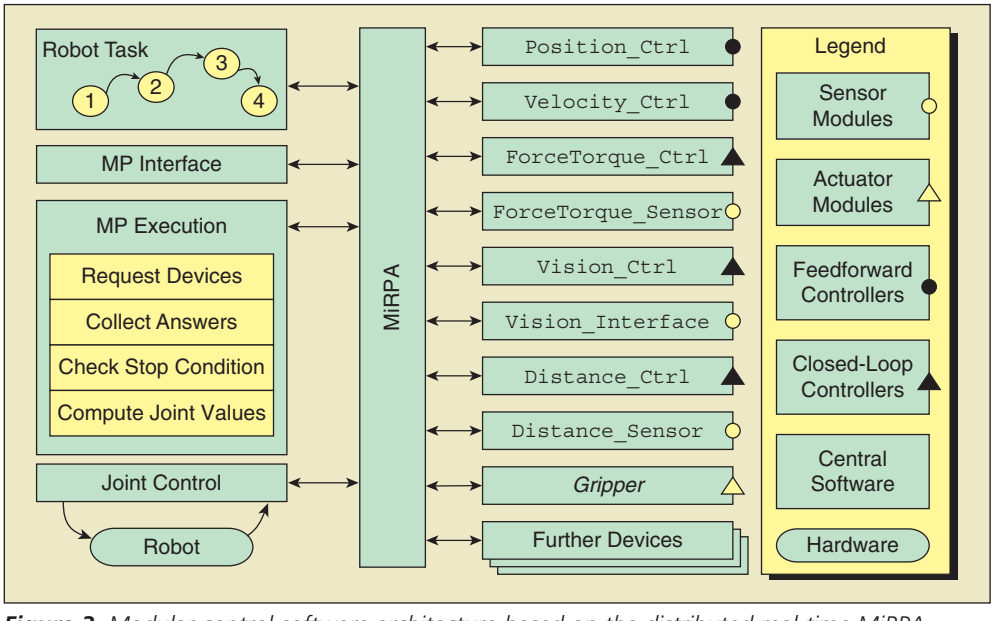

Figure 3. *Modular control software architecture based on the distributed real-time MiRPA.*

This exhibit shows the potential of multisensor integration and opens new possibilities for industrial manipulation.

Besides the hybrid motion command and the stop condition, a MP consists of a third part, the tool command. It addresses the control of further actuators in work cells. In this concrete case, it only opens or closes the gripper.

The consistency of this approach is ensured by using the adaptive selection matrix [9], which assigns exactly one appropriate controller to each DoF. Depending on the current system state, each controller checks whether it is able to control the manipulator in the current state or not. As a result, the responsibility for stability has been taken away from the user. A force control module, for example, would not be able to generate any reasonable output signal as long as the manipulator's end effector remains in free space, i.e., the fused data of the acceleration and force/torque sensors remains under a certain threshold value. In such a case, an alternative controller can be chosen depending on the parameters of the currently executed MP, e.g., the module `Velocity_Ctrl` in Figure 3 could lead the end effector into contact such that the `Force_Ctrl` module could, subsequently, take over in the moment of contact transition.

Control Architecture

The concept of MPs requires a hybrid control system that is able to react on (sensor) events within one control cycle of the MP Execution module, since the point in time where the stop condition becomes true is unpredictable. (In this context, a hybrid controller is a switching control system, which discretely switches between a number of continuous subsystems [32].) As a result, set points for the hybrid controller might change arbitrarily from one control cycle to another. Also, coordinate frames, e.g., the task frame (see [13], [14], and [15]), might change ad hoc. The stability of the resulting overall system is another issue that cannot be neglected [32]. The key part for the realization of these requirements is the online trajectory generator [30], which is represented by the blocks `Position_Ctrl` and `Velocity_Ctrl` in Figure 3. These modules are able to handle and proceed with any state of motion (position, velocity, and acceleration) and in any space (task space, world coordinate, joint space, etc.).

Both modules, `Position_Ctrl` and `Velocity_Ctrl`, compute set points for a synchronized trajectory as desired for the currently executed MP. The `Position_Ctrl` generates a manipulator trajectory, which lets the manipulator reach a desired pose exactly. The boundary conditions for this trajectory (maximum velocity, maximum acceleration, and maximum jerk) depend on the currently executed MP as well as the space in which the trajectory is generated. In comparison to the `Position_Ctrl` module, the `Velocity_Ctrl` module independently generates a trajectory that accelerates all the desired DoF to a certain MP-dependent target velocity.

The `Vision_Interface` provides the position and orientation data about each block of the Jenga tower. This data is subsequently used by the `Vision_Ctrl` module for visual servoing. It computes the poses in space for all blocks and monitors the tower's behavior (to detect a vibrating or collapsed tower).

To achieve high robustness while operating in contact with the environment, model-following-control structures are used for force/torque control in the block `ForceTorque_Ctrl`, which receives feedback signals via the `ForceTorque_Sensor` module. Similar to all controller modules on the right of Figure 3, the force/torque controller computes only a pose difference, which is subsequently interpreted by the MP Execution module to calculate a new absolute pose.

For rapid control prototyping purposes, the developer of a system has the possibility to create a process on one of the QNX PC nodes directly out of MATLAB/Simulink [33]. Here, Real-Time Workshop, Opal RT-Lab [34], and an in-house software interface module were used to establish the connection to MiRPA. Processes can be added and exchanged even during runtime such that users of the system can experiment with new sensor systems and new control approaches (e.g., trajectory computation, force/torque control, distance control, visual servoing, parameter estimation/identification, sensor data fusion etc.) very easily as desired for research purposes. During the development state, the processes on the right of Figure 3 are generated directly with MATLAB/Simulink, and these modules can subsequently be used for experimental verifications on the real target system.

Playing Jenga

Finally, we briefly describe the application program for playing Jenga. During the entire game, no strategy is applied. The blocks to be pushed out are selected randomly. The first step is to always try to push a block few centimeters out of the tower such that it can be subsequently gripped and pulled out from the opposite side. If the counter force during pushing gets too high or if the cameras detect a dithering tower, the manipulator stops immediately, moves back, and tries to push out the next randomly chosen block. In order not to damage the tower when gripping a block, we have to ensure that the block to be gripped does not move when closing the gripper, i.e., each block has to be gripped exactly centered. The spatial resolution of the three dimensional (3-D) model of the tower, which is estimated based on the CCD camera images, is approximately 1 mm in our setup, but this is not enough to calculate an accurate grip pose. This is the reason why a triangulation distance sensor signal is additionally needed to measure the pose of a block in the range of micrometers. The respective functionality is provided by the processes `Distance_Sensor` and `Distance_Ctrl`. To perform a high-precision measurement of the pose of a single block, the manipulator moves its end effector along the block such that the distance sensor records a distance profile, which is subsequently used to determine the block's exact pose. When the block has been gripped,

Figure 4. *Jenga-playing manipulator with a tower of 27 levels. Videos of this project can be found in [31] and [35].*

a force-guided MP is set up to pull the block out of the tower very carefully and to eliminate all transversal forces and respective torques. The last part of a single move is to put the block on to the top of the tower. This is done by a simple force-guarded MP, which moves the manipulator carefully toward the tower. After a certain force threshold is exceeded and contact has been established, the motion is stopped, and the gripper can be opened.

Figure 4 illustrates the manipulator with a tower of 27 levels. The record height was a tower of 28 levels, i.e., ten additional levels consisting of 29 ($9 \times 3 + 2$) blocks were put onto the top of the tower.

Conclusions and Future Work

This article describes an overview of a prototypical manipulation control system, which is able to play Jenga. The implementation of the Jenga game has been chosen to verify the integration of existing concepts such as force/torque control, distance control, real-time behavior of distributed control systems, sensor data fusion, online trajectory computation, and visual servoing in one exhibit. This exhibit has no direct industrial use, but it clearly shows the potential of multisensor integration and opens new possibilities for industrial manipulation. The scope of these kinds of systems is certainly not limited to industrial manipulation applications, e.g., the potential in the field of medical robotics is also very high and has to be investigated. A key part of this work is the online trajectory generator. Within this work, a second-order generator (rectangular acceleration signals) has been applied [30], but, for the aim of bringing the mentioned concepts into industrial practice, a jerk-limited generator will be necessary. This and further research on sensor fusion methods will be a major focus of our future work. Besides, the Jenga game could be used as an international benchmark for manipulation control concepts (including force/torque control, distance control, and visual servoing). It is well-known and, since the manufacturer [1] has only one place of production, the game is exactly the same all over the world.

Acknowledgment

The authors would like to thank QNX Software Systems for providing free software licenses.

Keywords

Robotic manipulation, multisensor integration, hybrid control, manipulation primitives, real-time middleware.

References

[1] Hasbro, Inc. (2007, Aug. 13). [Online]. Available: http://www.jenga.com

[2] D. E. Whitney, "Force feedback control of manipulator fine motion," *ASME J. Dynam. Syst., Measurement and Control*, vol. 98, pp. 91–97, 1977.

[3] M. T. Mason, "Compliance and force control for computer controlled manipulators," *IEEE Trans. Syst., Man, Cybern.*, vol. 11, pp. 418–432, June 1981.

[4] M. H. Raibert and J. J. Craig, "Hybrid position/force control of manipulators," *ASME J. Dyn. Syst., Meas. Control*, vol. 102, pp. 126–133, June 1981.

[5] C. Canudas, B. Siciliano, and G. Bastin, *Theory of Robot Control*. New York: Springer, 1996.

[6] B. Siciliano and L. Villani, *Robot Force Control*. Norwell, MA: Kluwer, 1999.

[7] J. Duffy, "The fallacy of modern hybrid control theory that is based on "orthogonal complements" of twist and wrench spaces," *J. Robot. Syst.*, vol. 7, no. 2, pp. 139–144, 1990.

[8] J. J. Craig, *Introduction to Robotics: Mechanics and Control*, 3rd ed. Englewood Cliffs, NJ: Prentice Hall, 2003.

[9] B. Finkemeyer, T. Kröger, and F. M. Wahl, "Executing assembly tasks specified by manipulation primitive nets," *Adv. Robot.*, vol. 19, no. 5, pp. 591–611, June 2005.

[10] J. Gámez García, A. Robertsson, J. Gómez Ortega, and R. Johansson, "Generalized contract force estimator for a robot manipulator," in *Proc. IEEE Int. Conf. Robotics and Automation*, 2006, pp. 4019–4024.

[11] K. Kozłowski, *Modelling and Identification in Robotics*. New York: Springer, 1998.

[12] O. Khatib, "A unified approach for motion and force control of robot manipulators: The operational space formulation," *IEEE J. Robot. Autom.*, vol. 3, no. 1, pp. 43–53, Feb. 1987.

[13] J. De Schutter and J. Van Brussel, "Compliant robot motion. I: A formalism for specifying compliant motion tasks," *Int. J. Robot. Res.*, vol. 7, no. 5, pp. 3–17, Aug. 1988.

[14] H. Bruyninckx and J. De Schutter, "Specification of force-controlled actions in the task frame formalism—A synthesis," *IEEE Trans. Robot. Autom.*, vol. 12, pp. 581–589, Aug. 1996.

[15] J. De Schutter and J. Van Brussel, "Compliant robot motion. II: A control approach based on external control loops," *Int. J. Robot. Res.*, vol. 7, no. 4, pp. 18–33, Aug. 1988.

[16] S. Huang and J. M. Schimmels, "Sufficient conditions used in admittance selection for force-guided assembly of polygonal parts," *IEEE Trans. Robot. Autom.*, vol. 19, no. 4, pp. 737–742, Aug. 2003.

[17] C. Natale, *Interaction of Robot Manipulators—Six-Degress-of-Freedom Tasks*, vol. 3 (Springer Tracts in Advanced Robotics). New York: Springer, 2003.

[18] J. Baeten and J. De Schutter, *Integrated Visual Servoing and Force Control*, vol. 8 (Springer Tracts in Advanced Robotics). New York: Springer, 2004.
[19] D. A. Forsyth and J. Ponce, *Computer Vision: A Modern Approach*. Upper Saddle River, NJ: Prentice Hall, 2003.
[20] O. Khatib, "A framework for task-level robotic manipulation," in *Proc. 6th Symp. Robotics Research*, 1994, vol. 6. pp. 287–304.
[21] J. De Schutter, J. Rutgeerts, E. Aertbeliën, F. De Groote, T. De Laet, T. Lefebvre, W. Verdonck, and H. Bruynickx, "Unified constraint-based task specification for complex sensor-based robot systems," in *Proc. IEEE Int. Conf. Robotics and Automation*, 2005, pp. 3618–3623.
[22] OROCOS. (2007, Aug. 13). *Open robot control software*. [Online]. Available: http://www.orocos.org
[23] OSACA. (2007, Aug. 13). *Open system architecture for controls within automation systems*. [Online]. Available: http://www.osaca.org
[24] T. Kröger, B. Finkemeyer, and F. M. Wahl, "A task frame formalism for practical implementations," in *Proc. IEEE Int. Conf. Robotics and Automation*, 2004, pp. 5218–5223.
[25] T. Kröger, B. Finkemeyer, M. Heuck, and F. M. Wahl, "Adaptive implicit hybrid force/pose control of industrial manipulators: Compliant motion experiments," in *Proc. IEEE/RSJ Int. Conf. Intelligent Robotic Systems*, 2004, pp. 816–821.
[26] R. Osypiuk, T. Kröger, B. Finkemeyer, and F. M. Wahl, "A two-loop implicit force/position control structure, based on a simple linear model: Theory and experiment," in *Proc. IEEE Int. Conf. Robotics and Automation*, 2006, pp. 2232–2237.
[27] T. Kröger, D. Kubus, and F. M. Wahl, "Force and acceleration sensor fusion for compliant manipulation control in six degrees of freedom," *Adv. Robot.*, vol. 21, no. 14, pp. 1603–1616, 2007.
[28] T. Kröger, B. Finkemeyer, S. Winkelbach, S. Molkenstruck, L.-O. Eble, and F. M. Wahl, "Demonstration of multi-sensor integration in industrial manipulation (poster)," in *Proc. IEEE Int. Conf. Robotics and Automation*, 2006, pp. 4282–4284.
[29] U. Thomas, S. Molkenstruck, R. Iser, and F. M. Wahl, "Multi sensor fusion in robot assembly using particle filters," in *Proc. IEEE Int. Conf. Robotics and Automation*, 2007, pp. 3837–3843.
[30] T. Kröger, A. Tomiczek, and F. M. Wahl, "Towards on-line trajectory computation," in *Proc. IEEE/RSJ Int. Conf. Intelligent Robotic Systems*, 2006, pp. 736–741.
[31] T. Kröger, B. Finkemeyer, S. Winkelbach, S. Molkenstruck, L.-O. Eble, and F. M Wahl, "Demonstration of multi-sensor integration in industrial manipulation (video)," in *Proc. IEEE Int. Conf. Robotics and Automation*, 2006.
[32] M. S. Branicky, "Multiple lyapunov functions and other analysis tools for switched and hybrid systems," *IEEE Trans. Autom. Control*, vol. 43, no. 4, pp. 475–482, Apr. 1998.
[33] The MathWorks. (2007, Aug. 20). [Online]. Available: http://www.mathworks.com
[34] Opal-RT Technologies, Inc. (2007, Aug. 20). [Online]. Available: http://www.opal-rt.com
[35] T. Kröger. (2007, Aug. 20). *Experimental videos of robot tasks*. [Online]. Available: http://www.rob.cs.tubs.de/research/projects/manipulation

Torsten Kröger studied electrical engineering at the Technical University of Braunschweig in 2002. In 2001, he did an industrial internship at Lenze Corp. in Atlanta. He is pursuing a Ph.D. degree at the Institute for Robotics and Process Control of the Technical University of Braunschweig. His major research interests are online trajectory generation, hybrid manipulation control, multisensor integration in robot work cells, and new robot programming paradigms. Since 2006, he has worked as a technical consultant for several companies dealing with robot technologies.

Bernd Finkemeyer studied electrical engineering at the Technical University of Braunschweig. Since 1998, he has been a research collaborator at the Institute for Robotics and Process Control of the Technical University of Braunschweig, from where he received his Ph.D. degree in 2004. His main fields of interest are modular distributed control architectures, multisensor integration in robot work cells, hybrid manipulation control, and new robot programming paradigms. Since 2005, he has been working as a project manager in the Research and Predevelopment Department of Kuka Robotics in Augsburg, Germany.

Simon Winkelbach studied computer science at the Technical University of Braunschweig. Since 2001, he has been a research assistant at the Institute for Robotics and Process Control, and he received his Ph.D. degree in September 2006. He was awarded by the Siegfried Werth Foundation and the Foundation for the Advancement of Science of the Technical University of Braunschweig for his research. His research interests focus on 3-D computer vision, surface acquisition and registration, object recognition, and medical imaging.

Lars-Oliver Eble studied electrical engineering with a specialization in the field of control, automation, and measurement engineering at the Technical University of Braunschweig. Since 2005, he has been working as a software developer for technical information systems at S&P Infosysteme GmbH in Braunschweig.

Sven Molkenstruck studied computer science at the Technical University of Braunschweig. He became a research assistant at the Institute for Robotics and Process Control at the Technical University of Braunschweig in 2005. His main research interests include vision systems in robot assembly, automated assembly and sensor planning, and 3-D data acquisition.

Friedrich M. Wahl received his diploma, Ph.D., and the "venia legendi" in digital signal and image processing at the Technical University of Munich in 1974, 1980, and 1984, respectively. From 1974 to 1981, he conducted research at the Institute of Communication Engineering at the Technical University in Munich in the fields of pattern recognition and signal and image processing. From 1981 to 1986, he worked at the IBM Research Labs in San Jose and Zurich in the areas of document analysis, industrial image analysis, and machine vision. Since 1986, he has been a professor of computer science at the Technical University of Braunschweig, Germany, where he set up the Institute for Robotics and Process Control. He became advisory professor of Shanghai University in 1992 and chair of the collaborative research center on robotic systems for handling and assembly in Braunschweig in 2000. His main interests are in robotics, computer vision, and algorithmic aspects of computer science.

Address for Correspondence: Torsten Kröger, Institute for Robotics and Process Control, Technical University of Braunschweig, Muehlenpfordtstrasse 23, 38106 Braunschweig, Germany. E-mail: t.kroeger@tu-bs.de.

Smart Radiation Sensor Management

Radiation Search and Mapping Using Mobile Robots

©PUNCHSTOCK

BY R. ANDRES CORTEZ, XANTHI PAPAGEORGIOU, HERBERT G. TANNER, ALEXEI V. KLIMENKO, KONSTANTIN N. BOROZDIN, RON LUMIA, AND WILLIAM C. PRIEDHORSKY

The current geopolitical situation requires automated tools for quick and effective assessment of threats. Modern threats are subtle and ephemeral and can be hidden across large areas. Classical information-extraction methods, where data are randomly collected and then subsequently filtered and analyzed by human operators in search of particular signatures, are no longer effective against today's modern threats. Data collection must be guided by querying world models that afford the span and resolution needed for multiscale problems.

Currently, searching for radiation sources is usually done manually, by operators waving radiation counters in front of them as they walk. This method does not provide any visual or statistical data map of the area in question. To quickly characterize the severity of the situation, an efficient way of obtaining this radiation map is needed. When searching for a weak radiation source, a speck of uranium, for example, manual methods are unlikely to yield results.

In nuclear search, the strength of the signal-to-noise ratio (SNR) falls with the square of the distance R to the source, as the latter increases. The relation between SNR and distance motivates bringing the sensor as close to the source as possible [1]. Mobile robots can carry sensors close to the source and position them accurately for the required measurement collection. Using traditional sequential testing theory, we can only confirm the presence of a source of a particular strength at a given location. For locations where these specific nuclear signatures are not detected, no information is given regarding the local radiation levels. A different approach is therefore needed if the objective is to map the radiation intensity over a certain area.

Digital Object Identifier 10.1109/MRA.2008.928590

In this article, we suggest two different motion planning strategies for radiation map building. In the first, named the *gradient-based Bayesian method*, an uncertainty metric is used to define a potential function, with which to bias the search toward particular areas of the map, where uncertainty regarding radiation levels is highest. In the second strategy, named the *sequential-based Bayesian method*, the robot visits every area cell along a predetermined path, and the time it spends at each cell depends on the local uncertainty levels.

The sequential-based Bayesian method ensures that each cell is visited only once, and thus it is time optimal. However, due to the motion plan of the sensor being predetermined, parts of the map that could be potentially the most interesting

1070-9932/08/$25.00©2008 IEEE

The current geopolitical situation requires automated tools for quick and effective assessment of threats.

could be revealed last. In addition, this method is not suitable when the prior is time varying, i.e., in the case of dynamic environments, since areas explored once are not revisited. The gradient-based Bayesian method, on the other hand, offers an approximate map of varying confidence at every time step, but it requires longer time for the completion of the map. However, the method outperforms the sequential-based Bayesian mapping in the initial stages of the area scanning, suggesting that when time constraints are imposed that will not allow the sequential-based method to terminate, a better map can be obtained with the gradient-based method. In addition, the gradient-based Bayesian method can accommodate real-time changes in the environment, through an online adaptation of the function that generates the potential field.

The methods described in this article are not only suited to applications of nuclear forensics, where we need to determine in the least possible time, and at a given probability of a false positive, whether fissile material has been processed in a given area. They are also applicable to the problem of assessing the contamination due to accidental or malicious release of radioactive isotopes. As a result of a radiation map, decision makers can single out safe from unsafe regions and quantify contamination as a first step toward containment and cleanup.

What Does a Map Show?

There are significant differences between mapping walls and door locations in an office environment and mapping the temperature distribution in the same space. Robot localization is typically linked to map building in the first case, whereas in the second it is not. Knowing where a measurement is taken is of paramount importance, but the two problems (localization and temperature mapping) are not linked. The second difference has to do with the underlying statistics: range measurements are typically associated with Gaussian distributions; measuring distributed quantities such as temperature, pressure, or radiation level may follow different statistical laws, which result from the type of sensors used as well as the nature of the underlying physical process. For this reason, we divide this section into three parts. The first refers to existing approaches to robot exploration and is conceptually related to our mapping problem because our robots essentially explore radiation distributions. The second focuses on expressing the spatial distribution of physical quantities, and the third part specializes the discussion on radiation mapping.

Exploring the World

Robot exploration typically involves creating a map of the known workspace, which depicts the location of obstacles and landmarks. The process is often based on an occupancy grid, which discretizes the area of interest into a large number of cells. The notion of grid maps or occupancy maps was first introduced in mobile robotics in [2] and subsequently used in [3] and [4]. In most cases, the cells of a grid map contain a probability value of whether that cell is occupied. Yamauchi [3] uses occupancy grids to define a new frontier for the robot to investigate and expand its knowledge of the environment. Romero et al. [4] uses occupancy grids to minimize the cost of traveling to an unoccupied cell for further investigation of the area. In this article, we use each cell of the grid map to hold a metric of the uncertainty regarding the radiation levels in that region. Our metric of uncertainty is the variance of a particular distribution over the expected radiation level at each spatial location.

Linking robot motion to uncertainty is not an entirely new concept but is lately gaining momentum in robotic exploration, localization, and mapping [5], [6]. Moorehead [5] uses the entropy, among other utility measures, to evaluate the benefit of visiting different locations. The entropy in [5] describes the uncertainty over a certain location being reachable. It is not directly associated with the quality of the model nor is it linked with the statistics of the measurements. In [6], the problem is to facilitate mobile robots in localizing target features in their environment, and mutual information is used as a metric of significance of different discrete locations in terms of sensing. Of course, the statistics for the detection problems addressed there are Gaussian, but the concept is nevertheless similar.

Mapping Spatial Distributions

Work on mapping the distribution of physical quantities over a region (e.g., gas concentration and temperature) is related to our approach in the sense that the map constructed is not related to the topology of the environment nor does it include landmarks or other location identifiers. In [7], maps of gas concentrations are constructed by maneuvering a robot using a predefined path that covers the entire area. An approach to search for ocean features is found in [8], in which multiple robots follow gradients to locate and track ocean features such as fronts and eddies. For the radiation mapping problem addressed here, sensor measurements at given locations are, in theory, random samples drawn from a Poisson distribution, and, therefore, vary widely, making gradient calculations meaningless. Our approach is to follow gradients of uncertainty, rather than those of measured radiation, and to steer the robot to locations where measurements make the most difference in situational awareness.

In [9] and [10], the focus is on efficiency. Kim and Hespanha [9] address the problem of determining the paths for a group of unmanned combat air vehicles that cooperate in their use of jamming resources, such that the risk of being tracked and destroyed by surface-to-air missiles is minimized. The minimum risk of path planning is reduced to a weighted anisotropic shortest path problem. Bertucelli and How [10] propose an approach to calculate the minimum number of observations needed to achieve a given level of confidence for target

existence in an uncertain grid-like environment. The authors use a beta distribution to model the imprecise knowledge of the prior probabilities in the individual cells. As in this article, [10] brings into play the variance of the distribution to strike a balance between the speed of observation and the uncertainty on the existence of a target.

Mapping Radiation

Sequential nuclear search allows us to quickly verify the existence of microscopic specks of radioactive material. When a gamma ray emitted from a source reaches a sensor, the latter is said to register a count. Radiation intensity is measured in counts per second, assuming that all emitted rays are detected and registered. Low rate counting of radiation from nuclear decay is described by the Poisson statistics. Classical sequential testing theory [11] suggests the stopping rules (i.e., when does one know with certain confidence that a source exists at a given point). These rules allow for rejection of certain sequences of observations at early stages. Either positive or negative identification can be made based on the likelihood ratio of the probability of observing a certain number of counts within some time period given that there exists a source emitting an average number of counts per unit time, μ_s, over the probability of these counts corresponding to background radiation. The stopping rule is determined from the desired false negative and false alarm rates P_{FN} and P_{FA}, respectively,

$$C = \frac{P_{\mathrm{FN}}}{1 - P_{\mathrm{FA}}}, \qquad A = \frac{1 - P_{\mathrm{FN}}}{P_{\mathrm{FA}}}. \tag{1}$$

The condition $\kappa_k \leq C$ rejects the hypothesis that the source is present at location κ_k, while the condition $\kappa_k \geq A$ confirms the presence of the source. When $C < \kappa_k < A$, a longer exposure is required to make a decision. An example of the stopping rule is illustrated in Figure 1, where the straight lines represent the limits of confidence intervals for the following conclusions: 1) when the radiation counts collected within a certain time period are in the upper region, the presence of a source is verified with a given confidence; 2) if the counts fall in the lower region, then they are most likely due to background radiation; 3) in between, no conclusion can be confidently drawn until more measurements are collected.

This strategy, however, is a detection strategy and not a mapping technique. To construct a contour radiation map using traditional sequential testing theory, one would have to scan the area for every single contour level. This approach is not time optimal, and the required completion time increases rapidly with the resolution of the desired map. There is also an important caveat here: the algorithm is sensitive to the assumed value of the strength of the source that is to be detected. If the source intensity is underestimated, the method will give a false negative by default, since the registered number of counts (triangles in Figure 1) remains within the threshold boundaries for the whole time interval of 2.4 s.

Mobile robots can carry sensors close to the source and position them accurately for the required measurement collection.

A Model for the Distribution of Radiation

Natural gamma ray background radiation has a cosmic ray component and a component from naturally occurring radioactive isotopes. Small detectors (such as the 1-in^3 La_2Br scintillator shown in Figure 4) typically record low count rates, and the probability of observing k counts, given a mean expected count rate λ, is well described by the Poisson distribution

$$P(X = k|\lambda) = \frac{\lambda^k e^{-\lambda}}{k!}. \tag{2}$$

We use a gamma distribution for the initial estimate of the expected mean count rate λ

$$\pi(\lambda) = \beta^{\gamma} \lambda^{\gamma - 1} e^{-\beta\lambda} \times \frac{1}{\Gamma(\gamma)},$$

where γ is the shape parameter, β is the scale parameter, and $\Gamma(\gamma) = \int_0^{\infty} t^{\gamma-1} e^{-t} dt$. The expected value and variance of the gamma distribution can be expressed in terms of its shape and

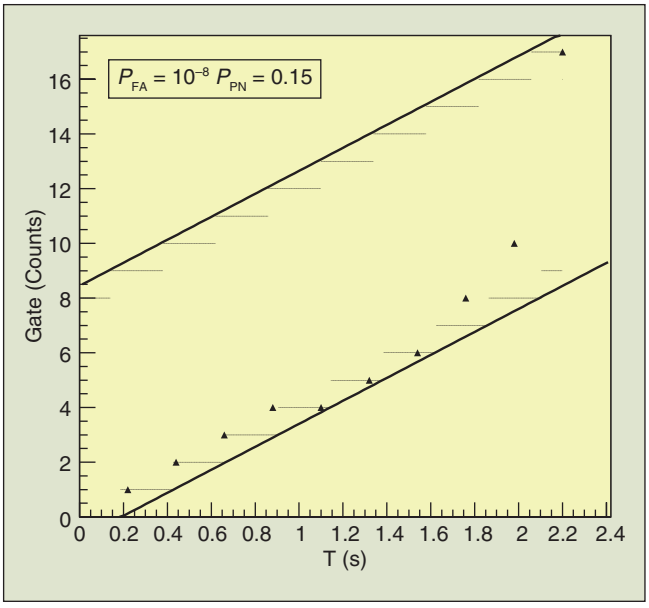

Figure 1. *Applying sequential testing theory to a nuclear detection problem, which involves calculating the thresholds for a positive confirmation or rejection of the source hypothesis [from (1)]. In the example depicted, the set of thin horizontal lines defines count thresholds for positive (top) and negative (bottom) identification of a ten counts per second source within one count per second background. The bold solid lines are the linear fit to the conservative boundaries of the thresholds.*

scale parameters

$$\mathbb{E}(\Gamma) = \frac{\gamma}{\beta}, \qquad V(\Gamma) = \frac{\gamma}{\beta^2}. \tag{3}$$

As new measurements are collected, the probability distribution of λ is updated using Bayes rule in the form of the recursive formula

$$\pi(\lambda|X) = \frac{P(X = k|\lambda)\pi(\lambda)}{\int P(X = k|\lambda)\pi(\lambda)d\lambda}.$$

Where to Move the Sensor

Area Cell Decomposition

Our main goal is to create a radiation field map of the area at a given uncertainty level (variance at most V_0). We decompose the workspace to $m \times n$ cells, which are arranged in a two-dimensional (2-D) array and indexed by i and j. In each cell, we assume an a priori radiation level, which is expressed in the form of an expected mean count rate λ_{ij} (Figure 2). Being uncertain about this estimate, we assume that this mean count rate follows a gamma distribution with mean $\lambda_{ij} = \gamma_{ij}/\beta_{ij}$, and variance $V_{ij} = \gamma_{ij}/\beta_{ij}^2$, according to (3).

Mapping Sequentially

One method of moving the robot and collecting measurements is through sequential search, by moving from cell to cell and drawing a statistically definitive conclusion. The method we describe here, however, is not an instance of the traditional sequential search because we do not verify a hypothesis about the existence of a certain source, but, rather, we position the sensor at a given location for sufficient time to reduce the uncertainty over our radiation level estimate below a certain threshold. The similarities stop at motion planning. In this hybrid approach for implementing Bayesian-based radiation mapping, motion planning is done sequentially, but the decision on the next movement is based on Bayes rule. We call this type of strategy *sequential-based Bayesian search*.

In this method, the robot stays in a cell and takes radiation measurements until the desired variance threshold is reached. Then, the robot moves to a neighboring cell along a certain direction and continues with mapping. The condition that enables the transition from cell (i,j) to, say, $(i+1,j)$, is $0 \le V_{ij} \le V_0$, where $V_0 \ge 0$ is the maximum acceptable variance. The mapping is completed when the robot has scanned every cell in the workspace.

Mapping Using Uncertainty Gradients

Searching sequentially is an open-loop strategy in the sense that the motion plan is predetermined, and the radiation map is ready only after the whole area is scanned. Instead, we can close the loop online and drive the robot where measurements are more critical for reducing uncertainty. These places change as the robot moves around and more measurements are collected. We thus use measurements as feedback to determine motion by means of an artificial potential field that is dynamically updated through Bayes rule. We construct a potential function of the form $\varphi = \gamma_d + 1/e^{\beta_o^{1/k}}$, where γ_d is the distance to the point where we want the robot to terminate the search, function β_o relates to the variance of each cell, and k is a positive tuning parameter.

The robot starts at cell (i,j), where $i \in \{1,\ldots,m\}$, $j \in \{1,\ldots,n\}$. A prior map of distribution of the average count rate over the area, in terms of parameters γ_{ij} and β_{ij}, is assumed to be given. From this distribution, we estimate the variance of the gamma distribution that expresses λ_{ij} (Figure 2) as $V_{ij} = \gamma_{ij}/\beta_{ij}^2$. Function β_o is then constructed as a strictly decreasing

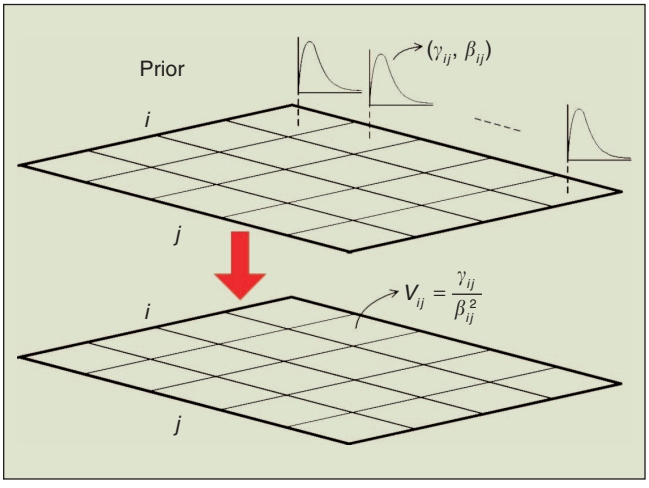

Figure 2. *The robot's workspace is decomposed in $m \times n$ cells. Prior knowledge of this area is a gamma distribution, with parameters γ_{ij} and β_{ij} in each cell. The mean value of the emission is λ_{ij}, and the variance is V_{ij} in any cell (i,j) of the grid.*

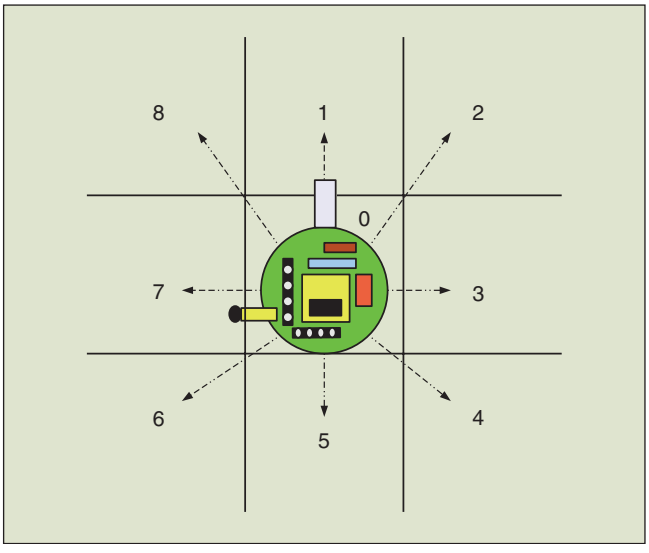

Figure 3. *The proposed area is decomposed into cells creating an $m \times n$ grid. The Khepera II mobile robot is allowed to move to the eight neighboring cells or stay in its current cell, depending on the calculated variance of the map, and based on the measurements obtained from the radiation sensor.*

function of V_{ij}. Although many choices are possible, for simplicity, we choose to set $\beta_{o_{ij}} = 1/V_{ij}$. From cell (i, j), the robot moves to an adjacent cell after comparing the values of φ at neighboring cells (Figure 3). To accelerate the search, instead of directly comparing variances in neighboring cells, we fit a smooth surface over the variance values of cells over the entire area. As a result, differences between adjacent cells are not skewed toward extreme values (zero or large positive and negative numbers) but are more uniformly distributed across the range of values. Using this method, we accelerate the mapping process by 10–15%. If the robot chases the global variance, maximum efficiency suffers. During both simulation and experimental tests of the gradient-based Bayesian mapping method, we observed a sharp increase in completion time as such maxima can appear in very distant regions of the area to be mapped. The robot travels back and forth, and the increased length of the robot's path translates directly to increased completion time.

The indices of the neighboring cell that the robot moves to are given as the solution to

$$\max \arg \varphi_{pq}, \quad i-1 \le p \le i+1, \quad j-1 \le q \le j+1. \quad (4)$$

If the radiation counts registered within the following time step are $x \in \mathbb{N}$, then, at the end of this time step, the cell parameters are updated as $\gamma_{ij}^{+} = \gamma_{ij} + x$ and $\beta_{ij}^{+} = \beta_{ij} + 1$, by applying the Bayesian rule on the gamma distribution. The variance is updated to $V_{ij}^{+} = \gamma_{ij}^{+}/\beta_{ij}^{+2}$. The loop is repeated until every cell on the radiation map has a variance below the predefined threshold. Note that the cell's variance is not necessarily decreased with any new measurement. Counts significantly different from the expected mean temporarily increase V_{ij}. Over time, however, the variance of revisited cells is decreased under a predefined threshold V_0. We refer to this strategy as *gradient-based Bayesian search*.

Algorithm Implementation

Hardware Description

Experimental tests were conducted using a Khepera II desktop mobile robot (Figure 4). The robot was equipped with a custom-built turret interfacing the cesium iodide (CsI) radiation sensor (Figure 4) with the robot's microprocessor, a Motorola 68331 running at 25 MHz. This processor executes the embedded C code that interprets and realizes motion commands coming from a desktop PC. On this PC, the search is planned, and the collected data are visualized in real time. Three analog inputs available through the input-output (I/O) robot interface are being used for sensor-robot communication, while collected sensor data are sent for visualization to a desktop computer through either a wireless or a cable RS232 link.

Gamma rays passing through the CsI crystal may deposit some or all of their energy. This energy excites electrons into higher-energy levels, which decay the emitting, visible light. The 4 cm long, 1.2 cm in diameter cylindrical CsI crystal is encapsulated into an aluminum casing with a Hamamatsu S3509

Linking robot motion to uncertainty is not an entirely new concept.

pin photodiode mounted on it to detect light induced in the crystal by passing photons. The sensor was assembled by Alphaspectra, Inc. Pulses generated by the diode are weak and are amplified using an Amptek A250 preamplifier with an external field-effect transistor. The amplified pulse is then shaped through a four-stage shaping amplifier. The shaping amplifier outputs an almost Gaussian waveform, the height of which corresponds to the energy deposited by the gamma ray in the active region of the detector. This signal is then processed using a digital board consisting of a low-power, high-speed, 8-National semiconductor ADC08200 and an Altera Cyclone 2910 field-programmable gate array (FPGA). The FPGA is programmed to perform peak finding and pulse counting. We estimate the total power consumption of the electronics to be below 200 mAh at 6 V, which allows us to power them for several hours with four rechargeable digital camera batteries. The pin photodiode is in reverse bias and consumes a negligible amount of power (on the order of nAh at 25 V).

The added weight of the sensor, digital board, and power supplies represents a challenge to the robot's motors. To reduce friction, a stainless steel ball caster wheel is attached to the base of the sensor. Without external measurements to be used for localization, odometry errors build up and cause the robot to deviate from the reference path connecting one cell to the next. To address this issue, we manually issue corrective motion commands to keep the localization error bounded.

Experiment Design and Implementation

The Khepera II robot is programmed to accept high-level, motion-correcting commands from a controller implemented on a laptop computer running MATLAB and interfaced with

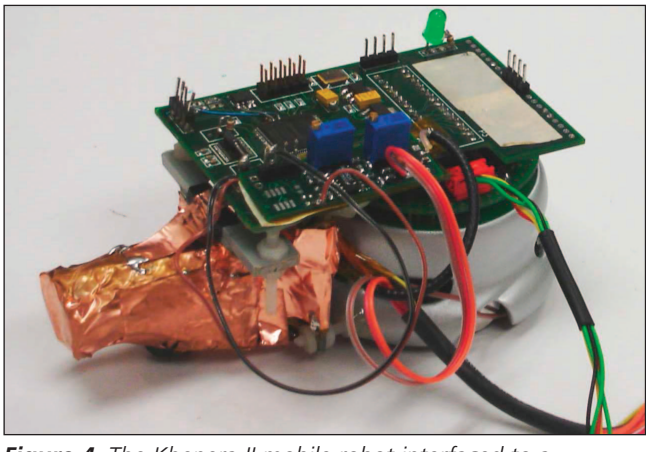

Figure 4. *The Khepera II mobile robot interfaced to a miniature radiation sensor that detects gamma rays. The robot communicates with a central computer via RS232 for real-time radiation map building and motion control.*

Sequential nuclear search allows us to quickly verify the existence of microscopic specks of radioactive material.

the serial port of the Khepera II. When sensor data are received from the robot, the central controller integrates them into the radiation map in real time.

The area to be mapped is a 60×60 cm surface, decomposed into a 15×15 grid. Initially, the robot is positioned at cell $(10, 10)$. We assume a distribution of radiation levels over this area, λ, represented in Figure 5(a). This distribution is unknown to the system, and the goal of the experiment is to reconstruct it up to a certain confidence level, using measurement data. Assuming that no initial information about the λ distribution is available, we start with a uniform distribution for both λ_{ij} and V_{ij}, as shown in the Figure 5(b) and (c), respectively. The desired variance threshold for the constructed map is set at $V_0 = 0.5$.

Snapshots of the experimental test are shown in Figure 6. Figure 6(a)–(c) shows the robot in different configurations on the grid, while Figure 6(d)–(f) presents screen captures showing how the map evolves and drives further measurements. In Figure 6(d)–(f), the upper left shows the real λ distribution of the area, the upper right shows the radiation map updated in real time as the robot moves around to take measurements, the lower left shows the updated variance distribution, and the lower right shows the potential function that steers the robot through its gradient field.

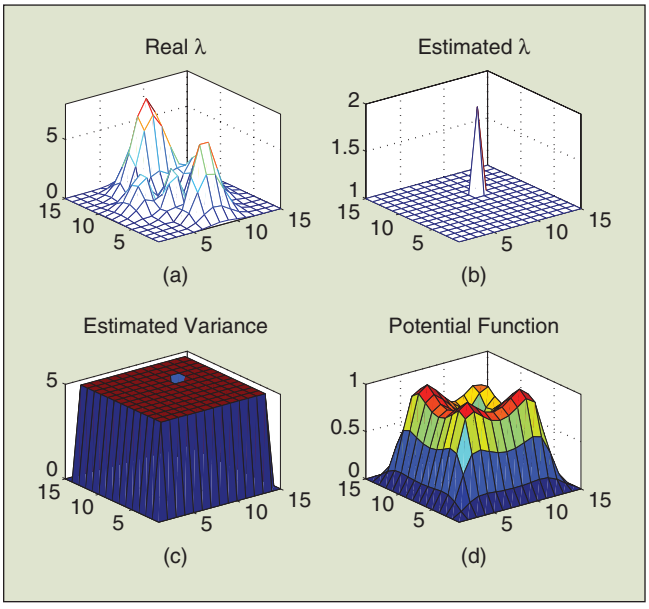

Figure 5. *Initial configuration of the area. (a) Real distribution of λ. (b) Uniform prior information of the distribution of λ. (c) Uniform prior information of variance. (d) Potential function based on surface fitting of variance data.*

Figure 7 shows 2-D representations of the variance distribution at different time instances during the experiment. All variance values in Figure 7(d) are below the threshold value of V_0, and thus the search terminates.

Figure 8 reveals how the completion time of the gradient-based and sequential-based Bayesian mapping methods is affected when the variance threshold (quantifying map uncertainty) is reduced. We observe an exponential increase in the time required for map completion.

Comparison of Different Navigation Strategies

We compare the proposed gradient-based Bayesian mapping algorithm with the uniform and sequential-based Bayesian mapping techniques. The uniform mapping consists of scanning the area cell by cell along each row and spending a constant fraction of time at each cell. At the end of the scan, the maximum value for the variance over all cells is compared with the threshold value, and, if found larger, the scan is repeated. Figure 9 shows the experimental results for the uniform search tested in the same scenario as for the Bayesian mapping algorithm.

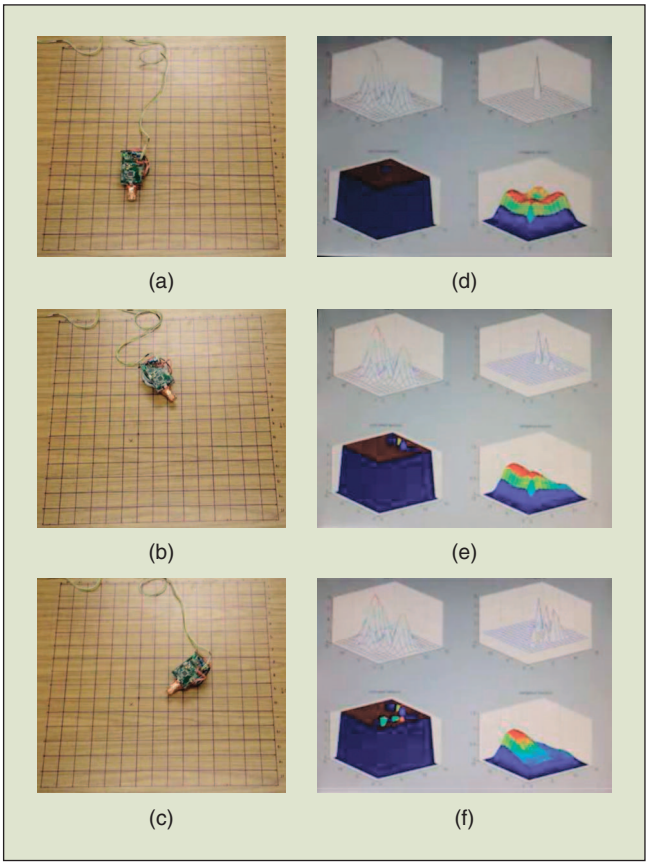

Figure 6. *Implementation of the gradient-based Bayesian mapping. (a)–(c) Snapshots of the real execution of the experiment. (d)–(f) Snapshots of the updated data during the experiment: Upper left: real distribution of λ; upper right: updated values of the distribution of λ as the robot is moving and the sensor is collecting radiation data; lower left: updated values of variance obtained during the experiment; and lower right: potential function based on surface fitting of variance data during the experiment.*

In the sequential-based Bayesian mapping, the time spent in each cell is adjusted to allow sufficient integration time for the sensor and enough measurements to be collected so that variance drops below the threshold before leaving the cell. Each cell is visited once. Figure 10 shows the experimental results for the sequential search and for the same mapping scenario.

The three mapping algorithms are compared in terms of completion time. The results indicate that the gradient-based Bayesian mapping is faster than uniform mapping but slower

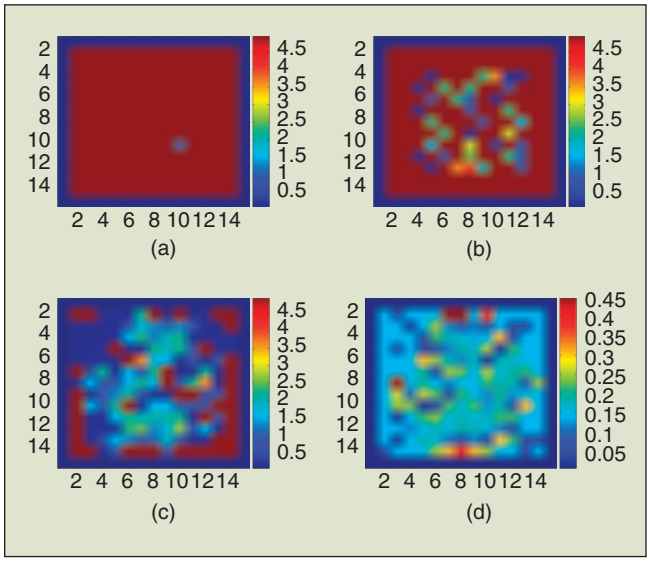

Figure 7. *Successive snapshots of the radiation map real-time construction using the gradient-based Bayesian algorithm, from the initial map (a) to the final map (d) after the completion of the algorithm. The numerals on the horizontal axis and the left column of the vertical axis on each matrix denote cell indices. The numerals on right column indicate the levels of variance of the gamma distribution for radiation intensity at each cell. (a) Initial map estimate. (b) Intermediate snapshot. (c) Shortly before completion. (d) Completed map.*

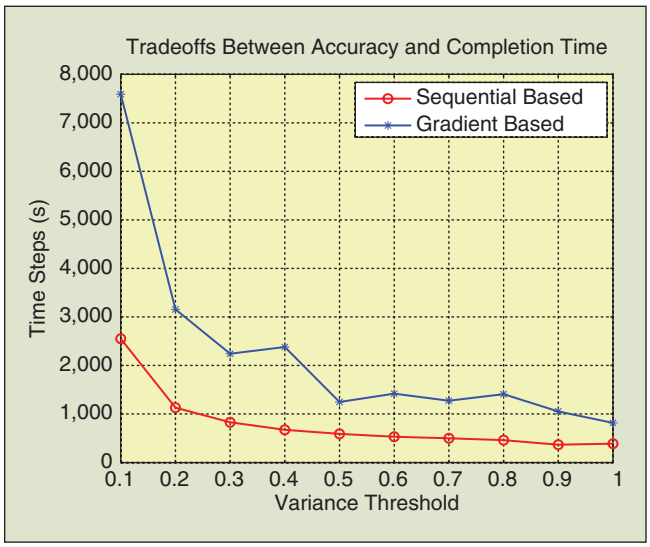

Figure 8. *The effect of the variance threshold choice on the completion time of the gradient-based and sequential-based Bayesian mapping algorithms. As the required accuracy increases, completion time appears to increase exponentially.*

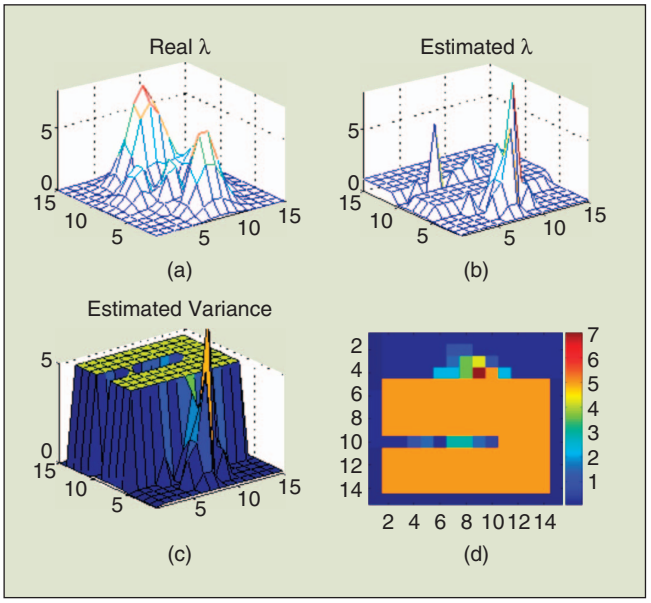

Figure 9. *Experimental implementation of the uniform-mapping algorithm. (a) The real distribution of λ. (b) The updated values of the distribution of λ as the robot is moving and the sensor is collecting radiation data. (c) The updated values of variance. (d) A 2-D representation of the variance distribution at an intermediate time step. More than one scan of the whole area will be needed to achieve the required confidence level.*

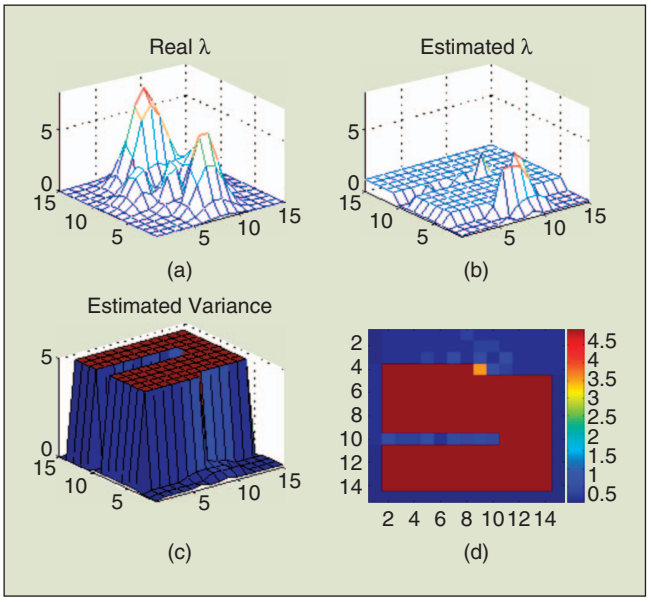

Figure 10. *Experimental implementation of the sequential-based Bayesian mapping algorithm. (a) The real distribution of λ. (b) The updated values of the distribution of λ as the robot is moving and the sensor is collecting radiation data. (c) The updated values of variance. (d) A snapshot of the 2-D distribution of radiation level variance over the area of interest.*

Our approach for implementing the Bayesian radiation mapping algorithms was to drive the robot over each segment of the search area.

than the sequential-based Bayesian mapping. In a typical run, the gradient-based Bayesian mapping requires approximately 1,300 time steps (simulation seconds), the uniform mapping requires roughly 3,000 time steps, and the sequential-based Bayesian mapping requires close to 600 steps to complete the map at the same level of confidence. Thus, the sequential-based Bayesian mapping algorithm outperforms the gradient-based Bayesian mapping algorithm, but the latter has the advantage over both other techniques such that, at each time step, there is an available map constructed with a confidence that is improved with time. This is particularly important if there are severe time constraints for the completion of the mapping task. No alternative mapping technique can adequately address the problem of producing a reasonably accurate map of the most interesting portions of the search area within a certain time interval. The information collected within 300 s by means of the gradient-based Bayesian algorithm may offer more clues for the distribution of radiation over the area than the half-built map, resulting from the sequential-based Bayesian search.

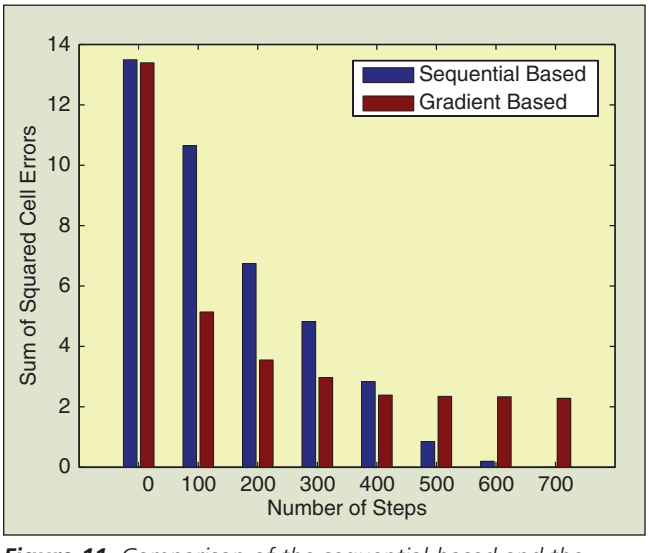

Figure 11. *Comparison of the sequential-based and the gradient-based Bayesian methods in terms of accuracy for uniform, constant prior. The gradient-based algorithm reduces the error rapidly in the initial stages but leaves a residual error after completion, which is proportional to the given variance threshold. The sequential-based algorithm terminates faster and yields a more accurate map after completion, but map confidence increases almost linearly with time. The choice of method thus depends on the time constraints, the initial prior, and the dynamics of the environment.*

The two algorithms that take advantage of the Bayesian update (the sequential-based Bayesian and the gradient-based Bayesian) offer different tradeoffs between optimality and flexibility (Figure 11). The gradient-based Bayesian algorithm offers the ability to partially investigate areas that are of more interest first. The price to pay is that these areas may have to be visited again. On the other hand, the sequential-based Bayesian algorithm is time optimal as the prior variance distribution is uniform. The gradient-based Bayesian method cannot outperform the sequential-based method in terms of map accuracy, as the latter is measured in terms of the residual sum of squared errors between the true radiation levels and the estimated radiation levels. This is because, strange as it may sound, in nuclear measurement, $1 + 1 \neq 2$! The Poisson statistics of nuclear measurement implies that visiting the same cell twice and spending a total of 2 s there is not the same as getting there once and have the sensor integrate for 2 s continuously. When the prior variance distribution is not uniform, however, a partially constructed map may be of limited value, depending on the initial position of the robot prior to exploration.

Summary

We developed two radiation mapping algorithms that can handle different situations based on prior information of the search area. The algorithms were developed in the framework of model-driven measurement, where a world model was used to drive measurement collection, and measurements were used to update the world model. We developed and experimentally tested a robotic implementation of two Bayesian-based radiation mapping strategies in two dimensions, using a commercially available desktop mobile robot fitted with a CsI radiation sensor. Our approach for implementing the Bayesian radiation mapping algorithms was to drive the robot over each segment of the search area, in real time, according to the radiation counts collected by the sensor. Future research directions include extensions to three-dimensional mapping; exploring and characterizing the tradeoffs between time efficiency, map confidence level, and utilization of prior knowledge information; as well as the implementation of Bayesian statistics for the online update of the world model.

Acknowledgments

Xanthi Papageorgiou was supported by Los Alamos National Laboratory Award STB-UC:06-36. Andres Cortez was supported, in part, by the aforementioned award and, in part, by the Department of Energy, University Research Program in Robotics Grant DE-FG52-04NA25590. The latter grant also supported Herbert Tanner and Ron Lumia. The authors thank Nick Hengarter and Chuck Alexander of Los Alamos National Laboratory for assistance in nuclear statistical modeling and experimental system integration, respectively.

Keywords

Nuclear search, radiation mapping.

References

[1] R. J. Nemzek, J. S. Dreicer, D. C. Torney, and T. T. Warnock, "Distributed sensor networks for detection of mobile radioactive sources," *IEEE Trans. Nucl. Sci.*, vol. 51, no. 4, pp. 1693–1700, Aug. 2004.

[2] A. Elfes and H. P. Moravec, "High resolution maps from wide angle sonar," in *Proc. IEEE Int. Conf. Robotics and Automation*, 1985, pp. 116–121.

[3] B. Yamauchi, "Frontier-based exploration using multiple robots," in *Proc. 2nd Int. Conf. Autonomous Agents*, 1998, pp. 47–53.

[4] L. Romero, E. Morales, and E. Sucar, "An exploration and navigation approach for indoor mobile robots considering sensor's perceptual limitations," in *Proc. IEEE Int. Conf. Robotics and Automation*, May 2001, pp. 3092–3097.

[5] S. Moorehead, "Autonomous surface exploration for mobile robots," Ph.D. dissertation, Carnegie Mellon Univ., Pittsburgh, PA, 2001.

[6] B. Grocholsky, J. Keller, V. Kumar, and G. Pappas, "Cooperative air and ground surveillance," *IEEE Robot. Automat. Mag.*, vol. 13, no. 3, pp. 16–26, 2006.

[7] A. Lilienthal and T. Duckett, "Building gas concentration gridmaps with a mobile robot," *Robot. Auton. Syst.*, vol. 48, no. 1, pp. 3–16, 2004.

[8] P. Orgen, E. Fiorelli, and N. E. Leonard, "Cooperative control of mobile sensor networks: Adaptive gradient climbing in a distributed environment," *IEEE Trans. Automat. Control*, vol. 49, no. 8, pp. 1292–1302, Aug. 2004.

[9] J. Kim and J. P. Hespanha, "Cooperative radar jamming for groups of unmanned air vehicles," in *Proc. IEEE Conf. Decision and Control*, Dec. 2004, pp. 632–637.

[10] L. Bertuccelli and J. How, "Robust UAV search for environments with imprecise probability maps," in *Proc. IEEE Conf. Decision and Control*, Dec. 2005, pp. 5680–5685.

[11] A. Wald, "Sequential tests of statistical hypotheses," *Ann. Math. Stat.*, vol. 16, no. 2, pp. 117–186, 1945.

R. Andres Cortez received his B.S. degree in mathematics from New Mexico Highlands University, Las Vegas, in 2005, and his M.Sc. degree from the University of New Mexico in 2007. He is currently working toward his Ph.D. degree in mechanical engineering at the University of New Mexico.

Xanthi Papageorgiou received her Eng. Diploma in mechanical engineering from the National Technical University of Athens (NTUA), Greece, in 2003. In 2006, she was a visiting research scholar at the Mechanical Engineering Department at the University of New Mexico. She is currently working toward her Ph.D. degree in mechanical engineering at NTUA. She is a Student Member of the IEEE.

Herbert G. Tanner received his Eng. Diploma and Ph.D. in mechanical engineering from the NTUA, Greece, in 1996 and 2001, respectively. From 2001 to 2003, he was a postdoctoral fellow at the Department of Electrical and Systems Engineering at the University of Pennsylvania, Philadelphia. In 2003, he joined the faculty of the Department of Mechanical Engineering at the University of New Mexico, where he is currently an assistant professor. In 2007, he was awarded the University of New Mexico School of Engineering Junior Faculty Research Excellence Award. He is also a recipient of the National Science Foundation Career Award.

Alexei V. Klimenko received his B.S. and M.S. degrees in electrical engineering from Moscow Institute of Steel and Alloys, Russia, in 1998 and 1999, respectively, and the M.S. and Ph.D. degrees in nuclear physics from Old Dominion University, Norfolk, Virginia, in 2001 and 2004, respectively. From 2004 to 2006, he was a postdoctoral research associate at Los Alamos National Laboratory, New Mexico. He is currently a staff scientist at Passport Systems, Inc., Acton, Massachusetts. He develops and models threat detection algorithms for nonintrusive cargo-screening systems.

Konstantin N. Borozdin received the M.S. degree in experimental nuclear physics from Moscow Engineering Physics Institute, Russia, in 1988, and the Ph.D. degree in astrophysics and radioastronomy from Moscow Space Research Institute in 1995. He is currently a technical staff member with the Space Science and Applications Group, Los Alamos National Laboratory, New Mexico. He has been working in the fields of astrophysics, physical modeling, information technologies, radiation detection, and national security applications. He received an Order of Merit medal for his involvement in the Mir-Kvant space experiments in 1997.

Ron Lumia has been a professor in the Mechanical Engineering Department of the University of New Mexico since 1994. He received a B.S. degree from Cornell University in 1972 and the M.S. and Ph.D. degrees from the University of Virginia in 1977 and 1979, respectively. He has worked for industry, government, and academia. Recently, he was elected as a Fellow of the IEEE for leadership in the development of open architecture control systems for applications in robotics and automation, and he has managed a variety of robotics, automation, and sensory processing research projects.

William C. Priedhorsky received the B.A. summa cum laude with honors in physics from Whitman College, Walla Walla, Washington, in 1973, and the Ph.D. degree in physics from the California Institute of Technology, Pasadena, in 1978. He has been at Los Alamos National Laboratory since 1978 and most recently as a program director at the Laboratory-Directed Research and Development Office. He has also been a visiting scientist at the Max Planck Institute for Extraterrestrial Physics, Garching, West Germany; the Danish Space Research Institute, Lyngby, Denmark; and the University of Melbourne, Australia; in 1985–1986, 1994, and 1995, respectively. His main research interests include high-energy astrophysics, X-ray and optical instrumentation, and various national security applications. He is a recipient of numerous awards and honors.

Address for Correspondence: Herbert G. Tanner, University of New Mexico, Mechanical Engineering, MSC01 1150, Albuquerque, NM 87131. E-mail: tanner@unm.edu.

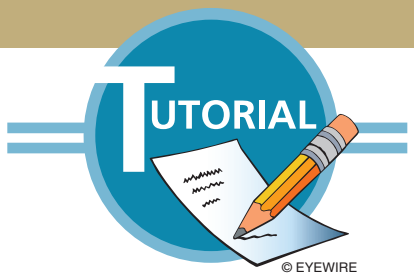

Surgical and Interventional Robotics: Part II

Surgical CAD-CAM Systems

BY GABOR FICHTINGER, PETER KAZANZIDES, ALLISON M. OKAMURA, GREGORY D. HAGER, LOUIS L. WHITCOMB, AND RUSSELL H. TAYLOR

A large family of medical interventions can be represented by a model that is analogous to industrial manufacturing systems. If the right information is available, they can be planned ahead of time and executed in a reasonably predictable manner. We, therefore, have classified them as surgical computer-aided design (CAD)–computer-aided manufacturing (CAM) systems, having three key concepts:

1) surgical CAD, in which medical images, anatomical atlases, and other information are combined preoperatively to model an individual patient; the computer then assists the surgeon in planning and optimizing an appropriate intervention
2) surgical CAM, in which real-time medical images and other sensor data are used to register the preoperative plan to the actual patient and the model and the plan are updated throughout the procedure; the physician performs the actual surgical procedure with the assistance of the computer, using appropriate technology (robotics, mechatronics, optical guidance, perceptual guidance, etc.) for the intervention
3) surgical total quality management (TQM), which reflects the important role that the computer can play in reducing surgical errors and in promoting more consistent and improved execution of procedures.

Digital Object Identifier 10.1109/MRA.2008.927971

Successful procedures are also included in procedural statistical atlases and fed back into the system for pre- and intraoperative planning. This article, primarily concerned with robotics and mechatronics, concentrates on the surgical action (surgical CAM), although for the sake of completeness, major issues in surgical planning (surgical CAD) and postoperative data analysis (surgical TQM) are also included. This article is the second installment of a three-part series on surgical and interventional robotics.

Medical Imaging Devices

All stages of surgical CAD-CAM are inseparable from medical imaging, which necessitates a brief review of imaging modalities used with surgical CAD-CAM. Fluoroscopy produces a projective live X-ray image on a television screen. It is versatile, easy to use, widely available, and relatively affordable. Fluoroscopy's soft tissue resolution is poor, but it shows bony anatomy quite well. It lacks depth perception and exposes the patient and surgeon to radiation. Fluoroscopic images are often distorted by electromagnetic noise. Computed tomography (CT) is essentially a tissue density map produced by rotating an X-ray imager. CT has good soft tissue and excellent bone visualization, but unfortunately, it is not generally real time. Some newer units can produce coarse real-time images but at the expense of even higher X-ray doses. Ultrasound (US) scanners transmit sound waves to the tissue and detect the echoes that they compute into images. US scanning is inexpensive, nontoxic, safe, and portable. However, image quality is dependent on the operator's skill,

1070-9932/08/$25.00©2008 IEEE

and fidelity is diminished by speckle, shadowing, multiple reflections, and reverberations. Soft tissues are perpetually deformed under the probe's pressure. Among all imagers, US imager alone does not show the surgical tool before introducing it into patient's body. Magnetic resonance imaging (MRI) creates a strong (1.5–3 T) static magnetic field around the patient. During scanning, magnetic dipoles resident in the human tissue are disturbed by magnetic pulses, and relaxation times are measured with induction coils. Relaxation times are closely related to soft tissue properties, and as a result, MRI produces the finest soft tissue imaging among all current imagers. Unfortunately, MRI is very expensive, lack of space inside the magnet excludes direct access to the patient, and high magnetic fields make instrumentation very difficult.

Driving Clinical Application Areas

Percutaneous Needle-Based Interventions

Image-guided percutaneous (through the skin) needle placement interventions have become the standard of care in many procedures, such as biopsies, aspiration, or tissue ablations. Needles offer several obvious advantages over traditional surgery, including less scarring, lighter anesthesia, reduced postoperative pain, reduced complications, and faster discharge from the hospital. Freehand needle punctures typically include three decoupled tasks: 1) touch down with the needle tip on the skin entry point, which requires three-dimensional (3-D) Cartesian motion, 2) orient the needle by pivoting around the skin entry point, which requires two independent rotations about intersecting axes, and finally 3) insert the needle into the body along a straight trajectory, which requires one-dimensional translation, possibly combined with some drilling effect. Releasing the therapeutic payload (injection, deployment of implanted seeds or markers, etc.) or collecting tissue (firing biopsy guns, etc.) may require additional degrees of freedom (DoF). Needle-based surgeries can be exceedingly complex interventions, where translation, rotation motions, bending and insertion forces make up a delicate procedure. A variety of methods exist from handheld tools to point-and-click robotic systems, with the system's complexity depending on the capabilities of the image guidance used and the accuracy requirements of the application, usually about 1–2 mm. One of the typical surgical CAD-CAM applications is prostate brachytherapy, where 80–100 radioactive pellets of the size of a rice grain are implanted into the prostate to kill cancer by emitting ionizing radiation. Under transrectal US (TRUS) imaging, the implant needles are inserted through a preplanned pattern of guide holes drilled in a template jig [26]. Robotic assistance lends itself naturally to image-guided needle placement. Following a flurry of initial activities, a few systems have actually entered clinical trials for TRUS-guided prostate brachytherapy [6] (Figure 1) and CT-guided (Figure 2) and MRI-guided abdominal biopsies [4].

Transcutaneous Interventions

Transcutaneous interventions are truly noninvasive, as they do not require surgical access. External beam radiation therapy (EBRT) is delivered by high-energy X-ray beams generated using a linear accelerator (linac), irradiating the patient from several directions. Based on a CT scan, the treatment is

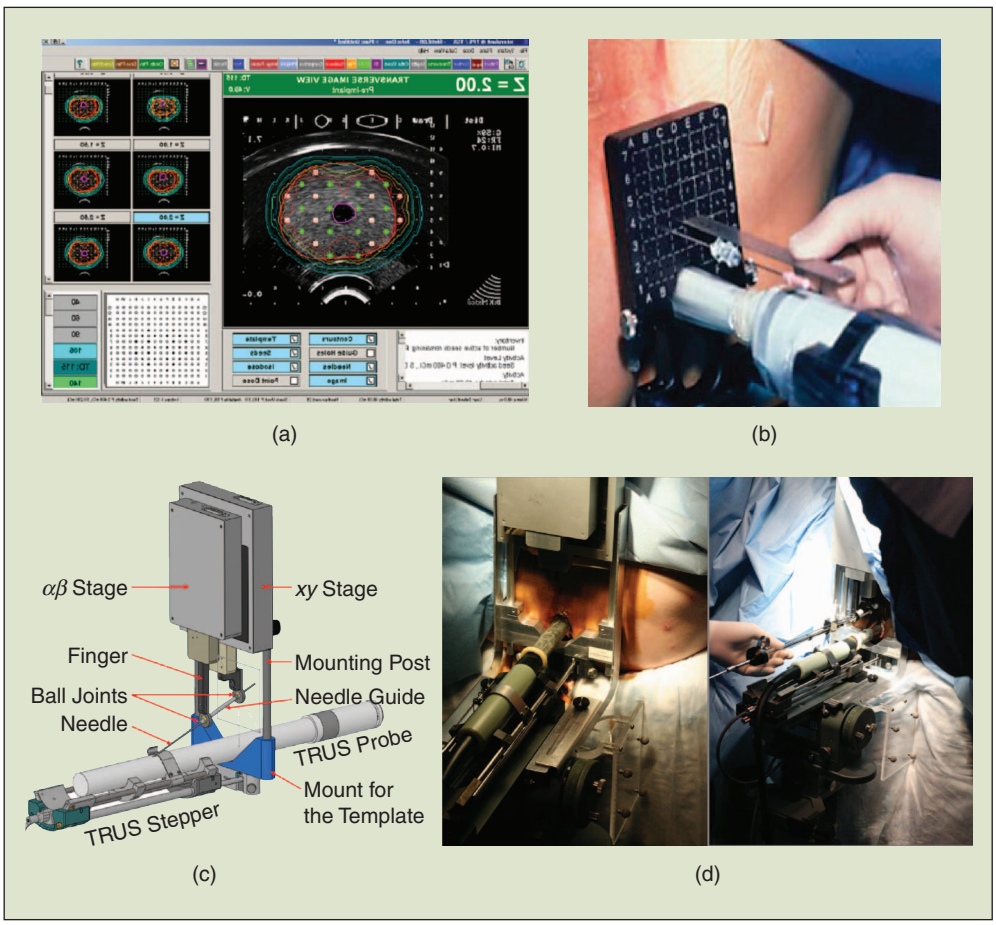

Figure 1. *Transrectal prostate brachytherapy [6]. (a) Implant and dose planning. (b) Classic manual needle placement under with template jig mounted over the TRUS probe. (c) Robotic needle positioner that replaces the template jig. (d) Patient treated with the robotic system. [Images courtesy of Everette C. Burdette (Acoustic MedSystems), Gabor Fichtinger, Danny Y. Song, and Peter Kazanzides (Johns Hopkins University).]*

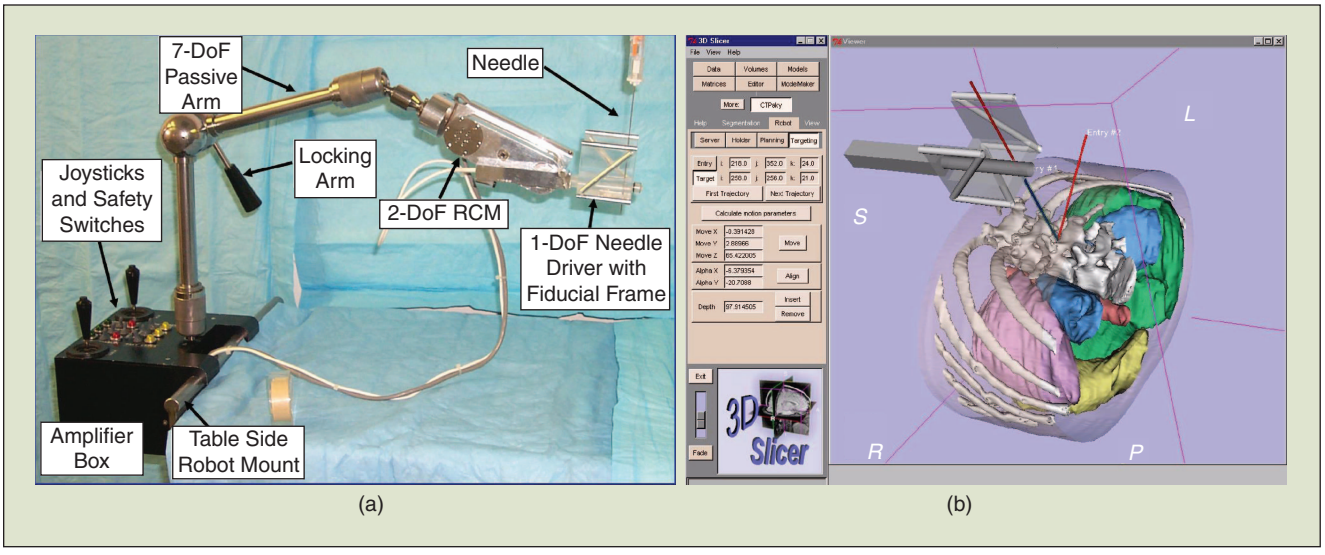

Figure 2. *System for CT-guided needle placement [17]. (a) 3-DoF remote center of motion robot is applied. The needle driver incorporates a stereotactic fiducial frame for image-based registration. (b) Screen shot of planning a spinal nerve root block, showing 3-D view of the reconstructed anatomy, end effector, and optimal needle path. [Images courtesy of Ken Masamune, Dan Stoianovici, Attila Tanacs, Russell H. Taylor, Gabor Fichtinger (Johns Hopkins University).]*

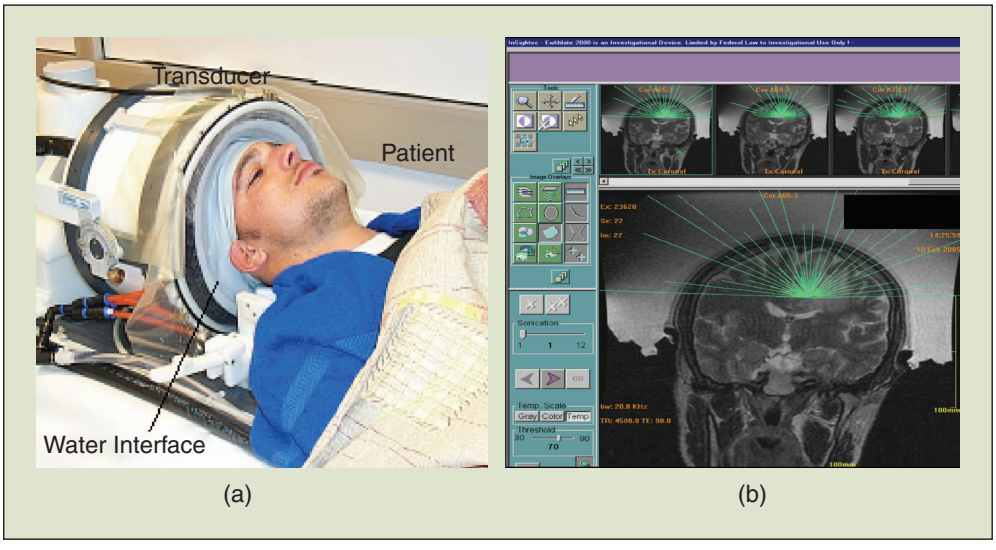

Figure 3. *MRI-guided focused US surgery of brain tumors [12]. (a) Patient in treatment position on the MRI couch. (b) Insonification planning interface. [Images courtesy of Ferenc Jolesz, Nathan Anmes (Brigham and Women's Hospital) and InSightec (Haifa, Israel).]*

carefully planned and simulated (surgical CAM). Generally, the EBRT dose is fractionated and spread out over several weeks to give normal cells time to recover, thereby demanding precise positioning of the patient before (and also during) each treatment fraction under the X-ray beam. EBRT delivery was among the first medical robot applications. Typically, the linac is placed on a large counterbalanced gantry that rotates around the patient lying on the couch. The couch has 3-DoF prismatic motion and 1-DoF rotation (recently, 3 DoF is used most often), where the axes of the gantry and couch rotations intersect in a single isocenter where the X-ray beam is aimed. Following the publicized Therac-25 accident [15], EBRT regulations were extremely conservative until the late 1990s. For example, no parameter other than gantry rotation was permitted to change while the beam was on. Nowadays, coach and gantry can move simultaneously while the beam is being collimated in real time by dozens of small shutters driven by separate stepper motors, in a process called intensity-modulated radiation therapy (IMRT). Modern treatment planning systems prescribe full four-dimensional motion sequences for the linac, couch, and beam collimator controller. At Stanford University, Adler et al. mounted a low-energy linac on a serial industrial robot. This system, available commercially under the name CyberKnife, specializes in precision treatment of tumors of the central nervous system [9].

In high-intensity focused US (HIFU) imaging, acoustic waves travel through the tissue, while part of them is absorbed and converted to heat. By focusing the beam, a precise zone of cell death can be achieved deep in tissue. Ideally, the HIFU unit is integrated with the image-guidance tool, such as MRI in [12] (Figure 3). First, the patient is scanned, and a precise sonification plan is created. During treatment, the temperature is monitored in real-time MRI. When the thermal dose reaches the prescribed level, sonification stops and the system moves to making the next lesion. Finally, a volume scan confirms the ablation zone, and additional sonification is used to

patch up cold spots. Another HIFU variant is the Sonablate (Focus Surgery, Inc.) used for transrectal ablation of benign prostate enlargement.

Intracavity Interventions

Interventions may be performed from within naturally accessible cavities of the body, such as the rectum, vagina, or cervix. (Interactive surgical assistant robots have been developed recently for surgeries in the nasal cavity and the throat, to be discussed in Part III of this tutorial series.) The most prevalent intracavity intervention today is core needle prostate biopsy performed through the rectum under TRUS guidance, where a spring-loaded biopsy gun is inserted into the prostate gland through a guide sleeve rigidly attached to the TRUS probe. Two inexhaustible sources of problems are found: 1) the prostate gland is under constantly varying deformation and dislocation during the procedure and 2) TRUS imaging provides poor imaging of prostatic tissues. TRUS-guided biopsy has poor sensitivity, and cancers as large as a sugar cube are routinely missed, a fundamental flaw that propelled MRI guidance to the attention of prostate cancer research. With a 3-DoF pseudorobotic device actuated manually by torsion cables, Krieger et al. performed accurate transrectal needle biopsies and implants in more than 50 patients using closed high-field MRI scanners [13]. Others proposed to make MRI-based targeting more affordable by real-time fusion of TRUS imaging and prior MRI (e.g., [30]).

Neurosurgery

Neurosurgery was one of the first clinical applications of surgical CAD-CAM, first with passive tool positioning devices (e.g., [2], [27]) and later with active robots (e.g., [14], [16]). The entry and target points are planned on CT or MR images, the robot coordinate system is registered to the image coordinate system (typically with fiducials affixed to the patient's head), and then, the robot positions a needle or drill guide (Figure 4). The fiducial structure may be a conventional stereotactic head frame, or, as in the Neuromate system, registration was achieved by simultaneous tracking of the robot and fiducials attached to the patient's skull [16].

Orthopedic Surgery

Orthopedic surgery is also a natural surgical CAD-CAM application. Bone is rigid and is easily imaged in CT and fluoroscopy, and surgeons are accustomed to doing preplanning based on these images. Geometric accuracy in executing surgical plans is very important. Spine surgery often requires screws and other hardware to be placed into vertebrae without damage to the spinal cord, nerves, and nearby blood vessels. In osteotomies, accurate cutting and placement of bone fragments are mandatory. Similarly, in joint replacement surgery, bones must be shaped accurately to ensure proper fit and positioning of components. The ROBODOC system [25] (described in Part I of this series [31]) represents the first clinically applied robot for joint reconstruction surgery in hip and knee replacement surgeries. In the surgical CAD phase, the surgeon interactively selects the desired prostheses and specifies their positions in preoperative CT images. In the surgical CAM phase, the robot is moved up to the operating table, the patient's bones are attached rigidly to the robot's base, and the robot is registered to the CT images by the use of either implanted fiducial pins or a 3-D digitizer to match bone surfaces to the CT images. After registration and initial positioning, the robot autonomously machines the desired shape with a high-speed rotary cutter while the surgeon monitors progress. Subsequently, other robotic systems for joint replacement surgery have been

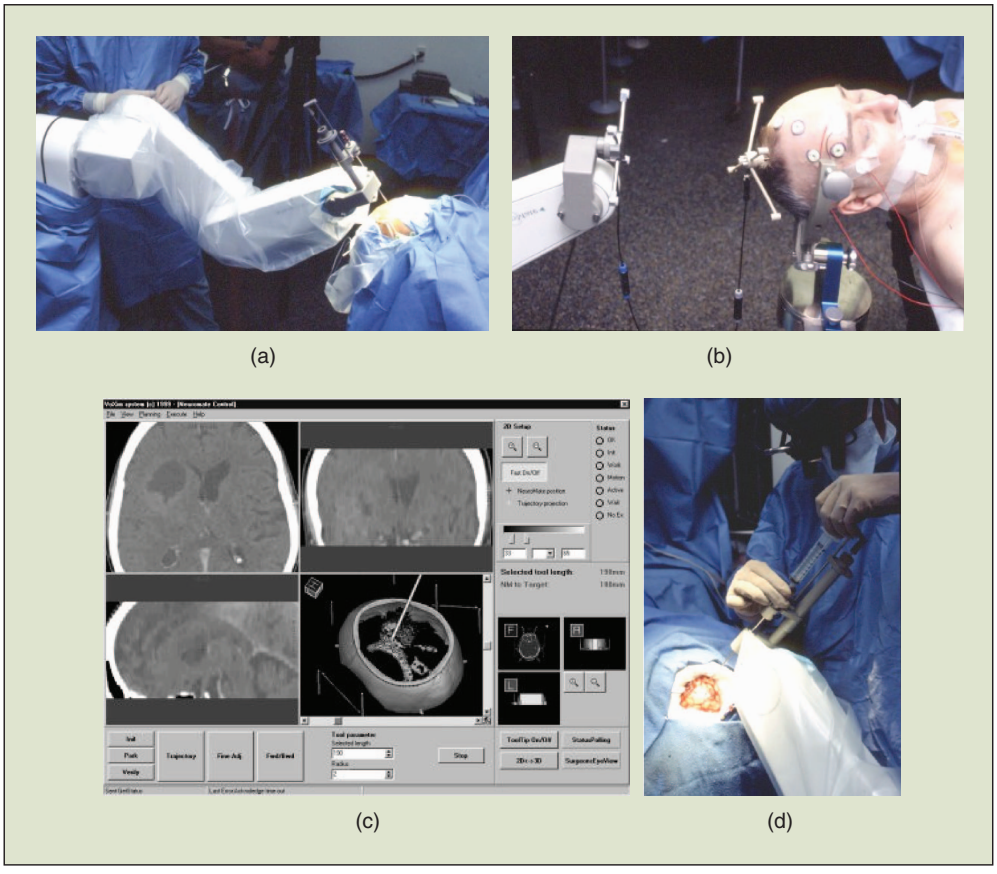

Figure 4. *Neuromate robot in brain surgery [16]. (a) The robotic arm holding an aspiration needle. (b) Robot-to-patient registration with optically tracked fiducials. (c) Screenshot from CT-based treatment planning. (d) Surgeon performing the aspiration. (Images courtesy of Integrated Surgical Systems.)*

investigated, including the hands-on guided Acrobot system [11] for knee surgery or various small robots that attach directly to the patient's bones (e.g., [3], [21], [22], [29]).

Point and Click Surgery

Surgical CAD: Intervention Planning

During the surgical CAD phase, the preoperative images are processed, and a computational model of the patient is created and interactively visualized for the surgeon. Often multiple imaging modalities are fused. Based on this patient-specific model, a surgical plan is created. The plan can be as simple as entry and target points for a biopsy, but it may be as delicately complex as an IMRT plan described earlier in the "Transcutaneous Interventions" section. Next, the physician simulates the surgery by performing a virtual dry run, like a computer game. For example, Figure 2(b) shows a screen from a simulation of robot-assisted spinal needle placement, with detailed 3-D rendering of the anatomy and a visual representation of the moving robot. In this case, for clinically more realistic planning, the robot was placed in the CT scanner with the patient during imaging. The robot was registered to CT image space with the fiducial frame attached to the end effector. In other applications, such as EBRT or brachytherapy, various approaches are tried out before converging on the optimal plan that envelops the target in the prescribed therapeutic dose while sparing the healthy tissues from collateral damage.

Linking CAD and CAM: Registration

Geometric relationships are fundamental to surgical CAD-CAM, and the registration of actors (robots, sensors, images, and the patient) is a perennial issue (e.g., [20], [23]).

As the final goal of registration is to determine the position of a surgical tool relative to the pathology targeted for intervention, it is desirable to perform the registration based on the image itself. One of the first uses of image-based registration was stereotactic neurosurgery [2], where a precision-machined a priori known rigid fixture (fiducial frame) was secured to the patient's head. After segmenting marks of the fiducial frame in CT, the transformation between the fiducial frame and image space was calculated. Since its initial introduction three decades ago, fiducial frames have taken the shape of helices, ellipses, lines, points, and endless combinations of these. Fiducial frames have appeared on the patient [Figure 4(a)], on end effectors of surgical robots [Figures 2(a) and 4(a)], and on surgical tools, and they have been used with all imaging modalities.

When a fiducial frame is not applicable, free fiducials are used in a more or less arbitrary constellation. Fiducials may be attached to the patient's skin (e.g., needle placement procedures), drilled in the patient's bone (e.g., orthopedic surgery, stereotactic neurosurgery), or locked in internal organs (e.g., clamps in breast surgery). In some cases, anatomical landmarks are picked as free fiducials. Intuitively, free fiducials are significantly less accurate and robust than precision machined fiducial frames, especially when the markers move relative to one another between planning and surgery.

When image-based registration is not practical or possible, external localization is applied. Typical external localizers are electromechanical, optical, electromagnetic, or ultrasonic, each with different pros and cons [20]. In some cases, optical lasers are used for indirect registration. For example, in EBRT setup, carefully calibrated laser lines mark the linac's isocenter. On typical CT and MRI scanners, transverse and parasagittal laser planes are available to align the patient and surgical tools. Lasers are usually used with bare eyesight or in combination with computational methods (e.g., [7], [19].)

Registration error analysis and prediction of the distribution of error over the region of interest have sizable literature to aid the developer in placing fiducials and tracking devices in the surgical scene. Generally, we are concerned with three metrics of registration performance: accuracy, consistency, and robustness, and, they are often at odds with one another. It may be counterintuitive but nonetheless true that accuracy is the least important of the three. Generally, surgeons can compensate for inaccuracies as long as the registration is robust and the error is consistent.

Surgical Augmentation Techniques

Robotic Assistant Devices

The mechanical design of a surgical CAD-CAM robot depends crucially on its intended application. (A comprehensive review of design principles and the state of the art is available in [23] and [24].) For example, robots with high precision, stiffness, and (possibly) limited dexterity are often suitable for orthopedic bone shaping or stereotactic needle placement, and medical robots have been developed for these applications (e.g., [16], [11], [21]). Other robots for needle placement surgeries in soft tissues require compactness, dexterity, and responsiveness. These systems (e.g., [4], [6], [17]) frequently have relatively high-speed, low-stiffness, and highly backdrivable mechanisms. Many medical robots (e.g., [9], [11]) were essentially modified industrial robots. This approach has many advantages, including low cost, high reliability, and shortened development times. If suitable modifications are made to ensure safety and sterility, such systems can be very successful clinically, and they can also be invaluable for rapid prototyping for research use. However, the specialized requirements of surgical applications have tended to encourage more specialized designs. One example is mechanically constrained motion of the surgical tool to rotate about a remote center of motion (RCM) distal to the robot's structure. In surgery, the robot is positioned so that the RCM point coincides with the entry point into the patient's body. This approach has been used by numerous research groups, using a variety of kinematic designs (e.g., [4]). Although most surgical robots are mounted to the surgical table, to the operating room ceiling, or to the floor, there has been some interest in developing systems that directly attach to the patient (e.g., [3], [21], [22], [29]), so the robot is stationary if the patient moves. Mechatronic and robotic systems intended for use in specific imaging environments pose additional design challenges. First, there is the geometric constraint that the robot (or at least its

end effector) must fit within the scanner along with the patient. Second, the robot's mechanical structure and actuators must not interfere with the image formation process, and the constraints for MRI are especially difficult (e.g., some examples in [4]). A perennially difficult issue is mounting robots inside imaging scanners. Standard clinical equipment is not designed to receive auxiliary structures, and their physical modification annuls the warranty. The most severe restrictions apply to the X-ray imagers with which integration of any sort is specifically forbidden.

Passive and Semiautonomous Devices for Needle Placement

A few researchers have proposed the use of passive, encoded manipulator arms for image-guided needle placement. After a registration step, these systems track the position and orientation of a passive needle guide and display the corresponding needle path in real time on CT or MR images. Semiautonomous systems allow remote, interactive image-guided placement of the biopsy tool. For example, Krieger et al. performed transrectal prostate interventions in a closed MRI environment [13]. The device is driven from outside the bore with torsion cables, while the needle driver is tracked in the MRI system with active coils and monitored using an interactive graphical interface.

Freehand Surgical Navigation Systems

In tracked surgical navigation systems, the positions of instruments relative to the reference markers on the patient are tracked using specialized electromechanical, optical, electromagnetic, or sonic digitizers or by more general computer vision techniques [20]. After the relationships among the key coordinate systems (patient anatomy, images, surgical tools, etc.) are determined through a registration process (explained previously), a computer workstation provides graphical feedback to the surgeon to assist in performing the planned task, usually by displaying the instrument positions relative to medical images. The main advantages of tracked surgical navigation systems are their versatility, their relative simplicity, and their ability to exploit the surgeon's natural dexterity and haptic sensitivity. Surgical navigation systems are achieving increasing acceptance in such fields as neurosurgery; ear, nose, and throat surgery; and orthopedics.

External tracking is superfluous in applications such as in most CT- or MRI-guided superficial needle placements (e.g., spinal nerve blocks and facet joint injections), where skin markers are used to locate the exact entry point, the scanner's alignment laser is used to control needle direction, and markers on the needle are used to control depth. In fluoroscopy, the typical procedure is to align the X-ray system so that it looks directly along the desired needle path, place the needle and stand it up so that its X-ray image is a dot, turn the X-ray system to look from the side, and insert the needle until it reaches the target. In US imaging, the primary reliance is on surgeon experience or the use of a needle guide attached to the probe in the plane of imaging. A variety of handheld mechanical guides have been tried out for use with all common image modalities. Computer-aimed laser guidance and augmented reality optical systems (e.g., [7]) have also been also proposed.

Adaptive Surgical CAD-CAM

Patient and Tool Tracking

Few issues are more important than tracking the anatomical target and surgical tool relative to one another, but this problem is still largely unsolved. Most current imaging modalities, except fluoroscopy, were originally designed for diagnostic imaging and thus are suboptimal for tracking the surgical tools and the anatomy. First, real-time image feedback is seldom available. With X-ray modalities, real-time imaging is not practical because of high doses. Commercial MRI installations do not allow sending imaging requests to the scanner, other than manual commands from the operator console. (Companies sometimes offer privileged access to research groups to the MRI scanner's internal application programming interface under research agreement.) Recently, open-architecture US scanners have appeared, permitting unfettered access to the beam former, thereby opening the way for real-time quantitative image guidance. For the first time, RF US image data can be utilized in the analysis of spectra and biological tissue speckle. Thus, in most applications, we are relegated to intermittent imaging and suffer from the fact that between two snapshots the anatomy and tool may have moved beyond the capture range of tracking. For example, target tracking has been a fundamental problem in EBRT delivery, where onboard X-ray imagers cannot show soft tissues, so surrogates are applied. One method is to implant radiopaque markers in the target and track those using X-ray image. One of the new exciting techniques is implanting active radar beacons (Calypso system by Calypso Medical Systems, Seattle, WA), which broadcasts a live homing signal for the couch controller to reposition the patient under the beam. On the negative side, implanted markers need some degree of surgery to get into the body in the first place, but this may be affordable in EBRT where regimens are spread into 25–40 fractions over several weeks. As a noninvasive option in EBRT, US imager can augment the linac's onboard X-ray imagers, but unfortunately therapists are usually not sufficiently trained in the acquisition and interpretation of US images. Other noninvasive methods include tracking of skin fiducials with optical localizers and various forms of respiratory gating, which are generally helpful but not quite accurate or reliable. In lieu of true image-based tracking, one must resort to surrogates. Surgical tools are often tracked externally (with optical or electromagnetic sensors), from which the tool tip can be predicted with reasonable accuracy, and some researchers track the tool tip with in-built electromagnetic sensors. Driven by the specific needs of image-guided surgery, some manufacturers started offering real-time tracking devices for navigation inside MRI scanners (e.g., EndoScout by Robin Medical, Inc.). In summary, intraoperative patient and tool tracking, combined with controlling the treatment delivery mechanisms (robots), is a problem-rich research area in which major breakthroughs are needed.

Tool Steering

Needles are widely used in surgical CAD-CAM procedures (see the "Percutaneous Needle-Based Interventions" section). Although classic needles have the advantage of being very minimally invasive, they have two major problems: 1) they

may deviate slightly from the desired path and thus miss the target and 2) they cannot reach targets inaccessible by straight (or close to straight) paths. Surgeons and interventional radiologists have long known that needles could be steered by hand, but methods for optimizing this technique have only recently been developed. New results in needle and tissue modeling, robot motion planning, and image-based control, as well as the design of specialized devices, have enabled steering of needles inside soft tissue, which improves targeting accuracy and avoids delicate areas or impenetrable anatomic structures.

There are two primary methods for steering needles: using the needle to manipulate the tissue and using the tissue to manipulate the needle. In the former method, significant forces are applied to the base of needles that are stiff relative to the tissue. This causes the tissue to deform, so that the needle's insertion direction is changed relative to obstacles or targets within the tissue (e.g., [5], [8]). In the latter method, needles have a lower structural stiffness than that of the tissue, and an asymmetric bevel tip or prebent tip causes the needle to bend when it is inserted into tissue. By pushing the needle forward from the outside and spinning it around its main axis, a robot can control the needle to acquire targets in a 3-D space with minimal trauma to the tissue, while avoiding obstacles as shown in Figure 5 (e.g., [18], [28]). In both methods, path planning should be used to determine the optimal insertion point and the sequence of the forces and torques (or velocities) applied to the needle base to both reach the target and avoid any obstacles along the way. The plan can be updated as the procedure progresses. The actual needle path for a given set of inputs is highly dependent on the tissue and needle properties, as well as the mechanics of their interaction [1]. Since patient-specific tissue models are difficult to acquire, real-time image-based control is essential to achieve the desired paths.

Process Monitoring and Plan Optimization

There are hardly any surgical CAD-CAM applications, except perhaps intracranial EBRT and some orthopedic surgeries, where the target anatomy is guaranteed not to deform or change between planning and execution. As the surgery progresses, deviations from the original plan are inevitable. As a result, certain aspects of the surgical plan, such as target location, tool trajectory, or therapeutic dose, need reoptimization before and/or during surgery. Some trivially occurring problems are patient motion, tissue deformation, and target dislocation, the detection and tracking of which we discussed in the previous section. In the simplest cases, such as biopsies, the surgical plan is essentially an ordered list of targets and preferred tool trajectories, and these can be more or less automatically updated if the target and tool are tracked (which, as we saw, is a significant problem in itself). The situation is more complicated when the clinical goal is to deliver some therapeutic dose over a prescribed target volume, such as radioactive seeds in the prostate or thermal dose to ablate a liver or kidney tumor. Here, the spatial and temporal accumulation of dose must be monitored and the plan reoptimized accordingly. This, in turn, increases the demand for sensitive, accurate, and fast intraoperative imaging techniques, as well as smart surgical instruments that incorporate physiological biosensors in the tooltip. Some current imaging modalities are capable of biological process monitoring, e.g., MRI can visualize tissue temperature [12] and both MRI and US imaging can show changes in tissue elasticity, but the present signal methodologies are not nearly sufficient to make use of these capabilities. Often, multiple spatially and temporally coregistered imaging modalities are needed for guiding and monitoring the surgery. For example, in prostate brachytherapy, a TRUS scanner visualizes the prostate, and a fluoroscope can show the implanted seeds [10]. Such a scenario, however, complicates the clinical workflow and increases procedure time and costs.

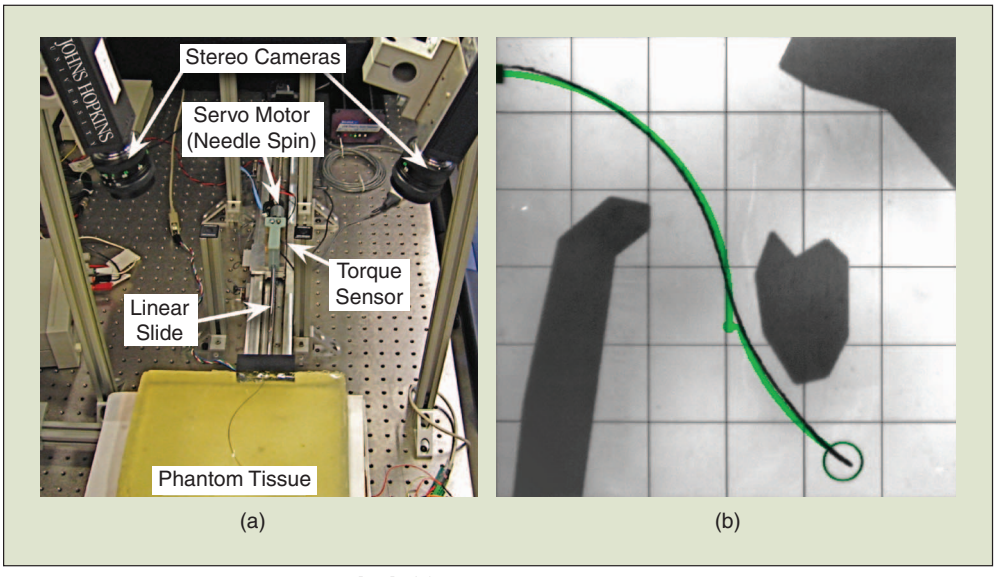

Figure 5. *Robotic needle steering [28]. (a) The vision-guided robot can work autonomously or teleoperated. (b) The needle (thin black line) follows planned trajectory (colored line) around obstacles in transparent artificial tissue. [Images courtesy of Kyle Reed, Robert Webster, Vinutha Kallem, Gregory Chirikjian, Allison Okamura, and Noah Cowan (Johns Hopkins University) and Ron Alterovitz and Ken Goldberg (University of California, Berkeley).]*

Future Directions

Regarding surgical CAM, the phase that most closely relates to robotics, a number of areas of future research can be identified.

- Highly dexterous and compact surgical robots that carry the surgical device inside the fields of intraoperative imaging devices, which need to be multipurpose, independent of imagers, and deployable in various clinical applications with minimum adjustment

- Robust registration and tracking of the surgical robot to the medical imager and the patient
- Steering and more dexterous manipulation of the tooltip based on imaging feedback to account for motion and tissue deformation
- Real-time target tracking and stabilization of instruments
- Smart end effectors combined with biosensors to detect biomechanical (stiffness), physiological (bleeding, edema, oxygenation), and morphological/pathological characteristics of tissues around the tooltip
- Building medical imaging devices with the resolution and accuracy of control required for interactions in the millimeter range and ultimately in the submillimeter range.

Effective surgical CAM requires that we integrate imaging and tracking devices into the robotic end effectors or surgical tools themselves to physically couple image and device coordinate frames, thus eliminating the traditionally greatest source of inaccuracy and operational hazard. The ultimate goal is local imaging, local guidance, and local actuation, all in one device.

As the capabilities of systems continue to evolve, the use of computer systems to model dynamically changing patient-specific anatomy will become more important. A diverse research community in medical image computing is addressing a broad range of research topics, including the creation of patient-specific models from medical images, techniques for updating these models based upon real-time image and other sensor data, and the use of these models for planning and monitoring of surgical procedures. As computing power and in-room imaging techniques improve, the planning and action come closer to each other, transforming the classic sequential paradigm to adaptive surgical CAD-CAM.

Acknowledgments

The authors gratefully acknowledge the National Science Foundation for supporting our work in this field through the Engineering Research Center for Computer-Integrated Surgical Systems and Technology (CISST ERC) Grant NSF EEC 9731748. Related projects have also been supported by Johns Hopkins University, the National Institutes of Health, the Whitaker Foundation, the Department of Defense, and industrial affiliates of the CISST ERC.

Keywords

Medical robotics, image-guided surgery.

References

[1] N. Abolhassani, R. Patel, and M. Moallem, "Needle insertion into soft tissue: A survey," *Med. Eng. Phys.*, vol. 29, no. 4, pp. 413–431, 2007.

[2] R. A. Brown, T. S. Roberts, and A. G. Osborne, "Stereotaxic frame and computer software for CT-directed neurosurgical localization," *Invest. Radiol.*, vol. 15, no. 4, pp. 308–312, 1980.

[3] J. H. Chung, S. Y. Ko, D. S. Kwon, J. J. Lee, Y. S. Yoon, and C. H. Won, "Robot-assisted femoral stem implantation using an intramedulla gauge," *IEEE Trans Robot. Automat.*, vol. 19, no. 5, pp. 885–892, Oct. 2003.

[4] K. Cleary, A. Melzer, V. Watson, G. Kronreif, and D. Stoianovici, "Interventional robotic systems: applications and technology state-of-the-art," *Minim. Invasive Ther. Allied Technol.*, vol. 15, no. 2, pp. 101–113, 2006.

[5] S. P. DiMaio and S. E. Salcudean, "Needle steering and motion planning in soft tissues," *IEEE Trans. Biomed. Eng.*, vol. 52, no. 6, pp. 965–974, June 2005.

[6] G. Fichtinger, J. Fiene, C. Kennedy, I. Iordachita, G. Kronreif, D. Y. Song, E. C. Burdette, and P. Kazanzides, "Robotic assistance for ultrasound guided prostate brachytherapy," *Med. Image Anal.*, to be published.

[7] G. S. Fischer, A. Deguet, D. Schlattman, L. Fayad, S. J. Zinreich, R. H. Taylor, and G. Fichtinger, "Image overlay guidance for MRI arthrography needle insertion," *Comput. Aided Surg.*, vol. 12, no. 1, pp. 2–14, Jan. 2007.

[8] D. Glozman and M. Shoham, "Image-guided robotic flexible needle steering," *IEEE Trans. Robot.*, vol. 23, no. 3, pp. 459–467, June 2007.

[9] W. Hara, S. G. Soltys, and I. C. Gibbs, "CyberKnife robotic radiosurgery system for tumor treatment," *Expert Rev. Anticancer Ther.*, vol. 7, no. 11, pp. 1507–1515, Nov. 2007.

[10] A. Jain, A. Deguet, I. Iordachita, G. Chintalapani, J. Blevins, Y. Le, E. Armour, C. Burdette, D. Song, and G. Fichtinger, "Intra-operative 3D guidance in prostate brachytherapy using a non-isocentric C-arm," *Med. Image Comput. Comput. Assist. Interv. Int. Conf. Med. Image Comput. Comput. Assist. Interv.*, vol. 10, pt. 2, pp. 9–17, 2007.

[11] M. Jakopec, S. J. Harris, F. R. y. Baena, P. Gomes, J. Cobb, and B. L. Davies, "The first clinical application of a hands-on robotic knee surgery system," *Comput. Aided Surg.*, vol. 6, no. 6, pp. 329–339, 2001.

[12] F. A. Jolesz and N. McDannold, "Current status and future potential of MRI-guided focused ultrasound surgery," *J. Magn. Reson. Imaging*, vol. 27, no. 2, pp. 391–399, Feb. 2008.

[13] A. Krieger, R. C. Susil, C. Menard, J. A. Coleman, G. Fichtinger, E. Atalar, and L. L. Whitcomb, "Design of a novel MRI compatible manipulator for image guided prostate intervention," *IEEE Trans. Biomed. Eng.*, vol. 52, no. 2, pp. 306–313, Feb. 2005.

[14] Y. S. Kwoh, J. Hou, E. A. Jonckheere, and S. Hayati, "A robot with improved absolute positioning accuracy for CT guided stereotactic brain surgery," *IEEE Trans. Biomed. Eng.*, vol. 35, no. 2, pp. 153–161, 1988.

[15] N. G. Leveson and C. S. Turner, "An investigation of the Therac-25 accidents," *IEEE Computer*, vol. 26, no. 7, pp. 18–41, July 1993.

[16] Q. Li, L. Zamorano, A. Pandya, R. Perez, J. Gong, and F. Diaz, "The application accuracy of the NeuroMate robot—A quantitative comparison with frameless and frame-based surgical localization systems," *Comput. Assist. Surg.*, vol. 7, no. 2, pp. 90–98, 2002.

[17] K. Masamune, G. Fichtinger, A. Patriciu, R. C. Susil, R. H. Taylor, L. R. Kavoussi, J. H. Anderson, I. Sakuma, T. Dohi, and D. Stoianovici, "System for robotically assisted percutaneous procedures with computed tomography guidance," *J. Comput. Aided Surg.*, vol. 6, no. 6, pp. 370–383, 2001.

[18] S. Okazawa, R. Ebrahimi, J. Chuang, S. E. Salcudean, and R. Rohling, "Hand-held steerable needle device," *IEEE/ASME Trans. Mechatron.*, vol. 10, no. 3, pp. 285–296, June 2005.

[19] A. Patriciu, S.B. Solomon, L.R. Kavoussi, and D. Stoianovici, "Robotic kidney and spine percutaneous procedures using a new laser-based CT registration method," in *Proc. MICCAI 2001*, pp. 249–257.

[20] T. Peters and K. R. Cleary, *Image-Guided Interventions: Technology and Applications*. Berlin: Springer-Verlag, 2008.

[21] C. Plaskos, P. Cinquin, S. Lavallee, and A. J. Hodgson, "Praxiteles: A miniature bone-mounted robot for minimal access total knee arthroplasty," *Int. J. Med. Robot. Comput. Assist. Surg.*, vol. 1, no. 4, pp. 67–79, 2005.

[22] M. Shoham, M. Burman, E. Zehavi, L. Joskowicz, E. Batkilin, and Y. Kunicher, "Bone-mounted miniature robot for surgical procedures: Concept and clinical applications," *IEEE Trans. Robot. Automat.*, vol. 19, no. 5, pp. 893–901, 2003.

[23] R. H. Taylor, A. Menciassi, G. Fichtinger, and P. Dario, "Medical robots and systems," *Springer Handbook of Robotics*, B. Siciliano and O. Khatib, Eds. Berlin: Springer-Verlag, 2008, ch. 52.

[24] R. H. Taylor and D. Stoianovici, "Medical robotics in computer-integrated surgery," *IEEE Trans. Robot. Automat.*, vol. 19, no. 5, pp. 765–781, 2003.

[25] R. H. Taylor, H. A. Paul, P. Kazanzides, B. D. Mittelstadt, W. Hanson, J. F. Zuhars, B. Williamson, B. L. Musits, E. Glassman, and W. L. Bargar,

"An image-directed robotic system for precise orthopaedic surgery," *IEEE Trans. Robot. Automat.*, vol. 10, no. 3, pp. 261–275, 1994.
[26] K. Wallner, J. C. Blasko, and M. Dattoli, *Prostate Brachytherapy Made Complicated*, 2nd ed. Seattle, WA: SmartMedicine, 2001.
[27] E. Watanabe, T. Watanabe, S. Manka, Y. Mayanagi, and K. Takakura, "Three-dimensional digitizer (neuronavigator): New equipment for computed tomography-guided stereotaxic surgery," *Surg. Neurol.*, vol. 27, no. 6, pp. 543–547, 1987.
[28] R. J. Webster, III, J. S. Kim, N. J. Cowan, G. S. Chirikjian, and A. M. Okamura, "Nonholonomic modeling of needle steering," *Int. J. Robot. Res.*, vol. 25, no. 5–6, pp. 509–525, May–June 2006.
[29] Wolf A, Jaramaz B, Lisien B, and A. M. DiGioia, "MBARS: mini bone-attached robotic system for joint arthroplasty," *Int. J. Med. Robot. Comput. Assist. Surg.*, vol. 1, no. 2, pp. 101–121, Jan. 2005.
[30] S. Xu, J. Kruecker, P. Guion, N. Glossop, Z. Neeman, P. Choyke, A. K. Singh, and B. J. Wood, "Closed-loop control in fused MR-TRUS image-guided prostate biopsy," *Med. Image Comput. Comput. Assist. Interv. Int. Conf. Med. Image Comput. Comput. Assist. Interv.*, vol. 10, pt. 1, pp. 128–135, 2007.
[31] P. Kazanzides, G. Fichtinger, G. D. Hager, A. M. Okamura, L. L. Whitcomb, and R. H. Taylor, "Surgical and interventional robotics—Core concepts, technology, and design," *IEEE Robot. Automat. Mag.*, vol. 15, no. 2, pp. 122–130, June 2008.

Peter Kazanzides received the B.S., M.S., and Ph.D. degrees in electrical engineering from Brown University in 1983, 1985, and 1988, respectively. He worked on surgical robotics in March 1989 as a postdoctoral researcher at the International Business Machines (IBM) T.J. Watson Research Center. He cofounded Integrated Surgical Systems (ISS) in November 1990 to commercialize the robotic hip replacement research performed at IBM and the University of California, Davis. As the director of robotics and software, he was responsible for the design, implementation, validation and support of the ROBODOC System. He joined the Engineering Research Center for Computer-Integrated Surgical Systems and Technology (CISST ERC) in December 2002, and currently, he is an assistant research professor of computer science at Johns Hopkins University.

Gabor Fichtinger received his B.S. and M.S. degrees in electrical engineering and his Ph.D. degree in computer science from the Technical University of Budapest, Hungary, in 1986, 1988, and 1990, respectively. He has developed image-guided surgical interventional systems. He specializes in robot-assisted image-guided needle-placement procedures, primarily for cancer diagnosis and therapy. He is an associate professor of computer science, electrical engineering, mechanical engineering, and surgery at Queen's University, Canada, with adjunct appointments at the Johns Hopkins University.

Gregory D. Hager is a professor of computer science at Johns Hopkins University. He received the B.A. degree, summa cum laude, in computer science and mathematics from Luther College, in 1983, and the M.S. and Ph.D. degrees in computer science from the University of Pennsylvania in 1985 and 1988, respectively. From 1988 to 1990, he was a Fulbright junior research fellow at the University of Karlsruhe and the Fraunhofer Institute IITB in Karlsruhe, Germany. From 1991 to 1999, he was with the Computer Science Department at Yale University. In 1999, he joined the Computer Science Department at Johns Hopkins University, where he is the deputy director of the Center for Computer Integrated Surgical Systems and Technology. He has authored more than 180 research articles and books in the area of robotics and computer vision. His current research interests include visual tracking, vision-based control, medical robotics, and human-computer interaction. He is a Fellow of the IEEE.

Allison M. Okamura received the B.S. degree from the University of California at Berkeley, in 1994, and the M.S. and Ph.D. degrees from Stanford University in 1996 and 2000, respectively, all in mechanical engineering. She is currently an associate professor of mechanical engineering and the Decker Faculty Scholar at Johns Hopkins University. She is the associate director of the Laboratory for Computational Sensing and Robotics and a thrust leader of the National Science Foundation Engineering Research Center for Computer-Integrated Surgical Systems and Technology. Her awards include the 2005 IEEE Robotics Automation Society Early Academic Career Award, the 2004 National Science Foundation Career Award, the 2004 Johns Hopkins University George E. Owen Teaching Award, and the 2003 Johns Hopkins University Diversity Recognition Award. Her research interests include haptics, teleoperation, medical robotics, virtual environments and simulators, prosthetics, rehabilitation engineering, and engineering education.

Louis L. Whitcomb completed his B.S. and Ph.D. degrees at Yale University in 1984 and 1992, respectively. His research focuses on the design, dynamics, navigation, and control of robot systems. He has numerous patents in the field of robotics, and he is a Senior Member of the IEEE. He is the founding director of the Johns Hopkins University Laboratory for Computational Sensing and Robotics. He is a professor at the Department of Mechanical Engineering, with joint appointment in the Department of Computer Science, at the Johns Hopkins University.

Russell H. Taylor received his Ph.D. degree in computer science from Stanford in 1976. He joined IBM Research in 1976, where he developed the AML robot language and managed the Automation Technology Department and (later) the Computer-Assisted Surgery Group before moving in 1995 to Johns Hopkins University, where he is a professor of computer science, with joint appointments in mechanical engineering, radiology and surgery. He is the Director of the NSF Engineering Research Center for Computer-Integrated Surgical Systems and Technology. He is the author of more than 200 refereed publications. He is a Fellow of the IEEE and AIMBE and is a recipient of the Maurice Müller award for excellence in computer-assisted orthopedic surgery.

Address for Correspondence: Peter Kazanzides, Department of Computer Science, CSEB 120, Johns Hopkins University, 3400 North Charles Street, Baltimore, MD, 21218, USA. E-mail: pkaz@jhu.edu.

ICRA2009

2009 IEEE International Conference
on Robotics and Automation
Kobe, Japan, May 12-17, 2009

IEEE
Celebrating 125 Years
of Engineering the Future

SCIENCE COUNCIL OF JAPAN

JSME SICE

Call for Participation

The 2009 IEEE International Conference on Robotics and Automation (ICRA2009) will be held in Kobe, Japan, during May 12 - 17, 2009. The theme of the conference is "**Robotics and IRT for Livable Societies**", reflecting the ever growing interests in research, development and applications in the dynamic and exciting areas of robotics and automation. Kobe is a fascinating city, and its attractions include one of the largest ports in the world, the beautiful natural setting of the Rokko Mountains and picturesque streets. Located in the central part of the Japanese archipelago, Kobe is 30 minutes from Kyoto and three hours from Tokyo by Shinkansen (the super express train).

We invite participation in the conference by researchers and engineers in all areas of robotics and automation. ICRA2009 will feature plenary speakers, invited sessions, strong technical sessions, a diverse array of workshops and tutorials, a robot challenge, student events, science/industrial forums, exhibits and social functions. For details, please visit the conference website.

Sponsors:
The IEEE Robotics and Automation Society
The Science Council of Japan

Technical Co-Sponsors:
The Japan Society of Mechanical Engineers
The Robotics Society of Japan
The Society of Instrument and Control

www.icra2009.org

Contact E-mail:
info@icra2009.org

Organizing Committee Chair
Fumio Harashima (Tokyo Denki Univ.)

General Chair
Kazuhiro Kosuge (Tohoku Univ.)

Program Chair
Katsushi Ikeuchi (Univ. Tokyo)

Program Co-Chairs
Kevin Lynch (Northwestern Univ.)
Raja Chatila (LAAS-CNRS)
Shigeki Sugano (Waseda Univ.)

Tutorials and Workshops Chairs
Yoky Matsuoka (Univ. Washington)
Cecilia Laschi (Scuola Superiore Sant'Anna)
Makoto Kaneko (Osaka Univ.)

Videos Chair
Peter Corke (CSIRO)

Science/Industry Forum Chairs
Hajime Asama (Univ. Tokyo)
Oussama Khatib (Stanford Univ.)
Ruediger Dillmann (Univ. Karlsruhe)

Publication Chairs
C. S. George Lee (Purdue Univ.)
Kazuhito Yokoi (AIST)
Zhidong Wang (Chiba Inst. Tech.)

Awards Chair
John M. Hollerbach (Univ. Utah)

Publicity Chairs
Hideki Hashimoto (Univ. Tokyo)
Ning Xi (Michigan State Univ.)
Max Meng (Chinese Univ. Hong Kong)

E-media Chair
Kenji Suzuki (Univ. Tsukuba)

Exhibitions Chairs
Tatsuo Arai (Osaka Univ.)
Frank Park (Seoul National Univ.)
Bill Smart (Washington Univ. in St.Louis)

Social Activities Chair
Zhi-wei Luo (Kobe Univ.)

Technical Visit Chair
Yasushi Yagi (Osaka Univ.)

Finance Chairs
Hiromi Mochiyama (Univ. Tsukuba)
Xiaoping Yun (Naval Postgraduate School)

Local Arrangement Chairs
Satoshi Tadokoro (Tohoku Univ.)
Koichi Osuka (Kobe Univ.)

Secretaries
Yasushi Nakauchi (Univ. Tsukuba)
Yasuhisa Hirata (Tohoku Univ.)

Digital Object Identifier 10.1109/MRA.2008.929823

IERA Forum and Award

The International Federation of Robotics (IFR)/IEEE Innovation and Entrepreneurship Forum was held on 11 June 2008 in Munich, Germany. It is cosponsored by the IEEE Robotics and Automation Society (RAS) and the IFR, whose members include robotics and automation manufacturers and suppliers and institutional members. The 2008 forum was hosted by the IFR in conjunction with Robotik 2008, Germany's largest robotics conference and exhibition, and Automatica 2008. The program comprised a workshop for entrepreneurs, which included talks by Bruno Siciliano of the Prisma Lab at the University of Naples, who discussed examples of successful collaborations between the university researchers and businesses, and by A. J. N. (Albert) van Breemen, founder of www.PersonalRobotics.nl, who spoke on the future of personal robotics.

The afternoon session featured presentations by the five finalists of the IFR/IEEE Invention and Entrepreneurship in Robotics and Automation (IERA) Award. Two teams were chosen as corecipients of the 2008 award.

- Mick Mountz and Pete Wurman of Kiva Systems (www.kivasystems.com), Woburn, Massachusetts, and Raffaello D'Andrea of ETH-Zurich and an engineering fellow of Kiva Systems were honored for their development of the Kiva Mobile Fulfillment System, in which pallets, cases, and orders are stored on inventory pods that are picked up and moved by a fleet of mobile robotic drive units to any operator on the factory floor.
- Thomas Brandstetter, Dieter Steegmüller, and Michael Zürn, all at Mercedes-Benz Cars, Stuttgart, Germany, were honored for their role in the development of the Assembly21: Innovative system and assembly concept for rear axle assembly for the new C-Class with cooperating robot teams.

"The winners (Kiva and Assembly21) were selected from different points of view. Kiva is really a start-up by a few persons and reached good business within just a few years, very much in line with the intention of the award," said Klas Nilsson, IERA Award cochair. "The Assembly21 at Daimler is an industrial and a very impressive system including 40 robots working together, with human operations included in the total work flow. Such innovations and the initiative to convince the top management in a big company (to put in the resources needed) is a very good example of outstanding or valuable results. In total, both winners (and the other finalist) very well represent and promote innovative robotics."

Other finalists were Rune Klausen Larsen and Ivar Balslev of Scape Technologies A/S, Odense C, Denmark: The Scape Bin-Picker; Elliot Duff of CSIRO-ICT, Australia: MINEGEMTM—An autonomous underground loader; and Joachim Melis and Matt Bjork of Adept Technology, Livermore, California: The Adept Quattro s650 Robot.

Information about all the finalists is available on the RAS Industrial Activities Board Web site www.ieee-ras.org/industrial.

Role of RAS in the 2008 UN Humanitarian Technology Challenge

Under the leadership of Gianmarco Veruggio, an informal group of volunteers has been established to lead the RAS volunteers with the other IEEE societies in a multiyear, joint project with the UN Foundation, called the Humanitarian Technology Challenge (HTC).

The HTC's objective is to bring together humanitarian organizations, first responders, experts, engineers, researchers, and educators to apply technology to address some critical world problems.

The project is based on selecting and thoroughly defining a set of humanitarian problems that would benefit from a technological solution, organizing a wide-scale solicitation of technology ideas to address them, working with nongovernmental organizations that would have responsibility for

From left: Dr. Michael Zürn, Daimler; Prof. Dr. Bruno Siciliano, IEEE-RAS president; Stefan Müller, IFR president; and Prof. Dr. Raffaello D'Andrea, Kiva Systems and ETH Zurich.

Digital Object Identifier 10.1109/MRA.2008.929194

applications of the solutions, and monitoring and, possibly, facilitating solution development and eventual implementation. Participation in the project will be worldwide, with a mixture of both personal interactions and Web-based interactions.

As Veruggio noted in a letter to the volunteers, "Since RAS already includes some sectors in the field of humanitarian technology (medical robotics, search and rescue, demining, telerobotics, etc.), it is important to give them the right visibility in the HTC."

Charter members of the RAS HTC committee include Gianmarco Veruggio, Robin R. Murphy, Maja J. Mataric, Ashley W. Stroupe, Surya P. N. Singh, Jorge Miranda Dias, Cristian Secchi, Machiel Van der Loos, Eugenio Guglielmelli, Shigeo Hirose, Jorge Solis, and Carol Reiley. The group has made a strong start and welcomes additional volunteers. See http://wiki.ieee-ras.org/tab:htc_activities_wiki_page for detailed information on activities to date and ongoing tasks.

Elsevier Adds IEEE-TASE and IEEE-CASE to Ei Compendex

The IEEE International Conference on Automation Science and Engineering 2006 (CASE 2006) and CASE 2007 have recently been indexed by Elsevier in preparation for inclusion in their online product, Engineering Index (Ei) Compendex. Although it has been indexed, the data are put through QA testing before they are uploaded; therefore, it will take approximately 4–6 weeks before they will be viewable in this product.

Since 2005, Elsevier has been receiving all IEEE conference titles for inclusion in its many databases, including Ei and Ei Compendex.

The arrangement between the IEEE and the Elsevier is that IEEE provides the conference content, but Elsevier retains the right to select content for inclusion to Ei/Compendex. Only Elsevier can issue a confirmation about content inclusion in the Ei/Compendex.

22nd IEEE International Conference on Micro Electro Mechanical Systems

MEMS 2009 Sorrento, Italy

25-29 JANUARY 2009 • HILTON SORRENTO PALACE

CONFERENCE CO-CHAIRS

Christofer Hierold
ETH Zürich, SWITZERLAND

Pasqualina M. Sarro
Delft University of Technology, THE NETHERLANDS

TOPICS

- Fabrication and Packaging Technologies
- Materials and Device Characterization
- Design, Simulation, and Theoretical Concepts with Experimental Verification
- Mechanical Sensors and Systems
- Physical MEMS
- RF MEMS
- Biomedical and Chemical Micro Sensors and Systems
- Micro-Fluidic Components and Systems
- Micro-Actuators
- Energy and Power MEMS
- Nano-Electro-Mechanical Devices and Systems

REGISTRATION DEADLINES

EARLY BIRD
15 October 2008

Advanced
16 October 2008 to 30 November 2008

Standard
1 December 2008 to 12 January 2009

On-Site After
12 January 2009

The MEMS Conference series began in 1987 and since 1999 it has been known as the IEEE International Conference on Micro Electro Mechanical Systems. Reflecting the rapid proliferation of microsytems in all venues of life due to the commitment and success of the research community, the MEMS Conference series has evolved into the premier annual event reporting research results on every aspect of microsystems technology. In recent years, it has attracted more than 800 participants, 750+ abstract submissions and has presented over 200 select papers in non-overlapping podium and poster/oral sessions. Its single-session format provides ample opportunity for interaction between attendees, presenters and exhibitors. The 22nd IEEE International Conference on Micro Electro Mechanical Systems (MEMS 2009) will be held in Sorrento, Italy on 25-29 January 2009 at the Hilton Sorrento Palace.

The city of Sorrento appears suddenly, just after the bend of Scutolo Point, on the road which takes you from Naples to the Amalfi Coast. The appearance is beautiful and yet dramatic, with rock peaks falling into the sea and with a breathtaking landscape. The town seems suspended between the blue sky and blue crystal clear sea. The legend tells that in the waters of Sorrento, the mythical Mermaids tempted Ulysses with an enchanting song, and when he refused to listen to the mermaids they decided to turn into rocks. Today, the rocks are called the Galli Islands. Visit nearby Sorrento attractions - from the coast of Capri to the culture of Pompeii, just 15 miles away.

Pre and Post-Conference tour options are outlined on the Conference web-site.

Unwind and enjoy the Hilton Sorrento Palace overlooking the Bay of Naples. A one hour drive from Naples Airport, this Sorrento hotel is a 10 minute walk from the beach and town centre. Stretch out in one of the hotel's terrace sunbeds, dive into the Roman-themed indoor swimming pool or enjoy a cocktail at Pagoda Bar and glimpse Mount Vesuvius in the distance.

www.mems2009.org

SPONSORED BY IEEE ROBOTICS AND AUTOMATION SOCIETY

The Fifth EURON/EUnited Robotics Technology Transfer Award

By Martin Hægele and Kostas Kyriopolis

The European Robotics Research Network (EURON) and the European Robotics Association EUnited Robotics have now for the fifth time presented their joint Technology Transfer Award in the recognition of outstanding achievements in the European robot technology. At their annual meeting in Prague on 28 March, the first prize was awarded to Nicola Canelli and Giancarlo Teti from the Italian startup company RoboTech for its successful I-Droid 01 robotic kit. More than 100,000 units of this small humanoid robot have been sold worldwide in the form of collect-and-build kits available in around 90 consecutive issues from newspaper kiosks.

The second prize was awarded to Nicola Tomatis, from the Swiss-based startup company BlueBotics, for autonomous navigation technology (ANT), a modular system to provide autonomous navigation to a large spectrum of unmanned vehicles such as automatic forklifts in logistics, mobile service robots, and self-propelled wheelchairs. Members of a Swedish consortium that joined forces to develop a robotic, force-controlled drilling tool were awarded the third prize. This tool is the basis for fully automated, high-accuracy, and cost-effective drilling for a variety of products ranging from aircraft to automotive. Tomatis was also the corecipient of the IEEE Robotics and Automation Society (RAS) 2008 Early Industry/Government Career Award.

The I-Droid 01 robot is a small robot for education and entertainment with an anthropomorphic appearance. It is composed of numerous parts such as a wheeled base, two arms with grippers, and visual and auditory sensory systems with speech and image recognition capabilities. Each issue contains robot components and a magazine with articles on robotics as well as instructions for assembling and programming the I-Droid 01.

The autonomous navigation suite from BlueBotics had its origin at the Swiss Federal Institute of Technology, Lausanne. The company faced its first technological challenge in 2002 with the successful development and implementation of 11 tour guide robots at the Swiss national exhibition Expo.02. Their current navigation suite ANT is a complete package for autonomous navigation solutions in indoor environments. Other robots equipped with ANT include mobile robots as diverse as machines from Nespresso, which freely navigate in buildings or autonomous 2-t forklifts.

SAAB Aerostructures has been pioneering the use of the novel robotic tool for drilling flexible airframe skin panels. The development successfully eliminated the sliding movement or skating of the tool, which usually results from the low mechanical stiffness of industrial robots. The presented solution is the result of a Swedish research project including ABB Robotics, a leading industrial robotic manufacturer, researchers from Lund and Linköping Universities, and DELfOi, an industrial IT solutions developer.

Digital Object Identifier 10.1109/MRA.2008.929590

"The EURON/EUnited Robotics Technology Transfer Award has firmly established itself as a permanent part of European robotics research," says Herman Bruyninckx from Katholieke Universiteit Leuven who is the technical and scientific coordinator of EURON.

The European robotics association EUnited Robotics was established in June 2004 by leading robot manufacturers and system integrators to act as a mouthpiece and platform for cooperation between all stakeholders from research institutes through national associations to end customers.

EURON sees its role as an excellence network that is aimed at advancing European research, teaching, publications, and cooperation between universities and industry in the field of robot technology and also at making Europe the world's number one in robotics.

The EURON/EUnited Robotics Technology Transfer Award is jointly presented each year by both institutions in recognition of outstanding innovations in the field of robotics and automation to promote excellence in applied research and technology transfer between research and industry. The award is financially supported by the European Community and sponsored by the EUnited Robotics members. For more information, visit http://www.euron.org/activities/techaward.html or http://www.eu-nited-robotics.net or contact Martin Hægele at haegele@pa.fhg.de.

Award winners and their jury. From left: Roland Siegwart, ETH Zurich (Switzerland), Jury member Henrik Kihlman, DELFoi (Sweden), third prize; Herman Bruyninckx, KU Leuven (Belgium), EURON coordinator and Jury member; Nicola Tomatis, BlueBotics (Switzerland), second prize; Stefan Sagert, EUnited Robotics (Belgium), Jury member; Nicola Canelli, RoboTech (Italy), first prize; Martin Hægele, Fraunhofer IPA (Germany), Jury member, organization of TechTransfer Award; Rainer Bischoff, KUKA Roboter (Germany), Jury member; Gisbert Lawitzky, Siemens (Germany), Jury member. The small robot in front is the small humanoid robot I-Droid 01, which has been sold worldwide in the form of collect-and-build kits.

2009 IEEE Conference on Automation Science and Engineering

August 22 – 25 2009, Bangalore, India
Sponsored by IEEE Robotics and Automation Society

Important Dates:
February 1, 2009:
Submission of papers, tutorials and invited/special sessions
April 30, 2009:
Paper acceptance notification
May 30, 2009:
Final paper submission due

Call for Papers

The fifth annual IEEE Conference on Automation Science and Engineering, IEEE CASE 2009, sponsored by the IEEE Robotics and Automation Society, will be held during August 22 - 25 2009 in Bangalore, India. The goal of the conference is broad coverage and dissemination of foundational research on automation among researchers, academicians and industry practitioners. The focus would be on scientific methods for machines and systems operating in structured environments over long periods, and also on the explicit structuring of environments. Special themes for the 2009 conference include: Green Technologies and Automation; Knowledge Services and Automation; Self Aware Automation; Internet Automation and Internet Search and Analytics.

CASE is an offspring of the IEEE Transactions on Automation Science and Engineering, IEEE T-ASE, (www.ieee.org/t-ase). High quality CASE papers will be recommended for publication in this flagship journal.

The technical program of IEEE CASE will consist of workshops, invited talks, posters and paper presentations. Submitted papers should describe original work in any of the following and other related areas:

- Ambient Intelligence
- Automatic Identification & Security
- Automation in Life Sciences: Biotechnology, Pharmaceutical & Health Care
- Business & Software
- Construction Automation
- Data Analytics for Automation
- Discrete Event Systems & Petri Nets
- Food Handling & Processing
  Green Technologies & Automation
- Human-Machine Interaction & Coordination
- Instrumentation & Measurement
- Intelligent Transportation
- Internet Automation
- Internet Search & Analytics
- Knowledge Services & Automation
- Laboratory Automation
- Manufacturing Automation
- Maintenance & Diagnosis
- Multi-sensor Fusion & Integration
- Micro/Nano-scale Automation & assembly
- Product Design, Development & Prototyping
- Planning, Scheduling & Coordination
- Self Aware Automation
- Semiconductor manufacturing Supply Chain Management
- System Modeling, Analysis & performance Evaluation
- Vision on Automation
- Workflow Analysis & Management

Paper Submissions: Author(s) should submit full papers electronically in double column IEEE-compliant PDF format. All papers will be peer-reviewed. Accepted papers will be published in CD-ROM. Detailed instructions for paper preparation and submission will be available on the conference web site: http:/www.ieee-case.org

Bangalore: Bangalore is currently destination number one for all global companies, especially those belonging to the IT sector. It is aptly called the Silicon Valley of India. It enjoys salubrious weather throughout the year and is known as India's air-conditioned city. It is home for India's premier research institutions including the Indian Institute of Science and numerous federal research labs.




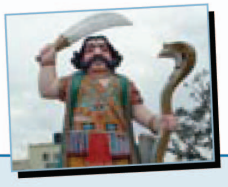


Digital Object Identifier 10.1109/MRA.2008.929905

By George A. Bekey

Springer Handbook of Robotics

Bruno Siciliano and Oussama Khatib, Editors, Springer-Verlag 2008. ISBN: 978-3-540-23957-4.

Robotics has come of age. It is now clear that it is not a passing fancy but rather that robots in one form or another are finding their way into more and more aspects of society. Robots are in the factory, in the home, on the battlefield, and many more venues, performing an incredible array of tasks, many of which were inconceivable even 20 years ago. What is perhaps even more remarkable than the enormous range of applications is that the field has grown up with a solid foundation in physics and mathematics. This may be because most robots were born in university laboratories around the world, where thousands of students enabled them to perceive, process information, learn, move, manipulate, and perform a wide range of tasks before they became sufficiently robust and reliable to become commercial products. Now, theory and applications, fundamental work in universities, and technology developed in the industry are mature enough to attempt a consolidated view of the entire field. This handbook accomplishes this task beautifully, both in style and substance.

The handbook is a very large and truly encyclopedic work, covering all aspects of robotics, from fundamental principles to applications. The book's 1,600 pages are subdivided into seven parts: Part A: Robotics Foundations, Part B: Robot Structures, Part C: Sensing and Perception, Part D: Manipulation and Interfaces, Part E: Mobile and Distributed Robotics, Part F: Field and Service Robotics, and Part G: Human-Centered and Life-Like Robotics. Each of the seven parts is subdivided into multiple chapters, all written by experts in their fields throughout the world. This reviewer tried to find aspects of robotics not treated in the book, and he failed: it is indeed a remarkably complete view of the field. The book also has four forewords by leading contributors to robotics, including Hirochika Inoue from Japan, Georges Giralt from France, and Bernard Roth and Rodney Brooks from the United States. They provide a most valuable introduction to the handbook from their perspective and experience, as all of them are among the founders of the field.

One may view the contents in another way. The first two parts provide the mathematical and physical fundamentals of robotics, including not only kinematics and dynamics and an introduction to motion planning and system architectures but also treatments of the physical elements of robots, such as mechanisms, hands, legs, and wheels. The third part deals extensively with sensors. The next two parts concern basic and applied issues in manipulation, grasping, motion planning and control, and distributed systems. Part F deals with what we might call contemporary applications, in space, under water, in agriculture, medicine, rehabilitation, and others. These are the applications that many people view as representing the significant impact of robotics on society. In Part G, these areas are supplemented by problems that still present major research challenges, including humanoid robots, human-robot interaction, neurorobotics, and a discussion of robot ethics.

This amazing book does an incredible job of balancing theory and practice throughout. It should be an immensely valuable reference for students and practitioners of robotics for many years to come.

Digital Object Identifier 10.1109/MRA.2008.928399

TC SPOTLIGHT

(continued from page 16)

The new event promoted by the IEEE Robotics and Automation Society (RAS) jointly with the EMBS, the International Conference on Biomedical Robotics and Biomechatronics (BioRob conference), which took place in Pisa, Italy, 20–22 February 2006, explicitly included a dedicated track on rehabilitation and assistive robotics, which was very successful.

Both the rehabilitation and the assistive robotics fields have already produced several commercial spin-offs, which brought to the market advanced systems that are currently being validated in extensive clinical trials worldwide.

The Rehabilitation and Assistive Robotics Technical Committee (TC) was the recipient of the RAS 2008 Most Active TC award. The committee was established in 2001 as the Rehabilitation Robotics TC. The name was changed this year to reflect the scientific progress and maturity reached by this broad research area. The TC currently has about 450 registered members worldwide and welcomes new members. See the Web site at http://www-arts.sssup.it/IEEE_TC_RehaRob/.

Recent activities of the TC include workshops at ICRA 2007 in Rome, technical sponsorship of the First EURON Summer School on Rehabilitation Robotics, and special issue on Socially Assistive Robotics (*Autonomous Robots*, January 2007), Rehabilitation Robotics (*Journal of Neuroengineering and Rehabilitation*), and *IEEE Transactions on Neural Systems and Rehabilitation Engineering* (September 2006).

2008

22–26 Sept. IROS 2008: IEEE/RSJ International Conference on Intelligent Robots and Systems. Nice, France. http://iros2008.inria.fr/

14–17 Oct. ICCAS 2008: International Conference on Control, Automation and Systems. Seoul, Republic of Korea. http://2008.iccas.org

19–22 Oct. BioRob 2008: International Conference on Biomedical Robotics and Biomechatronics. Scottsdale, AZ, USA. http://www.ieee-biorob.org/

21–24 Oct. SSRR 2008: IEEE International Workshop on Safety, Security, and Rescue Robotics. Sendai, Japan. http://www.rm.is.tohoku.ac.jp/ssrr2008/cfp.html

19–22 Oct. BioRob 2008: International Conference on Biomedical Robotics and Biomechatronics. Scottsdale, Arizona, USA. http://www.biorob2008.org

29–30 Oct. LARS 2008: Latin America Robotics Symposium Salvador, Bahia, Brazil. http://jri2008.dca.ufrn.br/LARS/index_en.php

6–9 Nov. MHS 2008: 2008 International Symposium on Micro-Nano Mechatronics and Human Science. Nagoya, Japan. http://www.mein.nagoya-u.ac.jp/mhs/

7–9 Nov. SCS 2008: 2008 International Conference on Signals Circuits and Systems. Submissions due by 31 July 2008. Nabeul, Tunisia. http://www.emc-lab.net/Conferences/SCS2008/

10–11 Nov. TePRA 2008: IEEE International Conference on Technologies for Practical Robot Applications. Woburn, Massachusetts, USA. http://www.ieeerobot-tepra.org/

17–19 Nov. DARS 2008: 9th International Symposium on Distributed Autonomous Robotics Systems. Tsukuba, Japan. http://www.robot.t.u-tokyo.ac.jp/DARS2008/

19–20 Nov. ICR 2008: 2nd Israeli Conference on Robotics. Herzlia, Israel. http://www.icr2008.org.il/

19–22 Nov. 2008: e-Manufacturing and DFM Symposium. Hinschu, Taiwan. http://www.tsia.org.tw/Seminar/eManufacturing/2008/

20–22 Nov. URAI: 5th International Conference on Ubiquitous Robots and Ambient Intelligence. Daejeon, Republic of Korea. http://www.robotweek.or.kr/

1–3 Dec. Humanoids 2008: 8th IEEE-RAS International Conference on Humanoid Robotics. Daejeon, Republic of Korea. http://humanoids2008.org/

2–5 Dec. ICARV: 10th International Conference on Control, Automation, Robotics and Vision. Hanoi, Vietnam. http://www.icarcv.org/2008/

4 Dec. SI Int.: 2008 IEEE/SICE International Symposium on System Integration. Nagoya, Japan. http://www.rm.is.tohoku.ac.jp/SIInt08/

14–17 Dec. ROBIO'08: IEEE International Conference on Robotics and Biomimetics. Bangkok, Thailand. http://www.robio.org

17–20 Dec. ICARCV: 10th International Conference on Control, Automation, Robotics and Vision. Hanoi, Vietnam. http://www.icarcv.org/2008/

2009

25–29 Jan. MEMS 2009: IEEE 22nd Annual Conference on Micro Electro Mechanical Systems. Sorento, Italy. http://www.mems2009.org/

11–13 Mar. HRI 2009: ACM/IEEE International Conference on Human-Robot Interaction. Submissions due by 15 September 2008. La Jolla, CA, USA. http://hri2009.org/

18–20 Mar. WHC 2009: World Haptics Conference Submissions due by 15 October 2008. Salt Lake City, UT, USA. http://www.worldhaptics2009.org

13–17 May ICRA 2009: IEEE International Conference on Robotics and Automation. Submissions due by 15 September 2008. Kobe, Japan. http://www.icra2009.org

1–3 June RoMoCo 2009: Technical Cosponsorship Download Event View on Map Poland. 7th Workshop on Robot Motion and Control. Submissions due by 15 January 2009. Czernie-jewo, Poland. http://romoco.put.poznan.pl/

22–25 June ICIA 2009: International Conference on Information and Automation. Submissions due by 15 January 2009. Zhuhai, Macao, China. http://www.cs.ualberta.ca/∼icia09/

23–26 June ICORR 2009: IEEE International Conference on Rehabilitation Robotics. Kyoto, Japan. http://www.icorr2009.org/

14–17 July AIM'09: IEEE/ASME International Conference on Advanced Intelligent Mechatronics. Submission due by 15 January 2009. Singapore. http://www.aim2009.org/

9–12 Aug. ICMA 2009: IEEE International Conference on Mechatronics and Automation. Submissions due by 20 March 2009. Changchun, China. http://www.ieee-icma.org

22–25 Aug. CASE 2009: IEEE International Conference on Automation Science and Engineering. Submissions due by 1 February 2009. Bangalore, India. http://www.ieee-case.org/

10–12 Sept. SYROCCO'09: 9th International IFAC Symposium on Robot Control. Gifu, Japan.

10–15 Oct. IROS 2009: IEEE/RSJ International Conference on Intelligent Robots and Systems. St Louis, MO, USA. http://www.ece.mtu.edu/resl/iros09/

2010

2–5 June HRI 2010: 5th ACM/IEEE International Conference on Human-Robot Interaction. Nara, Japan. http://www.hri2010.org/

3–7 May ICRA 2010: International Conference on Robotics and Automation. Anchorage, AK, USA. http://icra2010.grasp.upenn.edu/

6–8 Sept. IAV 2010: 7th IFAC Symposium on Intelligent Autonomous Vehicles. Lecce, Italy. http://iav2010.unile.it/

Digital Object Identifier 10.1109/MRA.2008.927700